

3rd International Workshop on Induced Polarization

6 - 9 April 2014

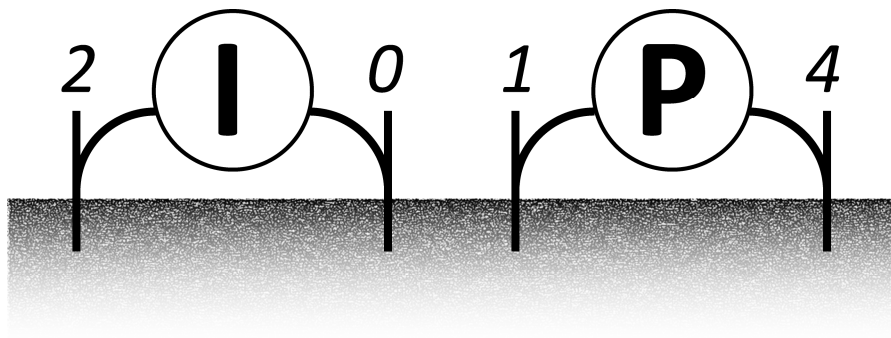
Ile d'Oléron - France



CAMERLYNCK C., CHAURIS H., MAINEULT A., SCHMUTZ M. (2014), *Proceedings of the 3rd International Workshop on Induced Polarization*, 6 – 9 April 2014, Ile d'Oléron, France.

**Proceedings of the
3rd International Workshop on Induced Polarization**

*6 – 9 April 2014
Ile d'Oléron
France*





FOREWORD

While Induced Polarization (IP) method was originally developed for ore prospecting and for the characterization of mineral deposits, its recent developments, in terms of instrumentation, understanding of the involved physical processes at the micro-scale for low frequencies (< 1000 Hz), macroscopic modelling and inversion procedures, are very promising for the study of environmental low-polarisable targets. In particular, interesting IP results were recently obtained in hydrogeophysics, biogeophysics or characterization of contaminated sites.

Two previous "International Workshops on Induced Polarization" were organised in Bonn (Germany) in 2009, and in Golden (Colorado, USA) in 2011. The first workshop presented the last developments and applications of the IP method for near-surface hydrogeological and environmental investigations; the second one focused on the understanding of the mechanisms generating IP signals in the Earth. They also dealt with data acquisition, petrophysical relationships, theoretical and laboratory studies, modelling and imaging, inverse problem, with environmental, hydrological and engineering applications. The goal of this third workshop is to discuss the recent IP developments and to open the discussion with scientists from other domains, such as agronomy or civil engineering.

We are pleased to see that many international scientists, coming from Europe, Israel, South Africa, Australia or USA, are attending this conference. We thank Areva for financial support, and the University Pierre-et-Marie Curie – Paris 6, the Institut Polytechnique de Bordeaux – ENSEGID, MINES ParisTech and the Centre National de la Recherche Scientifique (CNRS) for all the facilities.

C. Camerlynck, H. Chauris, A. Mainault and M. Schmutz
Organizing committee

N. Carlson, C. Doussan, N. Florsch, A. Kemna, J. Macnae, T. Martin, K. Titov and A. Weller
Scientific committee

* * *

In order to overcome more and more complex, deep or low contrasted targets exploration, geophysical methods are subject to continuous improvements whether it is hardware or software, data acquisition, processing or interpretation. This is the case when dealing with mining exploration where targets are becoming "deep and hidden".

Within this context, Induced Polarization and Spectral Induced Polarization are of importance for uranium resources exploration. One major objective for Areva Mines is to evaluate the suitability of SIP measurements as a guideline for the exploration of uranium mineralisation related to low disseminated sulphides contents, especially in roll-front context. Furthermore, SIP is foreseen as a tool for the survey of post-mining or remediation related topics.

Therefore, Areva Mines supports the 3rd International Workshop on IP. It is a real opportunity for Areva's geophysicists and geoscientists to exchange knowledge and experience with scientific community.

J.-M. Miehé
Geosciences Techniques Director & Geophysics Manager, Areva Mines

CONTENT

KEYNOTE LECTURE

- Martin T.** 2
Low frequency investigations on wood and trees

SESSION 1 – IP PETROPHYSICS

- Bairlein K., Hördt A., Bücker M., Nordsiek S.** 6
Experimental and theoretical studies of the temperature dependence of spectral induced polarization (SIP) based on a membrane polarization model
- Haegel F.-H., Esser O., Zimmermann E., Gao Z., Joblonowski N., Huisman J., Vereecken H.** 8
Induced polarization of carbon materials
- Hördt A., Bücker M.** 10
The salinity dependence of SIP parameters studied with an extended model of membrane polarization
- Hupfer S., Martin T., Noell U.** 12
Laboratory SIP-investigation on unconsolidated mineral-sand-mixtures
- Ingham M., Joseph S., Ilse K., Gouws G.** 14
IP and SIP – the practical link?
- Joseph S., Ingham M., Gouws G.** 16
Spectral induced polarization and hydraulic conductivity measurements on New Zealand unconsolidated sediments
- Kemna A., Weigand M., Zimmermann E.** 18
Resistivity and SIP response of rocks during freezing and thawing
- Kessouri P., Woodruff W., Revil A.** 20
Experimental study of the complex electrical conductivity of Fontainebleau sandstones
- Kremer T., Schmutz M., Keating E., Agrinier P., Maineult A.** 22
Spectral induced polarization monitoring of CO₂ injection in saturated sands: laboratory experiment and modelling
- Leroy P., Ghorbani A., Revil A., Cosenza P., Okay G.** 24
Modelling the induced polarization of bentonite-sand mixtures
- Masi M., Losito G.** 26
Spectral induced polarization for monitoring electrokinetic remediation processes
- Nordsiek S., Hördt A., Diamantopoulos E., Durner W.** 28
Estimation of the van Genuchten-Mualem parameter α and the saturated hydraulic conductivity from SIP measurements
- Placencia-Gómez E., Slater L.** 30
Electrochemical modelling of the SIP response to oxidation of disseminated metallic particles
- Revil A.** 32
POLARIS: a model to understand and interpret spectral induced polarization data in Earth sciences

Shefer I., Weinstein M., Furman A.	34
<i>Using SIP as a tool for identifying inorganic cations in a variably saturated soil</i>	
Shefer I., Schwartz N., Fel L., Furman A.	36
<i>The effect of free-phase NAPL on the spectral induced polarization signature of variably saturated soil</i>	
Treichel A., Binley A., Kemna A., Esser O., Zimmermann E., Vereecken H., Huisman J.	38
<i>Temperature-dependence of broadband complex electrical conductivity in unconsolidated porous media with variable clay content</i>	
Undorf S., Kemna A., Bücken M.	40
<i>A new numerical pore-scale model of membrane polarization</i>	
Weller A., Slater L.	42
<i>Improving understanding of the information content in induced polarization data: the value of empirical observations based on extensive, validated original datasets</i>	
Zhang Z., Weller A., Nordsiek S.	44
<i>Fractal dimension and induced polarization</i>	

SESSION 2 – IP METHODOLOGY

Abdulsamad F., Florsch N., Schmutz M., Camerlynck C.	48
<i>The paradox of the measuring electrodes in IP</i>	
Dahlin T.	50
<i>Factors affecting time domain IP data quality</i>	
Fiandaca G., Doetsch J., Binley A., Christiansen A., Auken E.	52
<i>2D time domain spectral polarization inversion - full wave modelling and Cole-Cole parameterization</i>	
Florsch N., Revil A., Camerlynck C.	54
<i>Inversion of generalized relaxation time distributions (GRTD) with a L-curve</i>	
Huisman J., Zimmermann E., Haegel F.-H., Treichel A., Vereecken H.	56
<i>Evaluation of a correction procedure to remove electrode contact impedance effects from broadband SIP measurements</i>	
Kelter M., Huisman J., Zimmermann E., Kemna A., Vereecken H.	58
<i>Imaging spectral electrical properties of variably saturated soil columns</i>	
Kenkel J., Kemna A.	60
<i>Anisotropic complex conductivity inversion</i>	
Macnae J.	62
<i>Newmont chargeabilities, apparent time constants and finite bandwidths</i>	
Macnae J., Kratzer T.	64
<i>Airborne induced polarization</i>	
Ntarlagiannis D., Slater L., Curatola F., Evdokimov K.	68
<i>SIP instruments for laboratory testing: current state of the technology and limitations</i>	
Olsson P.-I., Dahlin T., Auken E., Fiandaca G.	70
<i>Optimizing the acquisition time for time domain spectral IP by measuring during the on-time</i>	
Postic F., Doussan C.	72
<i>Test of different metal electrodes for IP measurement in time domain</i>	

Radic T.	74
<i>Measuring IP effects at high frequencies: first lab and field data from 0.001 Hz - 250 kHz</i>	
Schmutz M., Ghorbani A., Vaudelet P., Blondel A.	76
<i>Cable arrangement to reduce EM coupling effects in spectral induced polarization studies</i>	
Titov K., Gurin G., Tarasov A., Akulina K.	78
<i>Spectral induced polarization: frequency domain versus time domain</i>	
Zimmermann E., Zhao Y., Huisman J., Treichel A., Wolters B., van Waasen S., Kemna A.	80
<i>Numerical modelling of electromagnetic coupling effects in EIT borehole measurements</i>	
Zorin N.	82
<i>On the application of differential phase parameter in spectral IP</i>	

SESSION 3 – IP FOR GEOPHYSICAL CASE STUDIES

Auken E., Fiandaca G., Christiansen A., Gazoty A.	86
<i>Characterization of a landfill using 2D time domain SIP</i>	
Blondel A., Schmutz M., Franceschi M., Carles M., Tichané F.	88
<i>Case of study of a hydrocarbon contaminated site using the spectral induced polarization method: contribution of laboratory measurements for the interpretation of field results</i>	
Camerlynck C., Longuevergne L., Roques C.	90
<i>TDIP imaging of watershed over crystalline basement</i>	
Carlson N., Bouzid N.	92
<i>Synopsis of mapping buried waste with IP effects</i>	
Dahlin T., Auken E.	94
<i>An overview of time domain induced polarisation for characterisation of underground structures and point source contaminations – large research projects in Denmark and Sweden</i>	
Doetsch J., Fiandaca G., Auken E., Christiansen A., Cahill A., Jakobsen R.	96
<i>Monitoring of a CO₂ injection by time domain SIP</i>	
Flores Orozco A., Bücker M., Williams K.	98
<i>Induced polarization imaging at the floodplain scale for the delineation of naturally reduced zones</i>	
Ghorbani A., Schmutz M., Camerlynck C., Parisot J.-C.	100
<i>TDIP and SIP characterization of disseminated ores</i>	
Giampaolo V., Capozzoli L., Votta M., Rizzo E.	102
<i>Optimizing investigation strategies of hydrocarbon contaminated site using multi-geophysical approach in surface and borehole (IP, ERT and GPR)</i>	
Gurin G., Tarasov A., Ilyin Y., Titov K.	104
<i>Application of the Debye decomposition approach to time domain induced polarization profiling data: an ore exploration example</i>	
Johansson S., Olsson P.-I., Lumetzberger M., Dahlin T., Rosqvist H., Sparrenbom C.	106
<i>Delineation of a free phase chlorinated hydrocarbon plume with resistivity and TDIP</i>	
Kremer T., Allègre V., Schmutz M., Williard E., Maineuil A.	108
<i>Monitoring of a shallow CO₂ injection using time lapse electrical resistivity and induced polarization methods</i>	

Kulikov V., Sterligova I. <i>Frequency-domain induced polarization: application to a paleovalley, Ugra national park (Russia, Kaluga region)</i>	110
Kulikov V., Sterligova I. <i>Spectral induced polarization in mineral exploration</i>	112
Llubes M., Macouin M., Lartiges B. <i>Monitoring sediments pollution of the Garonne River using induced polarization and magnetic susceptibility measurements</i>	116
Okay G., Cosenza P., Ghorbani A., Camerlynck C., Cabrera J., Florsch N., Revil A. <i>Interpretation of a clay rock's desaturation process with IP methods</i>	118
Scheibz J., Bazin S., Pfaffhuber A., Fiandaca G., Dahlin T., Cappelen P., Zadorozhnaya V. <i>Integrating ERT and IP measurements with traditional environmental sampling – ambiguity reduced or increased? A DNAPL case study from Norway</i>	120
Schwartz N., Furman A. <i>Spectral induced polarization response of soil organic matter</i>	124
Schwartz N., Shefer I., Furman A. <i>A comprehensive study of the SIP response of soil contaminated with organic pollutants</i>	126
Williard E., Mainault A., Béhaegel M. <i>Spectral induced polarization on roll-front type deposits</i>	128
Zadorozhnaya V., Abu Zeid N., Santarato G. <i>Membrane polarization from molecular to rock scale in dynamic regime</i>	130
Zadorozhnaya V., Abu Zeid N., Santarato G., Bignardi S. <i>New shape of TEM: membrane polarization, mechanism and possible interpretation</i>	132

SESSION 4 – OTHER IP APPLICATIONS

Kruschwitz S. <i>SIP responses of building materials, investigation of correlations with specific surface and dominant pore throat size</i>	136
Mary B., Saracco G., Peyras L., Mériaux P., Vennetier M. <i>Preliminary use of induced polarization measurement to study tree roots growing in earth dikes</i>	138
Noel C., Gourry J.-C., Ignatiadis I., Battaglia F., Guimbaud C. <i>Monitoring of the biodegradation of toluene-contaminated sand in columns by SIP measurements, CO₂ content and its ¹³C/¹²C isotopic signature</i>	140
Revil A. <i>A new model for the spectral induced polarization signature of bacterial growth in porous media</i>	142
Weigand M., Kemna A. <i>Imaging and characterization of crop root systems using electrical impedance tomography at the rhizotron scale</i>	144

KEYNOTE LECTURE

Low frequency investigations on wood and trees

T. Martin⁽¹⁾

(1) Federal Institute for Geosciences and Natural Resources (BGR), Berlin, Germany

The interest in non-destructive tomographical methods for tree investigations is growing since years. Geophysical methods can be an alternative to detect internal defects and assess tree failure. In addition to geoelectrical methods, which are already used, the low frequency investigation method SIP (spectral induced polarization) can provide information about cell structure and condition.

Starting with field application a multiplicity of tomographical measurements at different tree species and for different temperature conditions were carried out. With the SIP256c device (Radic 2008) up to 24 stainless steel nails could be used as electrodes. For the tomographical reconstruction of the data the modified inversion program DC2dTree was used, based on the algorithm by Günther et al. (2006).

To understand these field data and the various influencing factors, a considerable amount of laboratory measurements were arranged. Mainly, the SIP characteristics as function of anisotropy, saturation, fungal decay and wood species were investigated. For these purposes fresh and seasoned small wood samples are measured with the SIP-measurement device from Zimmermann et al. (2008). To provide constant temperature the measurements were conducted in a climate chamber.

Figure 1 shows exemplary laboratory results from different European wood species. The amplitude values differ between 10 and 200 Ωm . Owing to the different wood moisture content mostly due to seasonal influences the species can hardly be differentiated with regard to the amplitude. A differentiation seems to be possible using in phase. Due to the different cell structures of the particularly wood species, the phase characteristics are much more variable in both, phase amplitude and frequency of the phase maximum, respectively. Poplar shows the highest phase effect ($\sim |40|$ mrad), but the oak species show the phase maximum at the lowest frequency (~ 0.01 Hz). The imaginary parts of conductivity (σ'' in Fig. 1) show that oak and lime, which have approx. the same maximum phase magnitude ($\sim |25|$ mrad), differ clearly with regard to σ'' . So, the polarization structure in lime is higher than in oak.

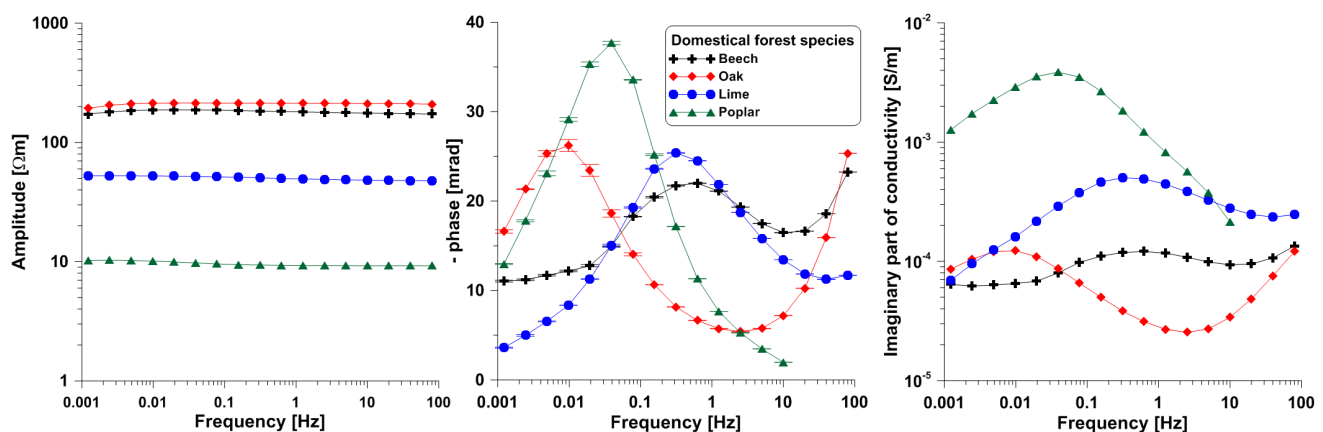


Fig. 1: Amplitude (left), phase spectra (middle) and imaginary part of conductivity (right) for different European wood species. Clear differences between the species can be found.

Figure 2 shows exemplary results of a tomographical field measurement at a lime tree for $f = 0.15$ Hz. The seasonal influence becomes very important for these field measurements. The tree changes with the season and, consequently, resistivity and phase change as well. In winter the tree stopped the water and nutrient transport, therefore, the sapwood is much drier. In early spring the sap flow starts again.

Both, resistivity (Fig. 2 left) and phase (Fig. 2 right) show a circle-concentric tree-typical setting. In contrast to oak trees the resistivity shows lower values (mainly < 200 Ωm). The phase shows a clear difference between sap- and heartwood. The “active” sapwood is characterised by low phase values whereas the “inactive” heartwood shows phase values up to $|2.5|^\circ$ ($> |40|$ mrad)

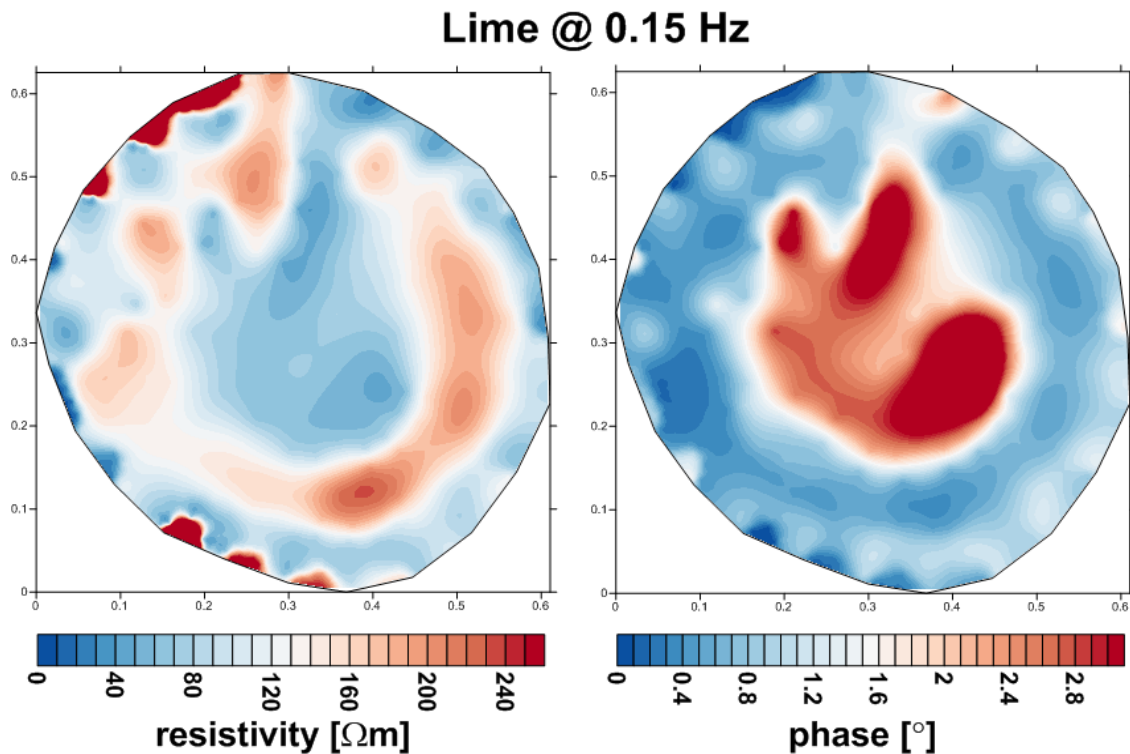


Fig. 2: Amplitude (left) and phase spectra (right) for lime (*Tilia*). Measurements were taken in February.

The results of these investigations can be summarized as follows:

- Anisotropy, saturation, and fungal decay influence the SIP characteristics of wood species in laboratory measurements (Martin 2012).
- Due to the different cell structures, varying tree species show very different phase behaviour.
- Tomographical field measurements show typically ring structures of heart wood trees. A differentiation between healthy and infected trees (fungal decay) could be observed (Martin and Günther 2013).

In conclusion, the SIP method seems to have potential as an additional tree investigation technique. Unfortunately, until now, it is not fully understood which factors and processes caused the polarization effect on the micro scale in wood. Further investigations are indispensable.

References

- Günther, T., Rücker, C. and Spitzer, K., 2006. 3-D modelling and inversion of DC resistivity data incorporating topography – part II: inversion. *Geophys. J. Int.*, 166, 506-517.
- Martin, T., 2012. Complex resistivity measurements on oak. *Eur. J. Wood Prod.*, 70, 45-53.
- Martin, T. and Günther, T., 2013. Complex resistivity tomography (CRT) for fungus detection on standing oak trees. *Eur. J. Forest Res.*, 132, 765-773.
- Radic, T., 2008. Instrumentelle und auswertemethodische Arbeiten zur Wechselstromgeoelektrik, PhD thesis, TU Berlin, Germany, www.radic-research.de.
- Zimmermann, E., Kemna, A., Berwix, J., Glaas, W., Münch, H.-M. and Huisman, J.A., 2008. A high-accuracy impedance spectrometer for measuring sediments with low polarizability. *Meas. Sci. Technol.*, 19, 094010.

SESSION 1

IP PETROPHYSICS

Experimental and theoretical studies of the temperature dependence of spectral induced polarization (SIP) based on a membrane polarization model

K. Bairlein⁽¹⁾, A. Hördt⁽¹⁾, M. Bucker⁽²⁾ and S. Nordsiek⁽¹⁾

(1) TU Braunschweig, Institute of Geophysics and Extraterrestrial Physics

(2) University of Bonn, Department of Geodynamics and Geophysics

Introduction

Knowing the temperature dependence of spectral induced polarization is essential for applications, where temperature changes, like seasonal variations or spatial variations at geothermal sites, are expected. The knowledge is also useful for comparing field and laboratory measurements and may help to understand the polarization mechanisms at the pore scale. Previous investigations indicated that the influence of temperature variation on the phase shift is not dramatic (e.g. Binley et al. 2010), but if we are interested in a wide temperature range and/or very precise measurements, temperature effects have to be considered. We compare the temperature dependence of SIP-parameters from measurements on several samples to calculations with an extended membrane polarization model.

Membrane polarization model

The membrane polarization model we use in this study is based on the one-dimensional equations developed by Marshall and Madden (1959). They study the movement of the ions through active and passive zones, which represent the narrow and wide pores, characterized by different mobilities of cations and anions. This model was extended by Bucker and Hördt (2013) to the description of the pores as cylinders of two different lengths (L_1 and L_2) and radii (r_1 and r_2). The ions moving through these pores are influenced by the electrical double layer, leading to a gradient of ion concentration along the pore.

Ion diffusion coefficients, Debye length, and Zeta-Potential, obviously vary with temperature. Ion mobility and Debye length are also affected by the temperature dependence of dynamic viscosity and relative electrical permittivity, which can be described by empirical equations.

The phase shift was calculated for different pore lengths and radii. Figure 1 shows that a variation of the pore radii lets the highest phase values (deep red colours) appear at higher temperatures and slightly higher frequencies. Decreasing the pore radii shifts the highest phase values towards lower temperatures, whereas increasing the radii shifts them towards higher temperatures. The magnitude of the highest phase values slightly changes.

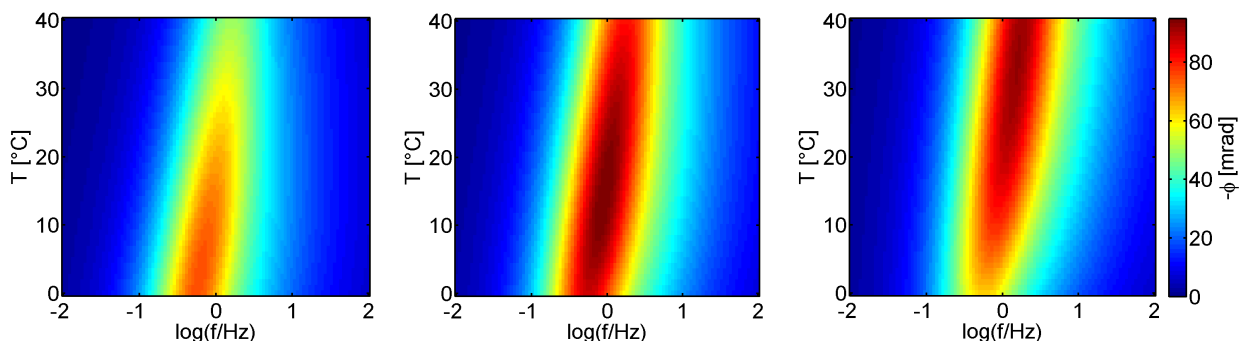


Fig. 1: Phase shift colour coded as function of frequency and temperature calculated with the model of Bucker and Hördt (2013) for different pore radii increasing from left to right. Left: $r_1 = 0.155 \mu\text{m}$, $r_2 = 0.009 \mu\text{m}$. Middle: $r_1 = 0.31 \mu\text{m}$, $r_2 = 0.018 \mu\text{m}$. Right: $r_1 = 0.62 \mu\text{m}$, $r_2 = 0.036 \mu\text{m}$. Pore lengths are $L_1 = 50 \mu\text{m}$, $L_2 = 0.5 \mu\text{m}$.

Measurements

Measurements were performed on several sandstones, limestones, and argillites. The samples were fully saturated with a sodium chloride solution, which had an electrical conductivity of 55 mS m^{-1} . The temperature was increased in steps of $5 \text{ }^\circ\text{C}$.

As an example, the temperature dependence of the phase shift of two sandstone samples in the temperature range of 0 to $40 \text{ }^\circ\text{C}$ is shown in Fig. 2. The phase shift of sample OK1 (Fig. 2, left) increases with temperature, whereas the phase shift of sample P8 (Fig. 2, right) decreases with temperature. We also note a shift of the maximum phase towards higher frequencies with increasing temperature.

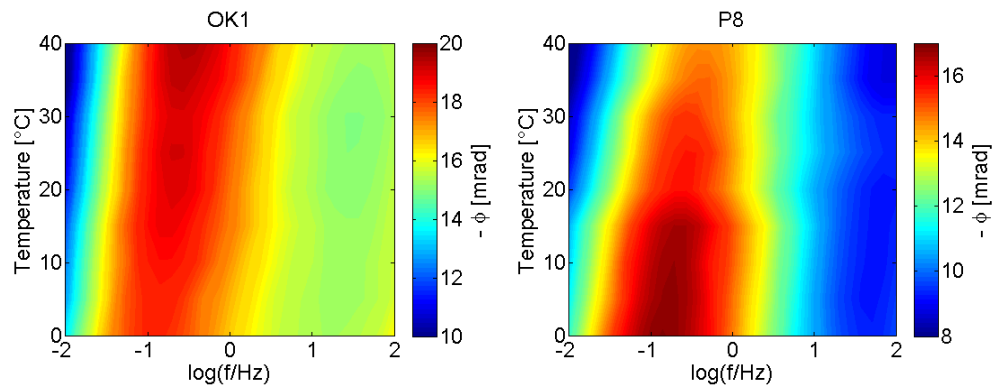


Fig. 2: Measured phase shift of two different sandstone samples OK1 (left) and P8 (right) as a function of frequency and temperature. Note that the colour scales are different.

Conclusions

Measured and calculated phase spectra show a qualitatively similar temperature dependence, indicating that our simple model can in principle simulate the polarization effects. Our modelling results show that the location of the highest phase values depends on the pore size, suggesting that the pore size may be important for the differences in the temperature dependence of the measured samples. Future analysis of the pore size distributions of the samples will provide additional information about the samples and might help to compare measurements and model results.

Acknowledgements

This work is supported by the ‘Niedersächsisches Ministerium für Wissenschaft und Kultur’ and Baker Hughes within the Geothermal Energy and High-Performance Drilling (gebo) research association. We thank Dorothea Reyer, Inga Moeck, Nicole Pastrok, Daniel Albrecht and Manfred Stövesand, who provided the samples and helped us preparing and characterizing the samples.

References

- Binley, A., Kruschwitz, S., Lesmes, D. and Kettridge, N., 2010. Exploiting the temperature effects on low frequency electrical spectra of sandstone: A comparison of effective diffusion path lengths. *Geophysics*, 75(6), A43-A46.
- Bücker, M. and Hördt, A., 2013. Analytical modelling of membrane polarization with explicit parametrization of pore radii and the electrical double layer. *Geophys. J. Int.*, 194, 804-113.
- Marshall, D. and Madden, T., 1959. Induced polarization, a study of its causes. *Geophysics*, 24(4), 790-816.

Induced polarization of carbon materials

F.-H. Haegel⁽¹⁾, O. Esser⁽¹⁾, E. Zimmermann⁽²⁾, Z. Gao⁽¹⁾,
N.D. Jablonowski⁽³⁾, J.A. Huisman⁽¹⁾ and H. Vereecken⁽¹⁾

(1) Institute of Bio- and Geosciences, Agrosphere (IBG-3), 52425 Jülich, Germany

(2) Central Institute of Engineering, Electronics and Analytics, Electronic Systems (ZEA-2), 52425 Jülich, Germany

(3) Institute of Bio- and Geosciences, Plant Sciences (IBG-2), 52425 Jülich, Germany

Introduction

Carbon materials exhibit more or less electronic conductivity and as a consequence they may show strong polarization effects when they are in contact with electrolytes and other less conductive materials, e.g. in supercapacitors or as biochar in soil. For an insulating mineral with a charged surface (e.g. sand), polarization is mainly due to a fast compression and dilatation of the diffuse electrical double layer and a slow movement of counterions in the Stern layer. Applying an electrical field to electronically conducting particles (e.g. graphite) induces a large dipole moment across the particle. This fast process is followed by a slow rearrangement of ions in the surrounding solution (Fig. 1). The time needed for the slow processes depends on the particle size. In contrast to ideal graphite, carbon materials made by pyrolysis from natural sources have functional groups and surface charges. Thus all mechanisms shown in Fig. 1 may influence their polarization. In addition, redox reactions taking place at the interface between the electronically conducting particles and the electrolyte or other solid material may lead to leakage currents that reduce the polarization. The goal of this work was to study the influence of the electronic conductivity, the particle size and the chemical composition of carbon materials on the induced polarization of their mixtures with a non-conducting material (sand) and an electrolyte.

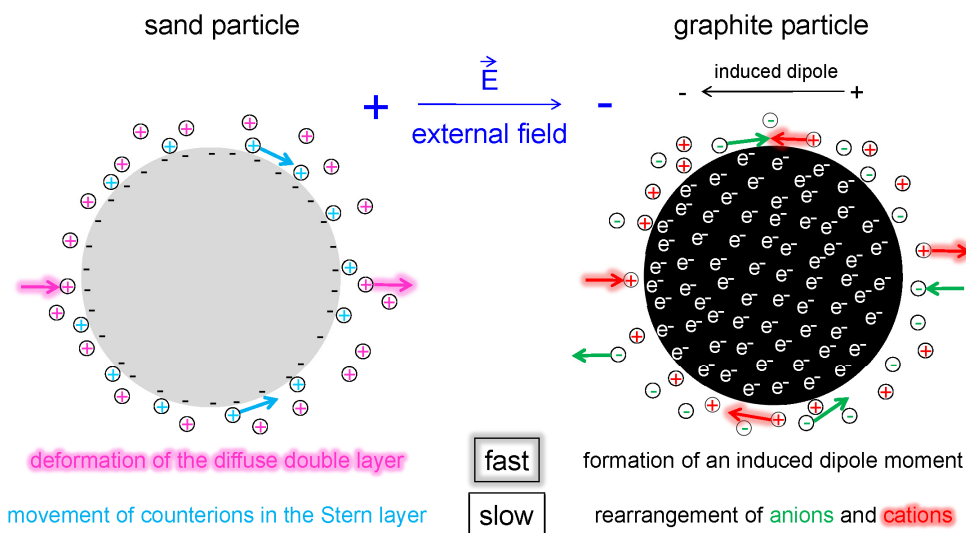


Fig. 1: Polarization mechanisms for sand particles and graphite particles.

Materials and methods

Series of commercial activated carbons with well-defined particle size and biochars made under different conditions were investigated. Sand with a particle size between 125 and 250 μm was used as non-conducting material.

The magnitude of the complex electrical conductivity $|\sigma^*|$ of some air-dry carbon materials and air-dry sand was determined in a two-electrode configuration between two bronze plates in the frequency range from 1 Hz to 45 kHz. The complex electrical conductivity $\sigma^* = \sigma' + i\sigma''$ of 2 % carbon in sand saturated with 4 mM NaCl was measured in the frequency range between 1 mHz and 45 kHz with an impedance spectrometer built at Forschungszentrum Jülich.

Results

The magnitude of the conductivity of carbon materials can vary over several orders of magnitude as shown in Fig. 2a. The conductivity of sand is ca. 10^{-8} S m^{-1} at 1 Hz and increases with frequency due to a capacitive current. This behaviour is typical for an insulator with a low leakage current. The conductivity of the charcoal with 1-2 mm size is somewhat larger, but still in the range of an insulator. The active carbons and the gasification coke show much higher conductivity in the range of semi-conductors and there is no significant capacitive current in the observed frequency range. The carbon materials with high conductivity show large polarization, but the charcoal with low conductivity also has a noteworthy polarization with a clear maximum of the imaginary part of the complex conductivity (Fig. 2b).

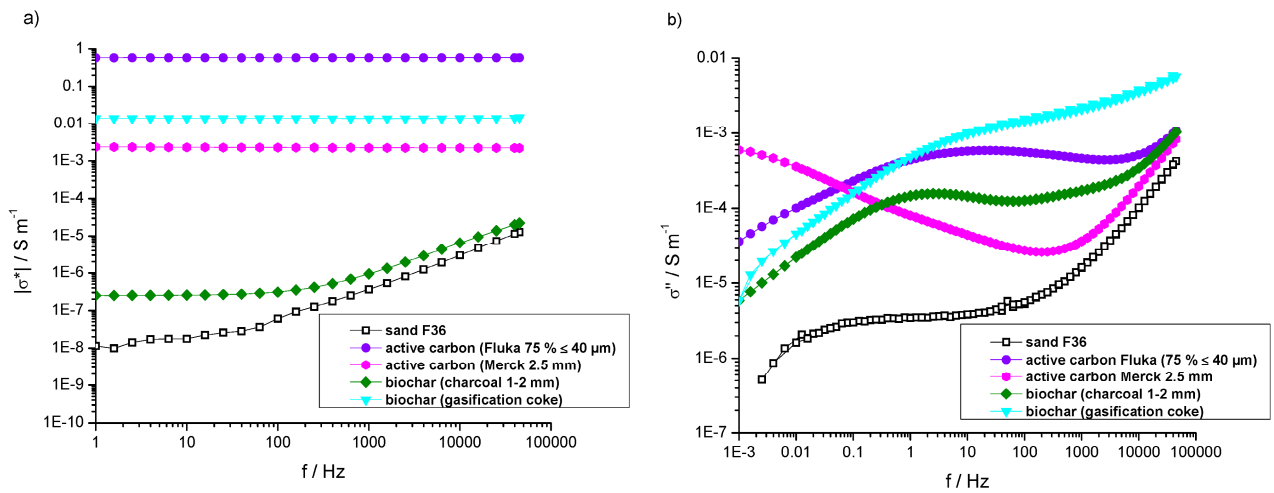


Fig. 2: a) Magnitude of the electrical conductivity of sand and different carbon materials. b) Imaginary part of the complex conductivity of sand with different carbon materials.

The frequency associated with maximum σ'' for active carbons and a series of different size fractions of the charcoal is dependent on the particle size, but two different lines are observed in a double logarithmic plot for charcoal and the active carbons with a slope that seems to be somewhat larger than expected for a diffusive relaxation mechanism (Fig. 3a). There is also some correlation between σ'' at a high frequency and the hydrogen/carbon ratio (Fig. 3b). This is related to the fact that the electronic conductivity increases, whereas leakage currents due to redox reactions and the hydrogen/carbon ratio decrease with increasing graphitization.

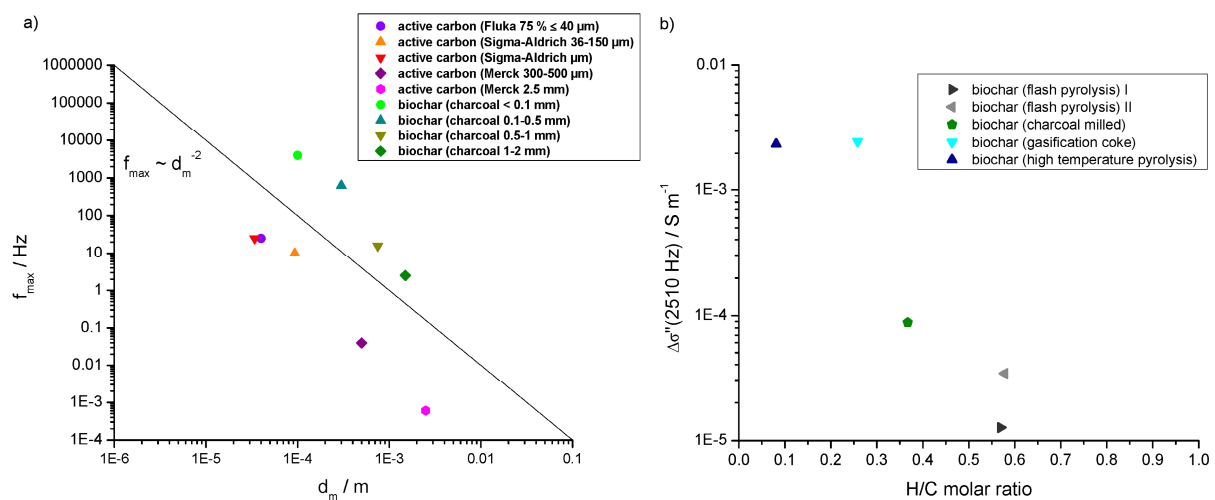


Fig. 3: a) Dependence of the maximum of σ'' on the particle size. b) Dependence of σ'' on the carbon/hydrogen ratio.

Conclusions

Electronic conductivity, particle size and H/C ratio influence the polarization of carbon material. Quantification of the effects still requires more data. We are currently extending our database with more measurements on a wide range of carbon materials.

The salinity dependence of SIP parameters studied with an extended model of membrane polarization

A. Hördt⁽¹⁾ and M. Bucker⁽²⁾

(1) TU Braunschweig, Germany

(2) University of Bonn, Germany

Introduction

An important parameter influencing the behaviour of induced polarization (IP) spectra is fluid salinity. Scott et al. (2004) observed that the phase shift may either increase or decrease with increasing salinity. Slater and Glaser (2003) and Kruschwitz et al. (2010) investigated the imaginary conductivity (around 1 Hz) and found an increase with fluid salinity. In order to understand the behaviour of SIP spectra from a mechanistic point of view, we carried out numerical simulations with a new model of membrane polarization (Bucker and Hördt, 2013). We discuss the results in the context of previously published experimental observations.

The model

In the original membrane polarization model by Marshall and Madden (1959), the IP effect is caused by different mobilities in two one-dimensional pore types. Assuming that the (apparent) mobility variation is related to the electrical double layer (EDL), Bucker and Hördt (2013) expand the model to a two-dimensional system with finite pore size (Fig. 1). The model is defined by the geometrical parameters r_1 , r_2 , L_1 and L_2 , the ion mobilities, the Zeta potential, the partition factor, and the parameters controlling the Debye length. The salinity influences the impedance as a constant factor, and through the definition of the EDL thickness.

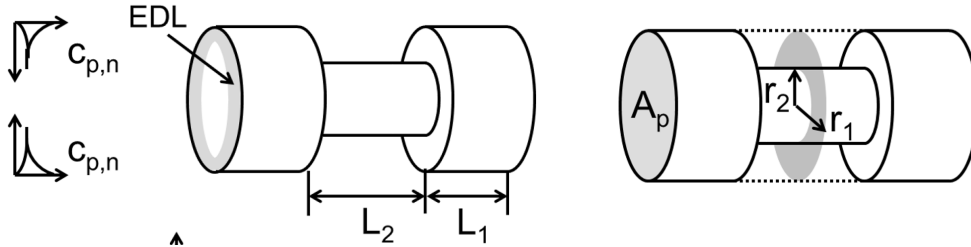


Fig. 1: Extended model to simulate membrane polarization. Left: Definition of pore lengths and schematic behaviour of anion and cation concentration c_p and c_n with distance from the pore surface within the EDL. Right: Definition of the two pore radii (after Bucker and Hördt 2013).

Results

The extended Marshall-Madden impedance was calculated as function of ion concentration, for fixed pore lengths and different combinations of pore radii (Fig. 2). The maximum phase shift (left panel) was determined from the spectra as a measure of the IP effect. It first increases, and then decreases with increasing salinity, where the peak salinity depends on the pore radii. This observation is qualitatively consistent with experimental results obtained by Scott et al. (2004), who observed that "...decreasing the salinity ... can cause the phase angle to either decrease or increase, depending on the sandstone".

The imaginary conductivity increases with fluid salinity for the parameter range (frequencies and pore radii) investigated here (Fig. 2, right panel). This trend can also be observed in experimental data (e.g. Slater and Glaser 2003; Weller et al. 2011). However, Weller et al. (2011) also find a decrease of imaginary conductivity at high salinities for some of their samples, which is not visible in our simulated results.

The relaxation times obtained with our model (not shown here) are fairly independent of salinity, consistent with experimental observations.

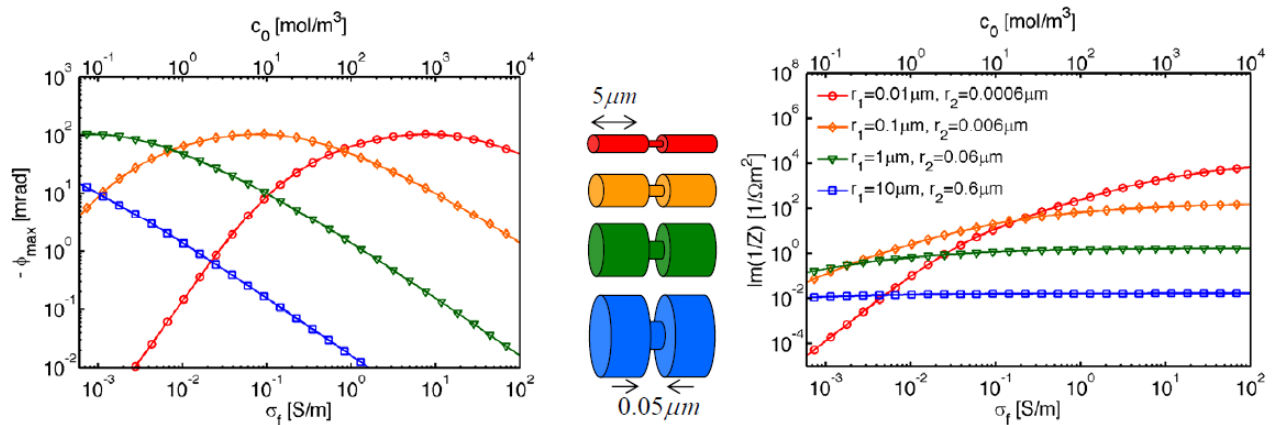


Fig. 2: Simulated phase shift (left) and imaginary conductivity (right) vs. fluid conductivity for different pore radii. The middle section illustrates the models (not to scale), where the pore lengths are constant.

Conclusions

We use an extended model of membrane polarization that explicitly includes pore radii and the EDL to simulate the influence of fluid conductivity on SIP spectra. The model is able to reproduce general trends observed experimentally, such as both decreasing and increasing phase shifts, and increasing imaginary conductivity. Some specific features of measured data, such as an increase of imaginary conductivity at high salinities, were not yet reproduced.

References

- Bücker, M. and Hördt, A., 2013. Analytical modelling of membrane polarization with explicit parametrization of pore radii and the electrical double layer. *Geophys. J. Int.*, in press.
- Kruschwitz, S., Binley, A., Lesmes, D. and Elshenawy, A., 2010. Textural controls on low-frequency electrical spectra of porous media. *Geophysics*, 75, WA113-WA123.
- Marshall, D. and Madden, T., 1959. Induced polarization, a study of its causes. *Geophysics*, 24(4), 790-816.
- Scott, J., Weller, A., Schleifer, N. and Barker, R., 2004. The effect of changing the salinity of the groundwater on SIP of sandstones. *10th Eur. Meeting Env. Eng. Geoph.*
- Slater, L.D. and Glaser, D.R., 2003. Controls on induced polarization in sandy unconsolidated sediments and application to aquifer characterization. *Geophysics*, 68, 1547-1588.
- Weller, A., Breede, K., Slater, L. and Nordsiek, S., 2011. Effect of changing water salinity on complex conductivity spectra of sandstones. *Geophysics*, 76, F315-F327.

Laboratory SIP-investigation on unconsolidated mineral-sand-mixtures

S. Hupfer⁽¹⁾, T. Martin⁽¹⁾ and U. Noell⁽¹⁾

(1) Federal Institute for Geosciences and Natural Resources (BGR), Berlin, Germany

The BMBF (German Federal Ministry of Education and Research) funded project ROBEHA aims at investigating abandoned mine dumps with regard to the potential reuse of the dumped mineral resources. Different geophysical methods (geolectric, radar, SIP, magnetic) were applied on a typical mining dump in the Harz mining area to study the dumps structure and extension. In order to evaluate the SIP signals obtained in the field, laboratory measurements were carried out on samples comprising those minerals typically expected in the abandoned mine dumps (pyrite, galenite, sphalerite).

For these laboratory measurements we created different synthetic unconsolidated mineral-sand-mixtures. For each of the three above mentioned minerals we investigated three different concentrations (volume percent of 0.5, 2 and 6 %) with three different grain size fractions (fine $\leq 63 \mu\text{m}$, middle = $112 - 200 \mu\text{m}$ and coarse = $630 - 1000 \mu\text{m}$). For these mineral-sand-mixtures a new measuring cell was constructed. This cell enabled to measure SIP and saturation simultaneously and the embedded samples can also be used for NMR-measurements. Each mineral fraction (e.g. pyrite, 2 %, coarse) was homogenised with quartz sand (density 1.5 g cm^{-3}) after DIN 19747 (2009) and fully saturated with tap water ($\rho \sim 13.6 \Omega\text{m}$). To provide constant temperature the measurements were conducted in a climate chamber using the SIP-measurement device from Zimmermann et al. (2008).

Figure 1 shows the results for the saturated 6 % pyrite-sand-mixtures with different grain sizes. The resistivity of the coarse and the fine/middle fraction differ significantly (Fig. 1, left) With decreasing grain sizes the phase amplitudes increase. Also the frequency of the phase maximum increase (Fig. 1, right). The peak of the finest fraction is at a very high frequency (15 kHz). Due to the accurate measurement device and the new measuring cell, the errors are very small.

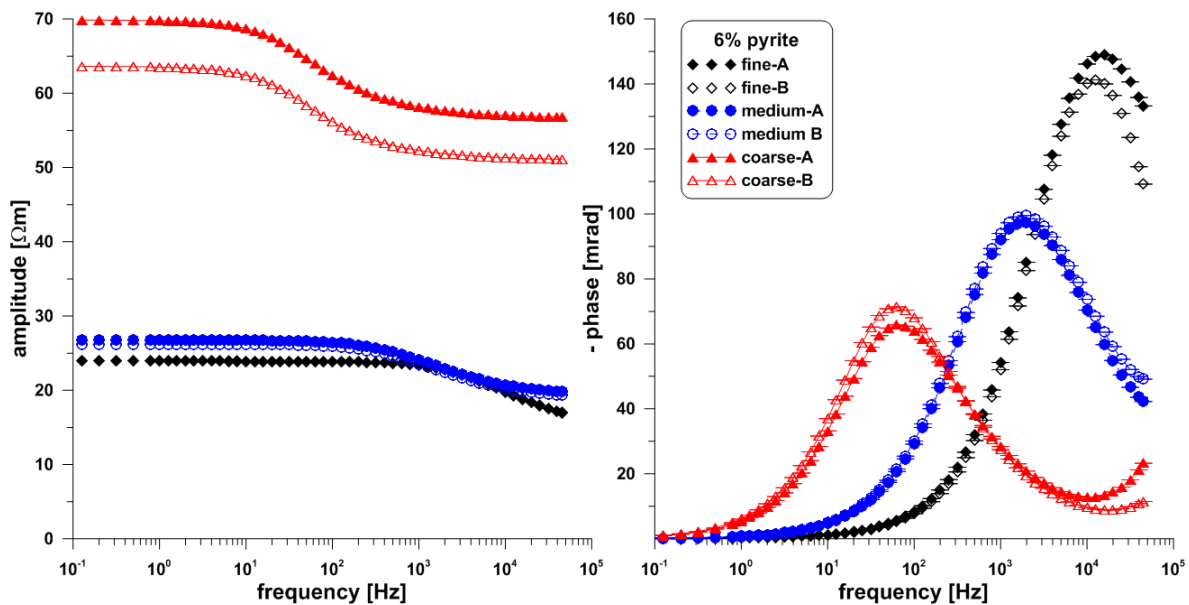


Fig. 1: Results of the saturated pyrite-sand-mixtures. The pyrite grain size changed from $<63 \mu\text{m}$ (fine) to $112 - 200 \mu\text{m}$ (medium) up to $630 - 1000 \mu\text{m}$ (coarse). Significant differences are visible in phase amplitude and in the frequency of the phase maximum. The error bars are very small.

Figure 2 left shows conductivities and phases of the coarse pyrite fraction for different concentrations. With increasing concentration the phase amplitude increases whereas the frequency of the phase maximum changes only slightly (from 60 Hz (6 %) to 120 Hz (0.5 %)).

The relationship between concentration and imaginary part of conductivity is pictured for all measured pyrite samples in Fig. 2 right. Both, the coarse and middle fraction as well as the fine pyrite fraction show a linear relationship. With increasing concentration the imaginary part of conductivity increases.

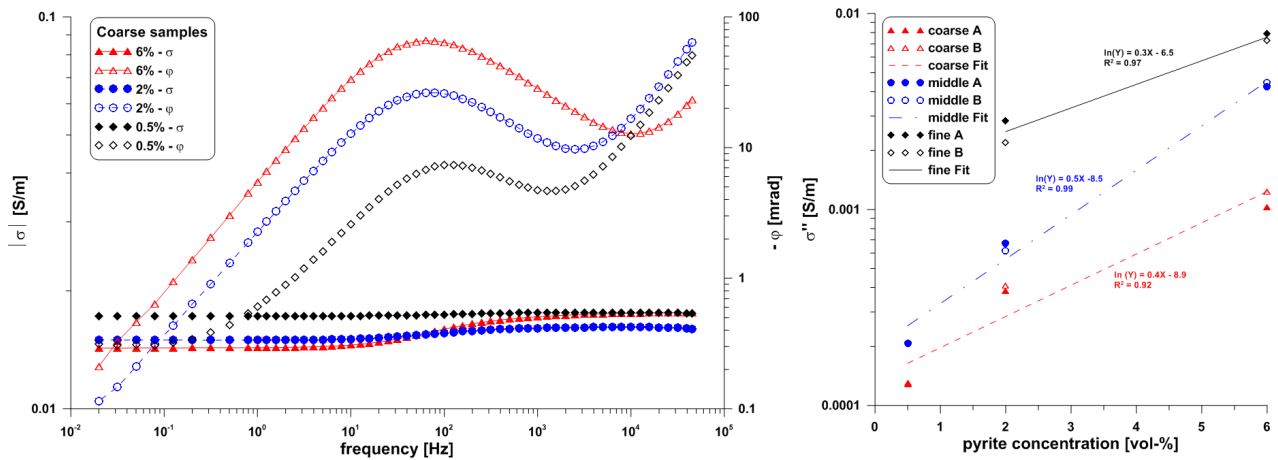


Fig. 2: Left: Comparison of saturated coarse pyrite-sand-mixtures with different pyrite concentrations. With decreasing concentration the phase maximum decreases. The frequency of the phase maximum is changing only slightly. Right: Pyrite concentration versus imaginary part of conductivity for all measured pyrite samples.

In summary we observed the following effects in our pyrite investigations:

- With increasing pyrite concentration the phase effect/imaginary part of conductivity increases.
- With decreasing grain size the phase amplitude/chargeability increases.
- With decreasing grain size the frequency of the phase maximum increases (decreasing of the relaxation time).
- No systematic relationship between conductivity and pyrite concentration is observed. Samples with the coarse pyrite show the highest conductivity with the lowest pyrite concentration (0.5 % vol.), samples with middle pyrite show the highest conductivity with 6 % vol. pyrite concentration and the samples with fine pyrite show the highest conductivity with 2 % vol. pyrite.

The results back the hypothesis that the minerals cause the polarisation effect and the effect increases with the mineral amount. The data seem to confirm that the size of the pyrite fraction and therefore the changing specific surface area influenced the polarisation in the mineral-sand-mixture (analogue to Slater et al. 2006).

Our results show a very significant relationship between mineral concentration/grain sizes and SIP-signature. So, at least in a laboratory environment SIP measurements can clarify the valuable mineral concentration. In field application this differentiation is much more complicated and could not be shown yet.

References

- DIN19747, 2009. Investigation of solids – Pre-treatment, preparation and processing of samples for chemical, biological and physical investigations, DIN-Deutsches Institut für Normung e.V.
- Slater, L., Ntarlagiannis, D. and Wishart, D., 2006. On the relationship between induced polarization and surface area in metal-sand and clay-sand mixtures. *Geophysics*, 71, A1-A5.
- Zimmermann, E., Kemna, A., Berwix, J., Glaas, W., Münch, H.-M. and Huisman, J.A., 2008. A high-accuracy impedance spectrometer for measuring sediments with low polarizability. *Meas. Sci. Technol.*, 19, 094010.

IP and SIP – the practical link?

M. Ingham⁽¹⁾, S. Joseph⁽¹⁾, K. Ilse⁽²⁾ and G. Gouws⁽¹⁾

(1) Victoria University of Wellington, New Zealand,

(2) Martin Luther University of Halle-Wittenberg, Germany

Laboratory measurements on both consolidated and unconsolidated samples suggest that spectral induced polarization (SIP) measurements have the potential to provide a proxy for hydraulic conductivity. Nonetheless there are several difficulties related to developing SIP as an effective field technique. These relate not only to the inductive and capacitive problems associated with using an alternating current when extensive cabling is laid on the surface of the electrically conductive Earth, but also to the time required to obtain accurate measurements at low frequencies. In contrast to SIP, induced polarization (IP) measurements are not as prone to the same problems. In theory, the square wave current used by an IP measurement can be represented as an infinite Fourier Series of sinusoidal waves of increasing frequency. This means in principle that if the full IP signal is able to be recorded at a sufficiently fast rate, the SIP response of the ground should be able to be derived from it.

The relationship between IP and SIP responses, and the limitations in obtaining the SIP spectrum from the IP response, have been explored in four stages.

- (1) By representing a measured IP voltage decay in terms of a mathematical function, such as a Debye relaxation, for which the Fourier Transform can be analytically calculated.
- (2) By creating a synthetic time series of such an IP decay and numerically calculating the resulting Fourier Transform.
- (3) By experimentally measuring both IP and SIP responses on laboratory samples and demonstrating that they related by Fourier Transformation.
- (4) Trial field measurements using a purpose built instrument capable of measuring both the SIP and IP response.

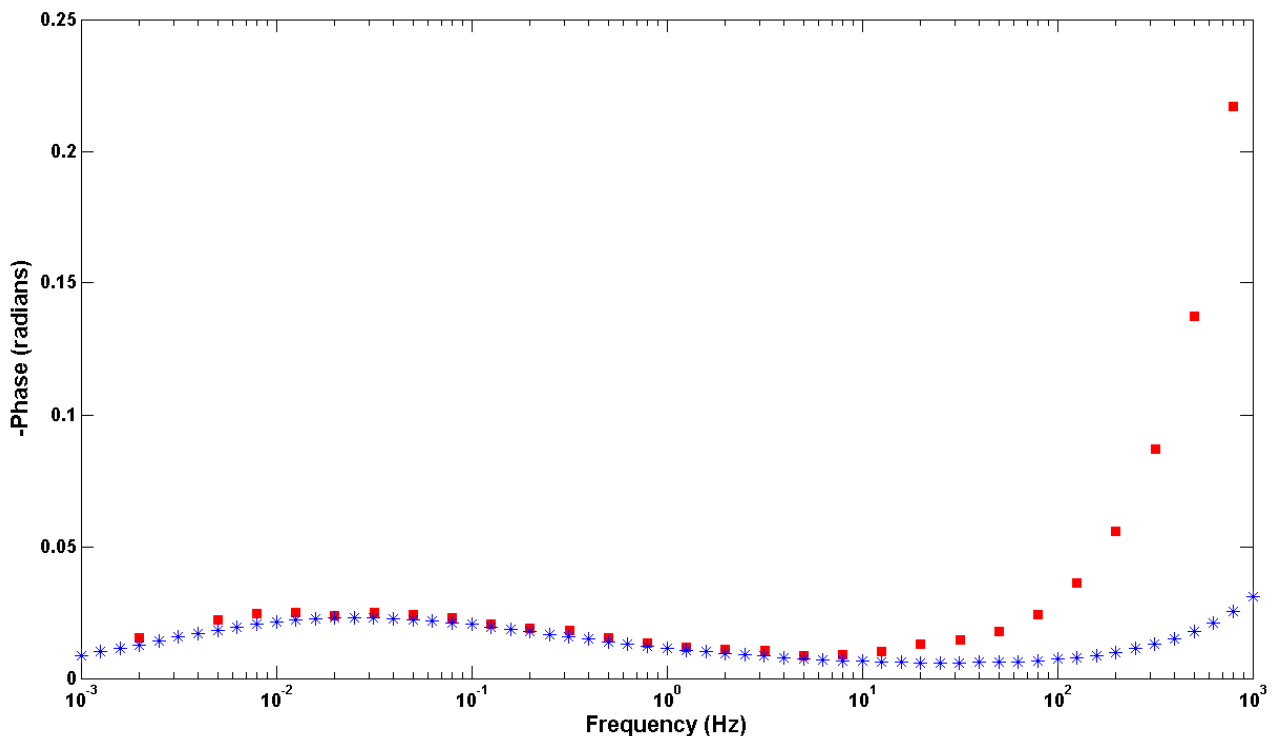


Fig. 1: SIP response of an unconsolidated sand sample measured in the laboratory. Blue stars – measured SIP response; red squares – SIP response calculated from the FFT of an IP measurement with pulse length 120 s.

The results of analytic calculations suggest that as long as the ratio of the IP pulse to the relaxation time of the principal relaxation is larger than about 5-10, the calculated Fourier Transform of the IP signal shows a perfect match to the SIP response. As this ratio decreases the frequency response is less well reproduced. When a synthetic time series is used as a basis for numerical calculation of the FFT, it is apparent that, in addition to the pulse length and the relaxation time, the overall length of the signal and the sampling frequency are important. This is further borne out by laboratory measurements on real samples. Such measurements also introduce measurement noise and demonstrate the need for suitable band averaging of frequency estimates calculated from the Fourier Transform. The quality of the calculated SIP spectrum can also be improved either by stacking of multiple measurements or by smoothing of the measured response. The efficacy of the second technique is illustrated in Fig. 1 which compares the laboratory SIP responses of an unconsolidated sand sample measured both directly and calculated from the FFT of a smoothed IP response using a 120 s pulse. The comparison between the measured and calculated responses in the region of interest at frequencies lower than 10 Hz is excellent.

The benefit of being able to derive an SIP spectrum from a measured IP signal is likely to be greatest for field measurements aimed at imaging the SIP response of the subsurface over both substantial depth and lateral ranges. Whereas a direct measurement of a single SIP spectrum over the frequency range 0.001-1000 Hz will take upwards of 25 minutes, depending on the number of individual frequencies that measurements are made at, the use of an IP pulse of 120 s pulse length will reduce the required time by at least a factor of 6. Adaptation of current commercial instrumentation is also possible meaning that new equipment is not required.

Spectral induced polarization and hydraulic conductivity measurements on New Zealand unconsolidated sediments

S. Joseph⁽¹⁾, M. Ingham⁽¹⁾ and G. Gouws⁽¹⁾

(1) Victoria University of Wellington, New Zealand

Spectral induced polarization (SIP) and hydraulic conductivity measurements have been made on unconsolidated samples representative of shallow coastal aquifers in New Zealand. The samples consisted of sands sieved into different fractions ranging from a mean grain size of 1.0 mm ($\phi = 0.00$) to 0.125 mm ($\phi = 3.00$).

To avoid the possibility that variations in SIP and hydraulic conductivity between samples might result from significant differences in the degree of packing of the samples into the sample holder a standardized measurement procedure was adopted consisting of the following steps. Initially each sample was thoroughly washed in distilled water over a period of two weeks and dried in an oven at 150 °C. The sample holder was filled with the dried sand and the mass of sand calculated by weighing the sample holder before and after filling. Water of a pre-determined (30-100 $\mu\text{S cm}^{-1}$) electrical conductivity was then passed through the sample until the electrical conductivity of the water coming out of the sample holder stabilized. The dc resistance of the sample was measured using a low frequency square wave and the formation factor calculated from the final recorded value of the pore fluid resistivity and the measured value of DC resistivity. Immediately after measurement of the formation factor the hydraulic conductivity of the sample was measured using the constant head method. Following the hydraulic conductivity measurement the SIP spectrum was repeatedly recorded for about 24 hours. The sample holder containing saturated sand was then reweighed to determine the mass of water saturating the sample and hence the porosity of the sample. The use of this standard procedure resulted, over all 13 samples, in an average formation factor F of 3.04 ± 0.11 , porosity of $41 \pm 2 \%$ and cementation exponent (calculated from Archie's Law) of 1.26 ± 0.07 . The resulting phase spectra measured for the all samples are shown in Fig. 1.

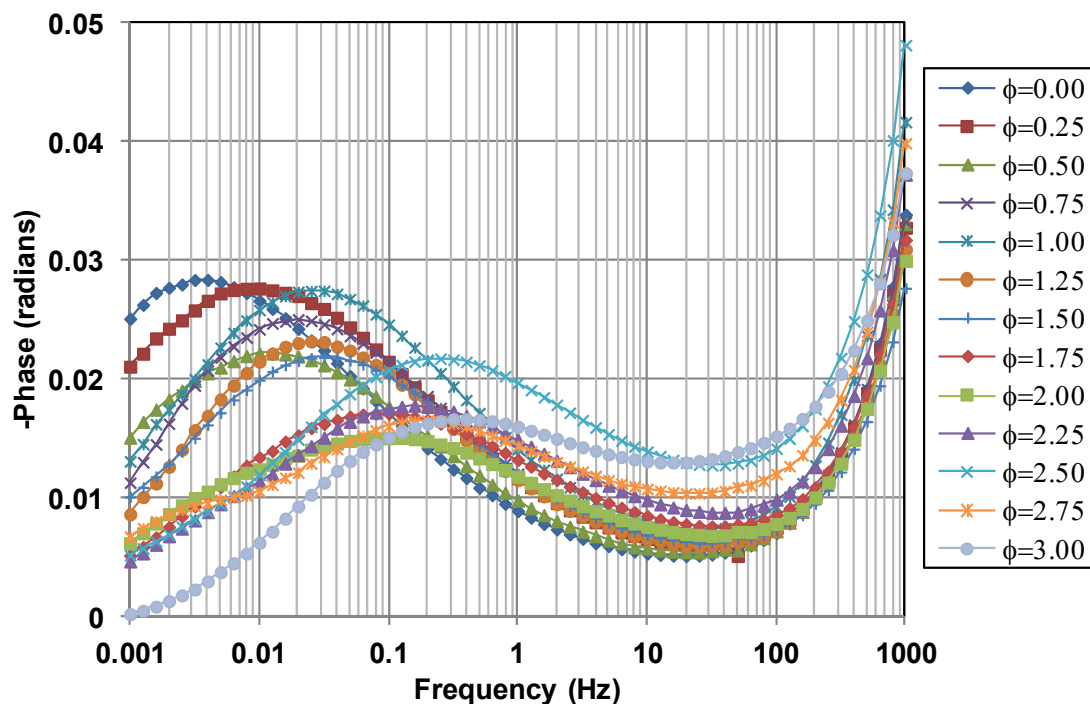


Fig. 1: SIP phase spectra measured on different sieved fractions.

To investigate any correlation between the electrical and hydraulic properties of the samples the SIP measurements were modelled using a Cole-Cole model (Cole and Cole 1941). Thus, for each sample, the complex conductivity representation:

$$\sigma^* = \sigma_o \left\{ 1 + m \left(\frac{(i\omega\tau)^c}{1 + (1-m)(i\omega\tau)^c} \right) \right\}$$

was used to fit the conductivity magnitude and phase in the frequency range 0.001-10 Hz. Such modelling shows that although there appears to be no clear variation of the Cole-Cole exponent c with the size of the sieved fraction, there is a systematic increase in the total chargeability, m , with increasing grain size (decreasing ϕ value). This latter result is consistent with that observed by Koch et al. (2012) for measurements on sieved sand fractions. The modelled relaxation time constant (τ) increases by two orders of magnitude between the smallest and largest sieved fractions.

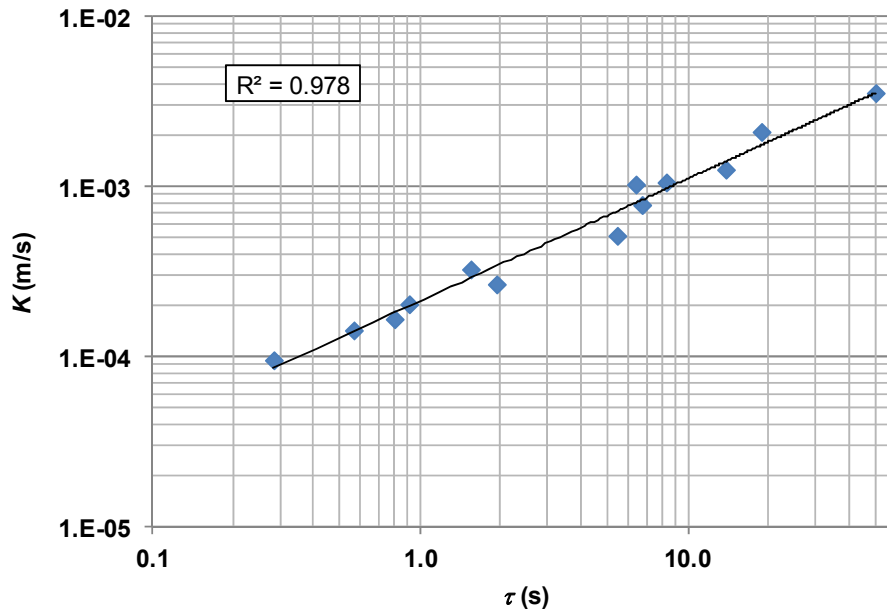


Fig. 2: Variation with of the measured hydraulic conductivity with relaxation time τ .

A plot of the measured hydraulic conductivity (K) against τ on a log-log scale is shown in Fig. 2 and demonstrates a strong correlation between the two parameters, reflecting the fact that both the SIP response and the hydraulic conductivity are controlled by the pore size and grain size structure. Assuming that polarization occurs within the Stern layer around grains, and based on the Kozeny-Carman equation, Koch et al. (2012) suggested that the permeability (k) can be related to τ by:

$$k = \frac{\tau D}{4n^2 F(F-1)^2}$$

where D is the diffusion coefficient of ionic species in the Stern layer, and n is the Archie's Law cementation exponent. Although previous results have suggested that this relationship underestimates the permeability by approximately an order of magnitude, the present measurements give a much closer agreement between predicted and measured permeability.

References

- Cole, K.S. and Cole, R.H., 1941. Dispersion and absorption in dielectrics. *J. Chem. Phys.*, 9, 341-351.
- Koch, K., Revil, A. and Holliger, K., 2012. Relating the permeability of quartz sands to their grain size and spectral induced polarization characteristics. *Geophys. J. Int.*, 190, 230-242.

Resistivity and SIP response of rocks during freezing and thawing

A. Kemna⁽¹⁾, M. Weigand⁽¹⁾ and E. Zimmermann⁽²⁾

(1) *Department of Geodynamics and Geophysics, University of Bonn, Germany*

(2) *Central Institute for Engineering, Electronics and Analytics, Electronic Systems (ZEA-2),
Forschungszentrum Jülich GmbH, Germany*

The use of electrical imaging methods for characterizing the frozen state of the subsurface requires the understanding of the low-frequency electrical soil/rock conduction and polarization properties as dependent on temperature in frozen and unfrozen regimes. While electrical resistivity tomography, measuring the quasi-static electrical conduction properties, is increasingly used in permafrost monitoring studies, relatively little attention has been paid so far to the measurement of electrical polarization properties for thermal state characterization. In particular, integrative models describing the low-frequency behaviour of both conduction and polarization properties below $T_0 = 0$ °C, where ice and water coexist in stable equilibrium, are still lacking.

We here present results from laboratory studies on sandstone and limestone samples with different pore size distributions, whose electrical conduction and polarization properties were measured in controlled freeze-thaw cycles (–30 to 10 °C) by means of impedance spectroscopy in the frequency range 1 mHz to 45 kHz. We used five different cylindrical samples, four sandstones and one limestone, of 10 cm length and 3 cm diameter. After saturating the samples with deionized water and waiting for chemical equilibrium, associated with some increase of pore water conductivity due to the dissolution of ions from the rock matrix, the samples were placed in a freezing chamber where they were cooled down from 10 to –20 °C by successively changing the temperature in steps between 0.2 and 1 °C; afterwards the samples were heated up again following the same procedure. After adjusting a new temperature, impedance measurements were only taken after thermal gradients in the sample had equilibrated, where waiting for two hours was found to be sufficient for the given size and thermal properties of the samples.

In Fig. 1, the spectral complex resistivity behaviour as a function of temperature for one of the sandstones, which was qualitatively observed for all sandstones, is shown. Resistivity magnitude varied only insignificantly with frequency below 1 kHz over the investigated temperature range, and thus the temperature dependence shown in Fig. 1a at 1 Hz is representative. The results reveal a distinct hysteretic behaviour, which is characterized by a critical transition of the sample at some temperature T_f during freezing, indicating abrupt ice crystallization in the pore space of the sample, and a gradually decreasing resistivity during thawing, suggesting continuous melting of the ice in the pores up to a temperature T_m . The observed resistivity hysteresis is qualitatively in agreement with the well-known hysteretic behaviour of other properties of porous media during freezing and thawing. Given the melting point depression of ice constrained in a pore according to the Gibbs-Thomson relationship, i.e., $T - T_m$ being inversely proportional to the pore size, the resistivity melting curve can be considered as reflecting the cumulative pore size distribution of the sample, similar to the concept of differential scanning calorimetry and NMR cryoporometry. Accordingly, the freezing curve clearly indicates that liquid water in the sample is supercooled down to the critical temperature T_f where sudden ice formation occurs.

The polarization properties likewise show a hysteretic behaviour as a function of temperature, which, however, is strongly frequency dependent. Inspecting the observed resistivity phase spectra, as exemplarily shown in Fig. 1b, one can identify the well-known relaxation of ice between 10^3 Hz and 10^5 Hz above –20 °C. The occurrence of this relaxation response during freezing and thawing is in correspondence with the above interpretation of the resistivity magnitude behaviour in terms of thermal state of the sample. In addition, polarization is observed in the lower frequency range, which in the unfrozen regime exhibits relatively weak frequency dependence between 1 Hz and 1 kHz. We attribute the response below 100 Hz to electrochemical polarization associated with electrical double layers (EDL) at the water-mineral interfaces. The observed phase

spectra suggest that upon ice crystallization this polarization mechanism partly breaks down, in particular at lowest frequencies representative of largest pores. This could be explained by ice formation in corresponding pores hindering the build-up of membrane polarization. However, water in smaller pores and films of premelted water around grains as well as ice nuclei could still maintain electrochemical polarization (in particular Stern layer polarization), potentially explaining the residual phase response with ongoing cooling.

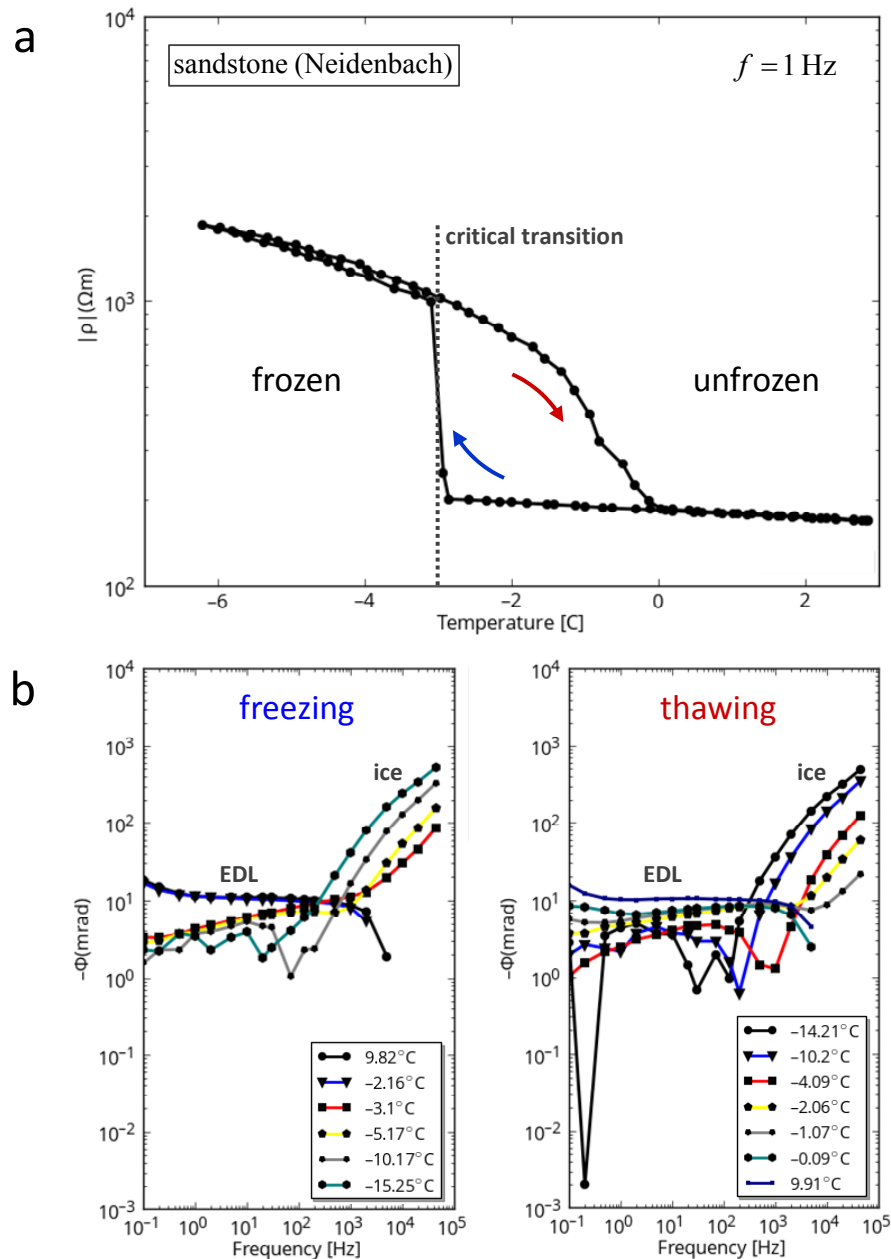


Fig. 1: Complex resistivity response measured on a sandstone sample during freezing and thawing. At each temperature step, measurements were taken after thermal equilibrium had re-established. a) Resistivity magnitude at 1 Hz as a function of temperature during freezing (bottom curve in hysteretic region) and thawing (top curve in hysteretic region). b) Resistivity phase spectra at selected temperatures during freezing (left) and thawing (right).

We conclude that low-frequency electrical properties measured in SIP offer direct access to the presence and amount of ice as well as liquid water (films) in frozen rocks. The hysteretic behaviour must be taken into account when electrical properties are, for example, to be used for monitoring seasonal temperature changes in permafrost environments. Studying the relationship between the critical temperature at which nucleation is triggered and the pore size distribution might provide improved insight into the mechanisms governing ice formation in porous rocks.

Experimental study of the complex electrical conductivity of Fontainebleau sandstones

P. Kessouri⁽¹⁾, W.F. Woodruff⁽¹⁾ and A. Revil^{(1),(2)}

(1) Colorado School of Mines, Dept. of Geophysics, Golden, CO, USA

(2) LGIT, UMR C559, Université de Savoie, 73376 Le-Bourget-du-lac Cedex, France

Fontainebleau sandstones possess remarkable properties that make them an interesting object to study. Indeed they are composed of pure silica grains (~ 99.8 %) and have a narrow grain size distribution (ranging from 150 to 300 μm with a mean grain size of 250 μm). Moreover, the silica grains can be more or less cemented by silica precipitation, so that the Fontainebleau sandstones have a large porosity spectra ranging from 3 to 30 %. Their study thus represents a good way to test the single influence of porosity in the complex electrical conductivity modelling and measurements.

A set of 67 Fontainebleau sandstones core samples has been studied in terms of complex electrical conductivities, surface conductivities but also porosities. To measure the surface conductivity, the DC electrical conductivity of the samples at 7 different water salinities (from $1.7 \cdot 10^{-3}$ to 18.7 S m^{-1}) was measured by a 2 electrodes device working at 4 kHz. The complex electrical conductivity was measured for a water salinity of $6.4 \cdot 10^{-2} \text{ S m}^{-1}$ using a 4 electrodes system linked with the ZEL-SIP04-V02 impedance meter working at frequencies ranging from 10^{-2} to 10^4 Hz. On this study we will only use the results at 0.1 Hz, this frequency having a good signal-to-noise ratio. The porosity was measured either using the formation factor and permeability measurements or using mercury intrusion measurements.

In Fig. 1, the intrinsic formation factor F ($F = a\phi^{-m}$ for a saturated medium with a porosity ϕ where a is the tortuosity factor and m is the cementation exponent) is compared to the apparent formation factor F_a ($F_a = \sigma_w / \sigma$ where σ_w represents the water electrical conductivity and σ is the electrical conductivity of the medium). For low water conductivities, until $1000 \mu\text{S cm}^{-1}$, there is a clear variation between the two formation factors. This variation shows the influence of the surface conductivity on the measurements. Until now, the surface conductivity of clay-free sandstones is generally neglected in the modelling. Taking into account these new data, the surface conductivity of clean sandstones needs to be taken into account, especially for low water conductivities, typically in fresh water aquifers contexts ($80 < \sigma_w < 1000 \mu\text{S cm}^{-1}$).

Moreover, the surface conductivity can give some information on the rock state properties. The bulk tortuosity α , defined as the intrinsic formation factor F multiplied by the sample porosity ϕ , is one of these properties. Indeed, for the Fontainebleau sandstones, a linear relationship exists between the log of the measured surface conductivities and the log of the bulk tortuosity (Fig. 2a). A similar relationship is observed between the measured quadrature conductivity and the bulk tortuosity (Fig. 2b). The same bulk tortuosity of the pore space can thus be used to evaluate the bulk and surface conduction processes. An interesting relation can also be found between the quadrature and the surface conductivity of the sandstones. These relationships are important because they can significantly improve the estimation of porosity, formation factor and salinity using IP measurements at only one water salinity.

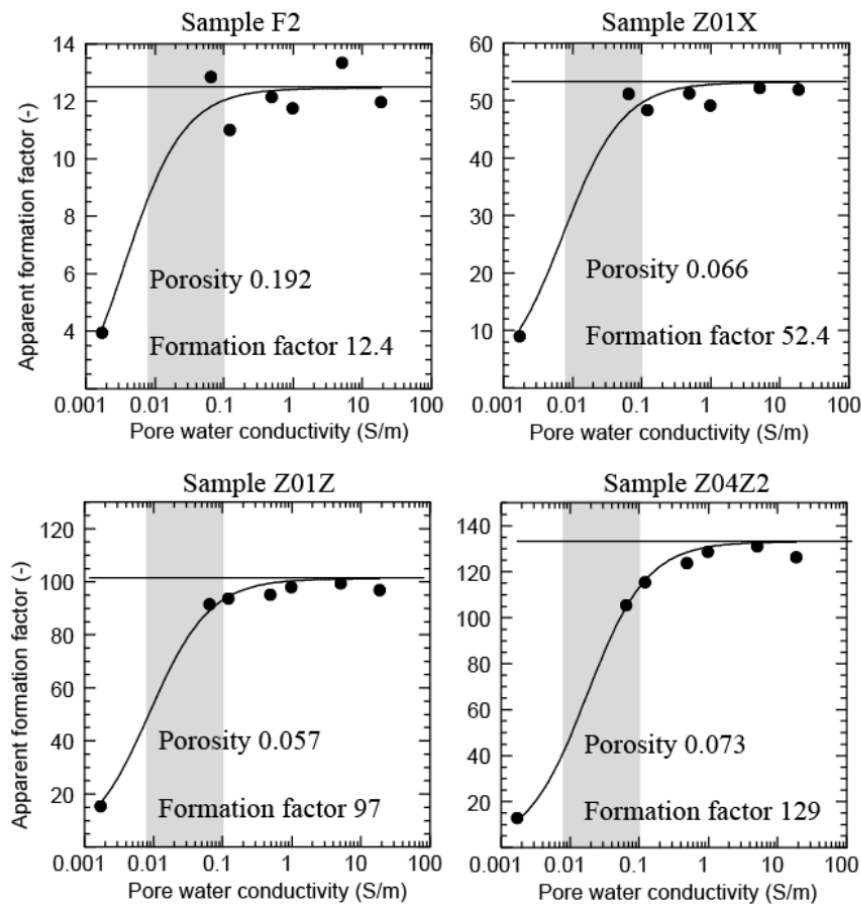


Fig. 1: Relationship between apparent formation factors F_a (defined as the ratio of the conductivity of the pore water by the sample conductivity) and intrinsic formation factors F ($F = a\phi^{-m}$ for a saturated medium with a porosity ϕ where a is the tortuosity factor and m is the cementation exponent). The horizontal line identifies the value of the intrinsic formation factor F while the continuous line identifies a fit with the equation $\sigma = \sigma_w/F_a + \sigma_s$ in terms of apparent formation factor. The grey areas correspond to typical conductivity values of fresh water aquifers (80 to 1000 $\mu\text{S cm}^{-1}$).

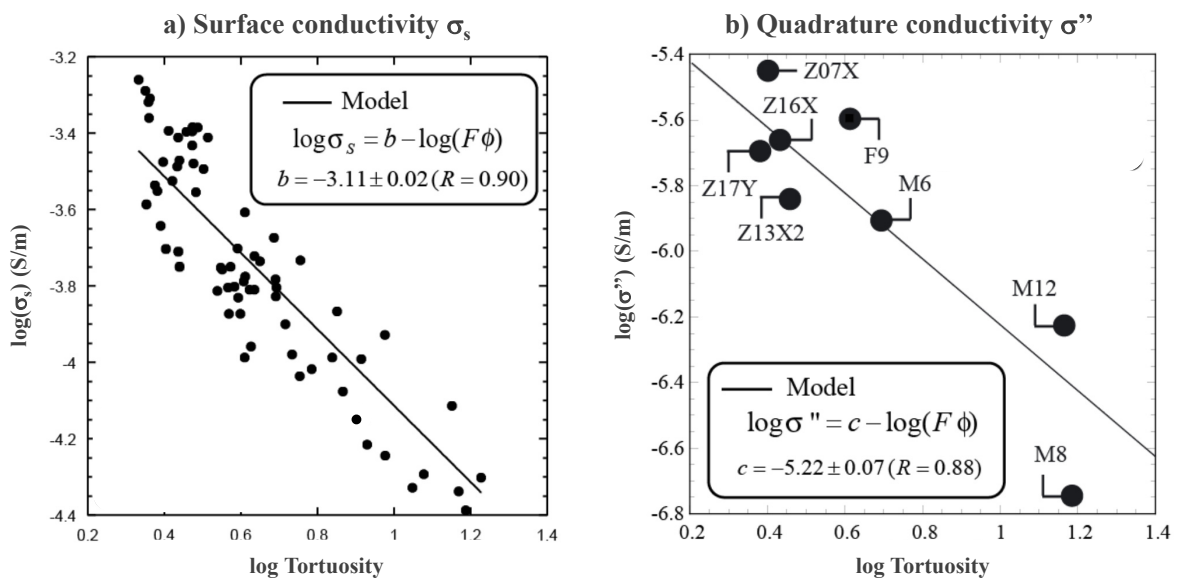


Fig. 2: a) Surface conductivity σ_s and b) Quadrature conductivity σ'' versus bulk tortuosity of the pore space ($\alpha = F\phi$ with F the formation factor and ϕ the sample porosity). The straight lines correspond to the best fit of the model equation.

Spectral induced polarization monitoring of CO₂ injection in saturated sands: laboratory experiment and modelling

T. Kremer^{(1),(4)}, M. Schmutz⁽²⁾, E. Keating⁽³⁾, P. Agrinier^{(1),(4)} and A. Maineult^{(1),(4)}

(1) *Institut de Physique du Globe de Paris, UMR CNRS 7154, France*

(2) *ENSEGID, EA4592 G&E, University of Bordeaux, France*

(3) *Earth and Environmental Sciences Division, Los Alamos National Laboratory, Los Alamos, New Mexico 87545, United States*

(4) *Centre de recherches sur le stockage géologique du CO₂ (IPGP / TOTAL / SCHLUMBERGER / ADEME), 1 rue Jussieu, 75238 PARIS cedex*

During the last decade, the interest of induced polarization methods for environmental studies has undoubtedly grown. Here, we present a set of laboratory experiments aimed at assessing the ability of spectral induced polarization (SIP) method to detect and monitor CO₂ transfers in the subsurface. The objectives were the quantification of the influence of various parameters on the SIP response, such as the water conductivity, the chemical reactivity of the solid and of the gas phases, and the injection rate. SIP measurements in the frequency range 50 mHz – 20 kHz were thus performed during gas (N₂ or CO₂) injections in a metric-scaled, cylindrical tank filled with unconsolidated granular material (quartz or carbonate sands) and fully saturated with water (Fig. 1).

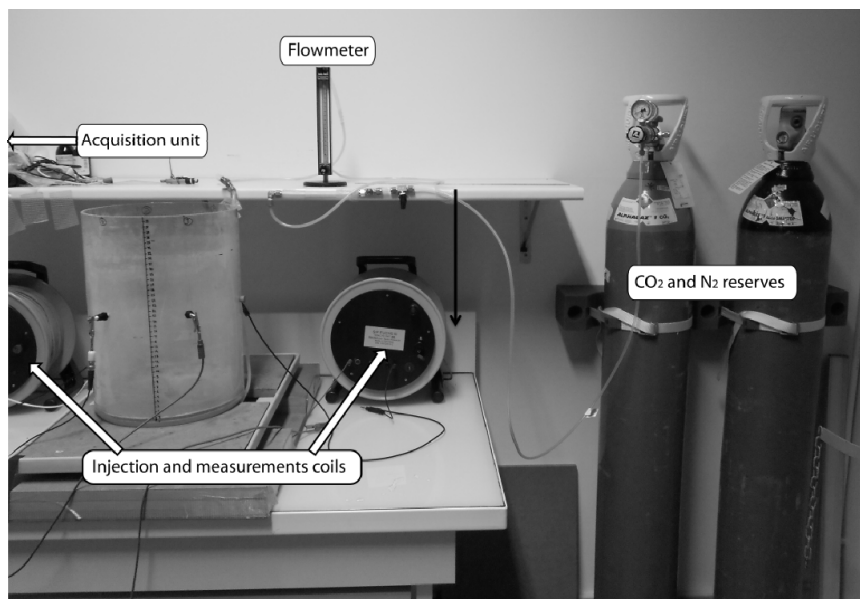


Fig. 1: Experimental set-up.

The system was most reactive to gas injection in the high frequency range (> 1 kHz). In quartz sand, the presence of gas in the medium tends to decrease the measured values of the phase angle. This effect becomes more important when increasing the injection rate, and thus the amount of gas trapped in the medium. The magnitude of this effect decreases when the water conductivity increases.

Dissolution processes (CO₂ in water and also solid matrix in the case of carbonated sand) were evidenced from chemical measurements (pH, conductivity and anionic concentrations). The increased ionic strength resulted in a decrease of the bulk resistivity and in an increase of the phase values at high frequency (Fig. 2). An interesting parameter is the ratio of the increase in phase to the decrease in resistivity. When dissolution processes are involved, this ratio increases strongly with the initial conductivity of the saturating fluid. Hence, in some cases the measured phase values still bring measurable information on the system evolution even if resistivity variations are very small.

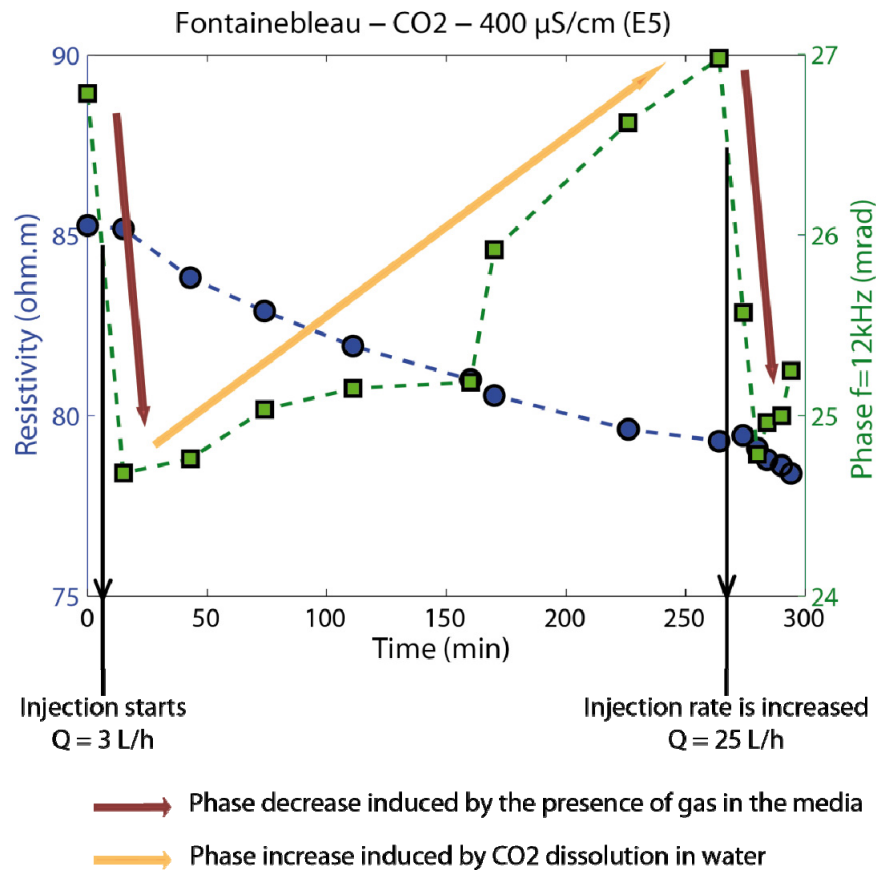


Fig. 2: Temporal evolution of the resistivity and the phase angle at the frequency 12 kHz for the experiment E5 (CO₂ injection in a Fontainebleau sand saturated with a 400 μS cm⁻¹ conductivity water). We can observe the effect of both gas invasion (red arrows – phase decrease) and CO₂ dissolution (yellow arrow – phase increase). Resistivity changes are less significant.

We were able to model these experiments using the numerical simulation code FEHM (Viswanathan et al. 2012), designed at the Los Alamos National Laboratory. Saturation evolution, CO₂ and carbonate dissolution, and dissolved species diffusion were described. We propose a theoretical framework to describe the high frequency behaviour of the SIP response in the high frequency range (100 Hz – 20 kHz). This theoretical model fits with the experimental data, and depends on the amount of ionic species present in the saturating water and the saturation state of the porous media.

References

Viswanathan, H., Dai, Z., Lopano, C., Keating, E., Hakala, J.A., Scheckel, K.G., Zheng, L., Guthrie, G.D. and Pawar, R., 2012. Developing a robust geochemical and reactive transport model to evaluate possible sources of arsenic at the CO₂ sequestration natural analog site in Chimayo, New Mexico. *Int. J. Greenhouse Gas Control*, 10, 199-214.

We gratefully acknowledge the support of the ADEME agency, Schlumberger and Total in this project and their permission to present this work. However, the views expressed here are those of the authors who are solely responsible for any errors.

Modelling the induced polarization of bentonite-sand mixturesP. Leroy⁽¹⁾, A. Ghorbani⁽²⁾, A. Revil^{(3),(4)}, P. Cosenza⁽⁵⁾ and G. Okay⁽⁶⁾

(1) D3E department, BRGM, Orléans, France

(2) Department of Mining and Metallurgical Engineering, Yazd University, Yazd, Iran

(3) Department of Geophysics, Colorado School of Mines, Golden, USA

(4) ISTerre, CNRS, UMR CNRS 5275, Université de Savoie, Le Bourget du Lac, France

(5) CNRS UMR 7285 IC2MP-HydrASA, University of Poitiers-ENSIP, Poitiers, France

(6) Department of Geomatics, Hacettepe University, Ankara, Turkey

Spectral induced polarization (SIP) has become an increasingly popular geophysical method for hydrogeological and environmental applications. These applications include for instance the non-intrusive characterization of the textural and interfacial physicochemical properties of bentonites used as permeability barriers in landfills or to store various types of contaminants including radioactive wastes. Bentonites are mainly constituted of smectites, which have very high specific surface areas (SSA) and cation exchange capacities (CEC). Therefore, these minerals have very high electromigration and polarization current densities responsible for very high in phase and quadrature conductivities, respectively. In addition, in diluted water, the diffuse layer of smectites occupies a large fraction of the pore space and may be therefore considered as part of the pore space.

In our approach (Okay et al. *subm.*), complex electrical conductivities of saturated unconsolidated bentonite and bentonite-sand mixtures are modeled at different salinities (NaCl) of the bulk pore water using a Donnan equilibrium model coupled to the revisited SIP model of Leroy and Revil (2009). Our complex surface conductivity model considers the DC contribution of the diffuse and Stern layers as well as the electrochemical polarization of the Stern layer coating the grains with different sizes. The macroscopic SIP model is based on the differential effective medium theory and considers the complex surface conductivity of the sand and smectite grains and the complex conductivity of the pore space. In our model, the diffuse layer of quartz sands occupies a small fraction of the pore space and is considered therefore as part of the surface of the grains.

Our SIP model predicts very well the low frequency (0.1 Hz – kHz) complex electrical conductivities of bentonite and bentonite-sand mixtures, except for very low frequencies (< 0.1 Hz) where membrane polarization may occur (Fig. 1). The in-phase conductivity of the sample with high clay content (20 % in volume) increases slowly with salinity because of the very high DC surface conductivity of smectite. The observed large increase of the in phase and quadrature conductivity of the samples with the clay content (1, 20 and 100 % in volume) is also predicted by our model. The quadrature conductivity of the samples with high clay content is fairly independent on the pore fluid salinity because it is strongly connected with the SSA, CEC and Stern layer of smectite (Fig. 1). The in-phase conductivity of the sample with low clay content (1 % in volume) increases quickly with the salinity because of its low DC surface conductivity. Its quadrature conductivity also increases quickly with salinity because of the formation of the Stern layer at the surface of quartz sand. Nevertheless, our SIP model cannot predict the quadrature conductivity spectra observed at very low frequencies ($< 10^{-1}$ Hz). The missing polarization mechanism may correspond to membrane polarization and there is an effort to be done to incorporate this contribution in a unified model.

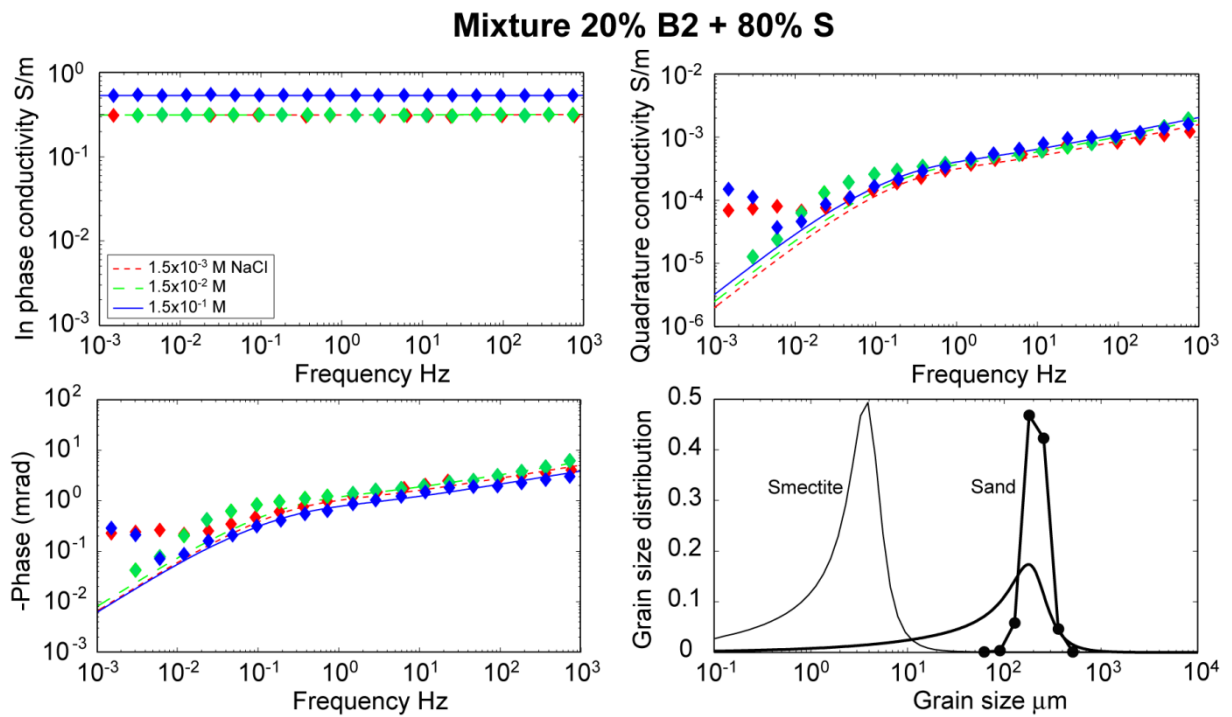


Fig. 1: Comparison between theory (lines) and experimental data (symbols) for bentonite-sand mixture (20 % clay content) at different pore water salinities (0.0015, 0.015, 0.15 M NaCl). The in-phase and quadrature conductivities of the sample are dominated by the diffusion of sodium counter-ions in the Stern and diffuse layers of smectite because of the very high SSA and CEC of this material.

References

- Leroy, P. and Revil, A., 2009. Spectral induced polarization of clays and clay-rocks. *J. Geophys. Res.*, 114, B10202.
- Okay, G., Leroy, P., Ghorbani, A., Cosenza, P., Camerlynck, C., Cabrera, J., Florsch, N. and Revil, A., 2013. Induced polarization of clay-sand mixtures. Experiments and modelling. *Submitted*.

Spectral induced polarization for monitoring electrokinetic remediation processes

M. Masi⁽¹⁾ and G. Losito⁽²⁾

(1) *University of Pisa, Department of Energy Engineering, Systems, Land and Construction (DESTEC), Italy*

(2) *University of Florence, Department of Civil and Environmental Engineering, Italy*

Electrokinetic remediation (EKR) is an emerging technology employed to extract heavy metals, radionuclides and organic compounds from saturated or unsaturated soils, sludge and sediments.

This technique relies on the application of a low-intensity electric field across electrode pairs placed on each side of the contaminated mass. The applied electric field induces the mobilisation of contaminants and water through the medium toward the electrodes due to three main transport mechanisms: electromigration, electroosmosis and electrophoresis. Electromigration is the transport of charged species through the pore solution towards the oppositely charged electrode, electroosmosis is the movement of pore fluid and electrophoresis is the transport of charged particles and colloids. Moreover, during the electrokinetic process, electrolysis reactions occur at the electrodes, producing oxygen gas and H⁺ ions at the anode and hydrogen gas and OH⁻ ions at the cathode. Water oxidation at the anode generates an acid front that migrates toward the cathode; conversely, water reduction at the cathode produces a base front migrating toward the anode. The pH profile across the porous medium significantly affects the efficiency of the remediation process. The advance of the acid front generally results into desorption and dissolution of metallic species, promoting their mobility. On the contrary, the advance of the base front typically has several negative effects such as adsorption and precipitation reactions that result in a decrease in the process efficiency. In some cases, the acid front may not be able to develop because of the high buffering capacity of the medium. Under this condition, it is necessary to use chemical reagents such as acids or chelants to control the pH to a desired level and achieve the solubilisation of contaminants.

Monitoring of electrokinetic processes both in laboratory and in field is usually conducted by means of point measurements and collecting samples from discrete locations. Geophysical methods can be very effective in obtaining high space and time resolution mapping for an adequate control of the electrokinetic processes. This study investigates the possibility of using geophysical methods to monitor electrokinetic remediation processes. Among the geophysical methods, the spectral induced polarization (SIP) technique has been selected because of its capability to provide qualitative and quantitative information about the physico-chemical characteristics of the porous medium.

Laboratory-scale electrokinetic remediation experiments were carried out on marine sediments contaminated by heavy metals, under different operating conditions. Four experiments (EXP1, EXP2, EXP3 and EXP4) were performed by changing the intensity of the applied electric field and the type of conditioning agent circulated within the system to enhance the extraction process. The experiments were conducted in a prismatic acrylic cell, consisting of four principal parts (Fig. 1): the sediment compartment, the electrode compartments, the electrolyte solution reservoirs and the power supply. Tap water was used as processing fluid in EXP1 and EXP2. To promote metal removal a 0.1 M solution of citric acid and 0.1M EDTA solution were used in EXP3 and EXP4, respectively. The applied voltage gradients were 50 V m⁻¹ (EXP1 and EXP3) and 80 V m⁻¹ (EXP2 and EXP4). The treatment duration was 10 days. At the end of each experiment, the material was sampled from five locations (S1 to S5) and analysed for pH and total metal content.

SIP measurements were performed on the sediments before and after the EKR treatments. Sediment samples were collected directly from the sampling locations S1 to S5 of the EKR cell. The measurements were performed on cylindrical sample holders, having a length of 200 mm and an inner diameter of 36 mm. They were made of acrylic, which produces no spurious phase response. The current electrodes were stainless steel plates. The potential electrodes were circular

silver wires placed inside grooves to keep them outside the current path, in order to reduce erroneous phase shifts due to their polarization. The samples were manually prepared and compacted, resulting in slight differences in porosity and water saturation which influenced the SIP response. Three repeated measurements were taken on each sample in the frequency range 10^{-3} - 10^3 Hz, each time by performing a new sample preparation. The mean resistivity and phase spectra were calculated. To quantitatively compare the SIP responses of the sediment samples, the Debye decomposition method was used to fit the data. Three parameters were determined for each spectrum: DC resistivity (ρ_0), total chargeability (m) and mean relaxation time (τ). By analysing the data, a linear relationship between the sample total chargeability (m) and pH was found (Fig. 2). This relation can be explained taking into account the electrical double layer (EDL) polarization mechanism. According to the EDL theory, a pH variation is responsible for a change in the zeta potential of the sediment, which is proportional to the amount of electric charge at the EDL. A variation of chargeability is thus directly associated with an alteration of electric charge at the EDL. Such a relationship has potential value for the interpretation of SIP data, encouraging the field-scale engineering implementation of the SIP method for monitoring EKR processes.

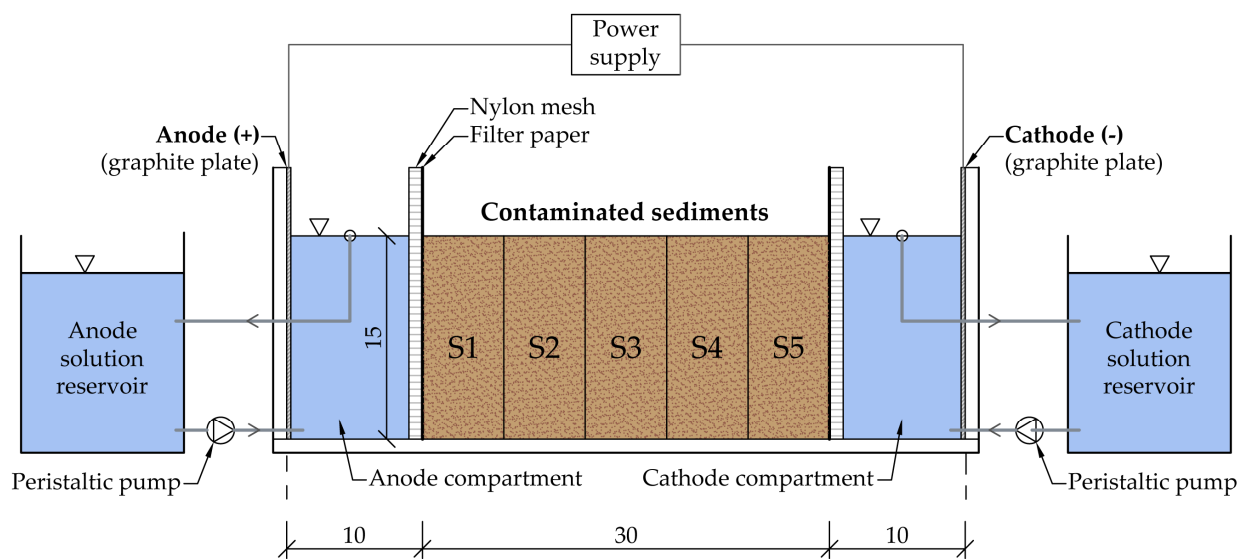


Fig. 1: Schematic diagram of the experimental electrokinetic cell. The material is divided into five equal sections (sampling locations) from S1 to S5. (Dimensions are in cm).

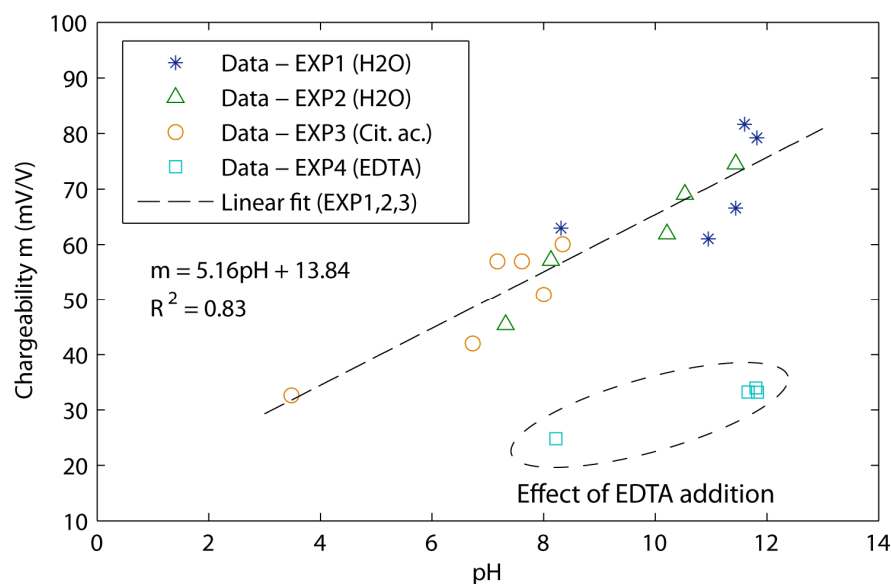


Fig. 2: Variation of chargeability with pH. Symbols show measured data. The line is determined by linear regression. The quality of fitting is indicated by the coefficient of determination R^2 .

Estimation of the van Genuchten-Mualem parameter α and the saturated hydraulic conductivity from SIP measurements

S. Nordsiek⁽¹⁾, A. Hördt⁽¹⁾, E. Diamantopoulos⁽²⁾ and W. Durner⁽²⁾

(1) TU Braunschweig, Institute of Geophysics and xtraterrestrial Physics, Germany

(2) TU Braunschweig, Institute of Geoecology, Germany

The application of hydrological methods to determine soil hydraulic properties can be time-consuming and may become more efficient when supported by geophysical methods. Due to the dependence of the complex electrical resistivity on the pore fluid, the porosity, the size of pores and grains, respectively, and the interface between the pore fluid and the matrix, SIP might be suitable to support the hydrological investigations (e.g. Hördt et al. 2009; Breede et al. 2011). To identify relationships between complex geoelectrical parameters derived from SIP spectra and soil hydraulic properties, we performed SIP and hydrological investigations in the laboratory on the same samples, containing different unconsolidated sediments, covering a wide range of texture classes. The so-called van Genuchten-Mualem model, which was suggested by van Genuchten (1980) based on a model by Mualem (1976), is a widespread approach in soil physics to describe the hydraulic conductivity:

$$K(S_e) = K_s S_e^l \left(1 - \left(1 - S_e^{1/m} \right)^m \right)^2$$

as a function of the effective saturation:

$$S_e(h) = \left(1 + \alpha |h|^n \right)^{-m}$$

with the pressure head h , the saturated hydraulic conductivity K_s and the empirical parameters α , l , n , and $m = 1 - 1/n$. We apply this model to interpret the results of hydrological laboratory investigations, which we performed using the multi-step outflow method and the evaporation method with the HYPROP© device (UMS GmbH, Munich), respectively. Detailed descriptions of these hydrological methods can be found e.g. in Breede et al. (2011) and Peters and Durner (2008).

For the SIP measurements, we studied the frequency range between 10 mHz and 100 Hz with a VMP 3 impedance spectrometer (Princeton Applied Research). The SIP spectra were evaluated with the Debye decomposition approach, which was suggested by Nordsiek and Weller (2008) to derive characteristic parameters like the mean relaxation time τ_{mean} , the normalized total chargeability m_n , and the non-uniformity parameter U_τ from the measured SIP spectra.

We considered eight samples of unconsolidated sediments. The set of investigated material covers a variety of different grain sizes. It includes fine-textured soil samples (GGL, WFB, VRD) as well as sandy soil samples (RBE, RBC, STO, SSU) and a sample of pure medium and coarse sand (LAB). All samples were saturated with calcium chloride solutions of different ionic strengths, ranging from 0.001 to 0.02 mol per litre.

We merged the results of SIP measurements at different ionic strengths of the saturating fluid and compared the SIP parameters with the hydrological van Genuchten-Mualem parameters. We found a strong correlation with a correlation coefficient of $R = -0.76$ between m_n and α from the van Genuchten-Mualem model. After reconsideration of the measured data and exclusion of two samples that might have been affected by equilibration processes after saturation, we formulated the empirical relationship:

$$\alpha_{SIP} = 1.69 \cdot 10^{-2} m_n^{-0.95}$$

with α_{SIP} in cm^{-1} and m_n in mS m^{-1} . The correlation coefficient is $R = 0.91$ and the adjusted coefficient of determination is $R_{adj}^2 = 0.81$. In Fig. 1 (left), we show the estimated parameter α_{SIP}

and the parameter α_{MSO} resulting from the hydrological investigations.

Another relationship was observed for the saturated hydraulic conductivity and the normalized chargeability. Here, we found the power law:

$$K_{s\ SIP} = 6.35 \cdot 10^{-11} m_n^{-1.60} \rho_0^{-1} \sigma_w^{-1}$$

with $R = 0.87$ and $R_{adj}^2 = 0.74$ for the estimation of the saturated hydraulic conductivity $K_{s\ SIP}$ (in $m\ s^{-1}$) from the normalized chargeability m_n (in $S\ m^{-1}$), the DC resistivity ρ_0 (in $\Omega\ m$), and the conductivity of the saturating fluid σ_w (in $S\ m^{-1}$). In Fig. 1 (right), we display the estimated hydraulic conductivity and the measured hydraulic conductivity $K_{s\ MSO}$.

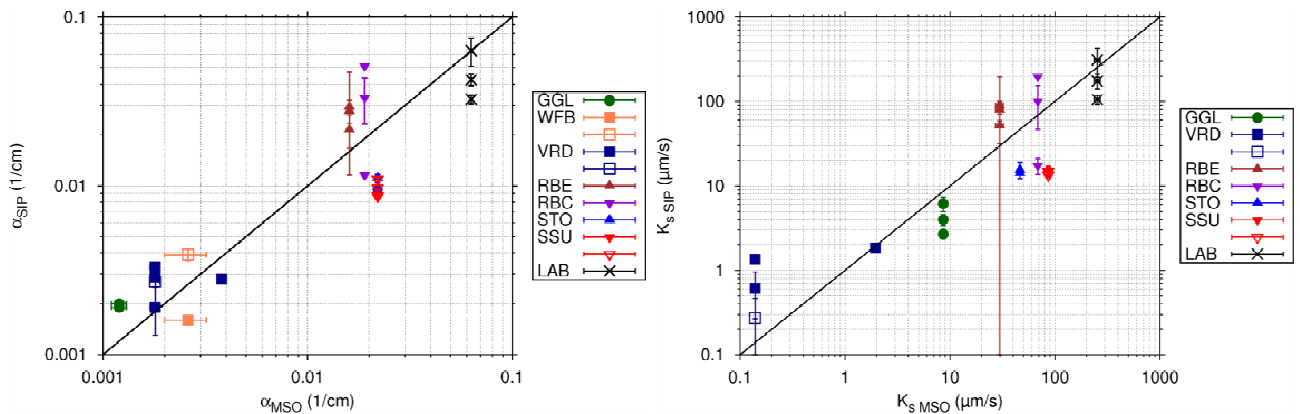


Fig. 1: Estimation of the van Genuchten-Mualem parameter α (left) and estimation of the saturated hydraulic conductivity (right) with parameters resulting from SIP measurements. The lines indicate identity between the measured values and the estimated values (Nordsiek et al. *subm.*).

Acknowledgements

We thank Ines Andrä, Sabine Mathesius, Katharina Bairlein, and Thomas Zimny (all TU Braunschweig) for providing and preparing the soil samples. This work was part of the project HO 1506/17-1 supported by the German Research Foundation (DFG).

References

- Breede, K., Kemna, A., Esser, O., Zimmermann, E., Vereecken, H. and Huisman, J. A., 2011. Joint measurement setup for determining spectral induced polarization and soil hydraulic properties. *Vadose Zone J.*, 10, 716-726.
- Hördt, A., Blaschek, R., Binot, F., Druiventak, A., Kemna, A., Kreye, P. and Zisser, N., 2009. Case histories of hydraulic conductivity estimation with induced polarization at the field scale. *Near Surface Geophys.*, 7, 529-545.
- Mualem, Y., 1976. A new model of predicting the hydraulic conductivity of unsaturated porous media. *Water Resources Res.*, 12, 513-522.
- Nordsiek, S. and Weller, A., 2008. A new approach to fitting induced-polarization spectra. *Geophysics*, 73, F235-F245.
- Nordsiek, S., Diamantopoulos, E., Hördt, A. and Durner, W. Relationships between hydrological parameters and induced polarization spectra of soil samples. *Submitted*.
- Peters, A. and Durner, W., 2008. Simplified evaporation method for determining soil hydraulic properties. *J. Hydrol.*, 356, 147-162.
- van Genuchten, M.T., 1980. A closed-form equation for predicting the hydraulic conductivity of saturated soils. *Soil Sci. Soc. Am. J.*, 44, 892-898.

Electrochemical modelling of the SIP response to oxidation of disseminated metallic particles

E. Placencia-Gómez⁽¹⁾ and L. Slater⁽²⁾

(1) *Aalto University, Finland School of Engineering, Department of Civil and Environmental Engineering, FI-00076 Aalto, Finland*

(2) *Rutgers University, Department of Earth & Environmental Sciences, Newark, New Jersey. U.S*

We investigated the SIP response of, and performed electrochemical modelling on, disseminated pyrite and pyrrhotite particles in sand, and mine waste material (tailings), in contact with electrolytic solutions composed of both inactive (non-oxidizing) and active (oxidizing) ions. The electrochemical model describes reasonably well the SIP response, and suggests that the activation of charge transfer reactions described by the corresponding model parameters can be used to evaluate the oxidation-diagnostic potential of the method.

Environmental relevance

The presence of metallic particles like sulphides, e.g., pyrite [Fe₂S] and pyrrhotite [Fe_{1-x}S], in granular media, constitutes a source of contamination to the soils, surface and ground waters which can affect some human activities and drinking water supplies. When these metallic particles enter in contact with oxidizing agents in conjunction with water, i.e., atmospheric oxygen (O₂) or dissolved in the pore water (DO), or with ferric iron (Fe³⁺) ions in solution, they tend to be dissolved by means of oxidative-weathering mechanisms driven by electrochemical cathodic (reduction) and anodic (oxidation) reactions. This results in the release of ferrous iron (Fe²⁺), sulphate (SO₄²⁻) and hydrogen (H⁺) ions to the pore-water. This acid metal-sulphate rich pore water forms a leachate which is transported down hydraulic gradient to impact water sources. The generation of such acid metal-rich contaminated plumes is documented to occur in mine waste dumps such as tailings impoundments and rock mine piles over the time of mining activities and is commonly termed acid mine drainage (AMD).

Materials and methods

Our study focused on investigating the SIP response and performing electrochemical modelling using the Wong (1979) model for (1) artificial sulphide-sand mixtures composed of disseminated pyrite and pyrrhotite particles, respectively, and (2) mine waste material (tailings) rich in pyrrhotite and pyrite collected from the Haveri Au-Cu mine tailings impoundment in Finland, exposed to oxidative-weathering conditions in laboratory columns. In the first case, using artificial sulphide-sand mixtures, the metal sulphides were subjected to oxidation promoted by O₂, both DO and atmospheric, and continuously monitored with SIP measurements. In the second case, tailings were subjected to alternating non-oxidizing (inactive) and oxidizing (active) ions in solution by saturating the pore space with CaCl₂ (inactive ions), FeSO₄ (active-inactive ions) and FeCl₃ (active-inactive ions) solutions.

The oxidation extent of metallic sulphides is deduced from the model parameters which contain information related to the charge transfer mechanisms, i.e., the oxidation-reduction reactions on the metal-electrolyte interface. The associated SIP signal due to the EDL polarization resulting from the type of ions in the electrolyte is analyzed here.

Results

The electrochemical model describes reasonably well the SIP response in both artificial and tailings material samples, and suggests that the activation of charge transfer reactions inferred by the model parameters can be used to diagnose the oxidation state of the system. Chemical analysis results on pore-water samples from artificial sulphide-sand mixtures showed that the greatest release of total iron (Fe²⁺ + Fe³⁺) associated with the oxidation extent of metallic particles occurred during atmospheric O₂ conditions. The SIP response to the atmospheric oxidation conditions resulted in depletion decrease of the phase angle (φ) (≈ 20 mrad) and imaginary conductivity (σ''),

along with a broader relaxation spectrum similar to a Warburg mechanism as suggested by Wong (1979); the latter is more evident in the case of pyrrhotite than pyrite minerals (Fig. 1). The sensitivity of the model parameters to the charge-transfer associated with the oxidation-reduction chemical reactions at the metal-electrolyte interface, such as the equilibrium exchange current density (i_0) and current reaction parameters (α) and (β), is consistent with the associated oxidation conditions promoted governing the changes in the modelled SIP spectra. The model suggests an increase of α , β and i_0 with an increase in the total iron released, defining SIP spectra consistent with the measured data following an increase in the oxidative-weathering (dissolution) on the metallic sulphides.

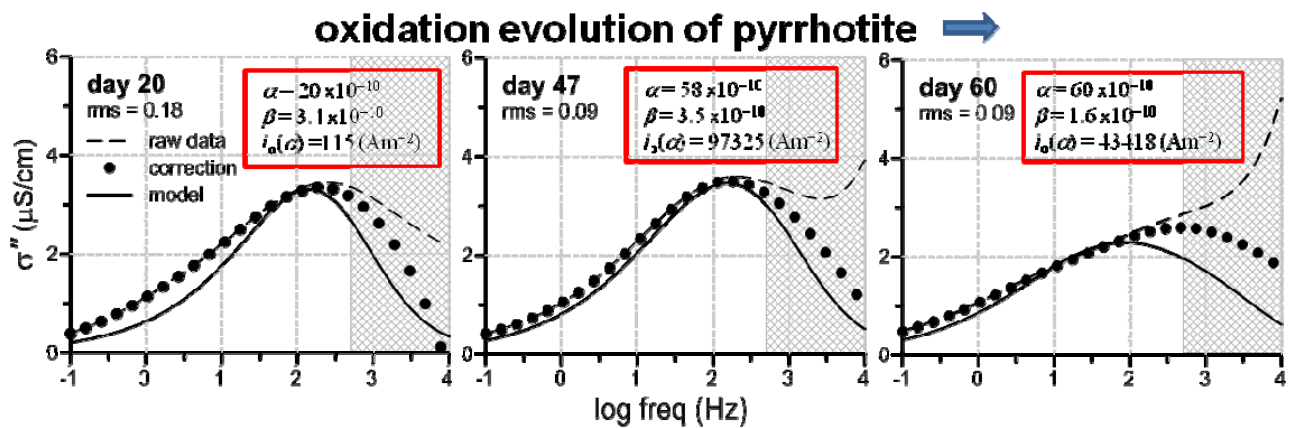


Fig. 1. Imaginary conductivity (σ'') spectra associated with the oxidation evolution of pyrrhotite on day 20 during DO oxidations conditions, and day 47 and day 60 during atmospheric oxidations conditions.

The SIP response of tailings due to inactive and active (ions) electrolytes filling the pore space is a reduction of φ with an increase in the total Fe released as an oxidation by-product. Both σ' and σ'' increases with the total Fe released. However, the shape and magnitude of the measured φ and σ'' spectra appear to be determined by the *in-situ* oxidation conditions. In summary, the electrochemical modelling seems to be consistent with the *in-situ* oxidation of tailings in most of cases.

Reference

Wong, J., 1979. An electrochemical model of the induced-polarization phenomenon in disseminated sulfide ores. *Geophysics*, 44, 1245-1265.

**POLARIS: a model to understand and interpret
spectral induced polarization data in Earth sciences**

A. Revil^{(1),(2)}

(1) *Colorado School of Mines, Golden, CO. USA*

(2) *CNRS, ISTERRE, Grenoble, France*

A model combining low frequency complex conductivity and high frequency permittivity is developed in the frequency range from 1 mHz to 1 GHz. The low frequency conductivity depends on pore water and surface conductivities. Surface conductivity is controlled by the electrical diffuse layer, the outer component of the electrical double layer coating the surface of the minerals. The frequency dependence of the effective quadrature conductivity shows three domains. Below a critical frequency f_p that depends on the dynamic pore throat size, the quadrature conductivity is frequency dependent. Between f_p and a second critical frequency f_d , the quadrature conductivity is generally well described by a plateau when clay minerals are present in the material. Clay-free porous materials with a narrow grain size distribution are described by a Cole-Cole model. The characteristic frequency f_d controls the transition between double layer polarization and the effect of the high frequency permittivity of the material. The Maxwell-Wagner polarization is found to be relatively negligible. For a broad range of frequencies below 1 MHz, the effective permittivity exhibits a strong dependence with the cation exchange capacity and the specific surface area. At high frequency, above the critical frequency f_d , the effective permittivity reaches a high-frequency asymptotic limit that is controlled by the two Archie's exponents m and n like the low-frequency electrical conductivity. The unified model is compared with various datasets from the literature and is able to explain fairly well a broad number of observations with a very small number of textural and electrochemical parameters. I will discuss also the effect of pore size on the distribution of the relaxation times and the relationship between the quadrature conductivity and the surface conductivity.

Using SIP as a tool for identifying inorganic cations in a variably saturated soil

I. Shefer⁽¹⁾, M. Weinstein⁽¹⁾ and A. Furman⁽¹⁾.

(1) Civil and Environmental Engineering, Technion – Israel Institute of Technology

In this work the potential of SIP as a tool for identifying and distinguishing between different inorganic cations in the soil's adsorbed phase is experimentally tested. A red sandy loam ('Hamra') had undergone five types of treatments with particular brine solutions: sodium, calcium, magnesium, potassium and ammonium chlorides. In order to achieve near homo-ionic conditions for each treatment, the soils were prewashed with the proper concentrated brine. The soil in each treatment was washed in the ratio of 1:2 soil to solution weight, seven times with descending concentrations until reaching salinity in the same order of magnitude as tap water ($\sim 1 \text{ mS cm}^{-1}$). Samples of the washing solutions were chemically tested to make sure the dominant cation is the one we are interested in. Following drying of the soils, 10 % (by weight) distilled water were added, mixed, and packed in sealed glass boxes (five replicates each). The electrical SIP measurements were taken five days after packing and complementary chemical measurements were conducted to measure the adsorbed and the solution's cations composition.

Preliminary results of the electrical SIP measurements are presented in Fig. 1, for the real and the imaginary part of the complex conductivity.

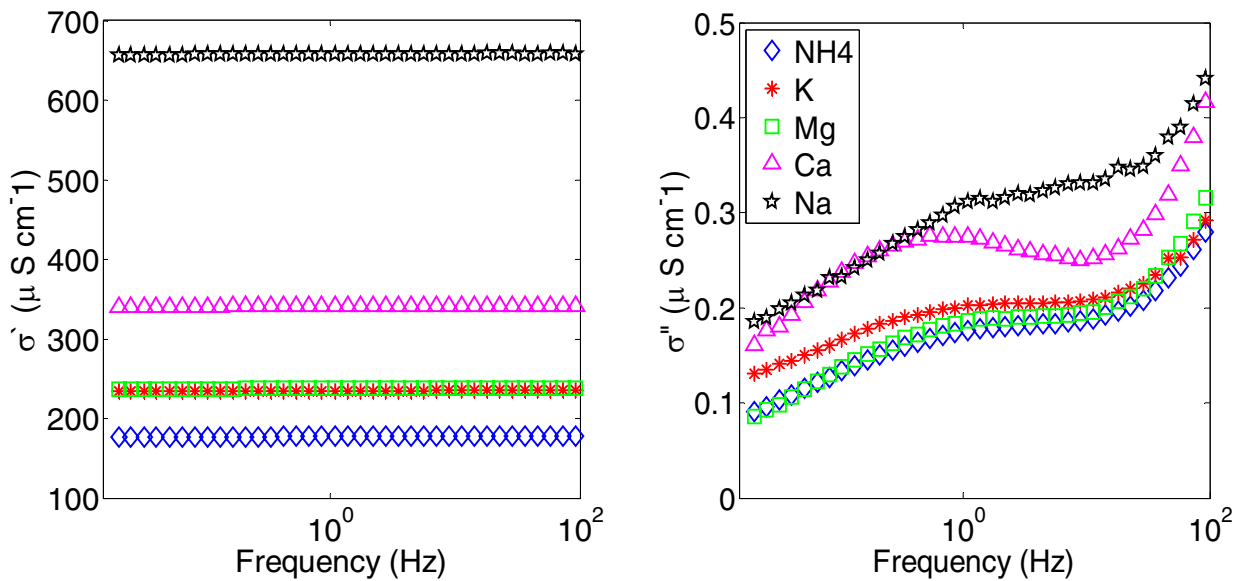


Fig. 1: mean values of the real part complex conductivity (left) and mean values of the imaginary conductivity (right) for the different treatments as a function of frequency. Error bars of the standard deviation are the same order of magnitude as the curves markers, therefore not presented.

A clear distinction can be made between the sodium treatment, the calcium treatment and the other three cations (K, Mg, and Na) by looking at the imaginary conductivity values. The magnesium's lower polarization effect compared to the calcium effect is somewhat surprising due to its lower adsorption selectivity to the solid surface (weaker binding) that allows greater mobility at the EDL. Moreover, its SIP signature greatly resembles the potassium's behaviour. The sodium's signature, though a bit noisy, has a very broad σ'' signature, while the calcium treated soil has clearer relaxation time. Although K and NH_4 are monovalent ions, they create strong bindings with the mineral surface which decreases their mobility and by that, apparently, their polarization decreases. As can be seen from the real part, Fig. 1 (left), the sodium's conductivity is prominently higher from the other treatments. This is a result of the difficulty to dry the sodium treated soil without losing the material. Nonetheless, the sodium's high salinity did not diminish its polarization effect as seen from Fig. 1 (right).

The electrical measurements results were fitted to a double Cole-Cole model (with the method presented by Chen et al. (2008)). The relaxation time parameter τ_1 (s) is depicted in Table 1. As prominent from this table, the calcium treatment relaxation time is longest, corresponding to its stronger surface interactions, while the sodium on the other hand, has the shortest time constant. Potassium, ammonium and magnesium have similar time constants. These time constants match the apparent peak frequencies obtained from Fig. 1 (left), with Na as an exception. Combining these constants with the σ' signatures of the different treatments enables the characterization of each cation's effect.

	Ca	K	NH ₄	Mg	Na
τ_1 (s)	0.369	0.212	0.193	0.1923	0.046




Table 1: relaxation time constants of the different treated soils.

This work emphasises the practical potential of SIP to identify dominant species, with environmental and agricultural importance, in the vadose zone.

Reference

Chen, J., Kemna, A. and Hubbard, S., 2008. A comparison between Gauss-Newton and Markov-chain Monte Carlo-based methods for inverting spectral induced-polarization data for Cole-Cole parameters. *Geophysics*, 73, F247-F259.

**The effect of free-phase NAPL
on the spectral induced polarization signature of variably saturated soil**

I. Shefer⁽¹⁾, N. Schwartz⁽¹⁾, L. Fel⁽¹⁾ and A. Furman⁽¹⁾

(1) Civil and Environmental Engineering, Technion – Israel Institute of Technology

The SIP signature of an unsaturated soil contaminated with a free-phase non-aqueous phase liquid (NAPL), decane, was experimentally investigated. Using an accurate SIP measurement system, the soil's complex electrical conductivity was measured for two treatments: clean soil and decane contaminated soil. The water content of the two treatments was nearly the same, while for the contaminated treatment decane was added and mixed to the soil, thus replacing air and creating a four-phase system. This procedure was used to isolate the effect of the free phase NAPL from other related processes such as cation exchange processes. Complementary chemical analyses were conducted, alongside temporal measurements of the electrical response of the different treatments.

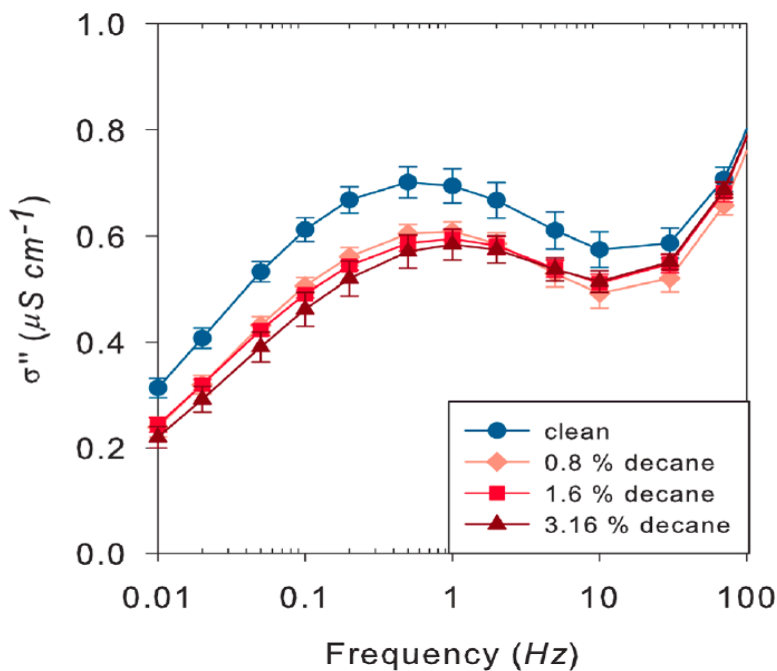


Fig. 1: The imaginary part of the complex conductivity for clean and decane contaminated are treatments. The error bars are the standard deviation values of replicates at each treatment.

The results show a clear decrease in the imaginary part of the complex conductivity for the decane contaminated soil. Moreover, a shift (reduction) of the relaxation frequency was observed for the contaminated soil (see Fig. 1). Furthermore, the amount of added decane virtually did not change the effect on the soil's polarization. These results are attributed to the membrane polarization mechanism, and specifically to its geometrical aspects. Chemical evidences support this argument and assure that the alternative mechanism of Stern layer polarization cannot explain our observations. Since no change in the solutions major ion composition was observed, we concluded that no ion exchange processes took place and there was no change in the Stern layer ion composition. Clearly, there was no change in the grain size distribution as the same soil was used for both treatments. Hence, the Stern layer model that depends primarily on the chemical composition of the Stern layer and on grain size distribution could not explain our results. We suggest that the addition of decane to the unsaturated porous media changes the distribution of liquid phase in the pore scale, thus affecting membrane polarization through its pore-scale geometrical component (while its chemical component is not being affected). Figure 2 depicts a solution of the

Young-Laplace equation for the interfaces created in our four-phase system, and shows a clear geometrical influence as a result of the decane addition. Moreover, once the addition of the free-phase fluid alters the geometrical distribution of the water in the pore throats, a supplementary amount does not significantly alter this distribution. Furthermore, we associate the time required for this liquid phase arrangement with the temporal changes of the soil's electrical signature. A clearer understanding of the SIP signature for soils contaminated with free-phase organic compounds can be achieved with this study's findings.

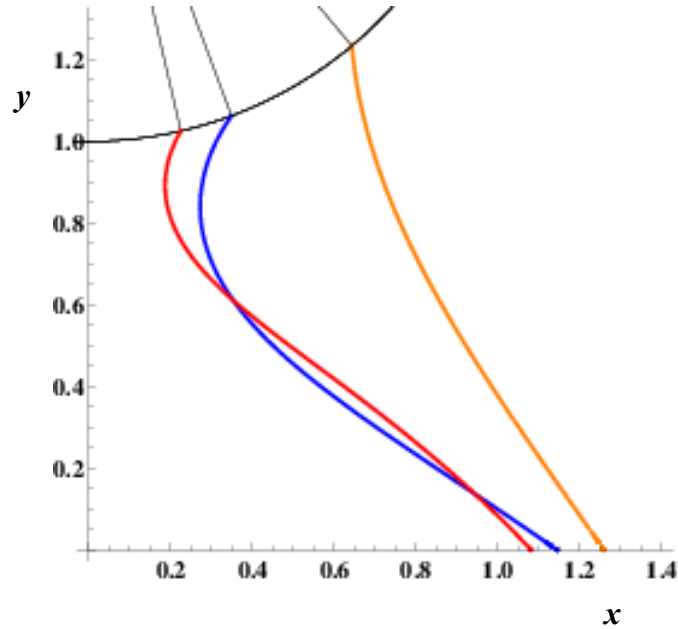


Fig. 2: Solution of the Young-Laplace equation for the described multiphase system.
Blue: the clean soil- water air interface; red: the water decane interface; orange: the decane-air interface.

Temperature-dependence of broadband complex electrical conductivity in unconsolidated porous media with variable clay content

A. Treichel⁽¹⁾, A. Binley⁽²⁾, A. Kemna⁽³⁾, O. Esser⁽¹⁾, E. Zimmermann⁽⁴⁾,
H. Vereecken⁽¹⁾ and J.A. Huisman⁽¹⁾

(1) *Institute for Bio- and Geosciences (IBG 3 – Agrosphere), Forschungszentrum Jülich GmbH, Germany*

(2) *Lancaster Environment Centre, Lancaster University, United Kingdom*

(3) *Department of Geodynamics and Geophysics, University of Bonn, Germany*

(4) *Central Institute of Engineering, Electronics and Analytics (Electronic Systems - ZEA 2), Forschungszentrum Jülich GmbH, Germany*

The complex electrical conductivity of porous media depends on temperature because the mobility of ions increases with increasing temperature. Although this dependence has long been recognized, temperature differences are not yet commonly considered in the interpretation of the complex electrical conductivity. Physically, it is not yet clear whether the temperature dependence of the real and imaginary part of the electrical conductivity is necessarily similar. The real part of the electrical conductivity is mainly determined by ions that can freely move in the bulk solution of the porous medium. Therefore, the temperature dependence of the real part of the electrical conductivity is expected to be similar to that of pure ionic solutions in the case of unconsolidated porous media. The imaginary part is determined by polarisation processes in the pore space, which are assumed to occur in the electrical double layer (EDL) at the mineral-electrolyte interface. This EDL can be separated in a diffuse layer with ionic mobilities similar to the bulk solution, and the Stern layer in which ions are tightly associated with the mineral surface and are typically assumed to have a reduced mobility. Depending on the dominant source of polarization and the associated ionic mobilities, the temperature dependence of the imaginary part of the electrical conductivity may be different. Within this context, the aim of this study is to investigate the temperature dependence of the complex electrical conductivity of unconsolidated porous media with varying amounts of clay in order to better understand polarization mechanisms in soils.

The complex electrical conductivity was determined in the frequency range between 1 mHz and 1000 Hz using spectral induced polarization (SIP). The temperature of the samples was varied from 5 to 25 °C. Two sample types are considered in this study. First, we obtained sample material from a heterogeneous aquifer at the Krauthausen test site. This aquifer mainly consists of sand and coarse gravel with a variable amount of clay. These samples were saturated with a CaCl₂ solution, because Ca²⁺ is the dominant cation at the Krauthausen test site. Second, we analyzed artificial sand-clay mixtures with variable amounts of Montmorillonite clay. These samples were saturated with NaCl solution because several experimental and modelling studies have previously used this type of solution. The measured complex electrical conductivity was first normalized to 25 °C for each frequency, and then the linear slope of the increase in real and imaginary part of the electrical conductivity was determined to obtain the frequency-dependent temperature sensitivity of the complex electrical conductivity.

The real part of the electrical conductivity showed the expected 2 % change per degree K for the artificial sand-clay mixtures (Fig. 1). The temperature dependence of the imaginary part of the electrical conductivity also varied around 2 % change per degree K, but consistent deviations were observed for different measurement frequencies and clay contents. The phase showed almost no change with temperature, but the same variations with frequency were observed as for the imaginary part of the electrical conductivity. In the remainder of this study, we prefer to interpret the phase of the complex electrical conductivity because it is less affected by errors in the temperature measurements. The presence of clay resulted in a measurable decrease in the temperature dependence of the phase of the electrical conductivity in case of the sand-clay mixture.

The samples from the Krauthausen test site also showed a measurable decrease in the temperature sensitivity of the phase (Fig. 2). No strong correlation with clay content was found

here, because the higher clay content in the top of the aquifer was not associated with a decreased temperature sensitivity of the phase for frequencies below 10 Hz. X-ray analyses were performed to determine the mineral type in the clay fraction. In the upper meters of the aquifer, the clay content was about 7 % and mainly contained muscovite/illite and chlorite. In the middle part of the aquifer, the clay content varied between 1 and 2 % and the main clay minerals were feldspars (microcline and albite). In the lower part of the aquifer, the clay content increased again and the main mineral type was albite followed by microcline. These results seem to indicate that the variations in temperature sensitivity of the phase are also related to the mineral composition of the clay fraction.

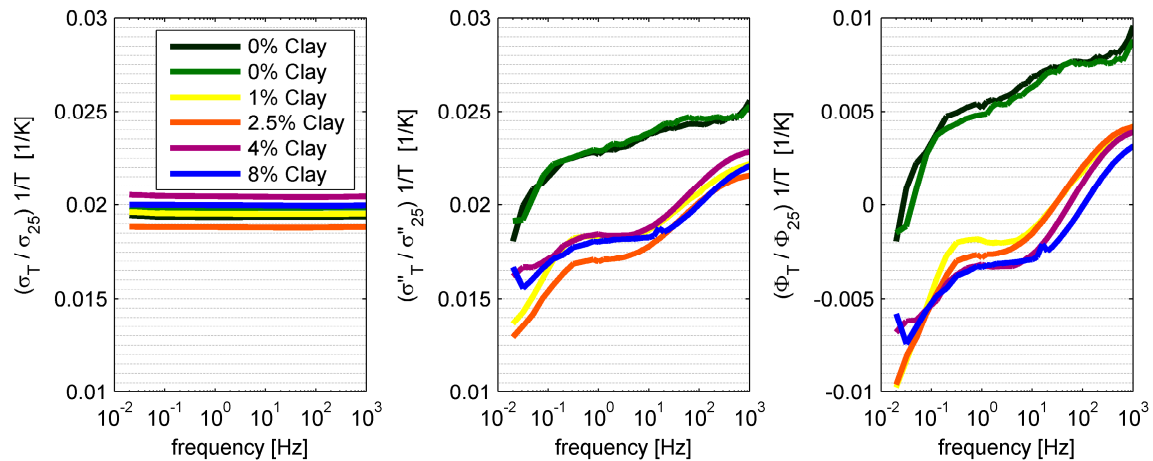


Fig. 1: Temperature dependence of the normalized real (left) and imaginary part (middle) and the phase (right) of the electrical conductivity as a function of frequency for the sand-clay mixtures.

The similarity of the temperature dependence of the real and imaginary part of the electrical conductivity indicates that both conduction and polarization are caused by ions with similar mobility. This seems to suggest that polarization is mainly associated with the diffuse layer. The observed variations in the temperature dependence of the imaginary part of the electrical conductivity could be caused by secondary contributions of the Stern layer. This is supported by the fact that the properties of the Stern layer are known to depend on the clay type.

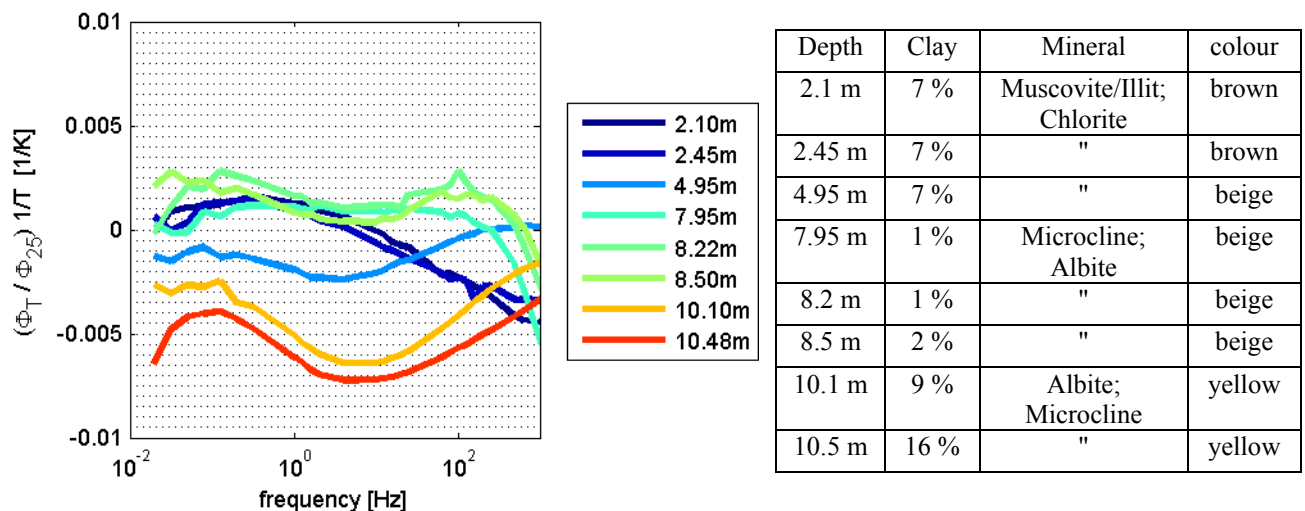


Fig. 2: Temperature dependence of the normalized phase of the electrical conductivity as a function of frequency for samples of the Krauthausen test site. Information on the variation in clay content, mineral type, and color with depth are also provided.

A new numerical pore-scale model of membrane polarization

S. Undorf⁽¹⁾, A. Kemna⁽¹⁾ and M. Bucker^{(1),(2)}

(1) *Department of Geodynamics and Geophysics, University of Bonn, Germany.*

(2) *Instituto de Geofísica, Universidad Nacional Autónoma de México.*

Existing membrane polarisation models

In membrane polarisation models, the motion of ions in the fluid-filled pore space in response to an applied AC voltage is considered. Existing analytic descriptions assume a sequence of active and passive zones, where the counter-ion mobility is reduced in active zones (Marshall and Madden 1959); they partly include some properties of the electrical double layer (EDL) at the matrix-fluid interface as essential source of the IP effect, as well as the finite pore width (most recent Bucker and Hördt 2013a, 2013b). Numerical models based on this conception have also been considered (Blaschek and Hördt 2009; Volkmann and Klitzsch 2010). However, each of these models is either 1-D, or assumes reduced counter-ion mobility in pore throats or close to the pore walls in order to mimic the effect of the EDL, or both, and thus has physical limitations, which are overcome by our model.

Model equations

As in existing models, our set of model equations describing the ions' migration and diffusion, and the associated electric potential, is given by the Nernst-Planck equations and the Poisson equation. The dependent variables are the cation concentration c_p , the anion concentration c_n , and the electric potential φ as functions of spatial position \underline{x} . If the spectral response is sought, it is advantageous with respect to computation time to solve the system of equations in frequency domain. A time-harmonic ansatz for the dependent variables is chosen:

$$\begin{cases} c_p(\underline{x}, t) = c_{p0}(\underline{x}) + c_p'(\underline{x}) \exp(i\omega t) \\ c_n(\underline{x}, t) = c_{n0}(\underline{x}) + c_n'(\underline{x}) \exp(i\omega t) \\ \varphi(\underline{x}, t) = \varphi_0(\underline{x}) + \varphi'(\underline{x}) \exp(i\omega t) \end{cases}$$

where i is the imaginary number, ω is the angular frequency of the applied AC voltage, and c_p' , c_n' , and φ' , and thus also c_p , c_n , and φ are complex-valued quantities. The frequency-domain equations are then given by

$$\begin{cases} 0 = D_p \Delta c_{p0}(\underline{x}) + \mu_p \nabla \bullet [c_{p0}(\underline{x}) \nabla \varphi_0(\underline{x})] \\ 0 = D_n \Delta c_{n0}(\underline{x}) - \mu_n \nabla \bullet [c_{n0}(\underline{x}) \nabla \varphi_0(\underline{x})] \\ \Delta \varphi_0(\underline{x}) = (F/\varepsilon) [c_{n0}(\underline{x}) - c_{p0}(\underline{x})] \\ i\omega c_p'(\underline{x}) = D_p \Delta c_p'(\underline{x}) + \mu_p \nabla \bullet [c_p'(\underline{x}) \varphi_0(\underline{x}) + c_{p0}(\underline{x}) \nabla \varphi'(\underline{x})] \\ i\omega c_n'(\underline{x}) = D_n \Delta c_n'(\underline{x}) - \mu_n \nabla \bullet [c_n'(\underline{x}) \varphi_0(\underline{x}) + c_{n0}(\underline{x}) \nabla \varphi'(\underline{x})] \\ \Delta \varphi'(\underline{x}) = (F/\varepsilon) [c_n'(\underline{x}) - c_p'(\underline{x})] \end{cases}$$

with cation and anion mobilities μ_p and μ_n , and diffusion coefficients D_p and D_n , respectively; F is the Faraday constant and ε the electrolyte permittivity. This approach differs from the already published numerical models by assuming a spatial dependence of the static parts of the variables (c_{p0} , c_{n0} , and φ_0).

Model geometries

The model equations are solved for a 3-D cylindrical pore system using the finite-element modelling tool COMSOL Multiphysics. In the model, a fixed surface potential at the pore wall is assumed, causing a dynamic EDL to build up. This means that no mobility contrast needs to be assumed like in previous model approaches, our model instead explicitly considers the (diffuse part of the) EDL. The AC voltage is applied along the cylinder axis. Simulations are run for different frequencies of this voltage in order to assess the spectral behaviour of ion fluxes within the 3-D

pore system, and thus to obtain the frequency-dependent impedance of the pore system.

With appropriate boundary conditions, the model can be applied to study a variety of different pore geometries. To have a classical membrane polarisation set-up, the model is in particular solved for a system of alternating wide and narrow pores (Fig.1). A grain-based pore geometry is considered, too.

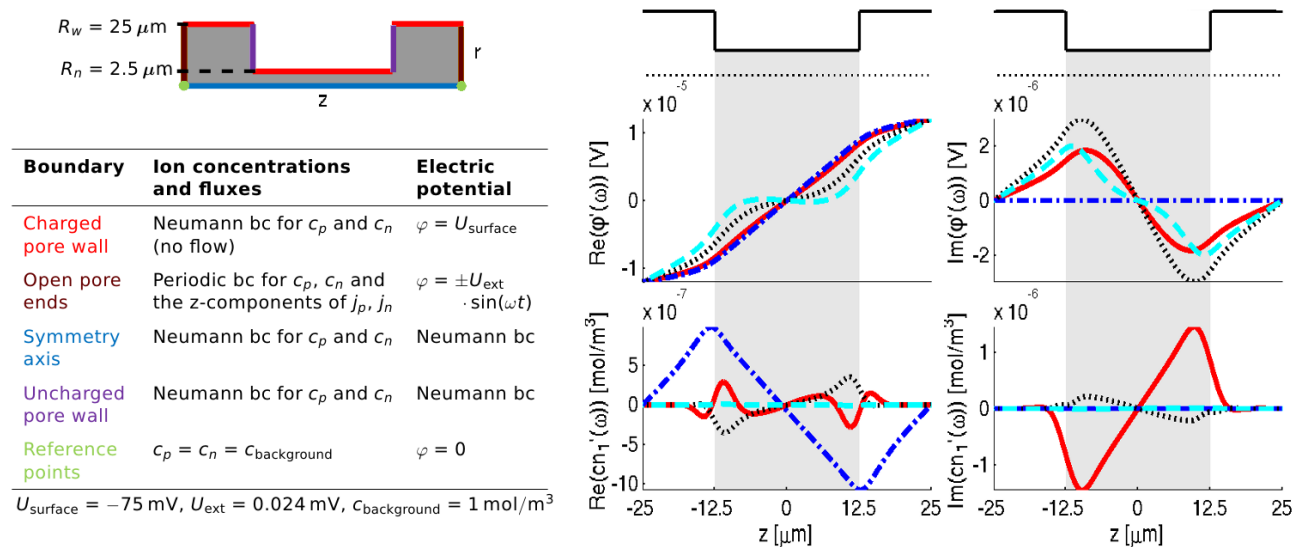


Fig. 1. Left: exemplary pore-based model domain with boundary conditions (bc) in time-domain formulation. Right: corresponding simulation results for both real and imaginary components: electric potential and co-ion concentration along the symmetry axis ($r=0$) at different frequencies (blue: 0.1 mHz, red: 270 Hz, black: 910 Hz, cyan: 3.1 kHz).

Results and future applications

The impedance spectra obtained from time and frequency domain calculations are found to be consistent. The geometry of alternating wide and narrow pores is considered with varying ratios of width and length. The obtained impedance spectra are compared to existing analytic solutions (in case of the grain-based geometry, e.g. with Fixman (1980).

Moreover, the time-dependent and frequency-dependent spatial distributions of the ions as function of position in the pore volume are analysed. For instance, an anti-cyclic oscillation of the counter-ion concentration in the EDL with respect to the counter-ion concentration outside the EDL and the co-ion concentration is found, and an explanation provided. The frequency-dependent spatial distributions of the ions (Fig. 1) are consistent with results of existing numerical studies.

Further analyses are made, for example an evaluation of the electric current through the pore. In the future, the model will be used to study pore-scale SIP signatures of rocks with multiphase pore fillings, such as water-air, water-NAPL (non-aqueous phase liquid), and water-ice, as relevant for hydrogeological, environmental, and cryospheric applications of SIP.

References

- Blaschek, R. and Hördt, A. 2009. Numerical modelling of the IP effect at the pore scale. *Near Surface Geophys.*, 7, 579-588.
- Bücker, M. and Hördt, A., 2013a. Analytical modelling of membrane polarization with explicit parametrization of pore radii and the electrical double layer. *Geophys. J. Int.*, 194, 804-813.
- Bücker, M., and Hördt, A. 2013b. Long and short narrow pore models for membrane polarization. *Geophysics*, 78, E299-E314.
- Fixman, M., 1980. Charged macromolecules in external fields. I. The sphere, *J. Chem. Phys.*, 72, 5177-5186.
- Marshall, D.J. and Madden, T.R., 1959. Induced polarization, a study of its causes. *Geophysics*, 24, 790-816.
- Volkman, J. and Klitzsch, N. 2010. Frequency-dependent electric properties of microscale rock models for frequencies from one millihertz to ten kilohertz. *Vadose Zone J.*, 9, 858-870.

Improving understanding of the information content in induced polarization data: the value of empirical observations based on extensive, validated original datasets

A. Weller⁽¹⁾ and L. Slater⁽²⁾

(1) Technische Universität Clausthal, Germany

(2) Rutgers-Newark, USA

There has been a recent surge in the publication of mechanistic formulations to describe the induced polarization response in terms of grain or pore based polarization mechanisms. In the POLARIS model, the importance of the mobility ratio i.e., the ratio of the mobility of the counterions in the Stern layer ($\beta_{(+)}^S$) to the mobility of the counterions in the diffuse layer ($\beta_{(+)}$), in reliably predicting induced polarization (IP) responses of porous media has recently been emphasized. The POLARIS model predicts two distinct values for this ratio, one for clean sands and one for clayey material. The mobility of the counterions at the surface of sand (silica) is assumed comparable to the mobility of the counterions in the diffuse layer, whereas in clay minerals the mobility of the counterions in the Stern layer is assumed to be much smaller ($\sim 1/350$) than in the diffuse layer. Recent publications have presented a limited amount of data in support of this argument, where sands are predicted to show an approximately two orders of magnitude increase in polarizability relative to clays with the same cation exchange capacity, a prediction that is not easily reconcilable with the majority of measurements in the literature. This strong difference in the mobility ratio for silica sands and clayey materials implies that any relationship between the surface conductivity and the quadrature conductivity will differ for clayey materials versus clean sands.

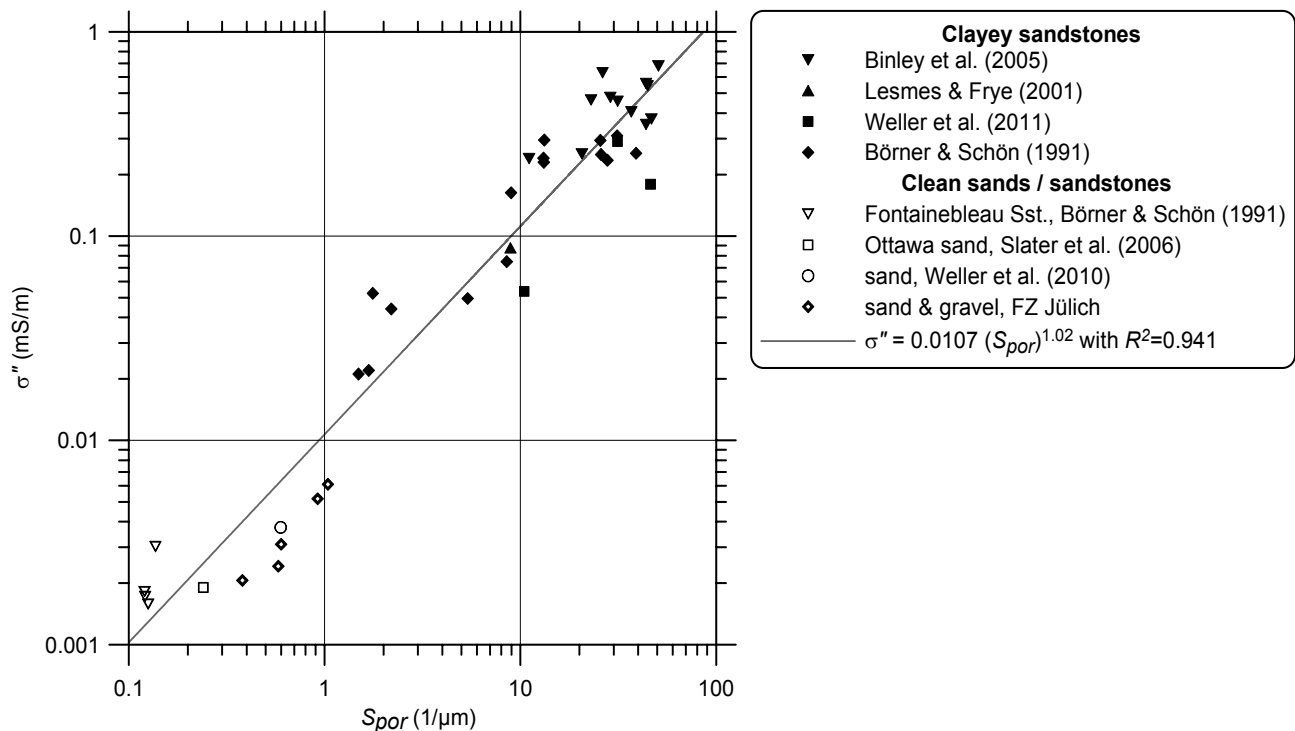


Fig. 1: Relation between imaginary part of conductivity (σ'') measured at a frequency of about 1 Hz and the specific surface per unit pore volume (S_{por}) for 42 samples originating from six laboratories. The data of the clean sand samples (F33, F34, F36, KH, and filter gravel) was kindly provided by Alexander Huisman, Forschungszentrum (FZ) Jülich, Germany. The samples have been saturated with natural water (Binley et al. 2005; samples F33, filter gravel) or a sodium chloride solution (all other samples) with a fluid conductivity of about 100 mS m^{-1} .

However, using a database composed of 63 sandstone and unconsolidated sediment samples covering nine independent investigations (including clayey, silty and clean material), we have identified a single strong, linear relationship between the real part of surface conductivity

determined from multi-salinity resistivity measurements and the imaginary conductivity measured with IP at a frequency of about 1 Hz (coefficient of determination of 0.911). This finding implies a more or less fixed ratio between quadrature conductivity and surface conductivity for our samples despite the wide range of mineral composition. Furthermore, the POLARIS model describes this extensive dataset, composed of a wide range of samples including coarse filter gravels, with an assumed single mobility ratio equal to 1/350. Even in the event that the mobility ratios are distinctively different for clay and quartz, our empirical findings indicate that they do not strongly affect the ratios between quadrature conductivity and surface conductivity. Similarly, we find a single strong relationship between imaginary part of conductivity measured at a frequency of about 1 Hz and specific surface per unit pore volume (S_{por}) for 42 samples originating from six laboratories spanning three orders of magnitude of S_{por} covering clean sands (including pure quartz sand), filter gravels, and Fontainebleau sandstones to clayey sandstones as demonstrated by Fig. 1. This finding is inconsistent with the proposed concept of large differences in the mobility ratio between sands and clays. In summary, if differences in the mobility ratios between clay and quartz do exist, experimental evidence suggests that such differences are not important for determining relationships between IP parameters and physical properties.

The strong empirical relations identified in our work can be readily used to significantly improve estimates of formation factor, water salinity and specific surface area in well logging and hydrogeophysical studies. We therefore suggest that, whilst mechanistic models are valuable for providing insights into the possible origin of IP responses, robust empirical petrophysical relations (similar to the classic Archie Law) that satisfy the widest possible range of available datasets may ultimately provide a more reliable means to relate IP measurements to fundamental physical properties of soils and rocks over a wide range of material types.

References

- Binley, A., Slater, L.D., Fukes, M. and Cassiani, G., 2005. Relationship between spectral induced polarization and hydraulic properties of saturated and unsaturated sandstone. *Water Resources Res.*, 41, W12417.
- Börner, F.D. and Schön, J.H., 1991. A relation between the quadrature component of electrical conductivity and the specific surface area of sedimentary rocks. *Log Anal.*, 32, 612-613.
- Lesmes, D.P. and Frye, K.M., 2001. The influence of pore fluid chemistry on the complex conductivity and induced-polarization responses of Berea sandstone. *J. Geophys. Res.*, 106, 4079-4090.
- Slater, L.D., Ntarlagiannis, D. and Wishart, D., 2006. On the relationship between induced polarization and surface area in metal-sand and clay-sand mixtures. *Geophysics*, 71, A1-A5.
- Weller, A., Slater, L., Nordsiek, S. and Ntarlagiannis, D., 2010. On the estimation of specific surface per unit pore volume from induced polarization: A robust empirical relation fits multiple data sets. *Geophysics*, 75, WA105-WA112.
- Weller, A., Breede, K., Slater, L. and Nordsiek, S., 2011. Effect of changing water salinity on complex conductivity spectra of sandstones. *Geophysics*, 76, F315-F327.

Fractal dimension and induced polarization?

Z. Zhang^{(1),(2)}, A. Weller⁽¹⁾ and S. Nordsiek⁽³⁾

(1) Technische Universität Clausthal, Institut für Geophysik, Clausthal-Zellerfeld, Germany

(2) China University of Geoscience, Wuhan, China

(3) Technische Universität Braunschweig, Institut für Geophysik und extraterrestrische Physik, Braunschweig, Germany.

Fractal theory is applied to describe the structure of geometric objects. The fractal dimension D of a straight line is equal one, but for a tortuous line it becomes larger than one. In a similar way, the fractal dimension of a smooth surface is equal two. A rough surface is described by a fractal dimension $D > 2$. A uniform pore size distribution corresponds to a fractal dimension of three, but a variation in the pore size distribution results in a fractal dimension $D < 3$.

The geometry of pore structure of reservoir rocks is described by the shape, size, distribution and connection of pores and pore throats. Pore space properties are important for the description and characterization of fluid storage and transport in reservoir rocks. We used the fractal concept to describe the geometrical structure of the pores of 25 samples from a Tertiary sandstone formation in China. The fractal dimensions of the sandstone samples were determined from capillary pressure (CP) curves and transverse relaxation time distributions of nuclear magnetic resonance (NMR).

An additional study should show whether complex conductivity spectra can be used to determine the fractal dimension of the pore space. We transformed the relaxation time distribution of complex conductivity spectra determined by Debye decomposition (DD) into a curve showing the cumulative intensity as a function of increasing relaxation time τ . The total chargeability is attributed to the total pore volume. A reliable relation between relaxation time and pore radius r is needed to transform the relaxation time distribution into a distribution of pore radii. The theory suggests a power-law relation $\tau \sim r^b$ with an exponent $b = 2$. Figure 1 displays the comparison between mean relaxation time τ_{mean} resulting from DD and an effective pore radius r_{eff} , which has been determined from permeability and formation factor. The slope of the fitting line indicates a considerably lower exponent ($b = 0.35$). Studies of other authors identified lower exponents, too. Therefore, we decided to assume for a first test a linear relation with an exponent $b = 1$. In this case, the volume fraction $S_v = V(<r)/V$ corresponds to the ratio of cumulative intensity to total intensity.

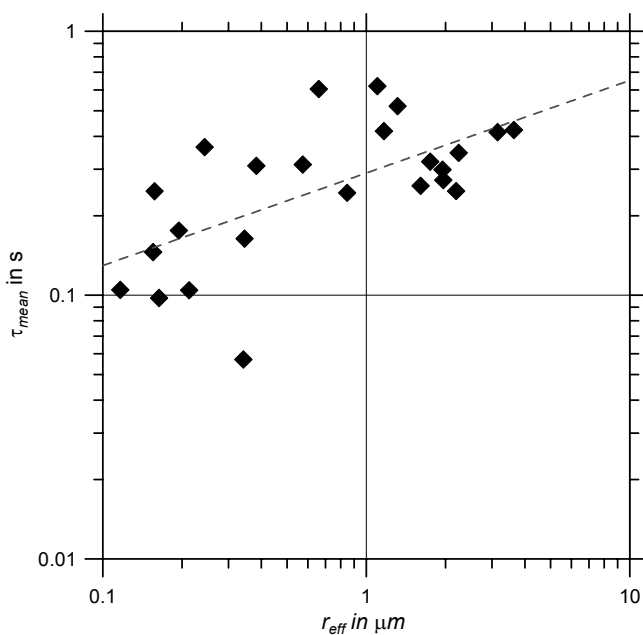


Fig. 1: Relation between mean relaxation time and effective pore radius for 25 sandstone samples. The dashed line indicates the power-law fit with a slope of 0.35.

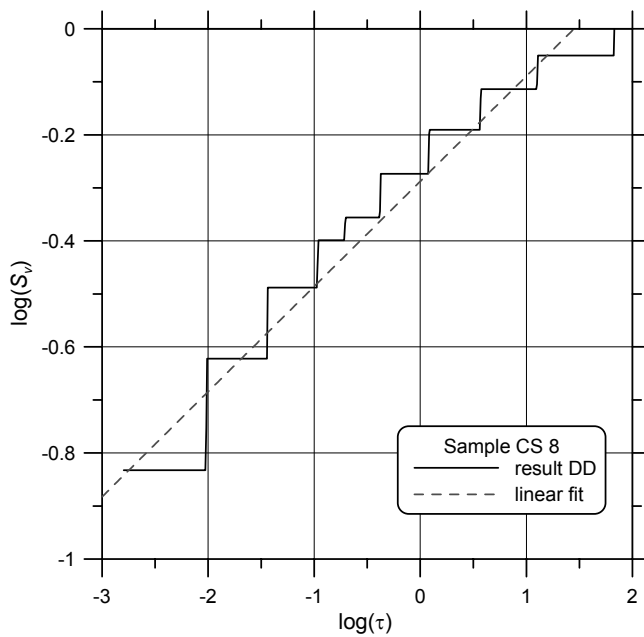


Fig. 2: The fractal dimension D_{IP} of sample CS 8 is determined from the slope of the linear fitting equation $\log(S_v) = 0.198 \log(\tau) - 0.288$ ($R^2 = 0.958$) with $D_{IP} = 3 - 0.198 = 2.802$.

The cumulative curve is presented in a double logarithmic plot showing the relation $\log(S_v)$ versus $\log(\tau)$. Figure 2 displays this curve for sample CS 8. In the case of fractal behaviour of the pore volume distribution, the slope s of the fitting line is used to get the fractal dimension $D_{IP} = 3 - s$. The resulting fractal dimension varies for the investigated samples in a range between 2.75 to 2.88. The values of D_{IP} are comparable to the 'volume dimension' determined by CP curves and higher transverse relaxation times of NMR.

Figure 3 displays the fractal dimension D_{IP} as a function of the specific internal surface S_{por} . A similar increase of fractal dimension with increasing specific internal surface S_{por} has also been observed for the fractal dimensions derived from NMR data.

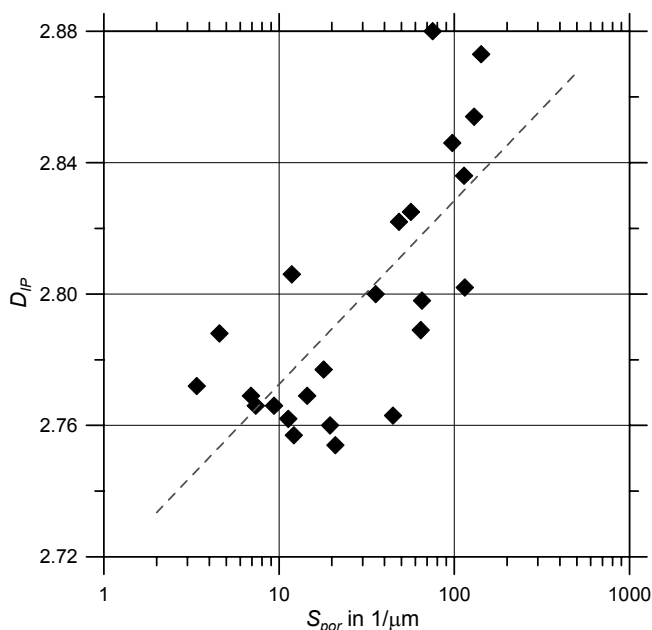


Fig. 3: The relation between the fractal dimension and specific internal surface. The dashed line indicates the fitting equation $D_{IP} = 0.0559 \log(S_{por}) + 2.685$ ($R^2 = 0.528$).

The study has shown that a fractal dimension can be determined on the basis of an IP relaxation time distribution. Further investigations will compare the fractal dimension D_{IP} with the fractal dimension derived from other methods. Additionally, it will be investigated how this fractal dimension can be integrated in models of permeability prediction.

SESSION 2

IP METHODOLOGY

The paradox of the measuring electrodes in IP

F. Abdulsamad⁽¹⁾, N. Florsch⁽²⁾, M. Schmutz⁽³⁾ and C. Camerlynck⁽¹⁾

(1) Sorbonne Université, UPMC-Université Paris 6, UMR 7619 Metis, Paris, France

(2) Sorbonne Université, UPMC-Université Paris 6, UMI 209 Ummisco, Paris, France

(3) ENGESID-IPB, Pessac, France

In the IP measuring chain, measuring electrodes sample the potential toward the very high impedance voltmeter. Modelled by a set of passive electronic components, the measuring electrodes should be invisible, thanks to the quasi infinite input impedance of the instrument input, as shown on Fig. 1. But they are not, from experimental evidence. Figure 2 shows the result obtained in a tank experiment by using three kinds of electrodes and two electrolytes: 1) copper and CuSO₄ solution, 2) non-polarisable electrode SDEC (Pb/PbCl₂) and NaCl, 3) stainless steel with tap water. Al though it is why one prefers non polarisable electrodes in practice, there is a paradox.

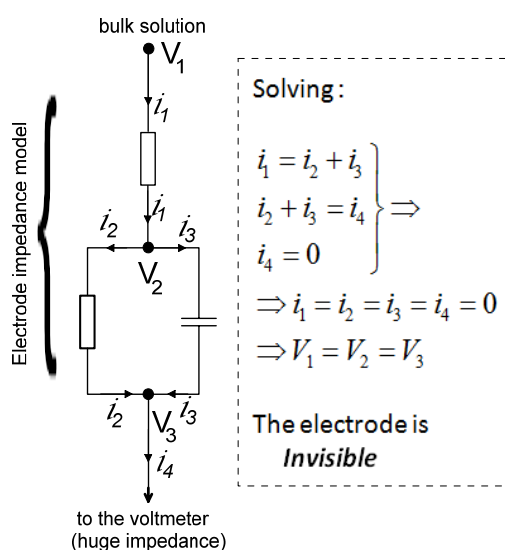


Fig. 1: IP measuring chain. Thanks to the huge impedance of the instrument input, any complex (passive) electrode should be neutral and not visible in a four-electrode array data set.

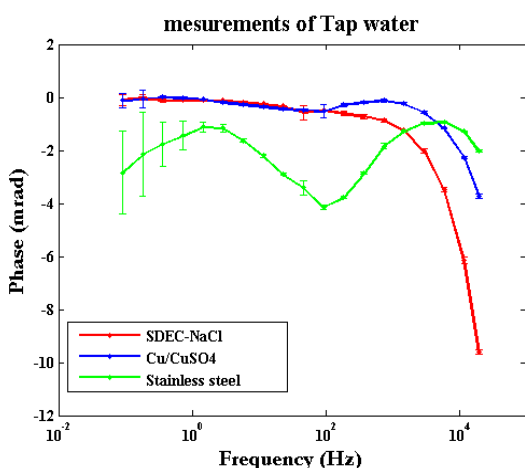


Fig. 2: Results of a classical measurement of tap water, showing the electrode impact on the data.

Clearly, the nature of the electrode impacts the data. It is particularly noticeable when using stainless steel electrode, where these effects at low frequencies are caused by the diffusion phenomena and can be modelled by a Warburg element. But the fact that at high frequencies the same behaviour and curve shape arises, when using non-polarisable or polarisable electrodes, suggests that the phenomenon could be general.

When considering the electrical double layer, a minimum voltage is required to get some “faradic current” crossing this redox potential barrier (it is the electrolysis threshold). But how does the same barrier behave when we try to “transport” passively the (small) potential from the bulk

electrolyte to the FET grid in the input stage of the instrumentation amplifier? The fact that the barrier is not overridden by the ordinarily small potential to be measured makes the current extremely low and even negligible. Actually, electrostatic influence is possibly the main phenomenon determining the potential in the metal of the electrode and finally on the FET grid.

Possibly, this kind of response should be taken into account in the whole protocol by introducing an equivalent electronic component between the potential electrodes P_1 and P_2 , at least to better analytically split the medium own response from the whole.

The objective of our work is to interpret all these effects and then model them as an equivalent electronic circuit. Impedance measurements of tap water or conductive solutions underline the strong effect of various types of electrodes. While “non-polarizable electrodes” give usually simpler results than metallic electrodes, the obtained frequency impedance is generally not reduced to the conductivity/permittivity response of the solution.

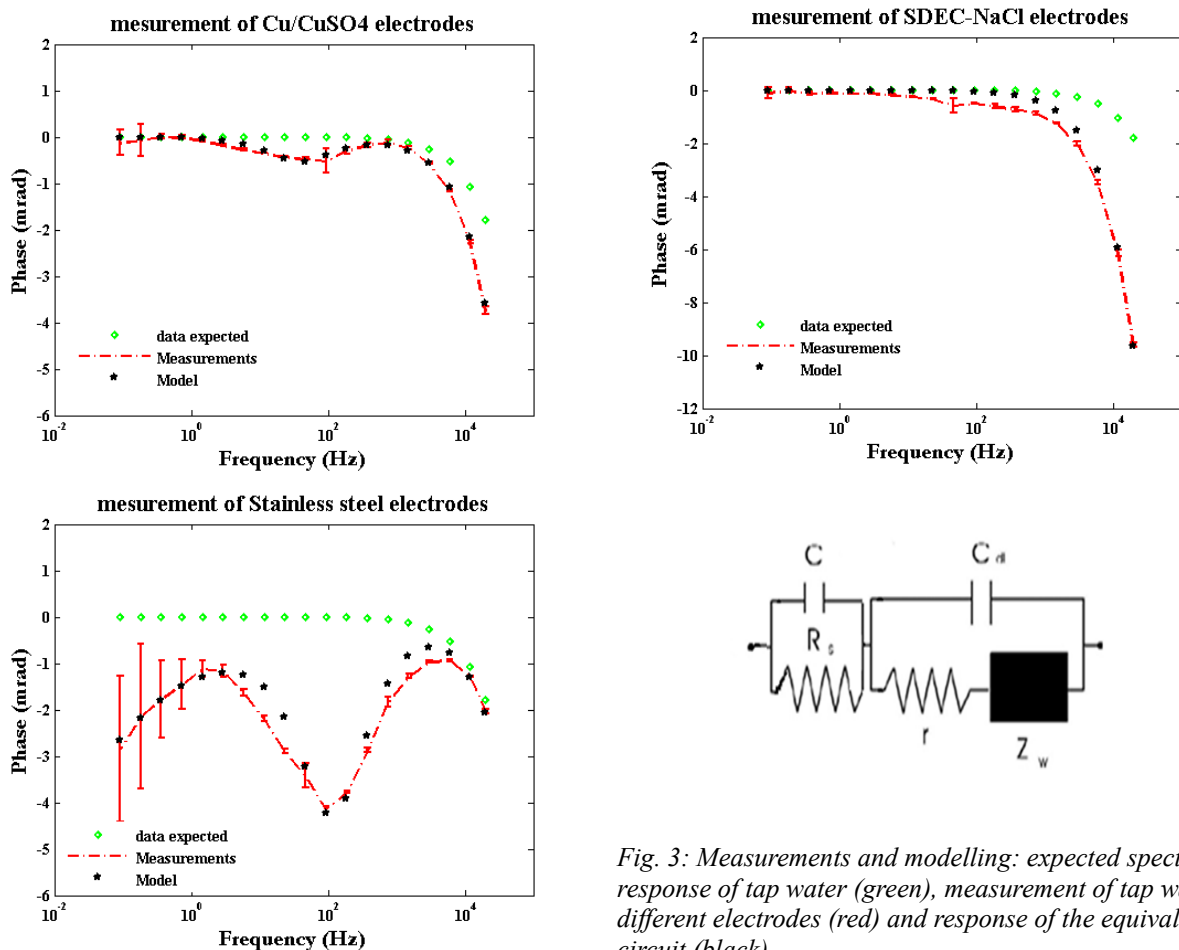


Fig. 3: Measurements and modelling: expected spectral response of tap water (green), measurement of tap water by different electrodes (red) and response of the equivalent circuit (black).

Figure 3 shows the equivalent circuit proposed to model the phenomena at high frequencies, and the modelling results for the three types of electrodes. Low frequency phenomena occur mainly with metal electrodes, and they are generally modeled by a “Warburg” type component (Boadu and Seabrook 2006, Ragheb and Geddes 1991). To adjust the high frequency discrepancy with respect to expected response, we have to add a capacitance element (C) connected in parallel with the resistivity of solution (R_s).

This work underlines the need of taking into account the influence of the electrodes on the spectral induced polarization measurements, over the the entire frequency band.

References

- Boadu, K.F. and Seabrook, C.B., 2006. Effects of clay content and salinity on the spectral electrical response of soils. *J. Env. Eng. Geophys.*, 11, 161-170.
- Ragheb, T., and Geddes, L.A., 1991. The polarization impedance of common electrode metals operated at low current density. *Ann. Biomed. Eng.*, 19, 151-163.

Factors affecting time domain IP data quality

T. Dahlin⁽¹⁾

(1) *Engineering Geology, Lund University, Sweden*

Acquisition of time domain IP data is logistically identical or similar to DC resistivity, but much more difficult from a measurement technical point of view due to the much smaller signals. In case of spectral IP it is also desirable to measure with short integration times, starting with as short delay as possible after current turn-off in order to achieve high frequency content. Signal levels of IP responses are often a fraction of the noise levels, making high dynamic resolution and adequate noise filtering key properties. Transmitted signal is also important, but there are logistical advantages of limiting the output power so that standard equipment of ERT type can be used.

An important factor for data quality is the signal-to-noise ratio, which varies strongly between different electrode arrays. Signal-to-noise ratio is often not a problem for resistivity data acquisition with modern good quality instruments, at least not for relatively small electrode spreads. For IP data acquisition, on the other hand, the signals are much smaller which makes them easily drown in noise. The signal levels are inversely proportional to the geometry factor, i.e. the larger the geometry factor the lower the signal-to-noise ratio. The Wenner array can be used as reference for calculating the relative signal-to-noise ratio of the other electrode arrays, and for the multiple gradient array (Dahlin and Zhou 2006) it falls in the range 0.3 – 1.6 (geometry factor 7.5 – 1.2) for s-factors respective n-factors going up to 7 or 8. For dipole-dipole array the relative signal-to-noise ratio is 0.01 – 0.3 (geometry factor 230 – 6.3) with the same range of n-factors. This means that 30 times more transmitted current is needed to achieve the same minimum signal-to-noise ratio when surveying with dipole-dipole array compared to multiple gradient array. Conversely, only 3.3 % of the transmitter output power is required to generate equivalent worst case signal-to-noise ratio for data measured with multiple gradient array compared to dipole-dipole array. Pole-dipole array is only a factor 2-3 weaker than the multiple gradient array for equivalent median depth of penetration, but it does require a remote electrode which is often problematic.

A common argument for using dipole-dipole array is to avoid coupling between the transmitter and receiver layouts. Coupling can be divided into inductive and capacitive coupling. Inductive coupling is not a problem for DC resistivity measurements, but can possibly be an issue for very early IP decay times. Capacitive coupling can become a serious problem when measuring IP using multi-electrode equipment with multi-core electrode cables used both for transmitting current and receiving signals. The problem appears to be strongly related to the electrode-to-ground contact (Dahlin and Leroux 2012). Experience shows that if the contact resistance is less than 1 k Ω , then IP data of very good quality can generally be recorded, whereas if the contact resistance is above 10 k Ω data quality can suffer significantly. In cases with high contact resistance, when it is not possible to reduce it with watering, putting extra electrode in parallel, etc., data quality can be improved by surveying with two sets of electrode cable spreads in parallel (Dahlin and Leroux 2012). Even if this means more complex field logistics and heavier equipment it is probably still more time and cost efficient compared to surveying with equipment designed for several kV and kW output which would be the alternative.

Electric noise from the power grid can be magnitudes larger than the IP signals, but it can often be efficiently suppressed for the integrated IP decay by averaging over multiples of the period of the base frequency. For spectral time domain IP the noise simple averaging is often not sufficient because of variation in the load on the power grid and since the base frequency can vary slightly. The standard EN50160 allows a frequency deviation up to ± 0.5 Hz if there is a sudden change in generation or load (Li et al. 2011). A more severe problem is electric noise from railway power systems (Fig. 1). In many countries the frequency is lower, 16 ²/₃ Hz, which means that the shortest

IP time window that can be extracted after averaging over a full power cycle is 60 milliseconds. This means that high frequency information from early time windows is lost. Another difficulty with noise from trains is that the disturbances are very dynamic in that the noise can vary strongly in amplitude when trains pass, and for surveys within kilometres of a railway with frequent train traffic this can have a severe impact on the data quality. Although data quality can be substantially improved by averaging over 60 millisecond intervals significant parts of the data may still be too noisy due to temporal variation in the noise (Fig. 2). Noise from DC powered trams and metro systems can also be difficult to handle. This calls for more advanced noise filtering approaches.

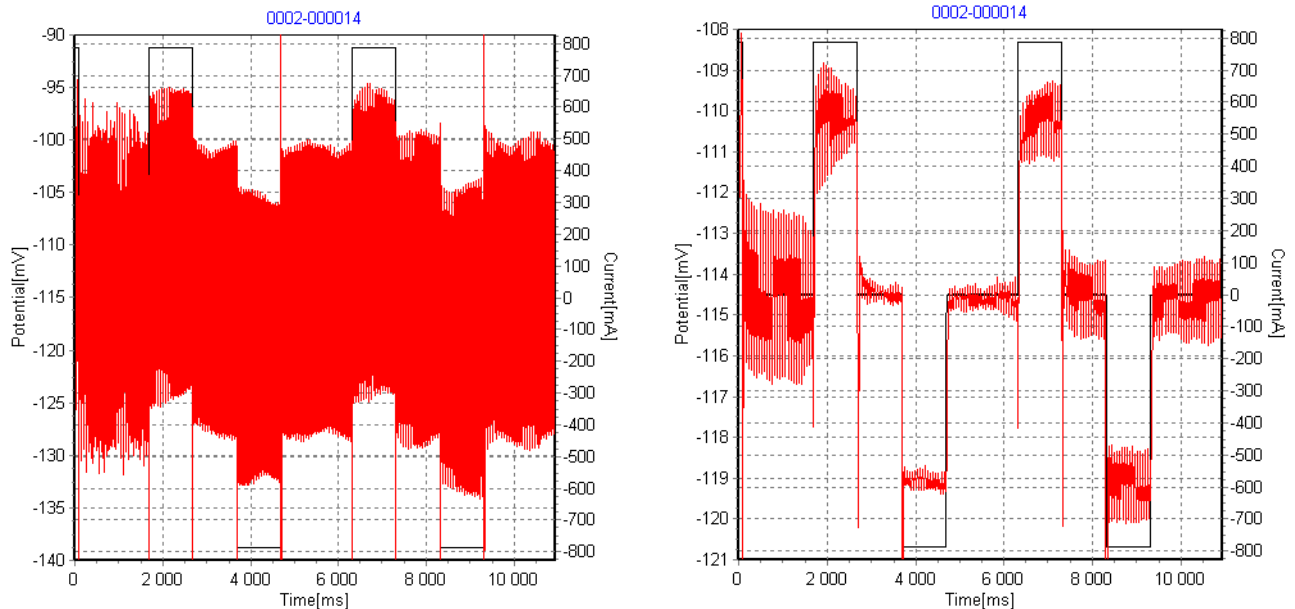


Fig. 1: Example of full waveform recording from IP measurement cycle with noise from railway traffic; a) unfiltered data, b) data averaged over 20 milliseconds (50 Hz).

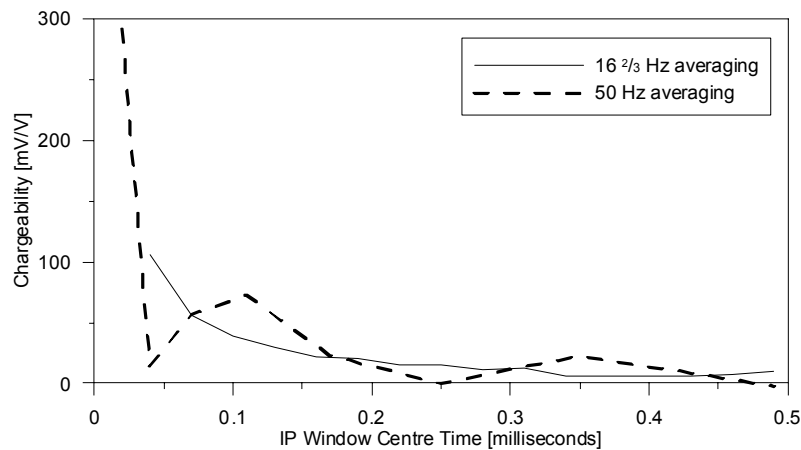


Fig. 2: Example of IP decay curve with railway noise (based on data in figure above) with data integrated over 20 ms multiples (50 Hz) and 60 ms multiples ($16^{2/3}$ Hz) respectively.

References

- Dahlin, T. and Leroux, V., 2012. Improvement in time-domain induced polarisation data quality with multi-electrode systems by separating current and potential cables. *Near Surface Geophys.* 10, 545-565.
- Dahlin, T. and Zhou, B., 2006. Multiple-gradient array measurements for multichannel 2D resistivity imaging. *Near Surface Geophys.*, 4, 113-123.
- Li, Z.W., Samuelsson, O. and Garcia-Valle, R., 2011. Frequency deviations and generation scheduling in the Nordic System, in *Procs. IEEE PowerTech*, 19-23 June 2011, Trondheim.

2D time domain spectral polarization inversion - full wave modelling and Cole-Cole parameterization

G. Fiandaca⁽¹⁾, J. Doetsch⁽¹⁾, A. Binley⁽²⁾, A.V. Christiansen⁽¹⁾ and E. Auken⁽¹⁾

(1) Aarhus University, Department of Geoscience, Denmark

(2) Lancaster University, Lancaster Environment Centre, UK

Field-based time domain induced polarization (TDIP) surveys are usually modelled by taking into account the integral chargeability only, thus disregarding spectral content. Furthermore, the effect of the transmitted waveform is commonly neglected, biasing inversion results. Given these limitations of conventional approaches, a new 2D inversion algorithm has been developed using the full voltage decay of the induced polarization response, together with an accurate description of the transmitter waveform and receiver transfer function. This allows reconstruction of the spectral information contained in the time domain decay series.

The new inversion algorithm is based around a 2D complex conductivity kernel that is computed over a range of frequencies and converted to the time domain through a fast Hankel transform. The same time-domain (TD) transform is applied to both the frequency-domain (FD) forward response and Jacobian, which in frequency-domain is computed through the adjoint method. The model space is defined in terms of Cole-Cole parameters (Cole and Cole 1941), the most widely used in literature for describing the polarization phenomenon.

The effects of the current waveform, stacking procedure and (eventual) instrumental filters are modelled following Fiandaca et al. (2012), but using a 2D implementation for the frequency domain kernels.

The duration of a current pulse transmitted by TDIP equipment is typically shorter than the time it takes for an IP signal to fully decay. This means that the pulse response obtained is actually a superposition of two time-shifted step responses. Due to this, the pulse response has smaller amplitude and decays faster than a step response. Stacking measurements, which is normal procedure to reduce noise content, can be expressed as a series of superimposed step responses (Fig. 1a). This averages different decays and therefore the number of stacks used for a given measurement can heavily affect the resulting signal. The typical stacked signal can differ from a single step response by 60–400 % (Fig. 1b). The receiver transfer function can also highly influence the measured data. TDIP meters, such as the IRIS Syscal Pro, have a digital filter implemented to reduce noise. This has the unwanted effect of distorting the IP signal at early times (Fig. 1c); these early time data should be rejected without proper modelling of the filter characteristics (Fig. 1e).

Several factors are involved in ensuring minimal computation time of the inversion algorithm, and therefore its applicability:

- (1) Fast computation of the TD Jacobian, by using a fast Hankel transform of the FD Jacobian
- (2) Parallel calculation is used for computing FD forward responses and Jacobians at different frequencies, as well as for the time-transformation of the FD kernels.

These features ensure fast computations, with the inversion time being comparable with that of dc algorithms.

With this new algorithm, field-based time domain induced polarization measurements give access to the spectral content of the polarization processes, opening up new applications in environmental and hydrogeophysical investigations.

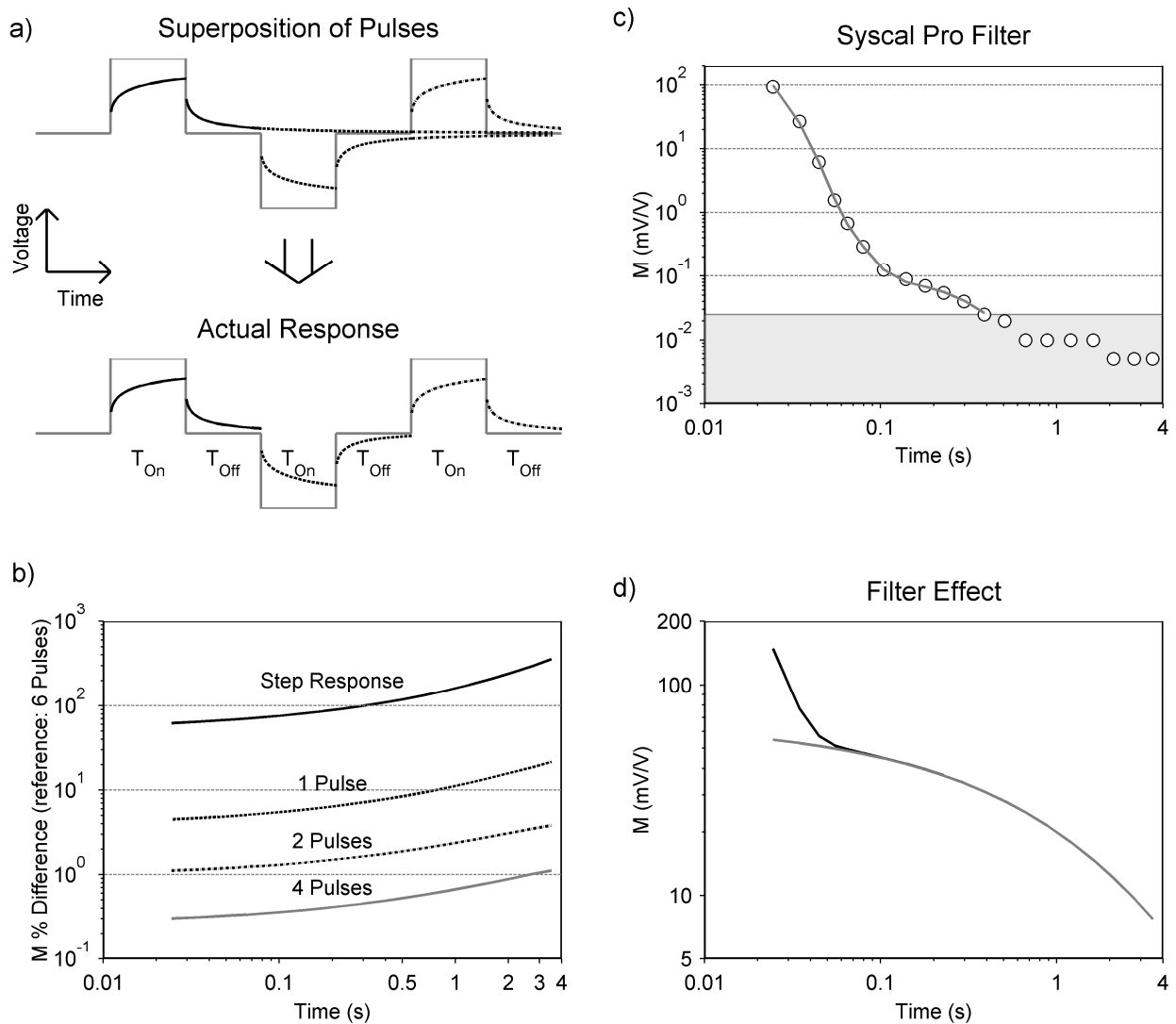


Fig. 1: a) Construction of the pulse response by superimposing two-step responses. b) IP percentage difference between decays with different number of stacks (a decay stacked six times is used as a reference) for the homogeneous half-space described by the Cole–Cole parameters ($m_0 = 100 \text{ mV V}^{-1}$, $\tau = 2 \text{ s}$, $c = 0.5$). Solid black line, step response; dashed line, 1 pulse; dotted-dashed line, 2 pulses; grey solid line, 4 pulses. The on- and off-times used for the waveform are: $T_{on} = T_{off} = 4 \text{ s}$. Note that the percent axis is logarithmic. c) IRIS Syscal Pro filter effect (circles) measured in the time domain on a non-chargeable resistor. The grey line represents the modelling of the filter, for which the measurements in the grey rectangle have not been taken into account (because the limit of the digitization of the data has been reached). d) Example of forward response with the filter implementation (black line) and without the filter implementation (grey line).

References

- Cole, K.S. and Cole, R.H., 1941. Dispersion and absorption in dielectrics. *J. Chem. Phys.*, 9, 341-351.
- Fiandaca, G., Auken, E., Gazoty, A. and Christiansen, A.V., 2012. Time-domain induced polarization: Full-decay forward modeling and 1D laterally constrained inversion of Cole–Cole parameters. *Geophysics*, 77, E213-E225.

Inversion of generalized relaxation time distributions (GRTD) with a L-curve

N. Florsch⁽¹⁾, A. Revil⁽²⁾ and C. Camerlynck⁽¹⁾

(1) *Université Pierre et Marie Curie, Paris (France)*

(2) *Colorado School Of Mine (USA, CO) and CNRS, Chambéry (France)*

From the beginning of the 20th century, retrieving the Relaxation Time Distribution (RTD) has been a challenge in the interpretation of spectra involving relaxation phenomena.

While physicists and electrochemists were the first involved in this questioning, the current revival of Induced Polarization in geophysicists today makes them fully concerned. The inversion of GRTD is a more general approach than the numerous models based on given transfer functions, like the popular Cole-Cole distribution and response. Numerous others provided catalogues of parametric models.

Generally speaking, the decomposition of observed spectra relies on a superposition principle involving elementary Debye relaxation, leading to the expression (given here for conductivity):

$$A_{\omega}(\omega) = a_{\Re} - \int_0^{+\infty} \frac{g_{\tau}(\tau)}{1+i\omega\tau} d\tau + i\omega C, \quad (1)$$

where $g_{\tau}(\tau)$ is the RTD, a_{\Re} a real constant, and C an empirical constant useful to accommodate the high frequency content (sometimes called the “high frequency dielectric term”). Parametric models are linked with associated distributions, and, in some cases, A_{ω} is known as well as the linked distribution itself (Cole-Cole in 1941, for instance, provided both functions).

The work introduced here deals with a more general problem, in which the Debye response may be replaced by any kernel like in the expression:

$$A_{\omega}(\omega) = a_{\Re} - M \int_0^{+\infty} g_{\tau}(\tau) \varphi(\omega, \tau) d\tau + i\omega C \quad (2)$$

For example, we may use a Warburg decomposition, in which:

$$\varphi(\omega, \tau) = \frac{1}{1 + \sqrt{i\omega\tau}} \quad (3)$$

Inversion scheme and example

A triple change of variable is first applied. The two first are classical and transform the equation above into an inhomogeneous Fredholm equation of the second kind:

$$\begin{cases} z = -\log(\omega) \Leftrightarrow \omega = e^{-z} \\ s = \log(\tau) \Leftrightarrow \tau = e^s \end{cases} \rightarrow A_z(z) = a_{\Re} - \int_{-\infty}^{+\infty} G_s(s) \Phi(z, s) ds + ie^{-z} C \quad (4)$$

This integral is computed by using Riemann's summation with step Δs , additionally to a spectrum sampling. Then, real and imaginary parts can be split into:

$$A_k^{\Re} = a_{\Re} - \Delta s \sum_{j=1}^{N_G} \Phi_{kj}^{\Re} G_j \quad \text{and} \quad A_k^{\Im} = -\Delta s \sum_{j=1}^{N_G} \Phi_{kj}^{\Im} G_j + Ce^{-z_k} \quad (5)$$

The third change of variable is applied to impose the required positivity of the RTD. The new unknowns are the G_j' defined by:

$$\forall j \in \llbracket 1, N_G \rrbracket \quad G_j = e^{G_j'} \quad (6)$$

This change guarantees the positivity of G_j , but makes the problem fully non linear. We solve it by using Tarantola and Valette generalized least square recursive formalism.

The properties of the kernel make the problem belonging to the ill-posed problem family. To control the regularization factor and damping, we make use of the notion of L-curve), which is no

more a canonical L-curve here due to non linearity, but remains usable. The optimum point (low left corner) is determined automatically.

The example given in Fig. 1 illustrates the inversion of a data set by using Warburg decomposition (with the recall of Debye decomposition).

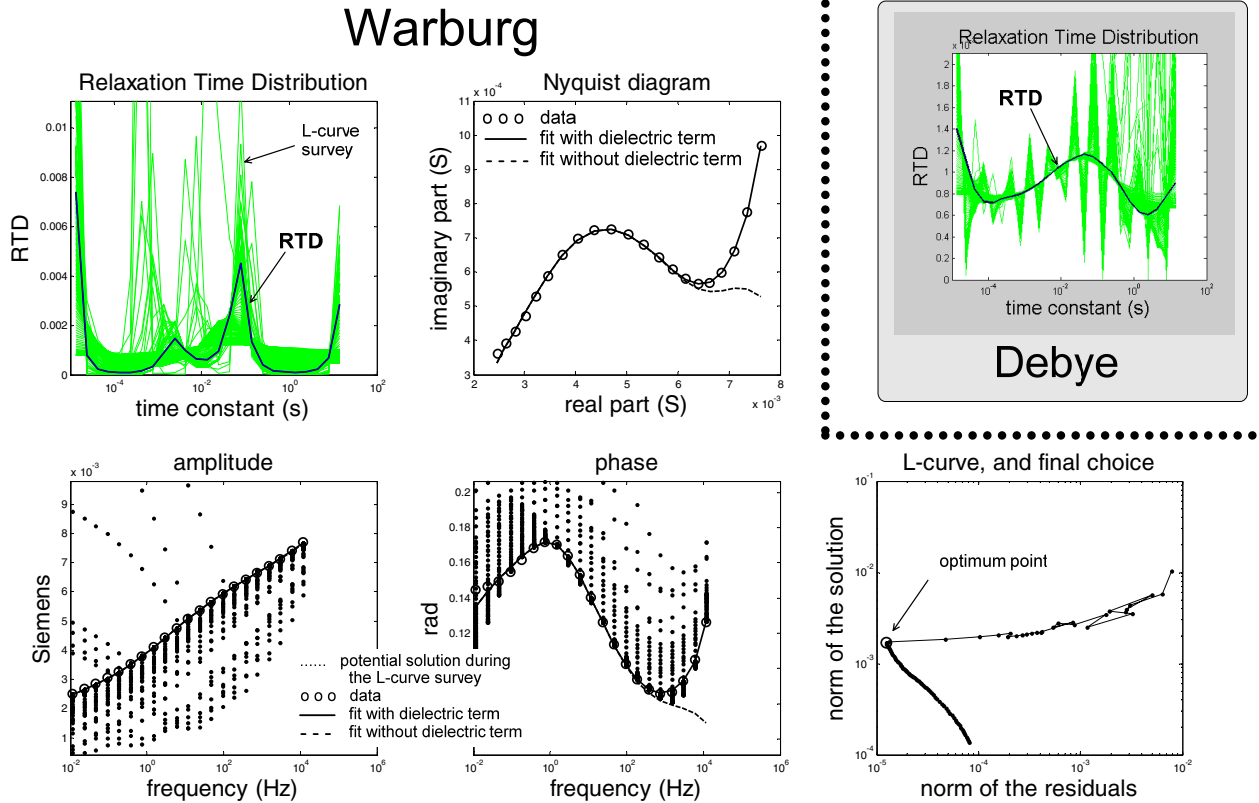


Fig. 1: Aulus data set is relative to the IP response of ancient metallurgic slag heaps. The inversion obtained by using a Debye decomposition leads to a wide bell-shaped distribution (top right), while the Warburg decomposition leads to a more tighten RTD (top left and other plots). The L-curve doesn’t look as it should be in the linear case, but permits setting an optimum damping parameter.

The program is available in a beta version by contacting the authors (nicolas.florsch@upmc.fr).

Evaluation of a correction procedure to remove electrode contact impedance effects from broadband SIP measurements

J.A. Huisman⁽¹⁾, E. Zimmermann⁽²⁾, F.-H. Haegel⁽¹⁾, A. Treichel⁽¹⁾ and H. Vereecken⁽¹⁾

(1) *Institute of Bio- and Geosciences, Agrosphere (IBG-3), Forschungszentrum Jülich GmbH, Germany*

(2) *Central Institute for Engineering, Electronics and Analytics, Electronic Systems (ZEA-2), Forschungszentrum Jülich GmbH, Germany*

Accurate measurements of the complex electrical conductivity using spectral induced polarization (SIP) in the mHz to kHz frequency range require sophisticated impedance spectrometers and carefully designed sample holders with appropriate geometry. Data correction procedures can be used to further improve the accuracy of the SIP measurements. A source of error in laboratory SIP measurements that has not yet been addressed is the effect of the contact impedance of the potential electrodes. This effect is particularly strong when SIP measurements are made on unsaturated porous media with a low electrical conductivity using high-impedance non-polarizing electrodes. In such a case, the accuracy of the imaginary part of the electrical conductivity is strongly affected by the high electrode contact impedance for frequencies above 100 Hz. Therefore, the aim of this study is to develop a correction procedure to remove electrode impedance effects from broadband SIP measurements and to evaluate this new correction procedure using measurements on water with known electrical conductivity and unconsolidated porous media.

Our proposed correction procedure is based on the electrical model of the sample and the measurement system shown in Fig. 1. Here, Z_x is the unknown sample impedance, Z_{e1} and Z_{e4} are the contact impedances of the current electrodes that also include part of the sample material, and Z_{e2} and Z_{e3} are the contact impedances of the potential electrodes. The model also considers the approximately known parasitic capacitances C_v of the amplifiers that lead to possible leakage currents during the SIP measurements. The aim of any SIP measurement is to estimate Z_x from the unknown voltage U_x and current I_x (Fig. 1). In previous work, we have shown how I_x can be accurately determined. So far, we have not yet considered procedures to correct U_x for the effect of Z_{e2} and Z_{e3} . Instead, we have attempted to minimize Z_{e2} and Z_{e3} to allow accurate measurements of U_x and Z_x , which is not always possible as detailed above. The electrical model shows that at least two measurements are required to estimate the five unknown impedances. We propose to use normal and reciprocal measurements where the current and potential electrodes are switched (Fig. 1). For the reciprocal measurement, we use a current injection with low intensity in order to avoid non-linear electrode processes. The contact impedance of the potential electrode Z_{e2} can then be determined from the voltage between node 5 and 2 and the associated known injected current in the reciprocal measurement. The potential at node 2 can be measured directly, and we assume that the potential at node 5 is identical to the measured potential at node 1, which is a reasonable assumption because of the high input impedance of the spectrometer. The electrode impedance Z_{e3} can be calculated in an analogous manner. Once the electrode impedances Z_{e2} and Z_{e3} are known, the unknown voltage $U_x = U_5 - U_6$ in the normal measurement can be calculated using:

$$U_x = U_2(1 + Z_{e2}j\omega C_v) - U_3(1 + Z_{e3}j\omega C_v) \quad (1)$$

where j indicates imaginary units, ω is the angular frequency, and U_2 and U_3 are the measured potentials at the electrodes. The corrected impedance can now be calculated using $Z_x = U_x / I_x$.

There are several challenges associated with the proposed correction method. First, the use of the low current intensity in the reciprocal measurement results in a low signal-to-noise ratio for the measured impedances, and it is clear that a compromise needs to be made between accurate impedance measurements and using a low enough current density to avoid non-linear electrode processes. Second, the electrode impedance is frequency dependent because of electrode polarization effects. However, initial analysis has shown that the electrode contact impedances are

relatively independent of frequency above 1 kHz, and we opted to use the mean electrode impedance between 1 and 2 kHz in our correction procedure. We neglect the frequency dependent behaviour because the observed low-frequency dispersion is not relevant for the correction of the SIP data because of the term $j\omega$ in Eq. 1.

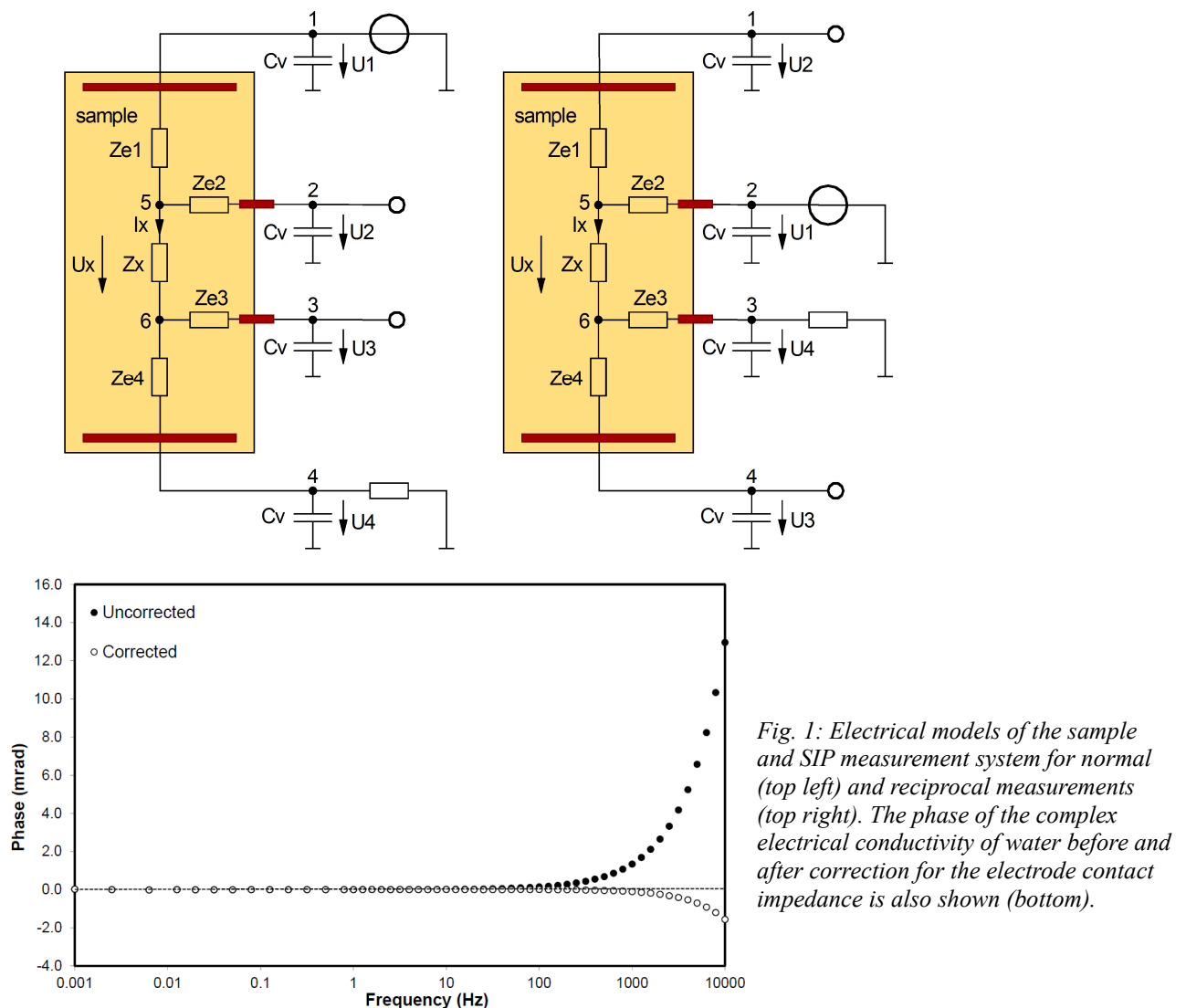


Fig. 1: Electrical models of the sample and SIP measurement system for normal (top left) and reciprocal measurements (top right). The phase of the complex electrical conductivity of water before and after correction for the electrode contact impedance is also shown (bottom).

The procedure to estimate the electrode impedances was tested using measurements on water with a known electrical conductivity of 0.0895 S m^{-1} . The uncorrected phase in Fig. 1 shows that the contact impedance of the potential electrodes introduced an error for frequencies higher than 100 Hz. The error was about 1 mrad at 1 kHz and increased to 13 mrad at 10 kHz. After correction, the increasing phase with frequency largely disappeared and the phase became negative for frequencies above 1000 Hz. This indicates that the required correction of the SIP measurements was slightly overestimated. When considering the potential error sources in the estimation of the electrode contact impedance, we estimate that the accuracy can be improved up to a factor of 10. However, greater improvement is not likely because of the need to know C_v with high accuracy. This estimated maximum possible improvement in accuracy is in reasonable agreement with the deviation of the corrected and the known phase of water at 10 kHz. The developed correction procedure was also applied to SIP measurements on unconsolidated porous media with variable water saturation. The corrected phase spectra were considerably below the uncorrected phase spectra for frequencies above 100 Hz. However, a direct validation of the corrections is not straightforward in this case because of the unknown contribution of the sample to the measured phase. We conclude that the developed correction procedure resulted in a considerable improvement of the SIP measurement accuracy.

Imaging spectral electrical properties of variably saturated soil columns

M. Kelter⁽¹⁾, J.A. Huisman⁽¹⁾, E. Zimmermann⁽²⁾, A. Kemna⁽³⁾ and H. Vereecken⁽¹⁾

(1) *Institute of Bio- and Geosciences (Agrosphere IBG 3), Forschungszentrum Jülich GmbH, 52425 Germany*

(2) *Central Institute of Engineering, Electronics and Analytics (Electronic Systems ZEA 2), Forschungszentrum Jülich GmbH, 52425 Jülich, Germany*

(3) *Department of Geodynamics and Geophysics, University of Bonn, 53115 Germany*

Accurate knowledge about the spatial distribution of soil hydraulic parameters is highly important for modelling the movement of water and solutes in saturated and unsaturated soils on several scales. Electrical impedance tomography (EIT) is a promising technique to non-invasively acquire information on hydraulic conductivity, because the measured complex conductivity is sensitive to soil properties that also control the hydraulic properties (water saturation, porosity, specific surface and pore/grain size distribution). Even more information is available if EIT is performed in a spectral manner (i.e. performing EIT measurements over a range of frequencies), which yields information on the spatial distribution of the spectral electrical properties of the soil. Relationships between spectral electrical and hydraulic parameters have shown strong correlations in several studies. Our ability to obtain such distributions of spectral electrical parameters in an EIT inversion approach is influenced by several factors, among which data accuracy, sensitivity and regularization strength and type are typically the most important. Numerical studies of the reproducibility of spectral electrical parameters in an inversion approach showed that an effective electrical relaxation time should be less affected by these factors than chargeability or DC-conductivity. In order to investigate this finding experimentally and to test the actual reproducibility of spectral electrical properties in an imaging approach, EIT measurements were conducted on a range of packed soil columns with materials which were well defined in terms of their spectral electrical properties using effective spectroscopic measurements.

Tomographic measurements were performed for frequencies ranging from 10 mHz to 45 kHz on homogeneous sand and sand-clay mixtures and on a heterogeneous column that consisted of a sand-clay anomaly embedded within a pure sand background for frequencies ranging from 10 mHz to 45 kHz. The dry material was homogeneously mixed with 10 percent by mass tap water and compacted manually in the column. After packing the columns, they were saturated with tap water from the bottom upwards. Hydraulic states of these soil columns were varied in order to investigate the spectral electrical properties and its reproducibility in imaging as a function of saturation. This was achieved by applying a defined suction at the bottom of the column. A three-dimensional complex resistivity inversion code was used to invert the spectral measurements, whereby each single frequency was inverted independently using the same regularization strength (spatial smoothing) for all frequencies. After inversion of each frequency, the spectral results of each volume element were decomposed into a superposition of 50 logarithmically distributed Debye-terms within a range from 0.01 to 100 seconds to obtain the relaxation time distribution. Reference spectral induced polarization (SIP) measurements were performed to independently determine the spectral electrical properties of all materials. These samples were prepared in a smaller sample holder using the same packing and saturation procedure and then drained by applying air pressure to the top of the sample.

Figure 1 shows the spectral imaging results in terms of normalized total chargeability and peak relaxation time determined using Debye-decomposition of inverted spectra of complex electrical conductivity for the saturated heterogeneous column. For the normalized total chargeability, the effect of spatial smoothing is clearly visible. However, the imaging results for the peak relaxation time allow a very distinct differentiation of the two different materials in terms of their quantitative values. In addition, the peak relaxation time shows no artefacts, whereas artefacts

are visible in the imaging results for the normalized total chargeability, especially near the boundaries, close to the electrodes. Spectral interpretation of the imaging results becomes more challenging with increasing drainage of the columns due to the higher contact impedances of the electrodes and the lower contrast in polarizability between the sand-clay anomaly and the sand background. Nevertheless the imaging results for the drained heterogeneous column can resolve the sand-clay inclusion as an anomaly with higher conductivity both in real and imaginary part and the inverted values are in reasonable agreement with the reference measurements. Differences from the reference data are in the range of reproducibility of the reference data itself and attributed to the packing procedure.

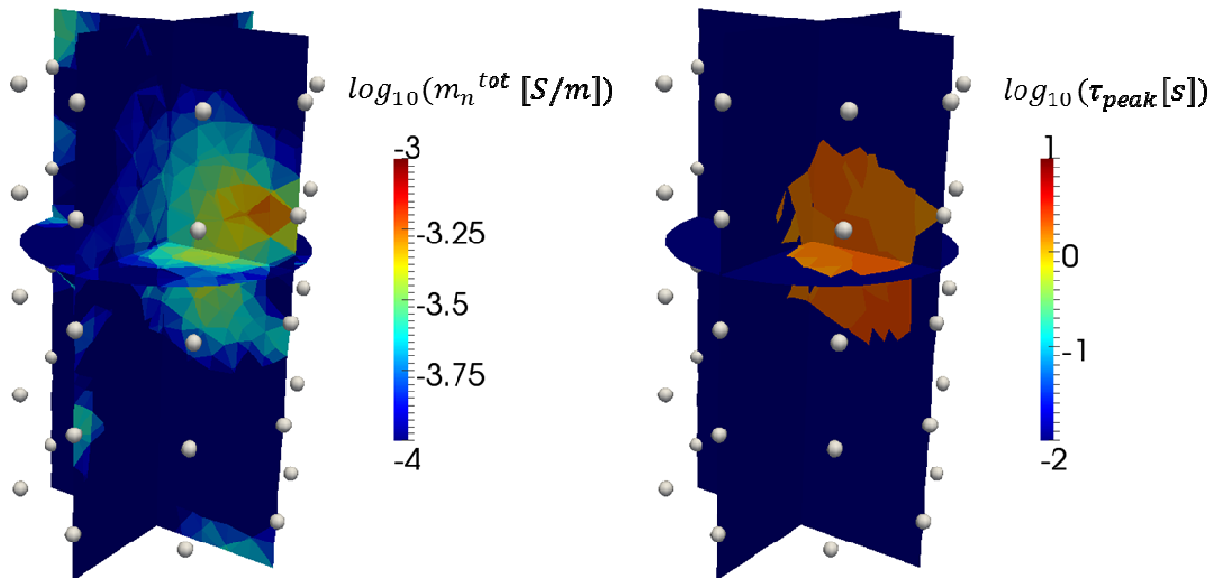


Fig. 1: Images of normalized total chargeability (left) and peak relaxation time (right) of spectral complex electrical conductivity for the sand-clay anomaly in a sand background in saturated conditions.

We conclude that the imaging results for the peak relaxation time are quantitatively much less affected by spatial smoothing than the normalized chargeability. Interpretation of the EIT measurements in the higher frequency range (> 10 Hz) was affected by phase errors that increased with increasing soil resistivity and electrode coupling impedances. This is due to the capacitive load of the electrodes which causes parasitic currents across the potential electrodes. These errors will be numerically corrected in the near future using advanced modelling of the measurement setup. The procedure of packing and saturating the columns proved to have a significant impact on the actual spectral response, which highlights the need for comparable and reasonable methodologies for sample preparation or the use of undisturbed natural soils for calibration purposes.

Anisotropic complex conductivity inversion

J. Kenkel⁽¹⁾ and A. Kemna⁽¹⁾

(1) *Department of Geodynamics and Geophysics, University of Bonn, Germany*

Introduction

In spectral induced polarization, impedance measurements at multiple frequencies are used to derive the subsurface spatial distribution of complex electrical conductivity by means of an inversion algorithm. Presently, these algorithms assume an isotropic complex electrical conductivity. However, as has been shown already for DC conductivity inversion, the assumption of isotropy can yield misleading or unnecessarily complex results (e.g. Nguyen et al. 2007). We propose a new inversion approach supporting anisotropic complex electrical conductivity distributions. The algorithm is based on CRTomo (Kemna 2000), an established code for isotropic complex electrical conductivity inversion. We present a synthetic study which highlights the improvements and limitations of an anisotropic complex conductivity inversion approach.

Inversion algorithm

The 2-D algorithm is based on 2.5-D finite-element forward modelling (Kenkel et al. 2012), and anisotropic complex conductivities are considered in the computation of the predicted impedances, the sensitivities, and the iterative model update in the Gauss-Newton inversion scheme.

We assume a diagonal complex conductivity tensor in terms of Cartesian coordinates. Correspondingly, the sensitivities are defined as derivatives of the complex electric potential, ϕ , with respect to the electrical conductivity values in the different directions, σ_i , as:

$$\frac{\partial \phi}{\partial \sigma_x}, \frac{\partial \phi}{\partial \sigma_y}, \frac{\partial \phi}{\partial \sigma_z}.$$

This allows the representation of anisotropy caused by horizontal or vertical structures (e.g. layering).

The iterative model update is carried out similar to the approach by Kemna and Binley (1996), but with extended equations accounting for the complex conductivity tensor. For regularization, a smoothness constraint is imposed for each component of the complex conductivity tensor. In addition, anisotropy is penalized, i.e., the most isotropic model possible is sought, by implementing an anisotropy penalty function which minimizes the term:

$$\begin{pmatrix} \sigma_x \\ \sigma_y \\ \sigma_z \end{pmatrix}^T \begin{pmatrix} 2 & -1 & -1 \\ -1 & 2 & -1 \\ -1 & -1 & 2 \end{pmatrix} \begin{pmatrix} \sigma_x \\ \sigma_y \\ \sigma_z \end{pmatrix},$$

for each model cell, following the approach of Pain et al. (2003).

Synthetic modelling example

We conducted a synthetic study where we imaged a perpendicular fault model from surface measurements. The original model and the inversion result are displayed in Fig. 1 as sections of the magnitude of the complex resistivity in x and y directions. It features an anisotropic fault region with resistivity values in x and z directions of 10 and 1 Ωm , respectively, embedded in an isotropic background of 1 Ωm . A dipole-dipole measurement configuration employing 40 surface electrodes is assumed. The anisotropic inversion algorithm is capable of correctly resolving the anisotropic fault region. However, the resistivity is slightly underestimated in x direction and overestimated in z direction. Nevertheless, the successful reconstruction of the shape and position of the anisotropic fault region in a relatively isotropic background seems promising.

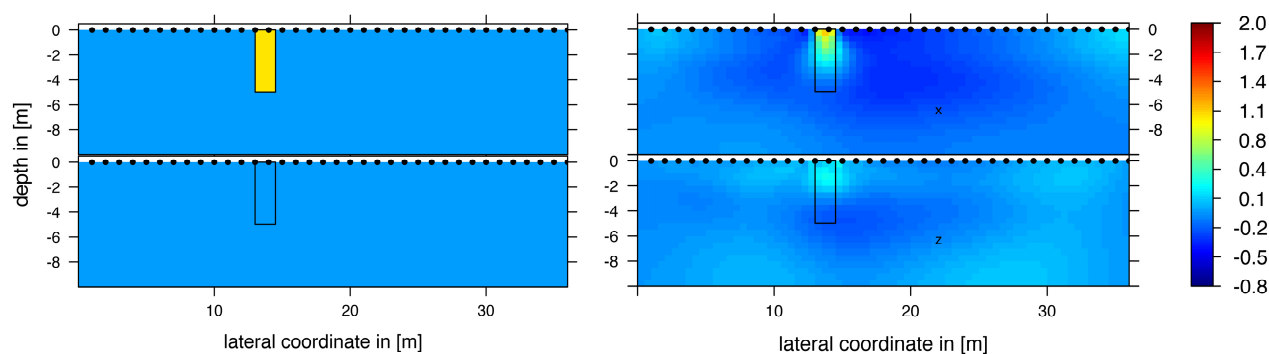


Fig. 1: Original (left) and reconstructed (right) resistivity in $\log_{10}(\Omega m)$ in x and y directions (top and bottom, respectively) featuring an isotropic fault region in an isotropic background ($1 \Omega m$). The fault region is characterised by resistivities of $10 \Omega m$ and $1 \Omega m$ in x and z directions, respectively. The black dots denote the electrode positions.

Conclusions

We think that accounting for anisotropy in complex conductivity inversion should improve the interpretation of resistivity/IP imaging data in many situations. We successfully verified our implementation with synthetic examples targeting the detectability of anisotropy. As a false test, we successfully inverted a synthetic example with isotropic conductivities. First results of the synthetic study indicate that the algorithm is able to resolve anisotropic conductivities while underestimating the original anisotropy factor.

We acknowledge support by the SFB/TR 32 "Patterns in soil-vegetation-atmosphere systems: monitoring, modelling and data assimilation", funded by the German Science Foundation (DFG).

References

- Kemna, A. and Binley, A., 1996. Complex electrical resistivity tomography for contaminant plume delineation. *Proc. 2nd meeting Environ. Eng. Geophys. Soc.*, 2-5 September 1996, Nantes, 196-199.
- Kemna, A., 2000. Tomographic inversion of complex resistivity - theory and application. Ph.D. thesis, Ruhr-Universität Bochum.
- Kenkel, A., Hördt, A. and Kemna, A., 2012. 2D modelling of induced polarization data with anisotropic complex conductivities. *Near Surface Geophys.*, 10, 533-544.
- Pain, C.C., Herwanger, J.V., Saunders, J.H., Worthington, M.H. and de Oliveira, C.E., 2003. Anisotropic resistivity inversion. *Inverse Probl.*, 19, 1081-1111.
- Nguyen, F., Garambois, S., Chardon, D., Hermitte, D., Bellier, O. and Jongmans, D., 2007. Subsurface electrical imaging of anisotropic formations affected by a slow active reverse fault, Provence, France. *J. Appl. Geophys.*, 62, 338-353.

Newmont chargeabilities, apparent time constants and finite bandwidths

J. Macnae⁽¹⁾

(1) RMIT University, Australia

There has been significant research into spectral methods in IP as applied to mineral exploration. However, most published IP field data examples from mineral exploration have IP amplitude estimated from phase differences between two frequencies or time domain systems use the Newmont chargeability as the IP parameter. For a Newmont measurement, an injected current is used with an alternating waveform: 2 second on, 2 second off (50 % duty cycle). The Newmont chargeability is the integral of the measured voltage response between 0.45 and 1.1 s after the turn-off, normalised to the peak voltage. The units of Newmont chargeability are typically ms. Most modelling for mineral exploration code however implements a Cole-Cole description of intrinsic IP parameters. This is a frequency domain model with parameters m , c and T (I am using T or capital τ for IP time constants)

Fundamental IP

My favourite description of sulphide mineral IP comes from Wong (1979). The Cole-Cole model has the form:

$$Z(\omega) = R_0 \left[1 - m \left(1 - 1 / \left(1 + (j\omega T)^c \right) \right) \right]$$

where Z is impedance, R_0 DC resistivity and ω angular frequency.

If $c = 1$, (sometimes called a “Debye” model); in time domain (off-time) the intrinsic decays are exactly exponential $\exp(-t/T)$ with time constant T . Basically $c = 1$ characterises EM and not sulphide IP decays, but can model clay (membrane) polarization decays.

If $c = 0.5$, (sometimes called a “Warburg” model); in time domain the intrinsic decays follow a simple mathematical expression $\text{erfc}((t/T)^{1/2}) \exp(t/T)$. This is the fundamental IP decay for a distribution of uniformly sized polarisable spheres (electronic conductors in an ionic medium). Such decays are illustrated in Fig. 1 with a Newmont system waveform.

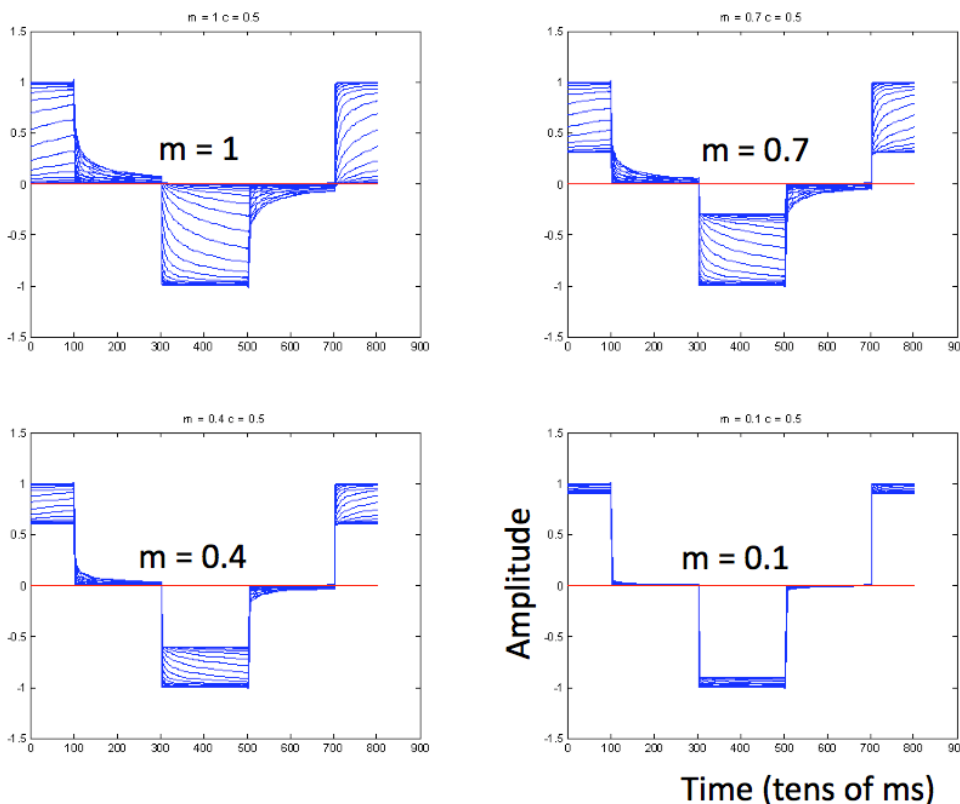


Fig. 1: IP decays with $c = 0.5$, with varying time constant T in four plots, each with a specific m value.

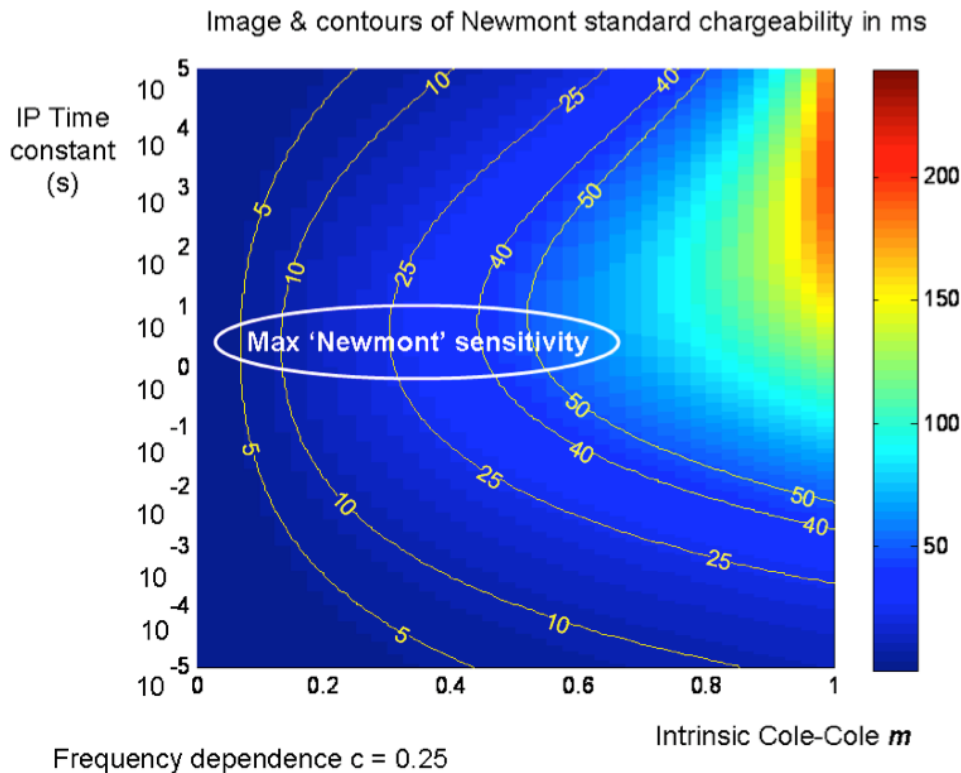


Fig. 2: Contours of Newmont chargeability in ms showing ambiguity with Cole-Cole parameters of a half-space.

If the Newmont chargeability of a half-space is estimated from decays such as those in Fig. 1, for a wide range of T and m , then it is clear that maximum sensitivity occurs for intrinsic T values around 1 to 10 seconds. Newmont chargeabilities over shallow, extensive economic sulphide deposits often exceed 25 ms. In this case, the minimum m value would be about 0.3, indicating a significant fraction of polarisable material.

Just as real EM decays can be synthesized from a spread of exponential decays (Stolz and Macnae 1998), real sulphide (electrochemical) IP decays can be synthesized from a spread of Warburg decays. The Cole-Cole model uses parameter $c < 0.5$ to simulate this spread, corresponding to varying grain sizes, each of which has an intrinsic Warburg T .

Further complications arise from target geometry and burial. The observed Newmont chargeabilities from a finite target are reduced in amplitude (called “dilution” in some historic literature). These can be modelled, but only with assumed Cole-Cole parameters. In this case, apparent time constants can be changed by orders of magnitude if observed responses are fitted with a basic Cole-Cole model.

Conclusions

Apparent chargeabilities estimated from field data are less than true chargeabilities (whether expressed as Newmont or m value).

Apparent time constants can be changed by orders of magnitude if observed responses from a buried target are fitted with a basic Cole-Cole model. Cole-Cole models apply to conductivity rather to decay shape (except to decays measured on lab samples or directly on uniform materials).

Apparent c value is always greater than intrinsic c value if observed data from a buried target are fitted with a Cole-Cole model without accounting for “dilution”.

It is tricky to use published field data (Newmont ms chargeability) to drive modelling. However, maximum m values and “typical” c values can be fairly safely assumed for modelling.

References

- Wong, J., 1979. An electrochemical model of the induced-polarization phenomenon in disseminated sulfide ores. *Geophysics*, 44, 1245-1265.
- Stolz, E.M. and Macnae, J., 1998. Evaluating EM waveforms by singular-value decomposition of exponential basis functions. *Geophysics*, 63, 1908-1913.

Airborne induced polarization

J. Macnae⁽¹⁾ and T. Kratzer⁽¹⁾

(1) RMIT University, Australia

Airborne IP (AIP) effects have been detected in many airborne electromagnetic (AEM) surveys to date (Smith and Klein 1996; Boyko et al. 2001; Smith et al. 2008; Kratzer and Macnae 2012). The IP effect on an AEM system is generally opposite in sign to an EM decay, and appears as negative data in the late off-time during measurements. Figure 1 is an example of a map of late-delay off-time amplitude from a VTEM survey in Quebec.

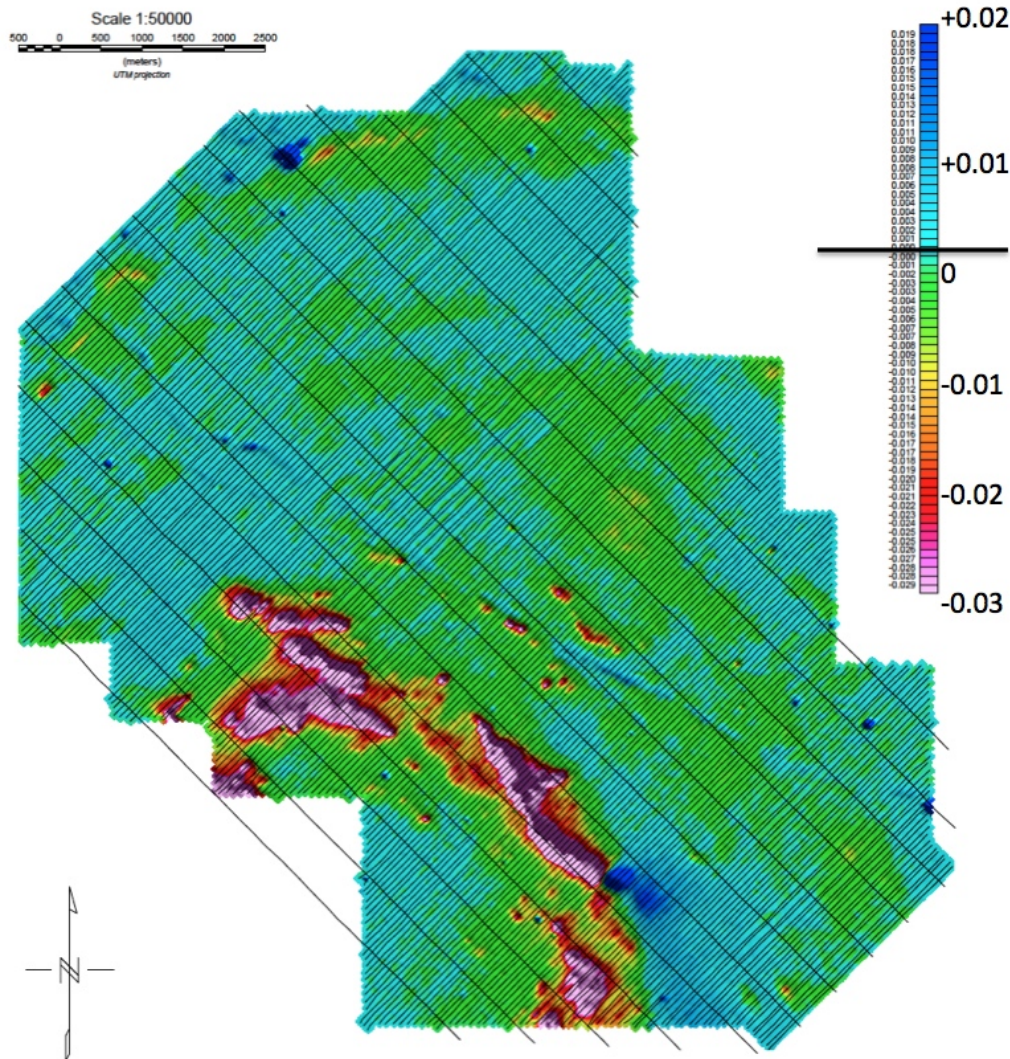


Fig. 1: Roughly 10 km by 12 km airborne VTEM survey in Quebec where large negative IP responses at late delay times were spatially coincident with Titanium mineralization. Data were collected at 3 m intervals along 170 flight lines spaced 100 m apart, with 16 tie lines.

All published AIP examples have the polarisable sources in the near surface. Recently, Kratzer and Macnae (2012) provided some quantitative fitting of AEM data with Cole-Cole models, taking into account the fact that the excitation current in the earth is of course conductivity- and geometry- dependent. This is because the transient current induced in the ground after the transmitter switches off expands downward and outward as it decays. Figure 2 shows the difference between Warburg decays from current injection, and those predicted for an AEM system flying over an area with a conductive overburden with a polarisable target within it and excited by the induced currents.

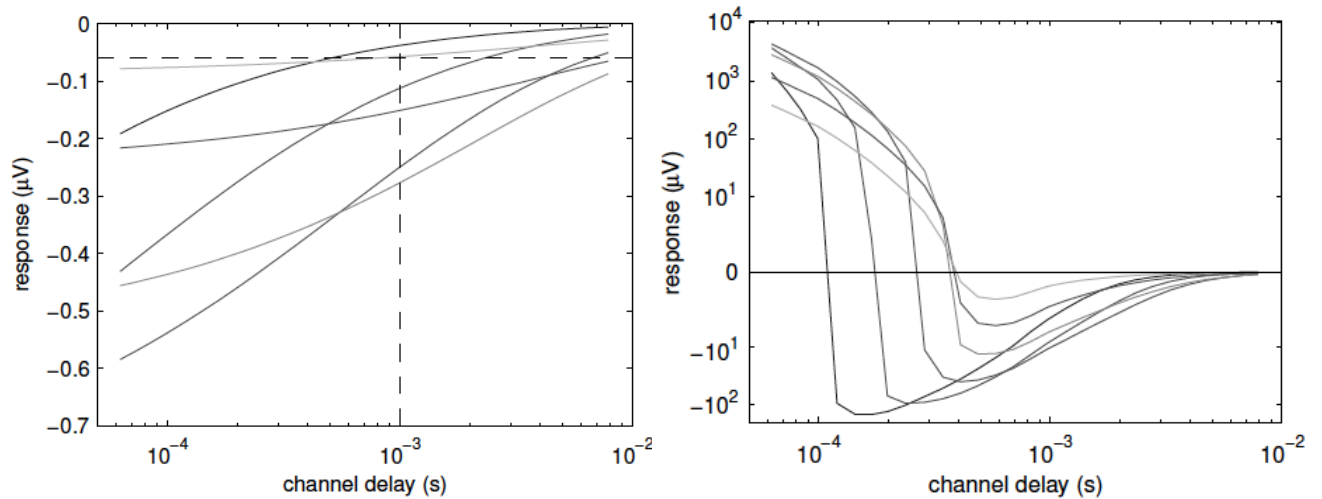


Fig. 2: Warburg IP decays with time constants of 1, 0.1, 0.01, 10^{-3} , 10^{-4} , 10^{-5} seconds from a 25 Hz injected square wave current (left) and Warburg IP decays with the same time constants as excited by induced currents from a 25 Hz square wave current in an airborne loop (right).

From Fig. 2, and a field data example (Fig. 3), we can generalise that AIP effects are seen as negatives of amplitude typically 4 to 5 orders of magnitude less than the peak amplitudes of the EM responses from induced currents. To see them at all has required 1) significant increases in the Signal/Noise ratio of AEM systems 2) significant improvements in the linearity and dynamic range of data acquisition systems and 3) poorly to moderately conductive cover of host rocks.

Even though the AIP effect is small, it can be useful in mapping tailings (Smith et al. 2008) and with technological advances could become more useful for contaminated site mapping.

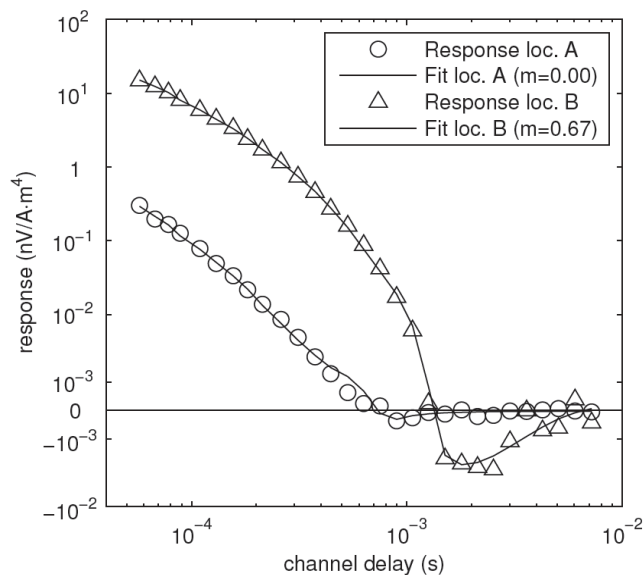


Fig. 3: Fit to AEM sample data at locations with (B) /without (A) polarisable material at surface.

The key questions for mineral exploration is the detection of AIP responses from targets at depth, as opposed to the surface examples from existing systems. Targets at depth will necessarily have smaller responses than those at surface. A large target at 100 m depth would have a response about $(140/40)^3$ or ~ 40 times smaller than the same target at surface (for an AEM system flying at 40 m above the ground). This is undetectable in existing systems with concentric transmitter-receiver geometry: assuming observed responses are a factor of 5 above noise level, it might be realistic to explore to a depth to top of target in the 50 to 60 m range. To achieve target detection at 100 m depth there are several options available from a conceptual framework. 1) Increase S/N by a factor of 4, possibly through use of a flock of UAV mounted receivers rather than a single receiver; there is little scope to increase transmitter signals at present; 2) locate the receiver closer to the smoke-

ring currents, such as occurs in the fixed-wing AEM system geometry where the receiver is towed in a bird behind the aircraft and transmitter and 3) lower the base frequency of the AEM system so that there is more transmitted energy at low frequencies, giving clearer negatives at late delay times. This last option has significant technical challenges attached to it. In much of Australia for example, cover is sufficiently conductive that EM response is dominant to even the latest measured delays (Fig. 4).

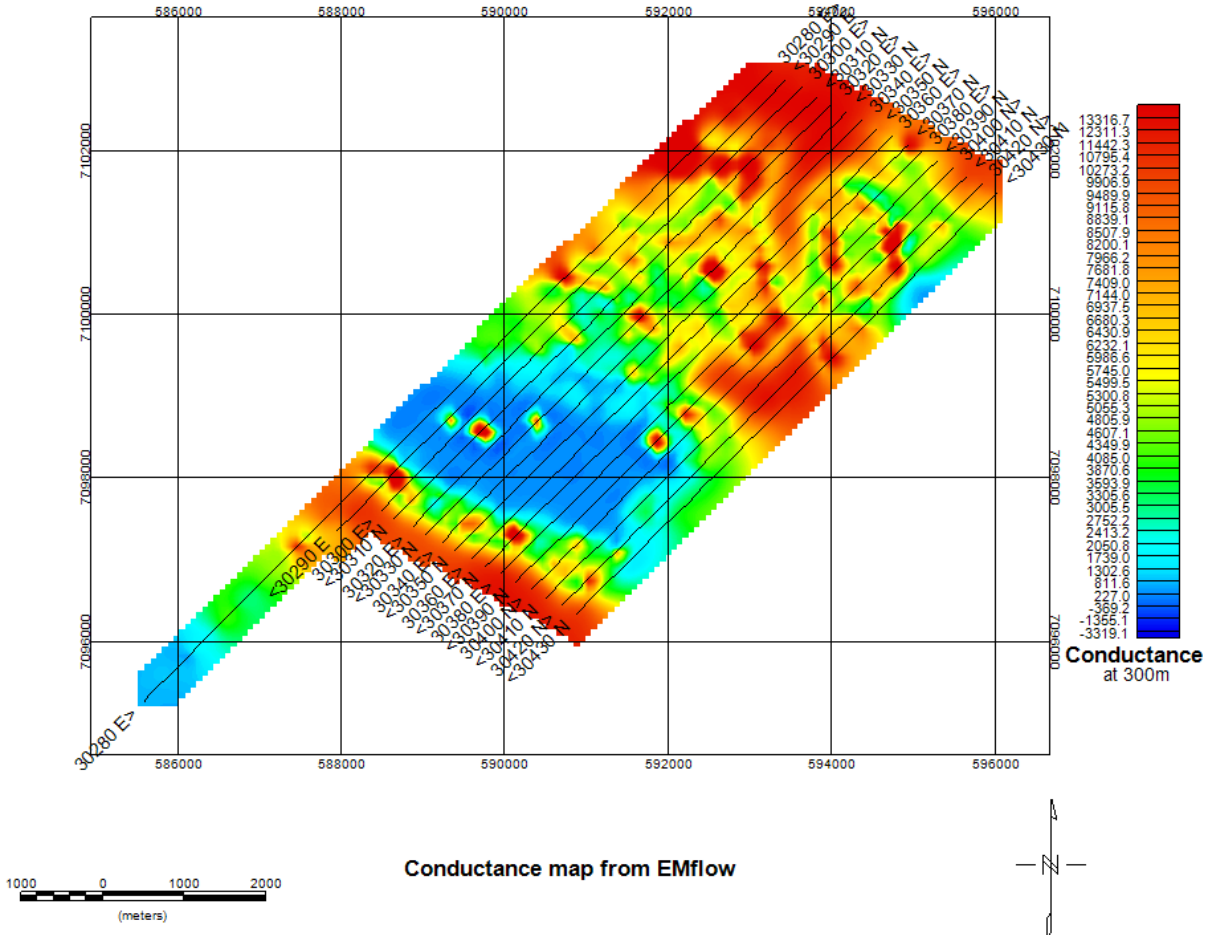


Fig. 4: Example of an airborne survey where AIP negatives (in dark blue, from clays) are only detectable where the cover is least conductive.

Conclusions

Airborne IP effects are seen as negatives of amplitude typically 4 to 5 orders of magnitude smaller than peak AEM responses. As a result, existing systems only “see” responses from targets in the top few 10s of metres. Significant challenges are the focus of current research to increase the reliable target depth detection range to 100 m and beyond.

References

Boyko, W., Paterson, N. and Kwan, K., 2001. AeroTEM characteristics and field results. *The Leading Edge*, 20 (10), 1130-1138.
 Kratzer, T. and Macnae, J., 2012. Induced polarization in airborne EM. *Geophysics*, 77, E317-E327.
 Smith, R.S. and Klein, J., 1996. A special circumstance of airborne induced polarization. *Geophysics*, 61, 66-73.
 Smith, R.S., Cheng, L.Z. and Chouteau, M., 2008. Mapping tailings around mine sites with reverse polarity airborne transient EM data. *SEG Technical Program Expanded Abstracts 2008*, 1313-1317.

SIP instruments for laboratory testing: current state of the technology and limitations

D. Ntarlagiannis⁽¹⁾, L. Slater⁽¹⁾, F. Curatola⁽²⁾ and K. Evdokimov⁽²⁾

(1) Department of Earth and Environmental Sciences, Rutgers University, Newark NJ, USA

(2) Ontash and Ermac, River Edge NJ, USA

Over the last decade the spectral induced polarization (SIP) method has resurged as a promising method for subsurface investigations (Kemna et al. 2012). The SIP method was originally developed for mineral exploration but advances in hardware and theoretical understanding of the IP signals, sources and generation have led to wide applications of the method in environmental and engineering disciplines.

The sensitivity of SIP to bulk and interfacial physicochemical properties permits a wider range of hydrogeophysical and environmental applications, including monitoring of biogeochemical transformations (Atekwana and Slater 2009; Knight et al. 2010). Improvement in hardware, including size and power requirements, along with faster acquisition capabilities and easy access to processing routines is encouraging more widespread adoption of the technique by non-experts. Instrumentation developments focus on resolving small signals to facilitate new applications. This requires accuracy and precision in the experimental set up, but in many cases instrument performance is often overlooked.

Motivated by the remarkably large range of recorded SIP signals on similar materials by different groups, we saw a need for a standardized procedure for SIP set up testing. This work presents our introductory efforts towards this goal, where we compare SIP measurements on different instruments in common used by the scientific community. The experimental samples used were both R-C networks that simulate electrical polarization recorded on earth media properties, and well characterized porous media.

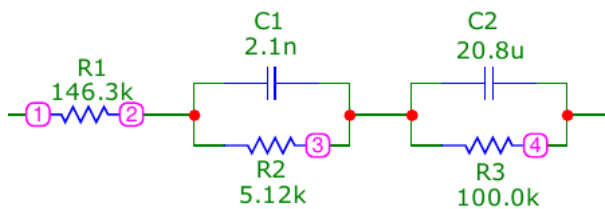
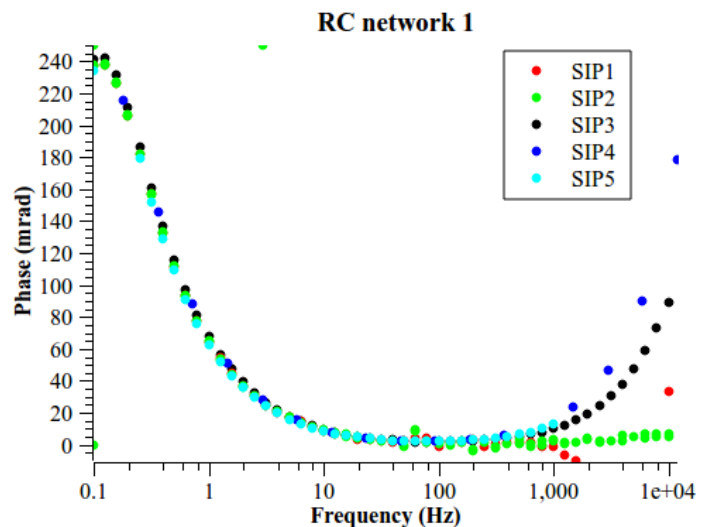


Fig. 1: Generalized schematic of the RC network architecture simulating earth media electrical properties, used for SIP system performance testing (Vanhala and Soininen, 1995).

Fig. 2: Characteristic phase response for 5 different SIP systems during preliminary tests with RC network 1 (peak ~ 0.1 Hz)



The first step of the testing procedure involved the use of R-C networks over a wide range of frequencies (1 mHz – 10 kHz). We created a set of four different R-C circuit boxes with different characteristics, one with pure ohmic characteristics and 3 which exhibit phase peaks around 0.1, 1, 10 Hz respectively (Fig. 1). This step permits identification of systematic errors when recording signals typical of real earth materials associated with the experimental set up, without the complexity (e.g. electrode performance) of interfacing with real samples. This step permits measurement of the speed of data acquisition in addition to the accuracy of the signal, and the precision of the measurement; during this step we will also evaluate data saving and recovery options after abnormal measurement termination (e.g. hardware failure, power outage). Preliminary testing showed the RC networks provide a valid means of comparison for different SIP instruments (Fig. 2).

The second step involves the testing of standardized earth media samples. We chose 5 different samples that exhibit different SIP properties (Table 1). All samples are fully saturated with

the same fluid ($300 \mu\text{S cm}^{-1}$ KCl) and are permanently sealed in an experimental column specifically designed for this type of testing (Fig. 3). The design of this column allows for high quality SIP measurements (as tested in our laboratory) while allowing for long term use of the sample samples. The latter was very important for the design selected since we envision sharing the standardized samples with other research groups interested in SIP research.

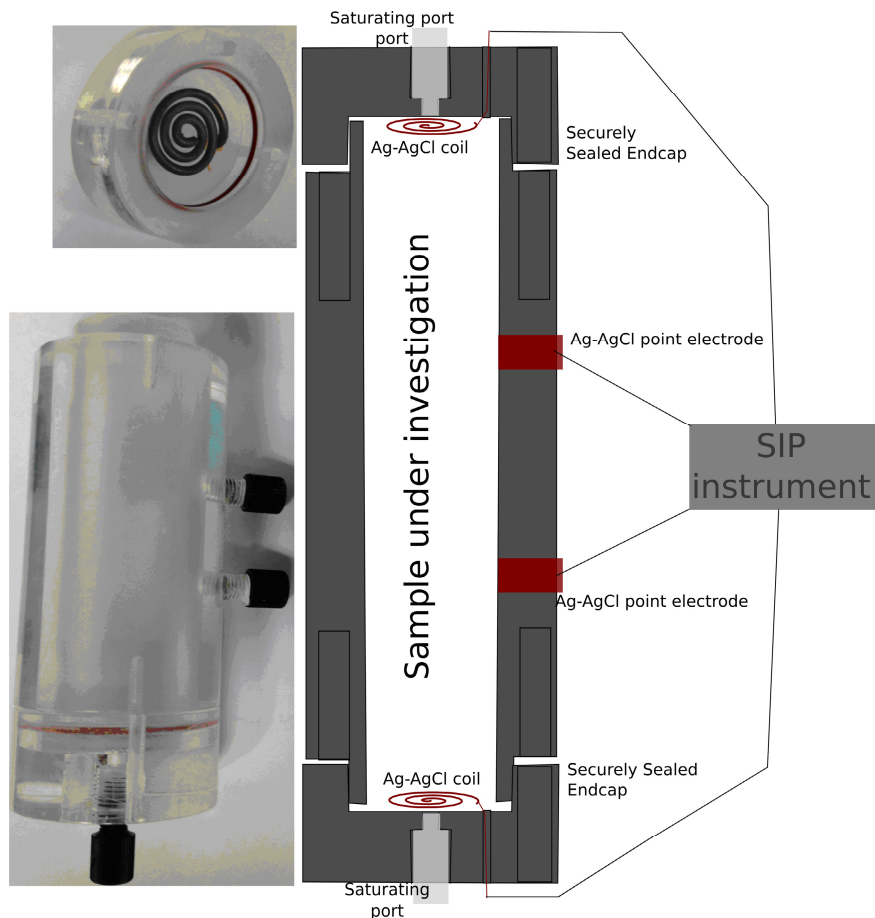


Fig. 3: Schematic and image of the sample holder for the standardized sample testing; after the sample has been packed and saturated, the endcaps are securely and tightly screwed on the main body to minimize any evaporation effects.

Sample	Ottawa Sand	Magnetite	Kaolinite
A	100	0	0
B	98	2	0
C	98	0	5
D	95	5	0
E	93	2	5

Table 1: Composition, by weight, of the five standardized samples.

References

- Atekwana, E.A. and Slater, L.D., 2009. Biogeophysics: A new frontier in Earth science research. *Rev. Geophys.*, 47(4), 1-30.
- Kemna, A., Binley, A., Cassiani G., Niederleithinger, E., Revil, A., Slater, L., Williams, K.H., Flores Orozco, A., Haegel, F.-H., Hördt, A., Kruschwitz, S., Leroux V., Titov, K. and Zimmermann, E., 2012. An overview of the spectral induced polarization method for near-surface applications. *Near Surface Geophys.*, 10, 453-468.
- Knight, R., Pyrak-Nolte, L.J., Slater, L., Atekwana, E., Endres, A., Geller, J., Lesmes, D., Nakagawa, S., Revil, A., Sharma, M.M. and Straley, C., 2010. Geophysics at the interface: Response of geophysical properties to solid-fluid, fluid-fluid, and solid-solid interfaces. *Rev. Geophys.*, 48(4), RG4002
- Vanhala, H. and Soininen, H., 1995. Laboratory technique for measurement of spectral induced polarization response of soil samples. *Geophys. Prospect.*, 43(5), 655-676.

Optimizing the acquisition time for time domain spectral IP by measuring during the on-time

P.-I. Olsson⁽¹⁾, T. Dahlin⁽¹⁾, E. Auken⁽²⁾ and G. Fiandaca⁽²⁾

(1) *Engineering Geology, Lund University, Sweden*

(2) *Department of Geosciences, Aarhus University, Denmark*

Combined direct current resistivity and time domain induced polarisation (DCIP) measurements are traditionally carried out with a current injection sequence using half of the time for transmission of current and the rest without transmission. With this sequence the resistivity is determined during the on-time and the IP from the potential decay during the off-time. However, if only resistivity is measured some commercial instruments use a square wave current injection, without any off-time between the positive and negative phases of current injection, and are thus able to reduce the time needed for these measurements.

In this paper we show that this approach could be implemented for DCIP measurements by also measuring the IP during the on-time. DCIP measurement using a square wave current injection signal, and measuring the IP response during current transmission, has been modelled numerically and tested in the field against a traditional IP measuring cycle with fifty percent current-on and fifty percent current-off.

The numerical modelling was conducted using superposition of step responses following (Fiandaca et al. 2012, 2013), but with a square waveform (Fig. 1). Sensitivity analysis was carried out in the software AarhusInv (version 6.20) on synthetic models with the square-waveform and the classical waveform. The comparison shows that with the square-waveform approach the IP parameters are resolved at least as well as with the classical approach.

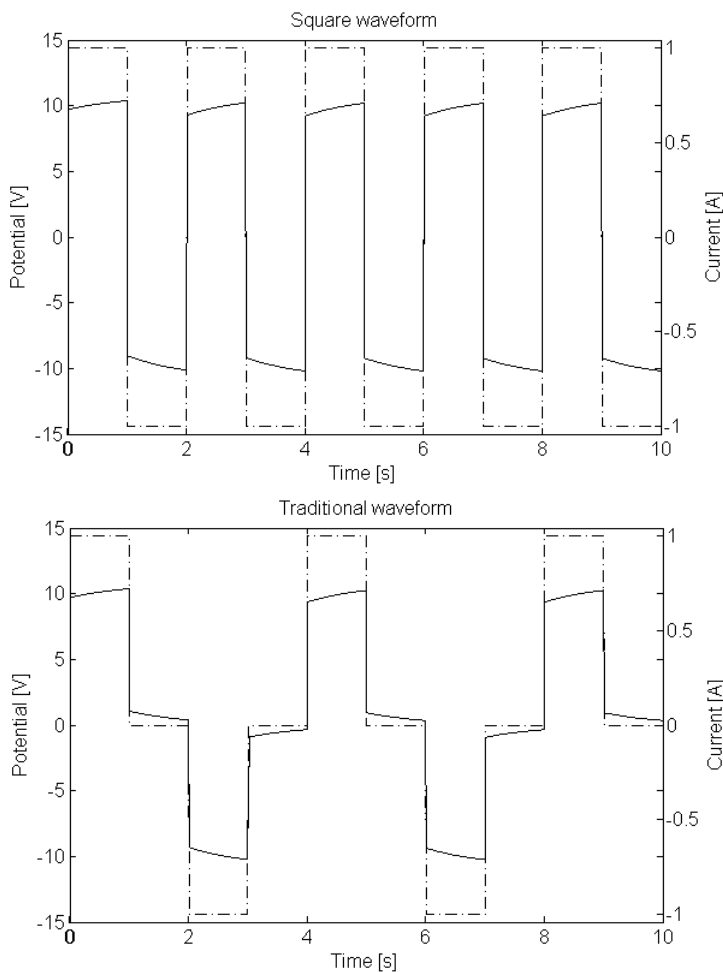


Fig. 1: Modelled waveforms using superposition of step response. The step response is calculated for a homogeneous half space ($\rho = 50 \Omega m$, $m_0 = 100 mV V^{-1}$, $\tau = 1.0 s$ and $C = 1.0$). The upper diagram shows the square waveform without off-time and the lower diagram shows the traditional waveform. Potential is drawn as solid and current as dash-dotted line.

The field test was done in an environment with Quaternary clayey till overlaying Silurian shale. A dolerite dyke in the shale creates an IP anomaly suited for the experiment. The DCIP

profile (202.5 meters, electrode spacing of 2.5 meters) was centred on top of the known IP anomaly and retrieved using a multiple gradient array (Dahlin and Zhou 2006) and the ABEM Terrameter LS instrument. To improve the IP data quality and reduce capacitive coupling separated cables were used for transmitting current and measuring potentials (Dahlin and Leroux 2012). The positions of all electrodes were determined using a differential GNSS system (Topcon GR3 and SWEPOS network-RTK).

Full waveform recordings from the field test for one of the electrode quadruples can be seen in Fig 2. The field test data show a clear IP effect during the current on time, but at the time of writing a complete processing and evaluation of the results is still ongoing.

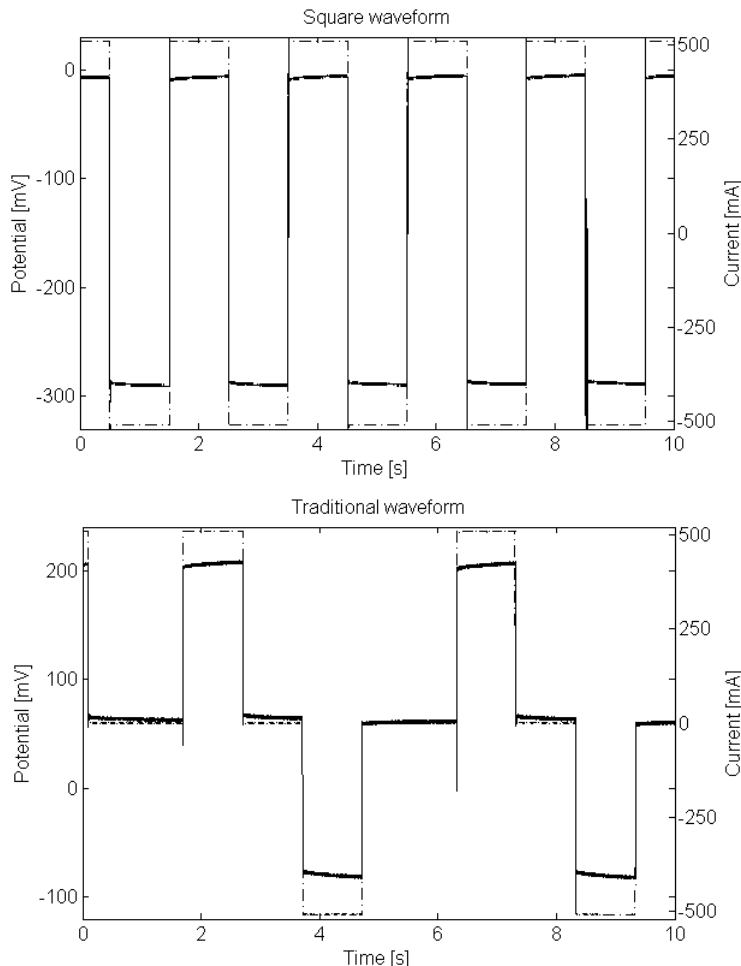


Fig. 2: Full waveform recordings from the field measurements for the same quadruple but with different current injection waveforms. Note that additional current pulses can be transmitted for the same measurement time when using the square waveform compared to the traditional. Potential is drawn as solid and current as dash-dotted line.

Our results support that the approach of using a square wave current injection signal is practically applicable and can reduce the measuring time substantially by measuring the IP-response during the current-on time.

References

- Dahlin, T. and Leroux, V., 2012. Improvement in time-domain induced polarization data quality with multi-electrode systems by separating current and potential cables. *Near Surface Geophys.*, 10, 545-656.
- Dahlin, T. and Zhou, B., 2006. Multiple-gradient array measurements for multichannel 2D resistivity imaging. *Near Surface Geophys.*, 4, 113-123.
- Fiandaca, G., Auken, E., Christiansen, A.V. and Gazoty, A., 2012. Time-domain-induced polarization: Full-decay forward modeling and 1D laterally constrained inversion of Cole-Cole parameters. *Geophysics*, 77, E213-E225.
- Fiandaca, G., Ramm, J., Binley, A., Gazoty, A., Christiansen, A.V. and Auken, E., 2013. Resolving spectral information from time domain induced polarization data through 2-D inversion. *Geophys. J. Int.*, 192, 631-646.

Test of different metal electrodes for IP measurement in time domain

F. Postic^{(1),(2)} and C. Doussan⁽¹⁾

(1) UMR EMMAH INRA/UAPV, Avignon, France

(2) ARVALIS Institut du Végétal, France

Standard IP survey requires the use of non-polarisable electrodes, which generally consist in a porous cup/wood filled with a liquid electrolyte, such as CuSO₄. If these electrodes give the best results in terms of measurement quality, their set up in the field is time consuming and requires a good soil-electrode contact with the inner electrolyte through the porous cup. Moreover, this kind of electrodes in long term survey (over 6 months to a year) for hydrological or agricultural applications for examining subsoil variations with time lapse acquisition, necessitate frequent refilling, are susceptible to leak out and to modify the soil environment next to the electrode. In that case, solid electrodes, such as metal electrodes, would be easier to handle and install, particularly for long term survey. However, it is known that metal electrodes may exhibit electrochemical reactions with the surrounding and soil and heterogeneous polarization among electrodes along the survey line. The magnitude of these parasitic effects may depend on the metal alloy used and a metal electrode exhibiting the closest behaviour to non-polarisable electrode would be a good balance between practicability and measurement quality.

In this study, we have tested 4 types of metal alloys for electrodes in IP measurements: bronze (CuSn₄Zn₄Pb₄), brass (CuZn₃₉Pb₃), cupronickel (CuNi₁₀Fe₁Mn) and stainless-steel, in conjunction with classical Cu/CuSO₄ non-polarisable electrode as a reference. These measurements were made in various conditions: grassland, crop field and fallow land. IP Measurements were conducted with Wenner protocol, electrode spacing from 0.5 m to 1.0 m, using an Iris Instruments Syscal pro. We used 20 time-windows up to 1000 ms. After a 20 ms delay, the first time-window length is 10 ms, then followed by 5 time-windows of 20 ms, 3 of 30 ms, 3 of 40 ms, 3 of 50 ms, 2 of 60 ms, 70 ms, 80 ms, 90 ms. Metal electrodes diameter was 12 mm except cupronickel 15 mm. Non-polarisable electrodes were made with porous ceramic cups from gardening equipment, filled with saturated CuSO₄ liquid solution and a copper rod immersed into the solution. Quadripoles of each electrode's types were left in the field for a long term monitoring.

From the data set acquired with these measurement settings, we extracted 4 variables describing the behaviour of each type of metal alloy electrode with respect to the non-polarisable electrode. At first, we compared the relative difference of chargeability: $\delta M = (M_i - M_n) / M_n$ between each metal alloy electrodes and the non-polarisable electrode, where M_i is the chargeability measured with metal alloy electrode, and M_n is the chargeability measured non-polarisable electrodes. This difference reports about the global quality of the measurement with each metal alloy. In order to express the sensitivity of the signal probed by each type of electrode to external electrical noise, we counted the relative number of negative voltage (RNN) values measured in each 20 time-windows over the all voltages measured. The difference between decay curves of metal/non-polarisable electrodes was estimated by the mean squared error (MSE) of each time windows. Finally, we fitted each IP decay curves that exhibited at least 2 decay times in our conditions with 2 power regressions. The first regression is applied to the first 3 time-windows, and the second to the rest of the decay curve. From these data fitted, we calculated the relative difference of the time exponents ($\delta\tau$) between each metal alloys and non-polarisable electrode, in the same manner as we did for the relative difference of chargeability value M .

The results for IP measurements done at a short time scales (i.e. a few minute-hour after electrode installation) show that the relative difference of the chargeability, δM (Fig. 1), was the smallest for bronze, reaching 16.6 % with non-polarisable electrode. Stainless-steel and brass are relatively close, with 26.2 and 30.2 % of relative difference respectively, while δM for cupronickel was as high as 88 %. Bronze had also the smallest relative number of negative voltage RNN ~ 0.16 % (Fig. 1), whereas brass and stainless-steel had RNN ~ 7 to 15 times higher. Non-polarisable electrode never showed negative voltages. Stainless-steel, and brass to a lesser extent,

exhibited a large variability in the number of erratic negative voltage, underlining sensitivity to noise. The smallest MSE was obtained by bronze, closely followed by stainless-steel and brass, while cupronickel gets at least a double score. Relatively good fits were obtained with a power regression for the voltage decay curves, mean r^2 ranged from 0.99 for the first decay to 0.82 for the second, with more variability in the signal measured. This fitting of time exponent of decay curves resulted also in the smallest relative difference of $\delta\tau$ for the bronze electrodes (8 to 9 % for the first and second time constants). For the others metal alloys, $\delta\tau$ ranged from 17 % to 73 %.

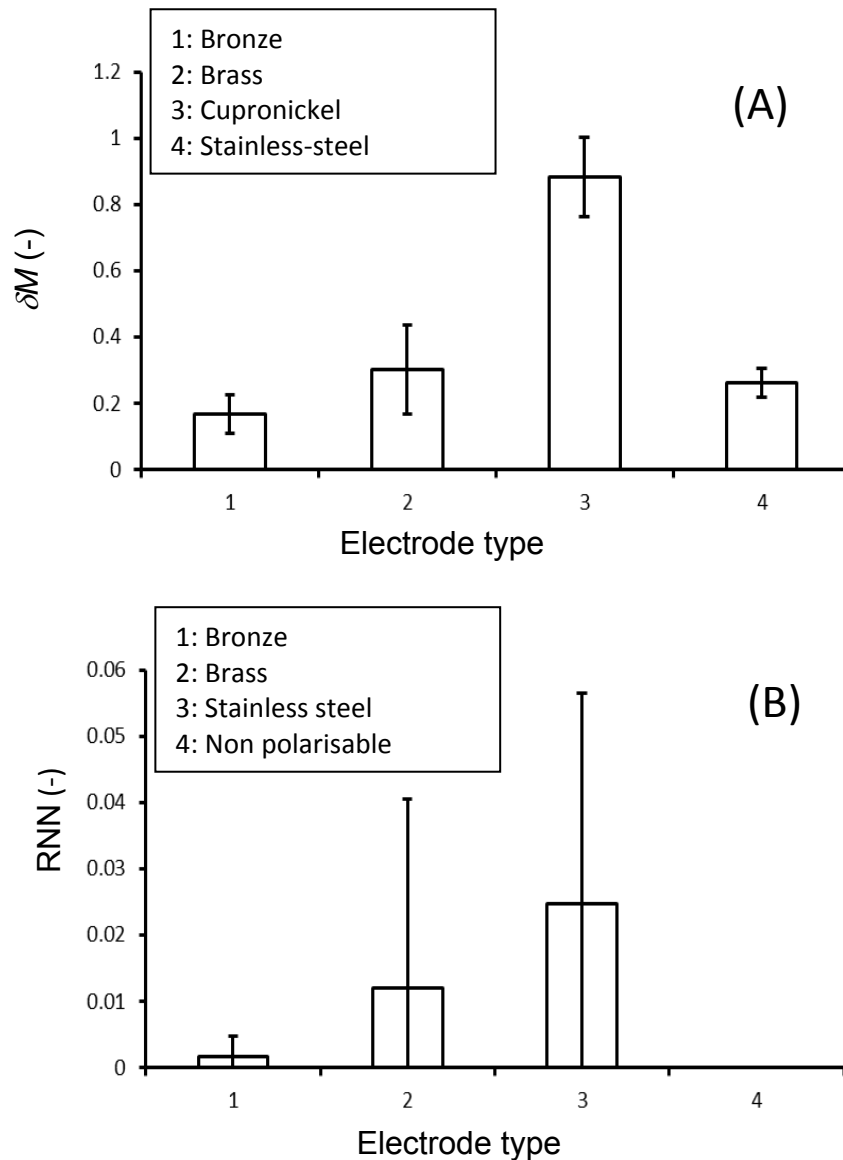


Fig. 1: (A) Relative difference of chargeability relative to non-polarisable electrode (δM) for bronze (1), brass (2), cupronickel (3) and stainless-steel (4) electrodes (mean \pm s.d.). (B) Relative number of negative voltage (RNN) measured in 20 time-windows of a IP decay curve for bronze (1), brass (2), stainless-steel (3) and non-polarisable (4) electrodes (mean \pm s.d.).

From this study, bronze exhibited best results for all the criteria studied relative to non-polarisable electrode (i.e. chargeability, mean error between decay curves, number of erratic, negative measurement, variability, and time decay constants) than other metal alloys for IP measurements on a short time scale (minutes to hours) and thus was closest to non-polarisable electrode behaviour. First measurements for a longer time-scale after installation for monitoring (i.e. ~ 3 months) tend to show that bronze electrodes are still effective for IP measurements.

Measuring IP effects at high frequencies: first lab and field data from 0.001 Hz - 250 kHz

T. Radic⁽¹⁾

(1) Radic Research, Berlin, Germany

The electrical resistivity of nearly all natural materials is more or less frequency dependent. This is caused by electrochemical interactions between the ions of the pore space fluids and the inner pore surfaces. These interactions express themselves as an additional conductivity mechanism, next to that of the fluids. In the frequency range one can observe with increasing frequency, a steady decrease of the resistivity. Accompanied by this is a phase shift between the injected current and the resulting voltage. In the first approximation, the phases are proportional to the increase of the resistance. Therefore the phase spectrum contains all information which can be obtained from electrical measurements, except the DC resistivity. Numerous investigations were done in the lab-scale on sandstone samples. Scott and Barker (2003) found a convincing correlation of dominant pore throat D_0 and the frequency at which the peak phase angle occurs for a range of sandstones obtained from sites across the UK. In doing so, large pore radii correlate with phases at low frequencies and small pore radii with phases at high frequencies. The determination of pore radii distribution is one of the most important parameters of Petrophysics. In order to determine the widest possible pore radii distribution with the method of Induced Polarization, the resistivity must, therefore, be measured over the widest possible frequency range.

Instrument and cable set-up

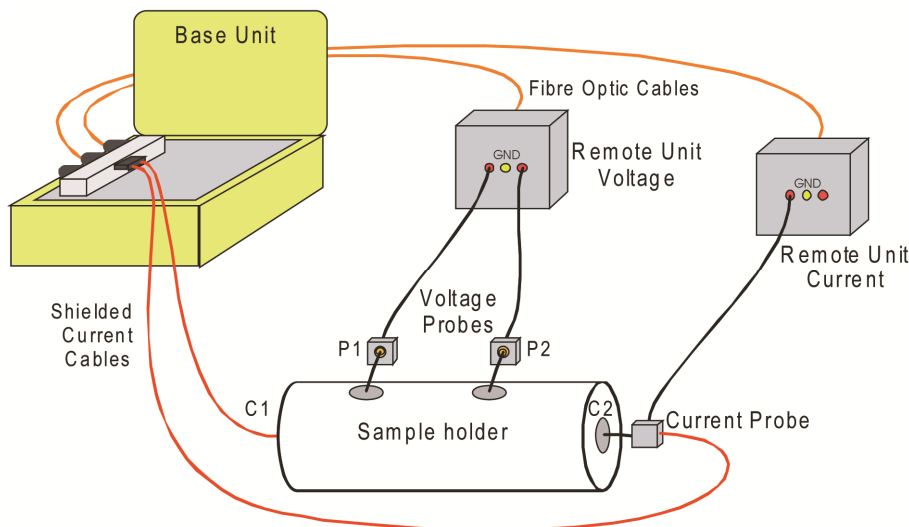


Fig. 1: Schematic diagram of the new instrument Chameleon. The base unit contains a signal source and transmitter. A minimum of two remote units digitize the analogue signals of the current and the voltage probes. The cylinder represents a container with sample material.

The expansion to high frequencies (up to 250 kHz) however, puts high demands on the measuring technique. For the measuring technique, the measuring instrument itself is important and also the indispensable measuring lines. To fulfil these requirements, we have developed a new type of measuring system called Chameleon (Fig. 1). We must demand a very high synchronicity of the measuring channels from the measuring instrument. In addition, unwanted couplings between them must be avoided. We achieve this through a physical separation of the system components. Optical fibres are used for data transfer and synchronisation; failing this, the required phase resolution would not be reached. Unwanted couplings can also appear between the measuring lines. These can be effectively stopped if the measuring lines are chosen to be as short as possible. Our measuring system permits the measuring electronics of every measuring channel to be placed directly at every electrode (here C2, P1, P2). An additional very important aspect for measurements at high frequencies is the input capacitance of the measuring electronics. With our apparatus it is just 1.5 pF. However, even this value is too high, as soon as the object has a low porosity or is unsaturated. As a rule both cause heighten the resistivity. This, together with the input capacitance,

has an effect like a low-pass filter on the resistivity measurement. Luckily, this effect can be almost exactly quantified and numerically compensated.

Case Study 1 - Sandstone Sample

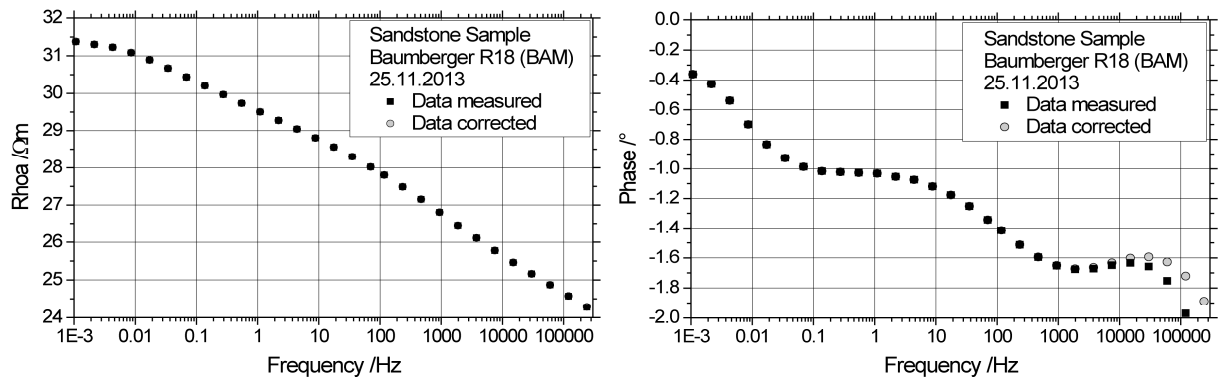


Fig. 2: Measured resistivity spectrum of a sandstone sample. Sandstone sample and sample holder were provided by Dr. S. Kruschwitz (BAM, Berlin).

Figure 2 shows a resistivity spectrum (amplitude and phase), which was measured from a fully saturated sandstone sample in our laboratory. The sandstone sample (Baumberger R18) as well as the sample holder were kindly supplied to us by Dr. S. Kruschwitz (Federal Institute for Material Research and Testing -BAM). Also shown next to the measured data (the black dots), are the corrected data, which are freed by effects from the input capacitance of the instrument (the red dots). The spectrum shows two phase maxima, one of which is at 0.2 Hz and another at 2 kHz. With regard to the directions given in the instructions, one can assume that this sample exhibits two dominant pore radii. The demonstrated maxima at 2 kHz, furthermore, shows that also at high frequencies relevant information exists about the pore space, and that we could clearly detect this with our new instrument Chameleon.

Case study 2 - Small-scale field measurement

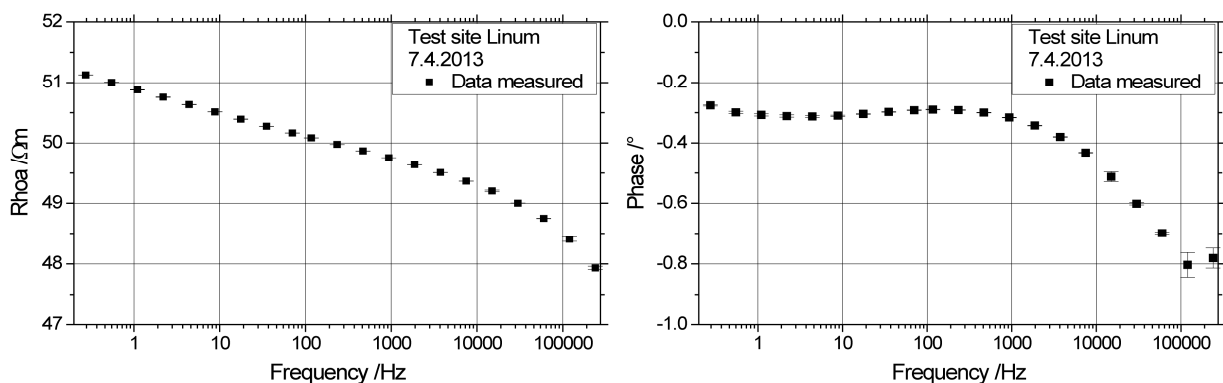


Fig. 3: SIP data measured at test site Linum (30 km north of Berlin). Squared array. Electrodes spacing: 1 m.

Figure 3 shows the result of spectral resistivity measurements at our test site Linum. The amplitude and phase were measured between 0.3 Hz and 250 kHz. For these measurements a squared array was used with an electrode space of 1 m. Despite the good conductivity of the ground, electromagnetic effects (inductive coupling, skin effect) can still be neglected by this small scale measurement set-up. The somewhat heighten error bar for both of the highest measured frequencies probably arises from disturbances from long wave range radio transmitters. The case study proves that the specific resistance with small-scale configurations can also be precisely measured at high frequencies. We see the application in the characterization of up to ~50 cm deep grounds. For example, information about the roots of trees and agricultural crops for food or bioenergy production can be obtained. We also see potential for application in archeology.

Reference

Scott, J.B.T. and Barker, R., 2003. Determining pore-throat size in Permo-Triassic sandstones from low-frequency electrical spectroscopy. *Geophys. Res. Lett.*, 30(9), 1450.

Cable arrangement to reduce EM coupling effects in spectral induced polarization studies

M. Schmutz⁽¹⁾, A. Ghorbani⁽²⁾, P. Vaudelet⁽³⁾ and A. Blondel⁽⁴⁾

(1) ENSEGID – IPB – EA 4592, Pessac, France

(2) Yazd University, Iran

(3) Terrascope, New Caledonia

(4) Geoscope, Cenon, France

Spectral induced polarization (SIP) is widely used for environmental and engineering geophysical prospecting and hydrogeophysics, but one major limitation concerns the EM coupling effect (Wynn and Zonge 1977; Wynn 1979). The phase angles related to EM coupling may increase even at frequencies as low as 1 Hz, depending on the ground resistivity, the array type and geometry.

To reduce EM coupling effects, one solution is to take into account the cable geometry and configuration. This has been done with the software CR1DMOD (Ingeman-Nielsen and Baumgartner 2006) – see Fig. 1. In a previous study we showed how to reduce, with the use of an appropriate cable arrangement, EM coupling effects both for modelling and for experimental data (Schmutz et al. 2014). In this presentation we try to explain why the software CR1DINV does not correct all the EM coupling effects: soil inhomogeneity, approximation in numerical resolution, non 1D medium, optic fibre (not taken into the modelling software account), cables modelled as for points.

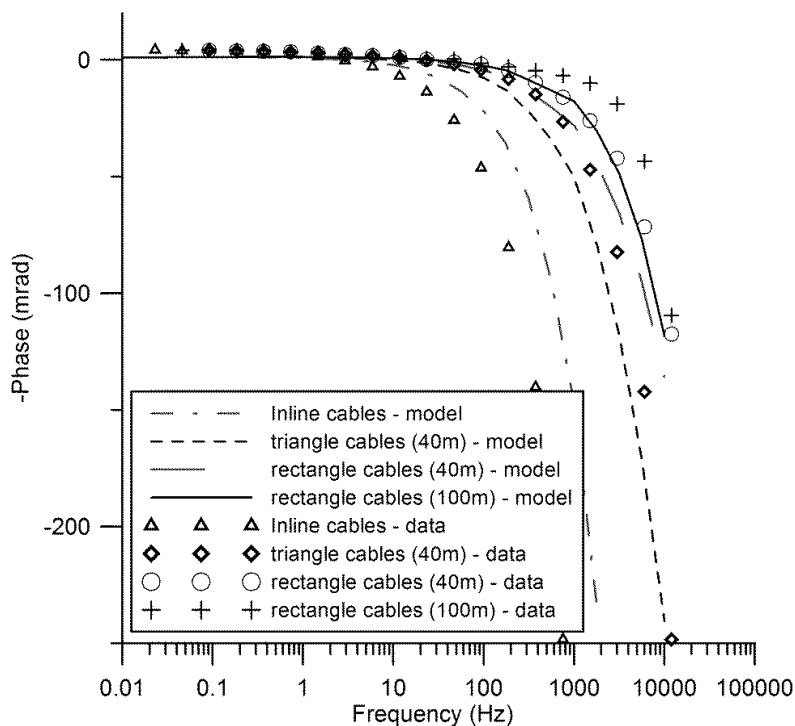


Fig. 1: Modelled and measured SIP phase spectra for Schlumberger array. Distance between the injection electrodes $AB = 30$ m and between the measurement electrodes $MN = 4$ m. The error bars are smaller than the symbol size. The solid lines are the spectra calculated by Cr1Dmod.

References

- Ingeman-Nielsen, T. and Baumgartner, F., 2006. A Matlab program to model 1D complex resistivity effects in electrical and electromagnetic surveys. *Comput. Geosci.*, 32, 1411-1419.
- Radic, T., 2004. Elimination of cable effects while multichannel SIP measurements. *10th Eur. Mtg. Env. Eng. Geophys. Exp. Abstr.*
- Schmutz, M., Ghorbani, A., Vaudelet, P. and Blondel, A., 2014. Reducing EM coupling effects in SIP studies. *Geophysics*, in press.
- Wynn, J.C., 1979. Electromagnetic coupling with a collinear array on a two-layer anisotropic Earth. *Washington, U.S. Govt. Print. Off.*
- Wynn, J.C. and Zonge, K.L., 1977. Electromagnetic coupling. *Geophys. Prospect.*, 25, 29-51.

Spectral induced polarization: frequency domain versus time domain

K. Titov⁽¹⁾, G. Gurin⁽¹⁾, A. Tarasov^{(1),(2)} and K. Akulina⁽¹⁾

(1) *St. Petersburg State University, St. Petersburg, Russia*

(2) *Rudgeofizika JSC, St. Petersburg, Russia*

Last decades, there has been a growing interest in the use of the Spectral Induced Polarization method in hydrogeology, contaminant hydrology, biogeophysics and mining geophysics. Field works are frequently carried out in a so-called Time Domain (TD), whereas the physics, which governs the IP phenomenon, is studied in lab conditions on the basis of Frequency Domain (FD) measurements. In FD, the complex dielectric constant, electrical conductivity (or its inverse, the resistivity) is measured in a wide frequency range (over 9 decades, from 1 mHz to 1 MHz, in laboratory conditions, and over 3 decades, from 0.1 to 100 Hz, in field conditions). For the resistivity, measurements are based on the Ohm's Law,

$$U(f) = \frac{1}{K} \rho(f) I(f), \quad (1)$$

where $U(f)$, $I(f)$ and $\rho(f)$, are the voltage, current and resistivity, respectively, f is the frequency and K is the geometrical factor.

In TD, voltage decays after cut-off of the electrical current are measured. The current waveform is a sequence of pulses of opposite polarity and pauses of the same duration. Decays after pulse sequences of different duration are obtained to cover three to six decades of time. Measurements are again based on the Ohm's Law, which is presented in the form of convolution,

$$U(t) = \frac{1}{K} \int_0^{\infty} \rho(t_0) I(t-t_0) dt_0, \quad (2)$$

where t is the time after switching the DC on, and t_0 is the integration variable.

From theoretical point of view, FD data are easier to interpret just because the product in Eq. (1) is simpler than the convolution in Eq. (2). Moreover the phase IP spectra frequently contain maxima, which is easier to analyze, comparing monotonous IP decays. However TD measurements are an attractive alternative because they are less time consuming than FD measurements. Table 1 presents IP parameters in TD and FD.

To date there is no universal link between the parameters measured in TD and FD. This link can be obtained on the basis of data fitting to empirical models (e.g., the Cole-Cole model). Then, on the basis of the model parameters, IP responses in FD or TD can be calculated. However these models are not universal.

We suggest using a Debye decomposition approach to link spectral data obtained in TD and FD. The Debye decomposition allows deconvolution of an IP signal to a sum of elementary polarizing responses describing by the Debye relaxation model and with different relaxation times. Distribution of magnitude of the Debye responses as a function of the relaxation time is obtained with DD. Although this approach is phenomenological it is universal because it can be applied to any type of data in FD and TD.

We applied the Debye decomposition approach to three datasets obtained in both TD and FD. These datasets are: (1) synthetic data calculated for an RC circuit shown in insert to Fig. 1b; (2) experimental data obtained on the same circuit; and (3) data measured on a mixture of calibrated commercial sand ($r = 0.2 \dots 0.3$ mm) and 10 % of commercial lead shot ($r = 2.2$ mm) saturated with NaCl solution ($\rho = 70 \Omega\text{m}$). Figure 1 shows the respective relaxation time distributions.

For the synthetic test (Fig. 1a) the RTDs obtained from FD and TD are very close, for the experimental test (Fig. 1b) the difference between them slightly increases, and for the experiment with lead shot the difference increases again. However for these three datasets the agreement between two types of RTD is reasonable. Only for the lead shot experiment the peak relaxation time values obtained from FD and TD data differ by a factor of about 2.5. This difference between RTD obtained on the basis of FD and TD data occurs because the Debye decomposition approach

resolves an ill-posed problem. However in the forward modelling both type of RTD allow robust calculation of TD and FD data. We suggest therefore the Debye decomposition approach as the link between FD and TD data. Based on RTD, FD data can be easily transformed to TD data and vice versa.

Parameter		Type of parameter
TD	FD	
Polarizability $\eta(t) = U(t)/U_0$, $U(t)$ and U_0 are the off-time and on-time voltages, respectively	Phase $\varphi = \arctan(\rho''/\rho')$, ρ' and ρ'' are the real and imaginary components of the resistivity, respectively	Local
Chargeability $m = \frac{1}{t_{\max} - t_{\min}} \int_{t_{\min}}^{t_{\max}} \eta(t) dt$, $ t_{\max} - t_{\min} $ is the integration time	Frequency effect $FE = \frac{\rho_{lf} - \rho_{hf}}{\rho_{lf}}$, ρ_{lf} and ρ_{hf} are the resistivity values at low and high frequencies, respectively	Partial
Normalized chargeability $m_n = m/\rho \sim \sigma''$	Metal Factor $MF = FE/\rho \sim \sigma''$, σ'' is the imaginary component of the conductivity	Normalized partial
Total chargeability, obtained numerically from the Debye Decomposition approach	Total chargeability $M = \frac{\rho_0 - \rho_\infty}{\rho_0}$, ρ_0 and ρ_∞ are the low and high frequency asymptotes of the resistivity, respectively	Global
Normalized total chargeability	Normalized total chargeability $M_n = \frac{\rho_0 - \rho_\infty}{\rho_0^2}$	Normalized global
Polarizability vs. time	Phase vs. frequency	Spectral

Table 1. IP parameters in FD and TD.

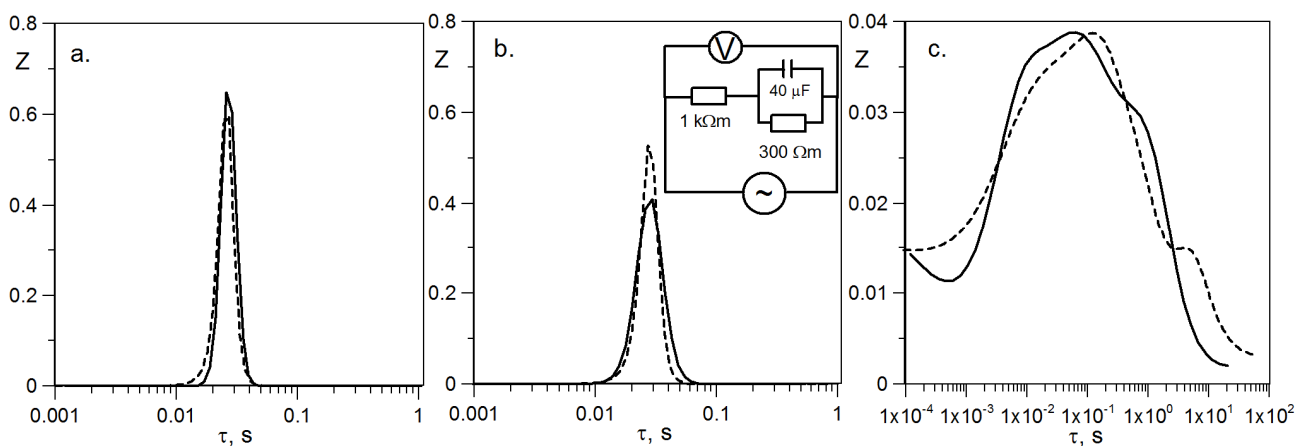


Fig. 1: Relaxation time distributions obtained for synthetic (a) and experimental (b) RC-tests and the lead shot experiment (c). Solid and dashed lines are RTDs obtained from FD and TD data, respectively.

Numerical modelling of electromagnetic coupling effects in EIT borehole measurements

E. Zimmermann⁽¹⁾, Y. Zhao⁽¹⁾, J.A. Huisman⁽²⁾, A. Treichel⁽²⁾,
B. Wolters⁽¹⁾, S. van Waasen⁽¹⁾ and A. Kemna⁽³⁾

(1) *Central Institute for Engineering, Electronics and Analytics, Electronic Systems (ZEA-2),
Forschungszentrum Jülich GmbH, Germany*

(2) *Institute of Bio- and Geosciences, Agrosphere (IBG-3), Forschungszentrum Jülich GmbH,
Germany*

(3) *Department of Geodynamics and Geophysics, University of Bonn, Germany*

The measurement of the impedance of low-polarizable soils and rocks in the mHz to kHz range with sufficient phase accuracy requires advanced data correction methods in addition to a sophisticated EIT measurement system. Several different electromagnetic effects currently limit the useable upper frequency range of the measured impedance to some tens of Hz in borehole EIT applications. In this presentation, we aim to discuss how improved EIT data acquisition and effective error correction procedures can be used to achieve higher phase accuracy for borehole EIT measurements in the frequency range between 10 Hz to 45 kHz.

EIT data acquisition was performed using a prototype spectral EIT system optimized for field applications. The prototype is based on a laboratory spectral-EIT measurement system with high phase accuracy. This laboratory system uses electrode modules with amplifiers for potential measurement and relays for current injection in order to minimize the capacitive load at the electrodes and to improve measurement accuracy. For EIT borehole measurements, similar electrode modules were integrated in electrode chains that consist of 25 m long shielded multicore cables each with eight electrode modules with a separation of one meter. In addition to the optimized system design, model-based numerical correction methods are used to remove several errors introduced by amplification errors, signal drift, current measurement errors, the propagation delay of the signal due to the long cables and other system dependent sources. Although these corrections improve the quality of the EIT measurements, a main source of errors in EIT field measurements above 10 Hz is the electromagnetic coupling associated with the long electrode chains and this error source will be treated in this study. Electromagnetic coupling consists of phase errors introduced by inductive coupling between the wires of electrode chains and phase errors due to capacitive coupling between the cable shield and the electrically conductive subsurface.

In the case of inductive coupling, the injected current induces a voltage in the wires used for potential measurement. This voltage is linearly added to the resulting voltage of the 'true' subsurface impedance Z_s , but with a phase shift of 90° and it therefore introduces a large phase error. The additional part of the induced voltage in the measured transfer impedance $Z = Z_s + j\omega M$, which is the quotient of the measured voltage and the injected current, is the mutual inductance M between the wires used for current injection and potential measurement. This shows that the measured transfer impedances can be corrected to obtain the subsurface impedance of interest by determining the mutual inductance. Therefore, we developed a method to determine the mutual inductance based on numerical modelling combined with calibration measurements. We differentiate two cases: i) coupling between wires in one borehole cable with small separations in the mm range and ii) coupling between different borehole cables with large separation in the m range. The mutual inductances between wires of different chains can be calculated numerically based on the position of the cable layout in the field. Sensitivity studies showed that the cable positions need to be known with cm accuracy only. To determine the inductance between wires in one chain, a calibration method is used because numerical calculations were not accurate enough due to insufficient knowledge of the positions of the wires in a multi-core cable. This calibration only needs to be performed once, since the mutual inductance is independent of the subsurface electrical conductivity and the wire positions are fixed within a single multi-core cable. In order to

correct the measurements of any configuration with two or more electrode chains, the different contributions to the mutual inductances are combined in a single universal pole-pole matrix. This enables the simple calculation of the mutual inductance for EIT field measurements using two electrodes for current injection and two electrodes for voltage measurement, because the mutual inductance now is a simple linear combination of the elements of the pole-pole-matrix corresponding with the current and potential electrodes.

The second source of errors is due to the capacitive currents between the soil and the shield of the cables. Due to the thin isolation of the multicore cables, these capacitances are relatively large ($\sim 1200 \text{ pF m}^{-1}$). The effect of this capacitance on the measured transfer impedances cannot be corrected a priori as in the case of inductive coupling because these parasitic currents depend on the unknown subsurface electrical conductivity distribution. To account for capacitive coupling, the complex admittance matrix of the forward electrical model is enhanced with additional admittances of the capacities of the cable segments. This enhanced admittance matrix is used for the forward modelling of the potential distribution in order to reconstruct the subsurface electrical conductivity.

In a first step, the developed correction methods were verified with borehole EIT measurements in water. The achieved accuracy in this controlled set-up was 1 mrad at 10 kHz using one electrode chain and 1 mrad at 1 kHz using two electrode chains. To demonstrate the method for actual subsurface characterization, borehole EIT measurements were made in a heterogeneous aquifer at the Krauthausen test site. The depth profiles reconstructed with 3D forward modelling and 1D inversion clearly showed the necessity of the correction for inductive coupling. The effect of the correction for capacitive coupling is also noticeable but much smaller (see Fig. 1). The presented work clearly is a major step towards more accurate borehole EIT measurements for frequencies above 10 Hz.

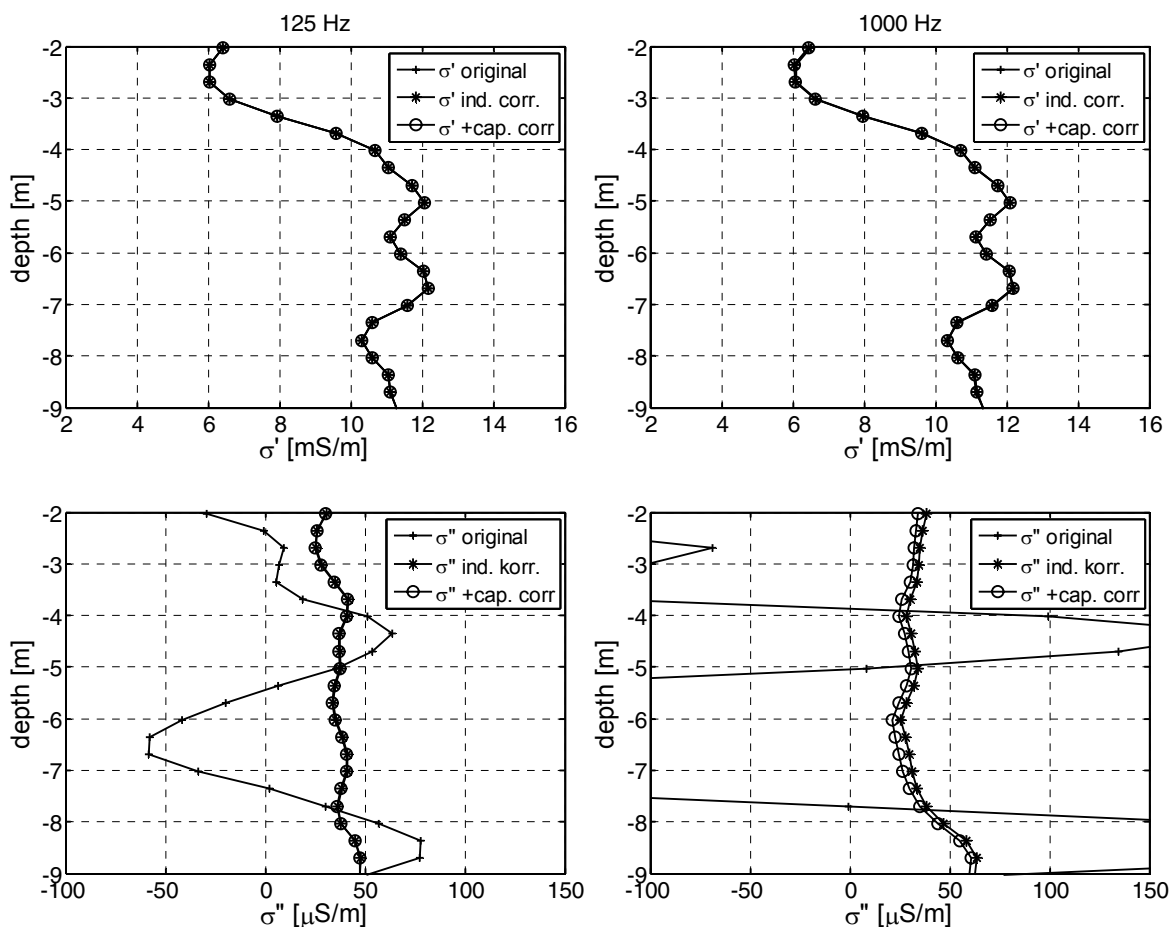


Fig. 1: Depth profiles of real (top) and imaginary (bottom) conductivity at 125 Hz (left) and 1 kHz (right) as obtained from borehole EIT measurements at the Krauthausen test site with and without corrections for inductive and capacitive coupling using a 1D inversion scheme.

On the application of differential phase parameter in spectral IP

N. Zorin⁽¹⁾

(1) *Moscow State University, Moscow, Russia*

Differential phase parameter (DPP) was brought forward in late 1970's and since then has been successfully used for suppression of inductive noise in IP phase measurements. In the near-field zone approximation, the phase shift of electric signal due to inductive effects in medium is directly proportional to frequency (Hallov 1974). In this context DPP was constructed in such a way that it eliminates the linear component of the phase shift, leaving the frequency-independent component untouched. Hence, DPP was originally invented for the constant phase angle (CPA) model of IP spectrum. We show the usefulness of DPP in more general case, when the IP phase curve is represented by a superposition of those of several models such as CPA and Cole-Cole. By doing so, we significantly expand its application area.

For two frequencies ω_1 and ω_2 DPP is defined as an operator Δ , which acts on an arbitrary continuous function $\varphi(\omega)$ as follows (Kulikov and Shemyakin 1978):

$$\Delta\varphi(\omega_1, \omega_2) \stackrel{\text{def}}{=} \frac{\varphi(\omega_1)\omega_2 - \varphi(\omega_2)\omega_1}{\omega_2 - \omega_1}. \quad (1)$$

Using the definition (1) it could be easily shown, that for any set of functions $\varphi_k(\omega)$ and coefficients a_k the following statements hold:

$$\Delta\left(\sum_k a_k \varphi_k\right) = \sum_k a_k \Delta\varphi_k, \quad (2)$$

$$\Delta(a_k) = a_k \text{ and} \quad (3)$$

$$\Delta(\omega a_k) = 0. \quad (4)$$

Thus, operator Δ turns out to be linear (2) and does not affect the constant part of the signal (3) while entirely suppressing its linear component (4). These properties of DPP shows that it may be successfully used to extract the IP phase value φ_{ip} from the phase $\varphi(\omega)$ of the measured electric signal if the former is virtually frequency-independent: in this case the value of $\Delta\varphi(\omega_1, \omega_2)$ equals to φ_{ip} for any frequencies ω_1 and ω_2 .

Although the CPA model has found its application in practice – for example, it describes well the IP spectra of some highly dispersive in grain size sedimentary deposits (Börner et al. 1993) – its field of use remains limited since most types of rocks show the frequency-dependent behaviour of IP phase and thus require alternative models to describe them. The highest popularity among such models was gained by the Cole-Cole function (Pelton et al. 1978), whose phase curve on logarithmic plot has a peak and two smooth branches, symmetrically tending towards zero. Chargeability η primarily affects the amplitude of the phase curve, time constant τ the peak frequency, and exponential parameter C the spectral width of the response. In case of asymmetrical phase behaviour one could use the so-called generalized Cole-Cole model (Pelton et al. 1983), with an additional independent parameter a .

In practice, the actual IP phase curve over an arbitrary geological section usually could be approximated with reasonable accuracy by that of one of the mentioned models or by their superposition. To get an idea of the distorting influence of DPP on a weighted sum of model curves (regarding the linearity of operator Δ and its perfect applicability to the CPA model), it is sufficient to give a consideration to its influence on a stand-alone Cole-Cole function. For that purpose we used the most popular in practice form of DPP with $\omega_2 = 3\omega_1$ and a Cole-Cole model with $\eta = 0.2$ and a set of C from 0.2 to 0.5. Chargeability was fixed in the modelling as it barely affects the IP curve shape, while the chosen range of C is typical for vast majority of rocks with most common

values from 0.2 to 0.35 (Pelton et al. 1978; Seigel et al. 1997). The result is given on Fig. 1.

It is clearly seen from Fig. 1 that for small C the Cole-Cole phase curve (solid line) virtually coincides with the DPP curve (dashed line). With a rise of parameter C the curvature of the Cole-Cole line increases, resulting in larger misfit with the corresponding DPP graph. It is also notable that this misfit tends to give the DPP curve more “contrast” – with slightly overestimated peak value and increased branch steepness. It is thus important to understand that for large C the resulting curve is not of the Cole-Cole type anymore, but some of its distinctive features such as spectral width or peak frequency remain almost the same or change negligibly.

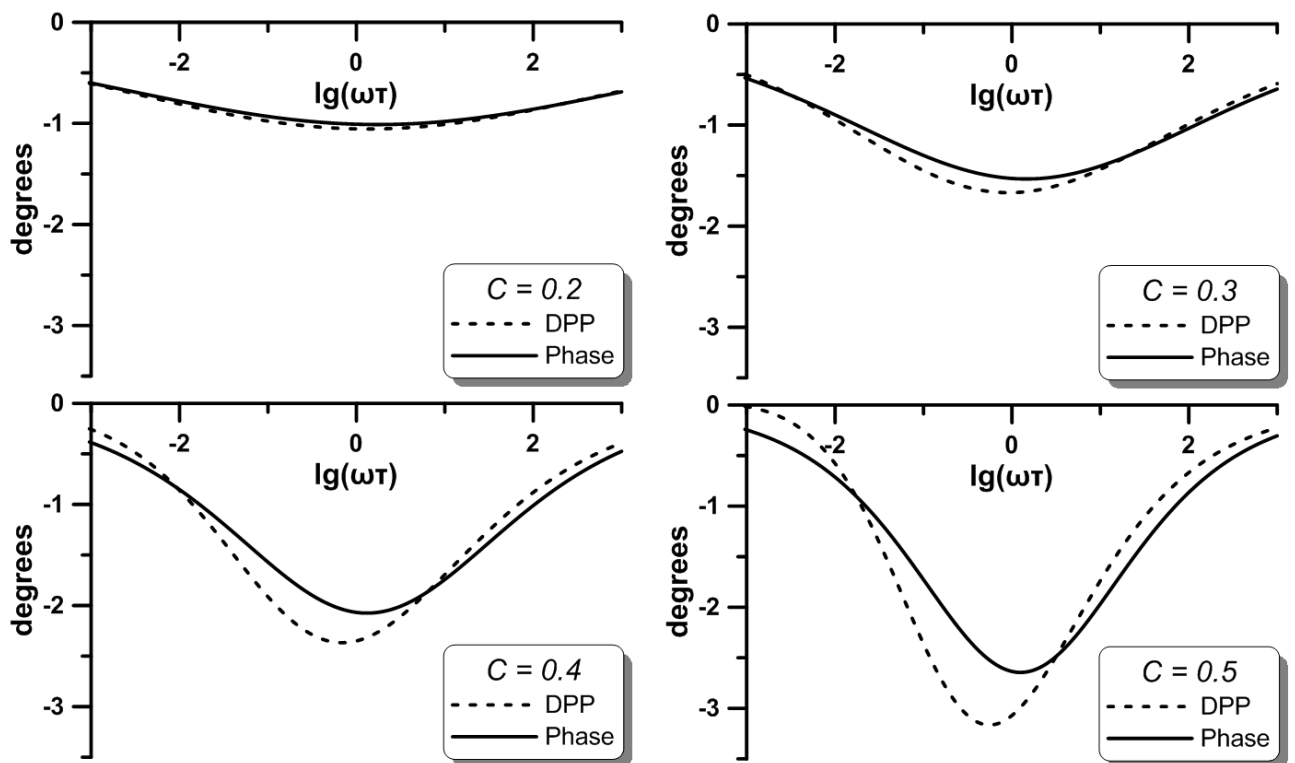


Fig. 1: Comparison between Cole-Cole phase curves ($\eta = 0.2$) and corresponding DPP curves.

To summarize, it may be concluded that DPP could be successfully applied not only for measurements of frequency-independent IP phase values, but also for discrimination of rocks distinguished by the standard IP parameters such as τ and C . Furthermore, by virtue of having more contrast, DPP curve may turn out to be even more useful than the IP curve itself. Taking into account high accuracy of obtained data and the significant suppression of inductive noise, it makes differential phase parameter a powerful instrument of low frequency electromagnetic prospecting.

References

- Börner, F.D., Gruhne, M. and Schön, J.H., 1993. Contamination indications derived from electrical properties in the low-frequency range. *Geophys. Prospect.*, 41, 83-98.
- Hallof, P.G., 1974. The IP phase measurement and inductive coupling. *Geophysics*, 39, 650-665.
- Kulikov, A.V. and Shemyakin, E. A., 1978. Geoelectric prospecting using phase method of induced polarization (*in Russian*). Nedra press, Moscow, 157 p.
- Pelton, W.H., Ward, S.H., Hallof, P.G., Sill, W.R. and Nelson, P.H., 1978. Mineral discrimination and removal of inductive coupling with multifrequency IP. *Geophysics*, 43, 588-609.
- Pelton, W.H., Sill, W.R. and Smith, B.D., 1983. Interpretation of complex resistivity and dielectric data. Part I. *Geophys. Trans.*, 29, 297-330.
- Seigel, H.O., Vanhala, H. and Sheard, S.N., 1997. Some case histories of source discrimination using time-domain spectral IP. *Geophysics*, 62, 1394-1408.

SESSION 3

IP FOR GEOPHYSICAL CASE STUDIES

Characterization of a landfill using 2D time domain SIP

E. Auken⁽¹⁾, G. Fiandaca⁽¹⁾, A.V. Christiansen⁽¹⁾ and A. Gazoty⁽¹⁾

(1) Aarhus University, Department of Geoscience, Denmark

Landfills are, or have been, the primary choice for municipal solid waste disposal in many parts of the world, as landfilling is seen as an easy and low-cost waste management option. Many landfills operational from 1950-1980 were designed without any kind of capture system underneath, leading to percolation through the waste and into the underlying geological layers and aquifer systems. Furthermore records of waste types and the deposited amount are often missing for old landfills. For large areas, it is very expensive to gain information on the landfill delineation using only drillings, and geophysics can be used for improving the knowledge in the whole area of interest. This work presents the characterization of the Risby landfill (Denmark) by a dense coverage of direct current (DC) and time-domain spectral induced polarization (SIP) profiles.

Risby landfill is an old and closed landfill that was used by the public authorities from 1959 to 1981 and privately by the Danish Forest and Nature Agency from 1981 to 1985. It is located in the vicinity of Copenhagen, on the island of Zealand, Denmark. No records explicitly report the waste types and the deposited amount, but aerial photos from 1945-1985 indicate the landfilling sequence. Furthermore, the aerial photos show that the landfill was placed on top of the old terrain without excavation.

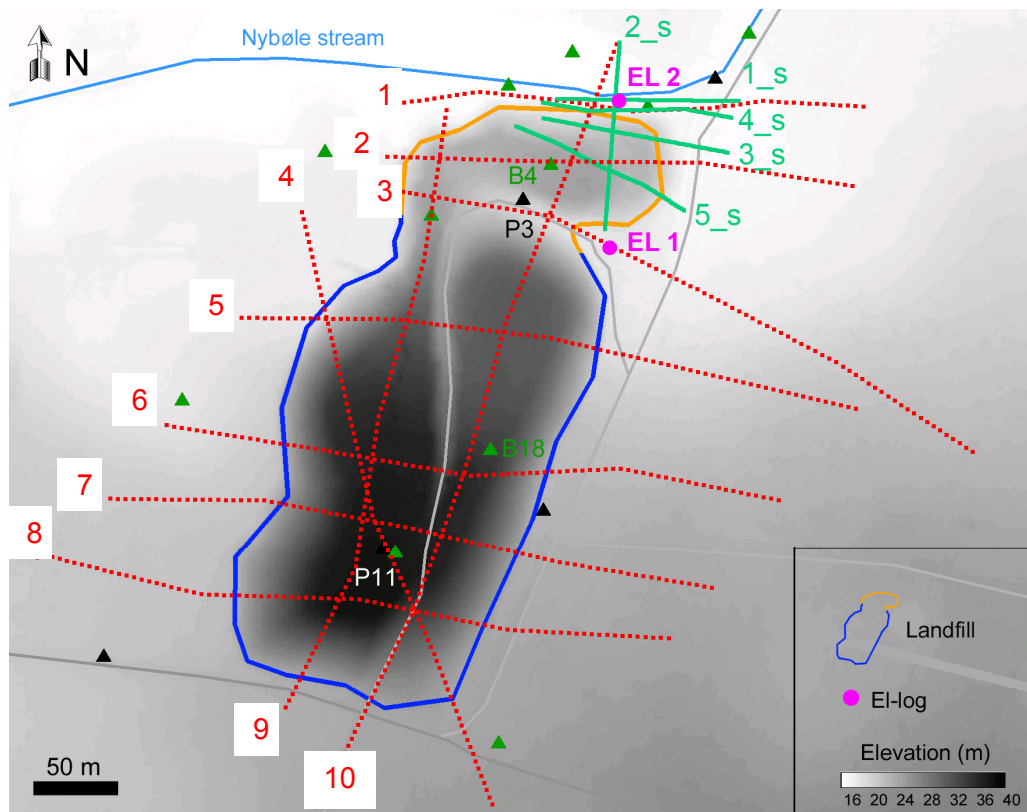


Fig. 1: Risby landfill and acquired profiles. Dotted lines: profiles with 5 m electrode spacing. Continuous lines: profiles with 1.5/1.0 m electrode spacing. Triangles: boreholes with lithology information. Circles: boreholes with in-borehole DC/IP measurements.

The survey consisted in the collection of 15 DC/IP profiles with electrode spacing of 5 m (Fig. 1, dotted lines) and 1.5 m (continuous lines, Fig. 1). Furthermore, 2 electrical loggings were carried out, with in-situ measurement of DC/IP data (Fig. 1, circles). The Syscal-Pro instrument (Iris Instruments) was used for the survey, with 4 seconds on- and off-time for current injection and 20

log-spaced time gates per quadrupole.

The DC data and the full IP decays have been inverted in 2D in terms of Cole-Cole parameters for extracting spectral information with AarhusInv, following Fiandaca et al. (2013). The inversion results have been compared with borehole information and the pre-landfill topography, obtained by kriging the DEM elevation at the landfill surroundings together with the waste/terrain interfaces in the boreholes P3, P11, B4 and B18 (Fig. 1).

The chargeability m_0 sections show anomalies with high values above the pre-landfill terrain (Fig. 2), where waste is present in the boreholes. In the north part of profile p10 and in profile p1 the chargeability anomalies appear below the pre-landfill topography and in situ DC/IP measurements (EL 2 in Fig. 2) confirm high-chargeability values below the waste, in a sand layer with polluted water. On the contrary, the resistivity sections do not show a good correlation with the waste thickness from boreholes nor with the pre-landfill topography.

These results highlight the added value of induced polarization in landfill characterization, when compared to the direct current method alone.

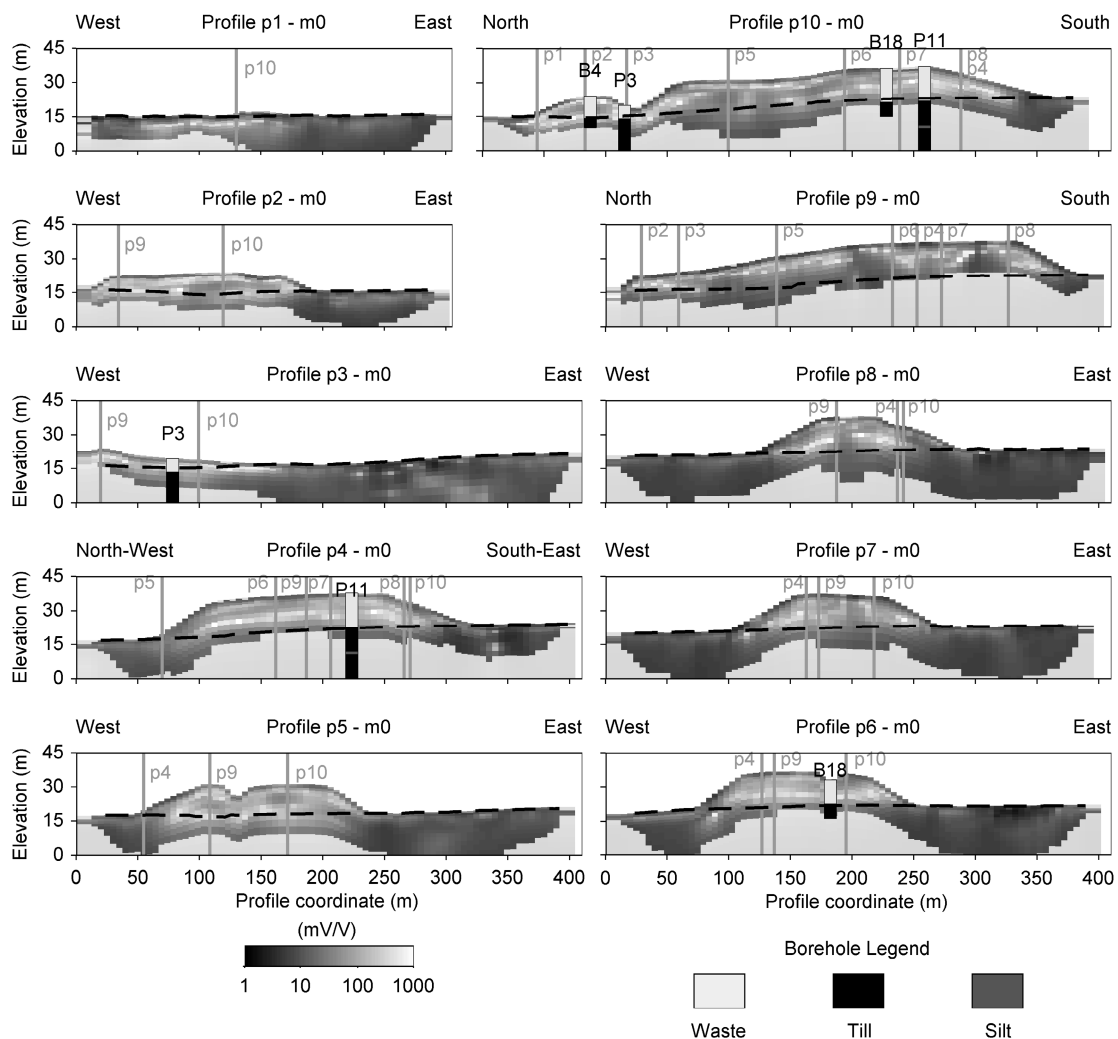


Fig. 2: Chargeability (m_0) sections for all the profiles with 5 m electrode spacing. Black dashed lines: pre-landfill topography. Grey vertical lines: crossing of profiles. Grey shading: poorly resolved area.

Reference

Fiandaca, G., Ramm, J., Binley, A., Gazoty, A., Christiansen, A.V. and Auken, E., 2013. Resolving spectral information from time domain induced polarization data through 2-D inversion. *Geophys. J. Int.*, 192, 631-646.

Case of study of a hydrocarbon contaminated site using the spectral induced polarization method: contribution of laboratory measurements for the interpretation of field results

A. Blondel^{(1),(2)}, M. Schmutz⁽¹⁾, M. Franceschi⁽¹⁾, M. Carles⁽¹⁾ and F. Tichané⁽³⁾

(1) *ENSEGID, EA4592 G&E, University of Bordeaux, France*

(2) *GEOSCOPE, 11 impasse Brunereau, 33150 Cenon, France*

(3) *TEREO, 11 impasse Brunereau, 33150 Cenon, France*

A geoelectrical study was initiated in 2012 in order to delineate a massive hydrocarbon spill, which occurred because of a petroleum pipe breakdown in 2009. These measurements have been compared with both field resistivity measurements made in 2009 and with laboratory measurements made on the petroleum oil at different stages of biodegradation.

From a physicochemical point of view, a hydrocarbon contamination has to be understood as a spatially and temporally varying object, responsible for a change in geoelectrical response (Atekwana et al. 2000; Sauck 2000; Revil et al. 2012). The pipe breakdown in 2009 has impacted a surface of 60 000 m². The initial contamination infiltration has created a residual zone that can be defined as the zone which presents a residual saturation of petroleum oil. According to Lee et al. (2001), this zone is the most favourable to the degradation of hydrocarbons by bacterial processes. Since 2010, a free phase of petroleum oil is also present at the top of the water table, with a maximal thickness of 1 m, at depths comprise between 8 and 11 m.

In a first time, to evaluate the evolution of the geoelectrical signal, laboratory induced polarization measurements were performed on a well-constrained sandy medium with both fresh and partially biodegraded petroleum oil, extracted from the site in 2012. The fresh oil (oil F) has been taken from the free-phase and seems not to be degraded. The partially degraded oil (oil B) has been taken from the top of a recovery tank where active biodegradation occurs. The non-degraded oil shows an increase in resistivity, normalized chargeability and quadrature conductivity with oil content (Fig.1). On the contrary, the partially biodegraded oil a slight decrease in resistivity but no modification of the phase-lag and chargeability parameters. According to the degradation state of the petroleum oil, different electrical behaviours are measured: the increase of the degradation state of the oil causes a modification of its physical properties.

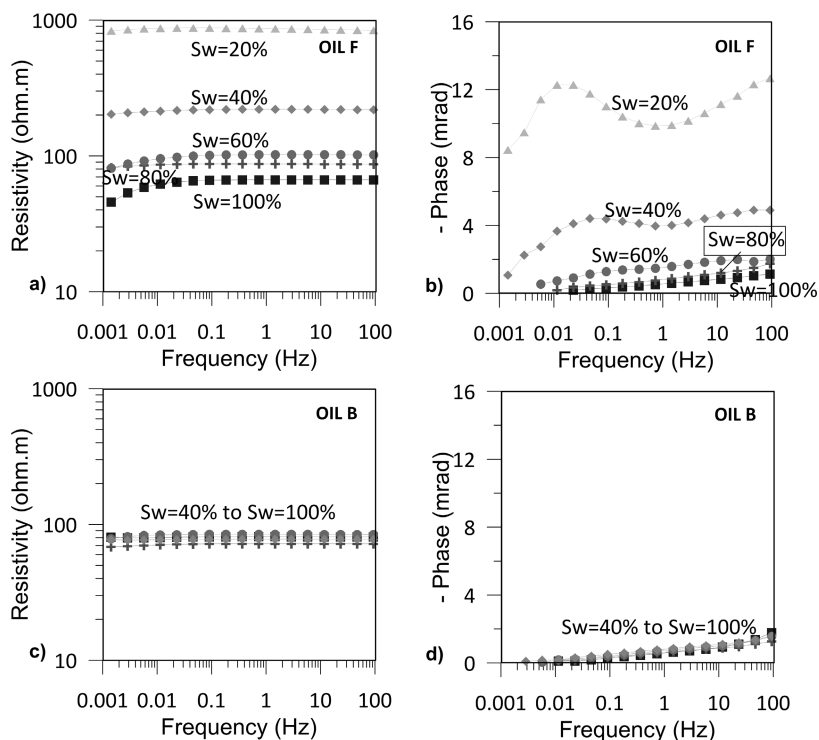


Fig. 1: SIP laboratory measurements acquired for non degraded Oil F: a) resistivity vs. frequency, b) phase-lag vs. frequency; and for partially degraded Oil B: c) resistivity vs. frequency, d) phase-lag vs. frequency.

On a second time, field measurements have been performed. Resistivity measurements were performed in 2009, just after the pipe breakdown. Only weak changes in the resistivity have been measured over the contaminated area (Fig.2). Resistivity measurements have also been made in 2012, three years after the pipe breakdown. It appears that the resistivity values in the residual zone are lower compared to the non-contaminated area. Moreover, over the contaminated area, in the first 10-m depth, we can notice a decrease of 40 % of the resistivity values between 2009 and 2012.

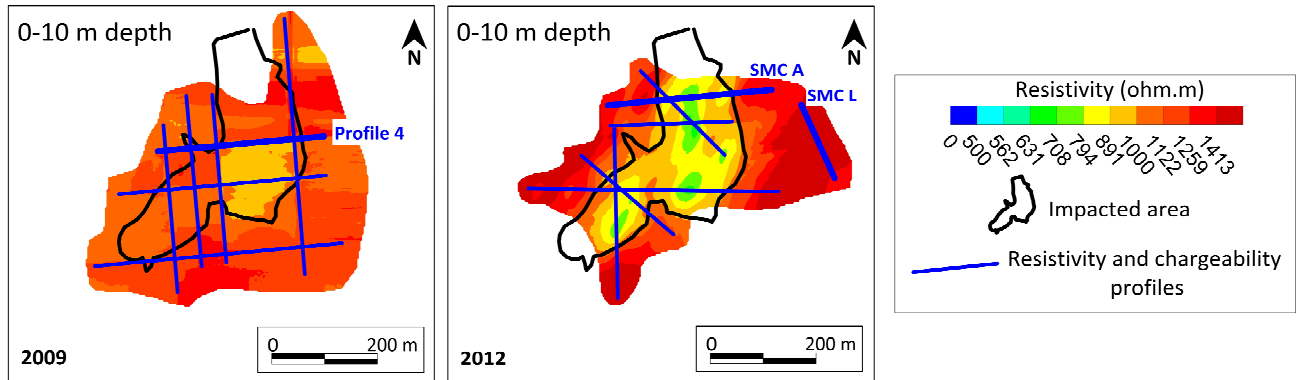


Fig. 2: Evolution of the resistivity values of the 0 □ 10 m deep slice for the period 2009-2012.

Actually, between 2009 and 2012, the bacterial degradation of the oil in the residual zone has caused an evolution of the physicochemical properties of the oil. This statement is confirmed by the laboratory measurements. Besides, bacterial processes produce conductive by-products, as bicarbonate ions, which modify the DC electrical resistivity measured on the field.

Temporal induced polarization tomographies have also been performed in 2012. No evolution has been noticed between the contaminated area and the non-contaminated area, neither for the chargeability parameter nor for the normalized chargeability parameter. Chargeability parameters seem not to be impacted by the presence of contamination or by its biodegradation, in spite of the presence of bacterial populations.

These observations led us to the conclusion that to made efficient geoelectrical measurements in the field, it is necessary to know whether the majority of the oil is non-degraded or degraded.

In the present study case, there is no need to acquire chargeability and phase-lag parameters to locate the contamination in the field, as they do not undergo any change. Nonetheless, chargeability parameters have been useful in this study case to characterize the lithological geometry.

On the other hand, the resistivity parameter is a good indicator of the presence of partially biodegraded oil. Resistivity measurements have led us to precisely locate contamination contours.

References

- Atekwana, E.A., Sauck, W.A. and Werkema, D.D., 2000. Investigations of geoelectrical signatures at a hydrocarbon contaminated site. *J. Appl. Geophys.*, 44, 167-180.
- Lee, J.-Y., Cheon, J.-Y., Lee, K.-K., Lee, S.-Y. and Lee, M.-H., 2001. Factors affecting the distribution of hydrocarbon contaminants and hydrogeochemical parameters in a shallow sand aquifer. *J. Contam. Hydrol.*, 50, 139-158.
- Revil, A., Atekwana, E., Zhang, C., Jardani, A. and Smith, S., 2012). A new model for the spectral induced polarization signature of bacterial growth in porous media. *Water Resources Res.*, 48, W09545.
- Sauck, W.A., 2000. A model for the resistivity structure of LNAPL plumes and their environs in sandy sediments. *J. Appl. Geophys.*, 44, 151-165.

TDIP imaging of watershed over crystalline basement

C. Camerlynck⁽¹⁾, L. Longuevergne⁽²⁾ and C. Roques⁽²⁾

(1) Sorbonne Université, UPMC-Université Paris 6, UMR 7619 Metis, Paris, France

(2) Université Rennes 1, Géosciences Rennes, UMR 6118, Rennes, France

Aquifers located in Brittany (Western France) are set over crystalline geology. Water is generally flowing through highly permeable fractures. We show the TDIP potentiality in picturing hydro-geophysical contexts. Those preliminary results need now to be confirmed by both sample measurement and in-situ characterizations.

Saint-Brice-en-Cogles (Northern Brittany, N48.422°, W1.377°)

The geological context comprises fractured schists with granite inclusions, located on a granite basement. Normal faults from Caledonian to Hercinian era define a horst/graben situation (Fig. 1). A borehole drilled thanks to the CASPAR program produced 43 m³ h⁻¹ during a preliminary pumping test, showing the high potentiality for consumable water production.

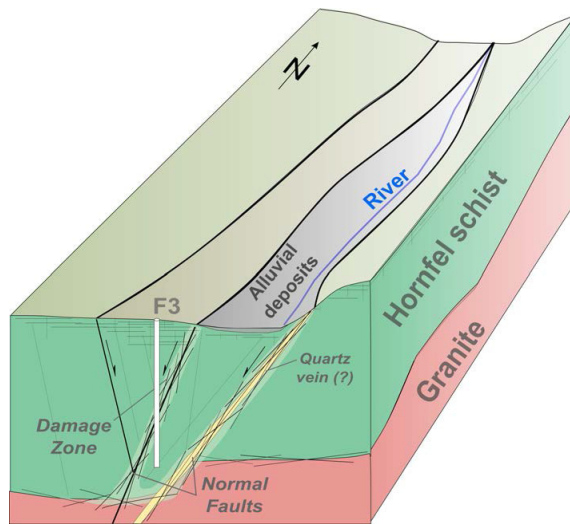


Fig. 1: Block diagram showing the aquifer situation.

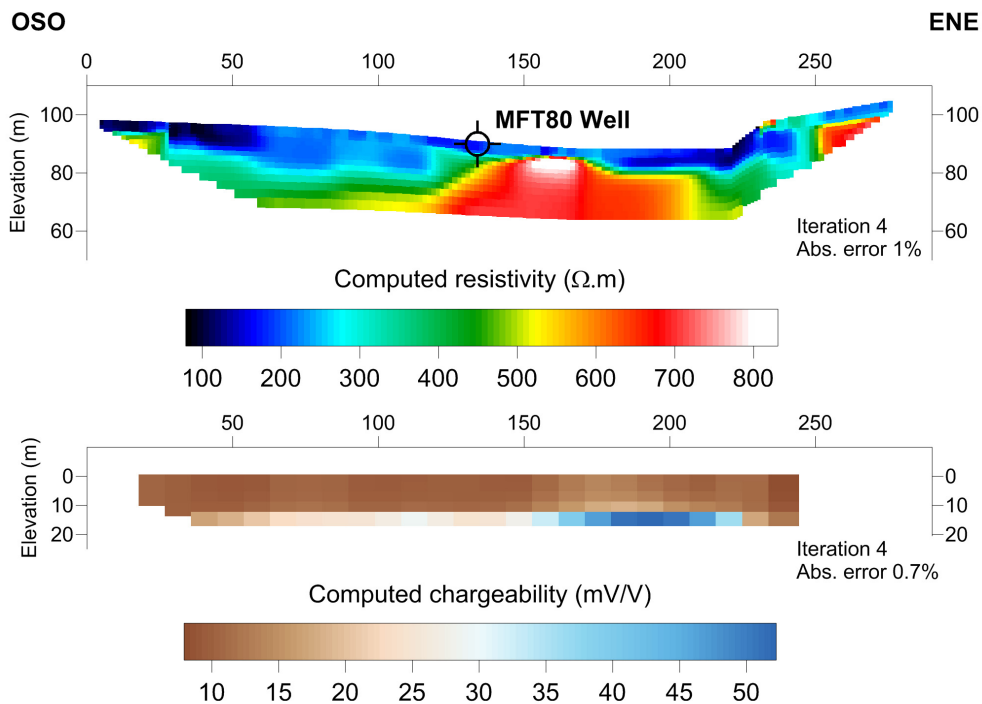


Fig. 2: Saint-Brice. a) Computed resistivity (Wenner-Schlumberger array, inter-electrode spacing = 3m). b) Computed chargeability (dipole-dipole array, inter-electrode spacing = 3 m).

Several electrical resistivity tomographies were performed in the west-east direction (Fig. 2). While the resistivity tomography shows a striking picture of the recharge zone associated with a conductive anomaly, the TDIP results make not coincide the highest chargeability with the MFT80 borehole location (close to productive F3 borehole) in which pyrite have been seen associated with fracturing in drilled sample. The association of fractures (so hydraulic transmissivity) with high chargeability response linked to pyrite is therefore to be discussed, with probable oxidation phenomena clearly visible on core drilling samples (Fig. 3).



Fig. 3: MFT80 core drilling. Oxidized (top, from 25 m depth) and unaltered (bottom) schist samples.

Guidel (Southern Brittany, N47.755°, W3.481°)

An unexploited aquifer could be considered in a pristine state, at the opposite of the more well-known Ploemeur aquifer located some kilometres to the east and pumped for the last 30 years. At least one borehole shows some artesian condition. A wet zone is probably supplied from below, with surface water properties very similar to those of deep water. Electrical resistivity tomography shows a discrepancy between resistivity and chargeability, both in measurements and inverted values (Fig. 4). We think that higher permeability and water circulations can be associated with a decreasing of induced polarization properties, probably through oxidation of polarisable materials.

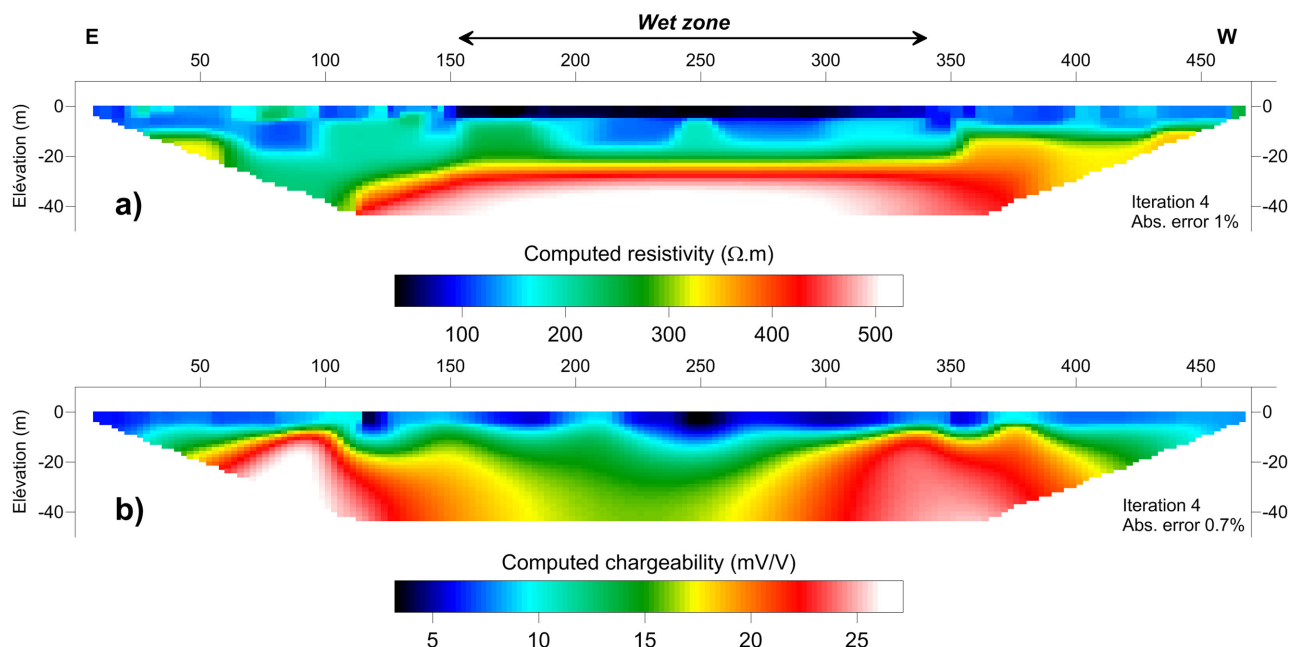


Fig. 4: Guidel (Wenner-Schlumberger array, inter-electrode spacing = 5m).
a) Computed resistivity. b) Computed chargeability.

Synopsis of mapping buried waste with IP effects

N. Carlson⁽¹⁾ and N. Bouzid⁽¹⁾

(1) Zonge International, Inc.

Although induced polarization (IP) effects measured over landfills were first discussed in a 1974 article in the journal *Science* (Angoran et al. 1974), it was assumed at the time that the primary source of the IP effect was metallic debris in the waste. For almost 20 years now, we have used the IP method regularly as a detailed mapping tool on more than 50 landfills in various environments and of differing types, including municipal solid waste (MSW), construction waste, green waste, and hazardous waste. Many of these projects were very extensive: 95 lines of dipole-dipole IP and resistivity data were acquired at one landfill alone. Although our work has been primarily in “applied” mode (as a mapping tool) rather than in “research mode” (to develop a better understanding of the IP effects), there are interesting, significant results from this very large data set.

Field techniques

IP surveys have been used in mineral exploration surveys for many decades in both time domain and frequency domain (also called phase domain), in a variety of geometries and arrays dependent on target depth and environment. Environmental applications were less common until the 1990's, since budgets for environmental geophysics were significantly smaller than for resource exploration, of course, and IP data are typically more time-consuming (i.e., more expensive) to collect for various reasons than other electrical properties such as resistivity. With the development of back-packable, battery-powered multichannel receiver systems with multiplexers, combined with flexible field logistics, however, the economics of acquiring IP improved tremendously. In order to maximize economic efficiency for environmental budget constraints, most of the landfill surveys summarized here were run in the time domain, usually using dipole-dipole arrays, measuring IP as the “Newmont Standard” chargeability, adjusted for a repetition rate of 0.5 Hz instead of 0.125 Hz (to increase survey speed).

Summary of results

One early result after comparing IP data with drilling and trenching results from numerous landfills was that the IP effects were not solely the result of metallic debris in the landfills as originally thought in 1974. The strength of the IP anomalies was not necessarily an indicator of metallic content, and eventually, several cases were evident where valid IP anomalies were measured despite the fact that little or no metal was present in the landfill. In one case, a buried “green waste” landfill containing vegetation waste (such as trees, branches, yard clippings, etc.) clearly exhibited an IP anomaly in good agreement with the landfill footprint from the historical records. In another case, trenching (and eventual clean-up) located little metallic waste, but IP anomalies appeared to be correlatable to plastic waste. At a different site, where asbestos from old demolished buildings was segregated from MSW and disposed of separately, a very weak but valid IP effect was detected over the buried asbestos. From a comparison of IP results over landfills comprised of different materials, it became evident that there are likely multiple potential sources of the IP effect at work, including metallic debris, fine-grained clays, wood or vegetable matter, some plastics, and possibly the biodegradation decay processes themselves.

Another particularly interesting overall result was the change in the strength of the IP anomaly over an old, buried landfill after an accelerated degradation process was used for four years. In this case, air and water were circulated in the subsurface waste to increase the speed of the normal decomposition. In the semi-arid desert environment where this landfill was located, the decomposition time was reduced from an estimated 100 years to approximately 5 years.

Accelerating this process is beneficial because it allows more control over ground subsidence and methane production. IP and resistivity data had been acquired over this landfill prior to the start of the accelerated degradation, and several lines of data were re-acquired after four years of the process, using the same survey parameters, equipment type, and data processing programs. The decrease in the strength of the IP anomaly over four years was very strong (see Fig. 1). The change in IP response was not completely uniform, however, suggesting that IP surveys could be used to monitor these degradation processes, helping to identify areas of the landfill where the degradation process is hindered due to poor circulation of air and water, for example.

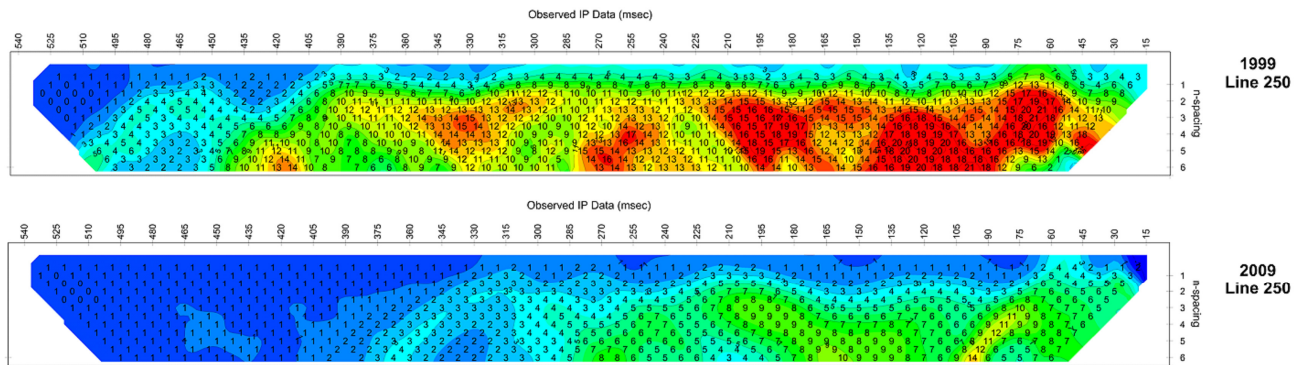


Fig. 1: Raw IP data in traditional pseudosection format, prior to modelling, showing the change in IP effects after four years of accelerated biodegradation of an old, buried, municipal solid waste landfill. Posted values are chargeability in milliseconds.

Summary

Although not acquired as research data *per se*, examination of hundreds of lines of IP and resistivity data over dozens of different landfills in a variety of environments has been useful in that it clearly illustrates that there is no single mechanism as the source of IP effects, and that differences in IP effects may in fact be useful in differentiating the types of waste in the subsurface at a given landfill. The IP method also shows promise as a tool for monitoring the accelerated biodegradation processes being developed now for landfill remediation.

Reference

Angoran, Y.E., Fitterman, D.V. and Marshall, D.J., 1974. Induced Polarization: a geophysical method for locating cultural metallic refuse. *Science*, 184, 1287-1288.

An overview of time domain induced polarisation for characterisation of underground structures and point source contaminations – large research projects in Denmark and Sweden

T. Dahlin⁽¹⁾ and E. Auken⁽²⁾

(1) *Engineering Geology, Lund University, Sweden*

(2) *Institute for Geoscience, Aarhus University, Denmark*

Two large research projects in which the time domain induced polarisation method plays a key role are underway in Sweden and Denmark, focusing on characterising underground structures in geotechnical engineering contexts and description of percolate flows from old landfills to surface water and streams respectively. Both projects involve development of new codes, instruments, field methodology etc. Scientists and engineers with multi-disciplinary backgrounds and from both universities are jointly involved in the projects.

Research and development on data acquisition techniques of DCIP (DC resistivity and induced polarisation) for environmental and engineering applications has been carried out at Lund University for over 10 years (e.g. Dahlin et al. 2002; Dahlin and Leroux 2012). Much of the research has focused on mapping, characterisation and monitoring of landfills (e.g. Dahlin et al. 2010), see example in Fig. 1, in later years within the MaLaGa project¹.

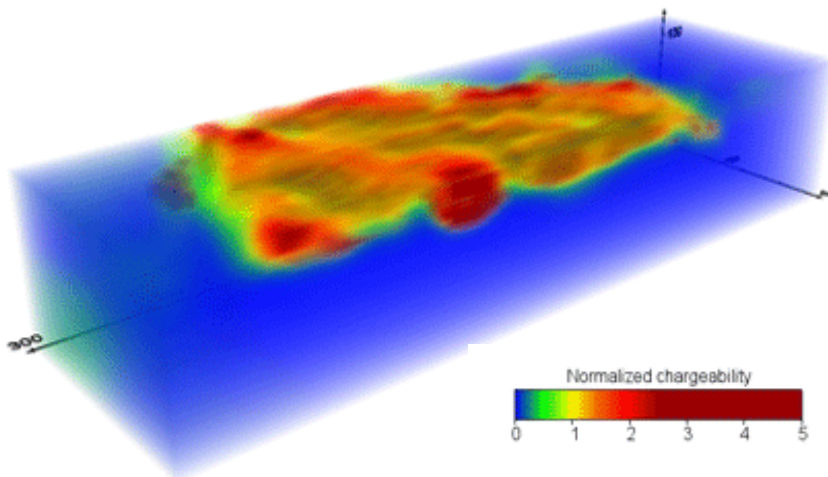


Fig. 1: 3D normalised chargeability model showing extent of waste in the Ekeboda buried landfill in Sweden (Dahlin et al. 2010).

During the last six years there have been two large projects in Denmark funded by the Danish Council for Strategic Research in which DCIP has been the key geophysical method. The first project focused on the mapping of landfills and percolate outflow to underlying groundwater reservoirs (Gazoty et al. 2012a, 2012b). Among other things this project allowed the development of efficient field methodologies for measuring IP in the time domain (Gazoty et al. 2013) and the development of the first modelling code where the entire decay curve including waveform and instrument transfer function could be modelled using e.g. the Cole-Cole model (Fiandaca et al. 2012). This code was based on the 1D LCI formulation. In the second project we could expand this code to a 2D solution (Fiandaca et al. 2013), and hardware was developed to a fully automated measurement system where 384 electrodes were set up in a time lapse experiment measuring full decay time domain IP and DC data (Auken et al. 2014). This experiment lasted almost 6 months and a clear correlation between Cole-Cole parameters and tracer metals released by CO₂ injected into the shallow aquifer was seen.

The on-going Swedish project is part of the Geoinfra-TRUST framework that is working towards developing techniques for more cost efficient underground construction in urban areas². This project aims at development and adaptation of DCIP imaging for use in urban environments and demonstration and evaluation of geoelectric mapping in this context. Establishing how well

¹ <http://malagageophysics.com>

² <http://www.trust-geoinfra.se/>

engineering and environmental key parameters can be estimated from models based on time-domain spectral IP is another aim. One part of the work is 3D data acquisition methodology and strategies, including different electrode arrays and combinations of surface and borehole electrode arrays. Adaptation and evaluation of data acquisition equipment is included, where the evaluation comprises synthetic examples from numerical modelling as well as field experiments. Development of software for 3D inversion of spectral time-domain IP data is a key part of the project. Ways of integrating other types of data in the inversion process are also part of the task. The possibility of establishing a more accurate characterisation of engineering and environmental key properties, based on models derived from inversion of spectral time-domain IP data, will also be investigated. This includes soil and rock properties, tectonic structures, existence and character of buried waste and derelict industrial areas, as well as water and contaminant occurrence and transport.

Lately a new consortium consisting of, among others, two Danish regions and a private consulting company has received funding from the Danish Council for Strategic Research for development of an efficient methodology for characterisation of outflow of percolate from old point source contaminations to surface water. The geophysical part of this project is to develop new prototype DCIP equipment further and describe a more quantitative relation between the pore water chemistry and the Cole-Cole model parameters.

In later years the two research groups at Lund University and Aarhus University have joined forces to boost the developments of hardware, software, methodologies and applications. The Swedish and the Danish projects have clearly shown that DCIP measured in the time domain is a strong alternative to measuring in the frequency domain. Field procedures are simple and the equipment is stable and (more or less) off the shelf. The key parameter has been to understand how to measure reliable data in the field and the development of the new inversion codes in 1D and 2D. In our opinion the methodologies are so robust that they can be used in real field scale production surveys with a greatly enhanced resolution of geological structures as well as of a suite of contaminations.

References

- Auken, E., Doetsch, J., Fiandaca, G., Christiansen, A.V., Gazoty, A., Cahill, A.G. and Jakobsen, R., 2014. Imaging subsurface migration of dissolved CO₂ in a shallow aquifer using 3-D time-lapse electrical resistivity tomography. *J. Appl. Geophys.*, 101, 31-41.
- Dahlin, T., Leroux, V. and Nissen, J., 2002. Measuring techniques in Induced Polarisation Imaging. *J. Appl. Geophys.*, 50, 279-298.
- Dahlin, T., Rosqvist, H. and Leroux, V., 2010. Resistivity-IP for landfill applications *First Break*, 28(8), 101-105.
- Dahlin, T. and Leroux, V., 2012. Improvement in time-domain induced polarisation data quality with multi-electrode systems by separating current and potential cables. *Near Surface Geophys.* 10, 545-565.
- Fiandaca, G., Auken, E., Gazoty, A. and Christiansen, A.V., 2012. Time-domain induced polarization: Full-decay forward modeling and 1D laterally constrained inversion of Cole-Cole parameters. *Geophysics*, 77, E213-E225.
- Fiandaca, G., Ramm, J., Binley, A., Gazoty, A., Christiansen, A.V. and Auken, E., 2013. Resolving spectral information from time domain induced polarization data through 2-D inversion. *Geophys. J. Int.*, 192, 631-646.
- Gazoty, A., Fiandaca, G., Pedersen, J., Auken, E. and Christiansen, A.V., 2012a. Mapping of landfills using time-domain spectral induced polarization data: The Eskelund case study. *Near Surface Geophys.*, 10, 575-586.
- Gazoty, A., Fiandaca, G., Pedersen, J., Auken, E., Christiansen, A.V. and Pedersen, J.K., 2012b. Application of time domain induced polarization to the mapping of lithotypes in a landfill site. *Hydrol. Earth Syst. Sci.*, 16, 1793-1804.
- Gazoty, A., Fiandaca, G., Pedersen, J., Auken, E. and Christiansen, A.V., 2013. Data repeatability and acquisition techniques for Time-Domain spectral Induced Polarization. *Near Surface Geophys.*, 11, 391-406.

Monitoring of a CO₂ injection by time domain SIP

J. Doetsch⁽¹⁾, G. Fiandaca⁽¹⁾, E. Auken⁽¹⁾, A.V. Christiansen⁽¹⁾, A.G. Cahill⁽²⁾ and R. Jakobsen⁽³⁾

(1) *HydroGeophysics Group, Department of Geoscience, Aarhus University, Aarhus, Denmark*

(2) *Department of Environmental Engineering, Technical University of Denmark, Copenhagen, Denmark*

(3) *GEUS – Geological Survey of Denmark and Greenland, Copenhagen, Denmark*

Contamination of potable groundwater by leaking CO₂ is a potential risk of carbon sequestration. With the help of a field experiment, we investigate if surface monitoring of electrical resistivity and induced polarization can detect geochemical changes induced by CO₂ in a shallow aquifer. For this purpose, we injected CO₂ at a depth of 5 and 10 m and monitored its migration using 320 electrodes on a 126 m × 25 m surface grid. A fully automated acquisition system continuously collected direct current (DC) resistivity and time domain full-decay induced polarization (IP) data using a Syscal Pro resistivity meter. CO₂ was injected for a period of 72 days and DC/IP monitoring started 20 days before and continued until 120 days after the beginning of the injection. The DC/IP data were supplemented by chemical analysis of water samples collected in 29 wells at time intervals of approximately 10 days (Cahill et al. *subm.*).

The high temporal sampling of the DC/IP data allowed detailed analysis of the resistance time-series for each measurement configuration (quadrupole) for outlier detection and error estimation (for details, see Auken et al. 2014). The time domain IP decays were also estimated for each quadrupole and each of the 20 time gates, using data variation within 2-5 day time windows. Baseline and time-lapse DC data were inverted in 3-D using the finite-element program BERT (Günther et al. 2006). The time-lapse inversion used differences in measured resistances to invert for changes in resistivity. Figure 1 shows the DC inversion results as resistivity ratio between the time-lapse results and their pre-injection values and compares them to the water sampling resistivity results. Both methods independently show a consistent decrease in resistivity that is moving advectively with the groundwater. The decrease in bulk resistivity is therefore attributed to a decrease in water resistivity, caused by the dissolved CO₂.

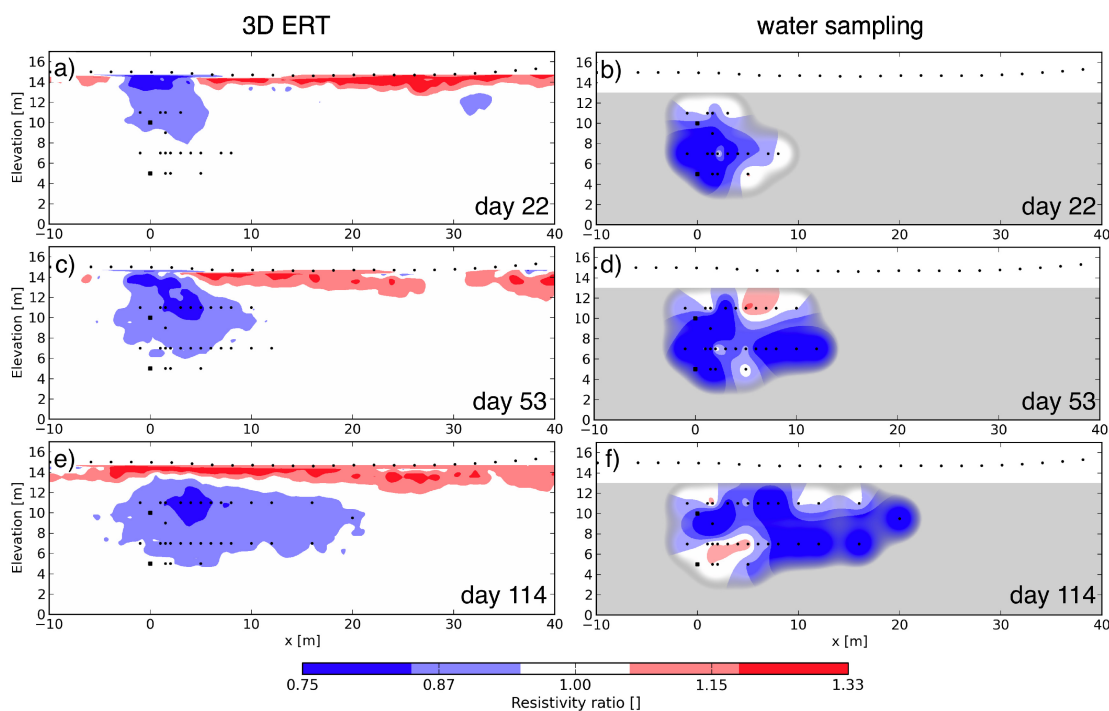


Fig. 1: Comparison of resistivity variation from 3D ERT inversion results (left panels) and groundwater samples (right panels) at 22, 53 and 114 days after the beginning of CO₂ injection. Shown resistivities are normalized by their pre-injection (baseline) values. Black dots at the surface indicate electrodes; black dots below the surface indicate water sampling locations. From Auken et al. (2014).

DC and IP data are inverted jointly using the 2-D algorithm AarhusInv (Fiandaca et al. 2013) that incorporates the full voltage decay of the IP response to resolve DC resistivity, intrinsic chargeability and spectral IP content parameterized using the Cole-Cole model. Following the injection, we use a time-lapse inversion where differences in the DC/IP data are inverted for changes to the Cole-Cole parameters. Data differencing is here used both for the DC-resistances and each time domain IP gate. The resistivity sections of the DC/IP inversion results are consistent with the 3-D DC-only results discussed above. Additionally, a chargeability (m_0) decrease has been observed after the injection, but in contrast to the decrease in DC resistivity, the chargeability anomaly remains localized around and slightly downstream of the injection wells throughout the experiment (Fig. 2). This chargeability decrease correlates in space and time with an increase in Al^{3+} , which is observed in the water samples and is caused by a decrease in pH. Consequently, we attribute this change in chargeability to pH-induced changes to the grains surfaces.

These results highlight the potential for monitoring of field scale geochemical changes by means of surface DC/IP measurements. Especially the different development of the DC resistivity and chargeability anomalies and the different associated geochemical processes, highlight the added value of induced polarization to resistivity monitoring.

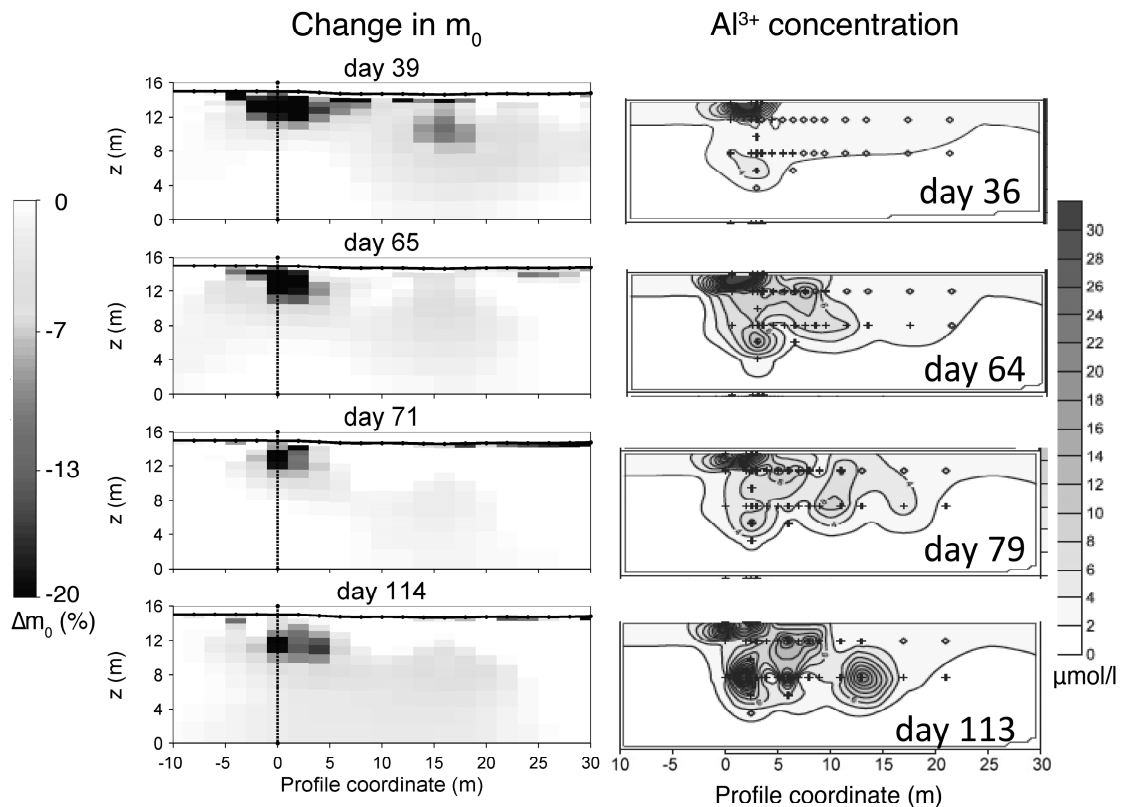


Fig. 2: Comparison of relative change in chargeability m_0 (left panels) and water-sample aluminium concentrations (right panels) for four times.

References

- Auken, E., Doetsch, J., Fiandaca, G., Christiansen, A.V., Gazoty, A., Cahill, A.G. and Jakobsen, R., 2014. Imaging subsurface migration of dissolved CO_2 in a shallow aquifer using 3-D time-lapse electrical resistivity tomography. *J. Appl. Geophys.*, 101, 31-41.
- Cahill, A.G., Marker, P. and Jakobsen, R., 2014. Hydrogeochemical and mineralogical effects of sustained CO_2 contamination in a shallow sandy aquifer: A field scale controlled release experiment. *Submitted*.
- Fiandaca, G., Ramm, J., Binley, A., Gazoty, A., Christiansen, A.V. and Auken, E., 2013. Resolving spectral information from time domain induced polarization data through 2-D inversion. *Geophys. J. Int.*, 192, 631-646.
- Günther, T., Rücker, C. and Spitzer, K., 2006. Three-dimensional modelling and inversion of dc resistivity data incorporating topography - II. Inversion. *Geophys. J. Int.*, 166, 506-517.

Induced polarization imaging at the floodplain scale for the delineation of naturally reduced zones

A. Flores Orozco⁽¹⁾, M. Bucker⁽²⁾ and K.H. Williams⁽³⁾

(1) Vienna University of Technology, Austria

(2) University of Bonn, Germany

(3) Lawrence Berkeley National Laboratory, USA

Measurements of time-domain Induced Polarization (TDIP) were performed in order to spatially delineate Natural Reduced Zones (NRZ's) at the floodplain scale, within an aquifer underlying a former uranium mill tailings at the U.S. Department of Energy's (DOE) Integrated Field Research Challenge site (IFRC) in Rifle, Colorado (USA). Previous experiments at the site have repeatedly demonstrated the ability of microorganisms to reductively immobilize uranium (U) in U tailings-contaminated groundwater accompanying organic carbon amendment. At the same time, geophysical monitoring during such amendment experiments has proven that Induced Polarization (IP) datasets can provide valuable information regarding geochemical changes induced by stimulated microbial activity, such as precipitation of metallic minerals (e.g. FeS) and accumulation of reactive, electroactive ions (Fe²⁺).

Based on these findings, we present a novel application of the IP imaging method. Specifically, we utilized time-domain IP measurements to delineate areas where fluviually deposited organic material within aquifer sediments naturally stimulates the activity of subsurface microorganism. Natural reduction of aquifer sediments leads to both the natural immobilization of uranium and accumulation of reduced end-products (minerals and pore fluids), and thus, capable of generating IP anomalies. These so-called 'naturally reduced zones' (NRZ's) are characterized by elevated rates of microbial activity relative to sediments having a lower concentration of organic matter. These zones are a critical component of the natural attenuation process enabling the slow but sustained removal of uranium from groundwater. The delineation of such NRZ's is an important aspect of assessing the potential for natural attenuation. Nonetheless, prospection of NRZ's at the floodplain by means of direct methods (drilling followed by further analysis of soil and water samples) is impossible; whereas geophysical methods permit the collection of almost continuous data on the subsurface with higher spatial resolution and in reduced exploration times.

As noted, and based on our previous experiments at the site, the accumulation of metallic minerals represents suitable targets for the exploration with IP tomographic methods. Here, we explore the application of the IP imaging method for the characterization of NRZ's at the scale of the floodplain. We present imaging results obtained through the inversion of 77 independent lines distributed along the floodplain (~600 m²). TDIP measurements were collected using an electrode separation of 1.8 m and a square-wave current injection with 50 % duty cycle and a pulse length of 2 s. Measurements were collected as normal and reciprocal pairs for estimation of the data error, where reciprocal measurements consist of those readings where current and potential dipoles are interchanged compared to the normal measurements. Inversion results presented here were obtained, as a first approach, with a 2D inversion algorithm, which permits to account for an improved error model in phase readings for the inversion of TDIP measurements.

Resistivity images (as presented in Fig. 1) show a strong correlation with the lithological units of the site, as noted in previous studies, permitting to delineate changes in the geometry (e.g., thickness) of the aquifer.

Moreover, as presented in Fig. 2, phase images revealed clear anomalies to the South of the floodplain, characterized by relatively high polarization values (absolute values above 5 mrad), suggesting the presence of NBZ's. A consistent response is also observed in those areas where previous biostimulation experiments resulted in the accumulation of metallic minerals and electroactive ions (Fe²⁺), sustaining our hypothesis.

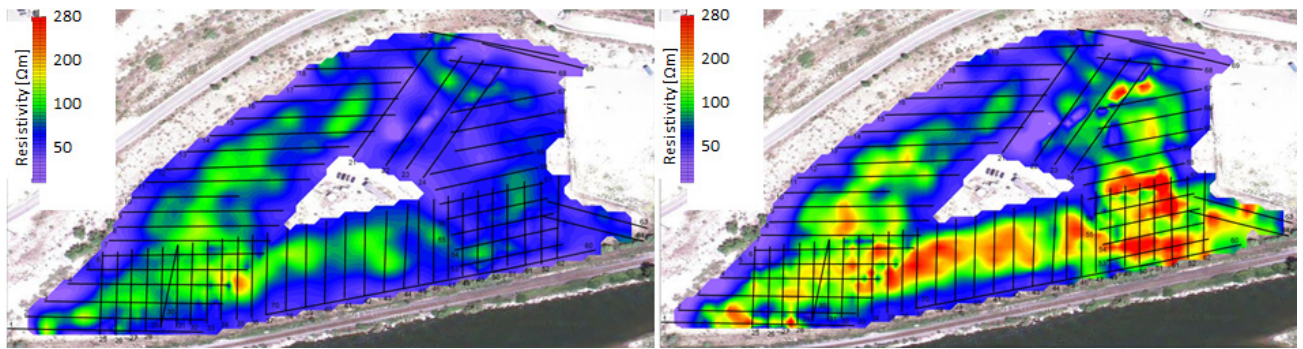


Fig. 1: Map of the electrical resistivity values computed for a depth of 3.5 m (left side) and 7 m (right side), accounting for the upper and lower levels of the aquifer.

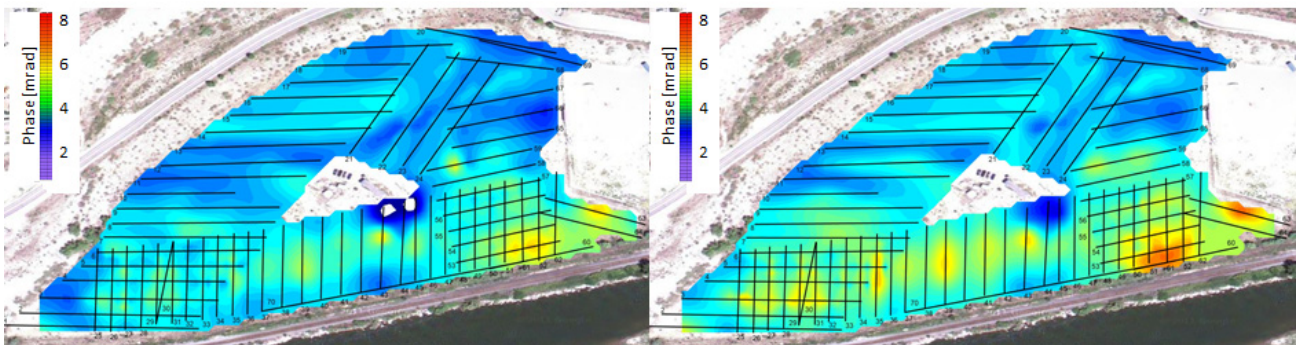


Fig. 2: Map of the phase values computed for a depth of 3.5 m (left side) and 7 m (right side), accounting for the upper and lower levels of the aquifer.

Imaging results are validated through comparisons with lithological data obtained from wells drilled at the site and laboratory analysis of sediment and groundwater samples. Our results show the applicability of the IP method for characterizing regions of the subsurface having a greater propensity for elevated rates of microbial activity, with such regions (themselves often highly localized within a larger sedimentary matrix) exerting an outsized control on contaminant (e.g. U) fate and transport.

TDIP and SIP characterization of disseminated ores

A. Ghorbani⁽¹⁾, C. Camerlynck⁽²⁾, M. Schmutz⁽³⁾ and J.-C. Parisot⁽⁴⁾

(1) University of Yazd, Department of Mining and Metallurgical Engineering, Yazd, Iran

(2) Sorbonne Universités, UPMC-Université Paris 6, UMR 7619 Metis, Paris, France

(3) ENGESID-IPB, Pessac, France

(4) CEREGE, Aix-en-Provence, France

The aim of this work is to show complementarity of temporal and spectral induced polarization, applied to ore body detection and differentiation. This study had been performed into well-known geological background through borings, geochemical measurements, and also through some electrical resistivity tomographies.

Time-domain induced polarization (TDIP) had been carried out with SYSCAL PRO equipment (Iris Instrument, Ltd.) transformed into ELREC PRO, by differentiating transmitter device (VIP generator manufactured by IRIS) from receiver one. The main interests are (i) to avoid internal coupling effects and between transmitter / receiver cables on soil, and (ii) to obtain higher electrical power (until 3000 W) necessary to reach 30-40 m depth. Voltage measurement is done through non-polarisable electrodes. Electrical chargeability and resistivity tomographies had been obtained by lateral array displacement. Pole-dipole array is selected because it offers the best compromise between minimizing coupling effects, getting enough power to reach wanted depth, and necessary lateral resolution.

Spectral induced polarization (SIP) was performed using SIP FUCHS II equipment (Radic Research). As the device is not configured into a multichannel way, and as one sounding is very time consuming (about 7 h), only 2 soundings had been performed, located on major chargeability anomalies.

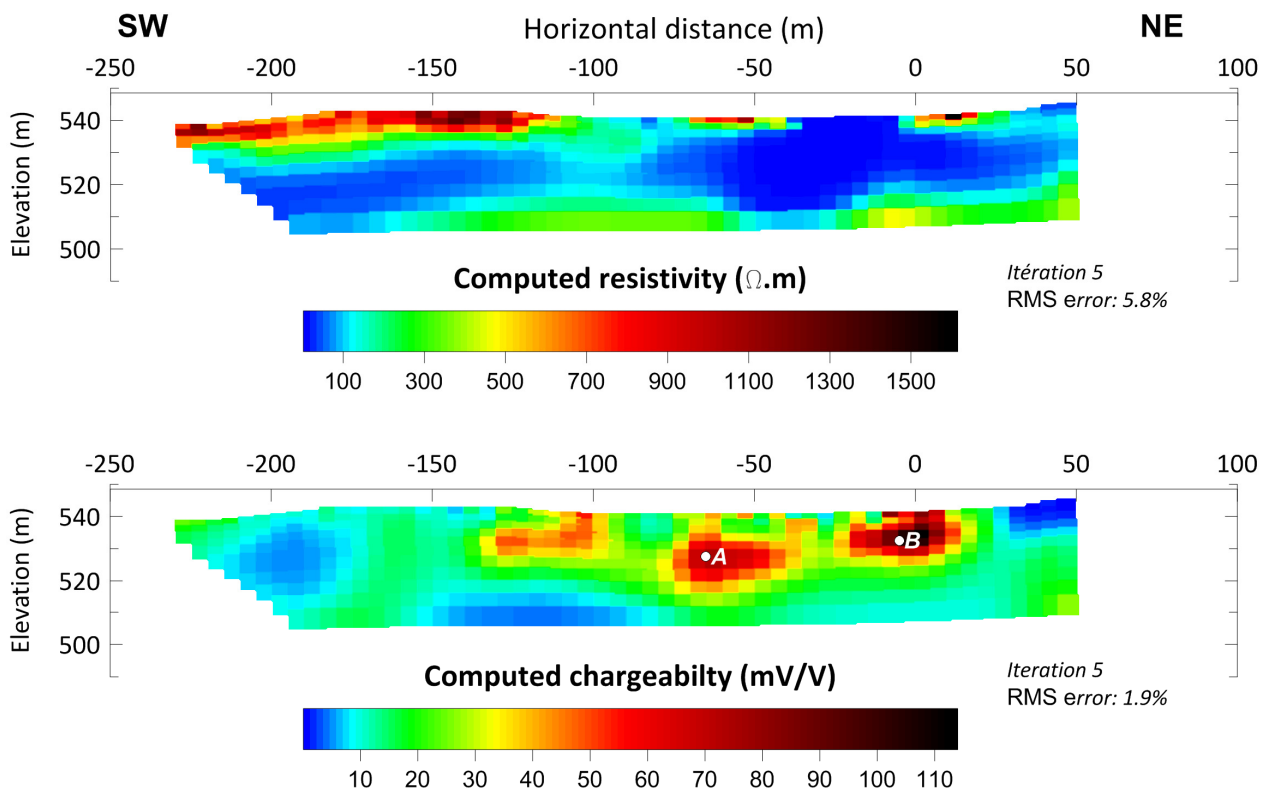


Fig. 1: Computed resistivity and chargeability sections (pole-dipole array, 10 m inter-electrode spacing). A and B indicate chargeability anomalies.

As results, a 3-layer model can be observed (Fig. 1): very a resistive level between 0 and 5 m depth (up to 1000 Ω m), a more conductive one between 5 and 20-25 m depth (50 Ω m), and

finally an increasing resistivity for the bottom layer. A finer analysis indicates some highly conductive zone 50 m wide ($50 \Omega \text{ m}$) from surface until 30 m depth. This could be explained by clay or ore body presence.

Induced polarization analysis indicates very high chargeability values at resistivity anomaly zone (up to 100 mV V^{-1}), whereas everywhere else values are less than 10 mV V^{-1} . Such high chargeability may only be explained by disseminated ore. At first sight, there should correspond to sulphide ore (geochemical analysis will indicate 2 different types).

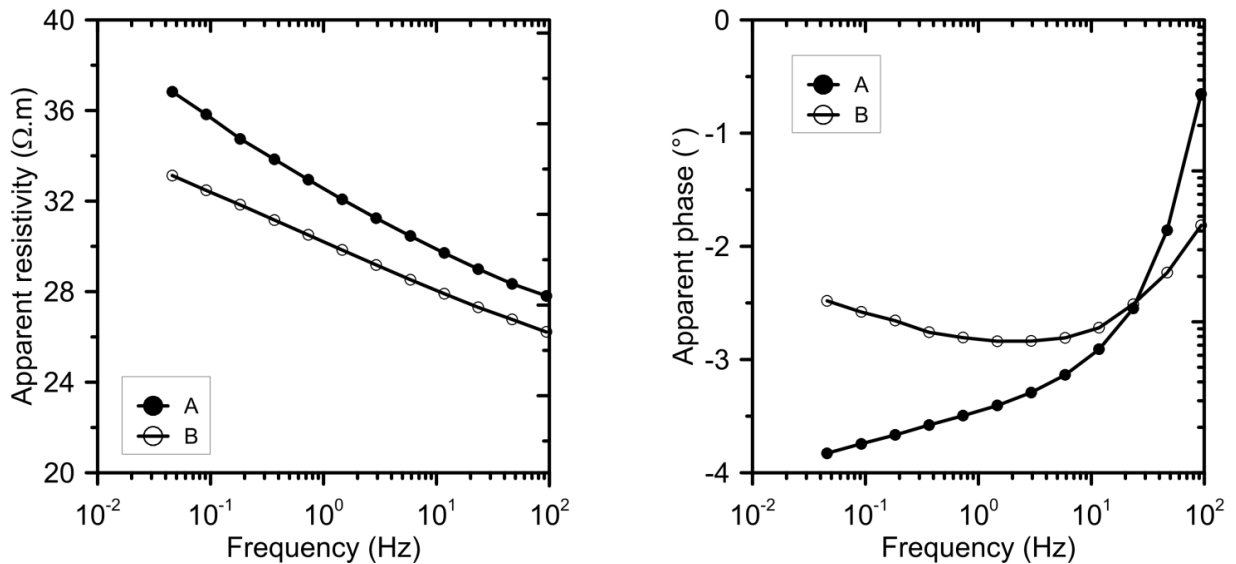


Fig. 2: SIP spectra for A and B positions.

Two SIP soundings have been done vertically above chargeability anomalies A and B (Fig. 2). There is no difference for the resistivity values, but the phase diagrams are very different (maximum absolute phase is 3 Hz for measurement B and less than 0.1 Hz for measurement A). Some SIP characterization has now to be done to better characterize the nature of the ore body.

As a conclusion, time and frequency domain measurements are actually complementary (speed for TD chargeability / strong capability of differentiation for SIP).

Optimizing investigation strategies of hydrocarbon contaminated site using multi-geophysical approach in surface and borehole (IP, ERT and GPR)

V. Giampaolo⁽¹⁾, L. Capozzoli⁽¹⁾, M. Votta⁽¹⁾ and E. Rizzo⁽¹⁾

(1) CNR-IMAA, Hydrogeosite Laboratory, Italy

The goal of this work is to characterize underground contaminant distributions and monitoring a remediation activity using a multi-geophysical approach (cross-hole IP and ERT, GPR). The experiments consisted in monitoring a simulated oil leachate into a box (1 m³) by multi-geophysical measurements with sensors located in surface and boreholes (Fig. 1a). The tank is filled with quartz-rich sand (95 % silica, $n = 0.43$, and $k = 1.16 \cdot 10^{-12} \text{ m}^2$) and an aquifer with tap water is located. The box is monitored by water content and piezometric sensors. Moreover, four boreholes were placed in the tank during the construction. The boreholes, spaced about 40 cm, were equipped each with 12 stainless steel ring electrodes, at 5 cm spacing, for cross-hole electrical resistivity and time-domain IP measurements. 25 additional stainless steel electrodes were installed at the surface of the tank. The steel electrodes were connected, by multichannel cables, to the georesistivimeter Syscal PRO (Iris instrument). The experiment was analysed before and after contamination process to compare zones characterized by absence or presence of hydrocarbon.

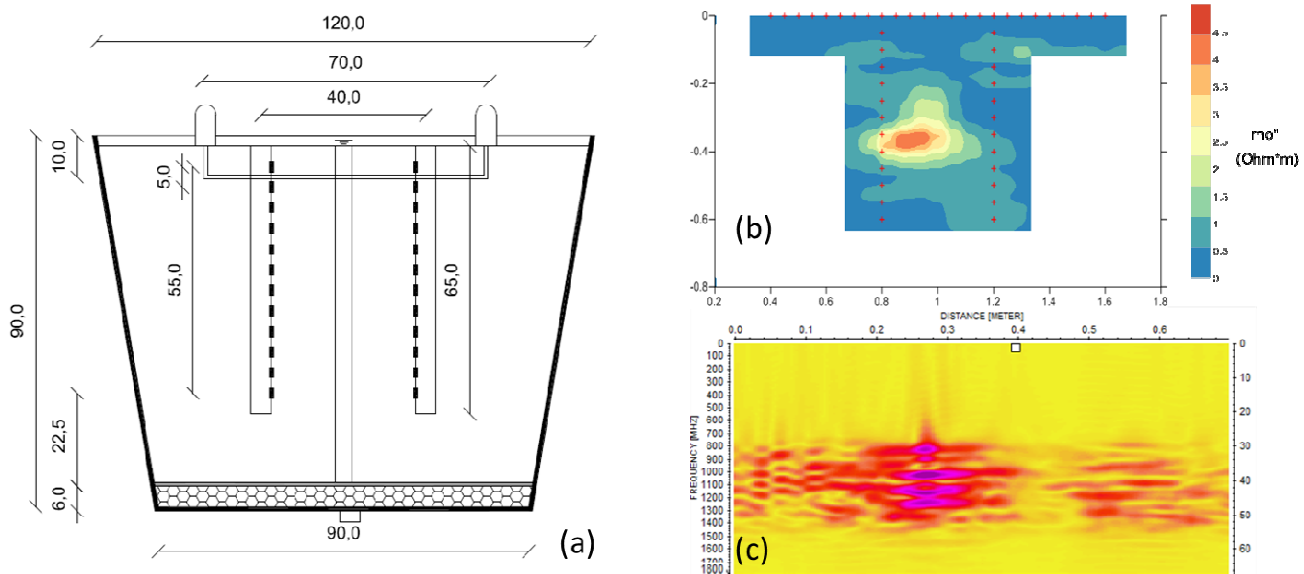


Fig. 1: Sketch of the sand box (a) with an IP image (b) and GPR spectrum data (c).

Two measurement phases were realized: first, we monitored electrical resistivity, IP, and dielectric conductivity of the uncontaminated soil; the second experimental phase consists in the geophysical monitoring of a crude oil controlled spill.

Surface and cross-hole ERT and IP were acquired with a new approach array and reciprocal configuration. IP measurements were collected using a square-wave current injection with 50 % duty cycle and a pulse length of 1 s, with integral chargeability measurements performed during voltage decay between 160 and 920 ms after current shut-off. For the inversion of IP measurements, chargeability values were linearly converted to frequency domain phase values (at the fundamental frequency of 0.125 Hz) using the approach of Kemna et al. (1997). Therefore, in the inversion, resistance (voltage-to-current ratios) and phase angle were used as parameters. Finally, the real resistivity and phase angle distribution were obtained using the smoothness-constraint inversion algorithms cR2 and R2 (Binley 2007a, 2007b) for electrical resistivity and IP data respectively.

Additionally, GPR was used to monitor the dispersion of hydrocarbon in the sand layer. For this purpose we used a GSSI SIR-3000 radar system equipped with four different frequency antennas (respectively 900, 1500 and 2000 Mhz) in monostatic and bistatic configuration to obtain

different kind of information in terms of resolution and depth. Raw data acquired were processed with Reflexw software to reduce noise and enhance information of the data.

The presence of the contaminant causes a variation in the frequency spectrum (Orlando 2002). Generally we have an attenuation of GPR signal linked to a centroid frequency downshift that can be attributed to dielectric losses frequency-dependent due to the presence of hydrocarbon. So, from the analysis of variations in the frequency domain is possible to localize the presence of contaminants in the subsoil. In this work, the spectral analysis was computed using a standard Fast Fourier Transform (FFT) algorithm that allows describing the e-m behaviour of the medium in the frequency domain.

Results showed significant changes in the responses of geoelectrical measurements in presence of a crude oil contamination. Instead IP results give a phase angle distribution related to the presence of hydrocarbon in the system but not so clear in the location of plume. Therefore, to clearly delineate the areas interested by contamination, we estimate the imaginary component of electrical resistivity by:

$$\rho''(\omega) = \rho'(\omega) \tan(\varphi)$$

where ω is the frequency, ρ' (Ωm) is the imaginary component of electrical resistivity while ρ'' ($\Omega\text{ m}$) is the real one and φ (rad) is the phase angle (Fig. 1b).

Finally, the electrical behaviour of the medium from GPR data, compared to geoelectrical measurements, was investigated by the analysis of the strength of EM-reflections and absorption of EM signal introduced by different antennas (Fig. 1c). In particular, the most contaminated areas are characterized by a variation of soil permittivity dielectric value. For this purpose, spectral signal analysis is also performed to study in frequency domain the phenomenon of hydrocarbon spill in the box. Furthermore, the frequency analysis show a significant downshift of the frequency in correspondence of contaminated areas; for this reason the estimation of variation in frequency domain represents a supplementary approach to classical GPR signal data processing to increase quality information characterizing the acquired data.

In conclusion, the experiment was able to obtain information about contaminant distribution in the subsurface. Besides combining measurements from multiple geophysical measurements allow us to obtain more accurate characterization of contamination spatial variability.

References

- Binley, A., 2007a. *cR2: Summary*. Lancaster University, Lancaster, UK.
- Binley, A., 2007b, *R2: Summary*. Lancaster University, Lancaster, UK.
- Kemna, A., Räckers, E. and Binley, A., 1997. Application of complex resistivity tomography to field data from a kerosene-contaminated site. *Proc. 3rd Mtg. Environ. Eng. Geophys., Eur. Section*, 151-154.
- Orlando, L., 2002. Detection and analysis of LNAPL using the instantaneous amplitude and frequency of ground-penetrating radar data. *Geophys. Prospect.*, 50, 27-41.

Application of the Debye decomposition approach to time domain induced polarization profiling data: an ore exploration example

G. Gurin⁽¹⁾, A. Tarasov^{(1),(2)}, Y. Ilyin⁽¹⁾ and K. Titov⁽¹⁾

(1) *St. Petersburg State University, Russia*

(2) *VIRG-Rudgeofizika JSC, Russia*

In hydrothermal and metasomatic deposits, gold is frequently accompanied by sulphide minerals of different grain size and shape depending on degree of alteration of host rocks. We applied Time Domain (TD) Induced Polarization (IP) method combined with Debye Decomposition approach (DDA) to profiling data, in order to map zonality of the altered rocks within Julietta porphyry gold-silver deposit (Magadan region, Russia).

Gold is presented in veins. The veins are of complex shape and are surrounded with halos of low temperature altered rocks (beresite) with a thickness from 10 to 100 m. The altered rocks are of similar mineralogical composition (quartz, calcite, sericite, peach, sulphides) but with different metallic particle amounts, size and aspect ratio, which corresponds to different alteration degree. The veins are hosted by volcano-sedimentary deposits mainly of andesite composition, which are penetrated by numerous small intrusions (from rhyolites to basalts).

We carried out TD IP profiling with a pole-dipole (A120M40N) arrays, and with commercial instrument Cycle-IP-2 (current wavelength form was 2 s on-time and 2 s off-times with pulses of opposite polarity). IP decays were measured from 0.03 to 1.3 s in time windows (0.005 s), which allowed us applying the DDA. We also used a conventional magnetic survey.

In addition to traditional chargeability, based on DDA, for each station, we obtained the relaxation time distribution (RTD), the total chargeability and the mean relaxation time. In the data analysis we used previously obtained petrophysical relationships between the total chargeability (M) and volumetric content of the sulphide particles (ξ):

$$M \approx k\xi \tag{1}$$

and between the mean relaxation time (τ) and the particle radius (r):

$$\tau \sim r^2. \tag{2}$$

Figure 1 shows the traditional geophysical parameters (apparent resistivity, chargeability, and total magnetic field, Fig. 1a), the integral IP parameters obtained from DDA (total chargeability, mean relaxation time, Fig. 1b), RTDs typical of the studied area (Fig. 1c), and a geophysical model of the deposit (Fig. 1d).

Three types of altered rock were found (Fig. 1d). The first type is characterized by increased apparent resistivity values (1000 – 4000 Ωm), small values of the chargeability (1.5 %) and total chargeability (6 %), a monotonously decreased RTD. This geophysical signature is typical of quartz and quartz-carbonate zones with very small amount of sulphide minerals ($\xi \leq 1 - 1.5$ %), which is not detected by IP. These zones can be found by increased apparent resistivity values; however these values are also typical of small intrusions.

The second type shows values of the apparent resistivity, chargeability and magnetic field similar to those typical of host andesites. However, RTDs are characterized by large values at early time range (< 0.1 s). These values are produced by a relatively small amount (up to 3 %) of fine grains of sulphide minerals ($r < 0.1$ mm). Moreover, for this type of altered rocks the total chargeability increases up to 12 %. This geophysical characteristic is typical of silicification areas with quartz-carbonate veinlets and low amount of sulphides with small grain size. Zones of the second type can be mapped on the basis of the DDA parameters only.

The third type shows large values of the chargeability (5 – 6 %) moderate apparent resistivity values (1500 – 1800 Ωm) and decreased values of the magnetic field (which is a manifestation of high alteration degree). RTD shows increased values at late times (> 1 s), which is typical of large metallic grains (Eq. 2) or for the case of high aspect ratio of the grains. This

geophysical characteristic is typical of beresites (including pyrite, sericite, carbonate, quartz and illite), which contains veinlets (frequently with gold) with 2 to 7 % of pyrite, chalcopyrite and galena.

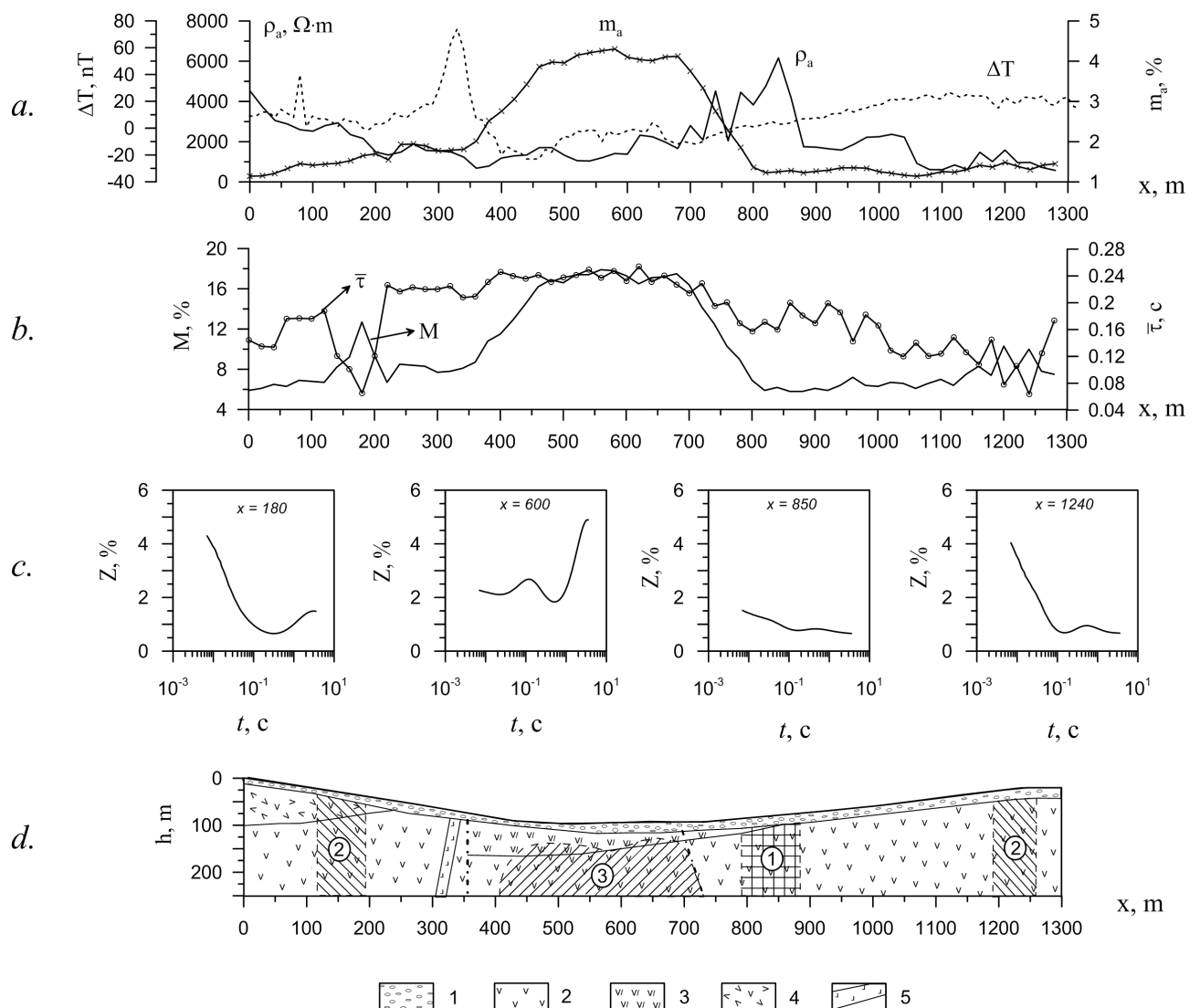


Fig. 1: Geophysical parameters along a line crossed altered rocks containing gold mineralization. a: apparent resistivity (ρ_a), chargeability (m_a) and total magnetic field (ΔT) distributions; b: total chargeability (M) and weighted average relaxation time (τ); c: typical RTDs, and geophysical model. 1 – Quaternary deposits, 2 – andesites, 3 – tuffs of andesites, 4 – porphyry andesites; 5 – andesite dyke.

Application of DDA to profiling data allows obtaining additional information comparing the standard processing procedure. One type of zones of altered rocks among three, which is economically important can be detected on the basis of RTD parameters only. The geophysical model (Fig. 1d) is confirmed by drilling results.

Delineation of a free phase chlorinated hydrocarbon plume with resistivity and TDIP

S. Johansson⁽¹⁾, P.-I. Olsson⁽¹⁾, M. Lumetzberger⁽²⁾, T. Dahlin⁽¹⁾, H. Rosqvist⁽³⁾ and C. Sparrenbom⁽³⁾

(1) *Engineering Geology, Lund University, Sweden*

(2) *Geosciences and Natural Resource Management, Copenhagen University, Denmark*

(3) *Geology Dept., Lund University, Sweden*

Drilling with subsequent laboratory tests on soil and groundwater samples is the conventional method used to delineate contamination plumes in soils. Chlorinated hydrocarbons, which belong to a group of fluids referred to as DNAPLs (Dense Non-Aqueous Phase Liquids), implicates especially severe conditions since they are very toxic and only a small amount can cause serious pollution of the ground water when dissolved. All pure DNAPLs are non-polar fluids and electrical insulators, and studies have shown that soil saturated with DNAPLs leads to a reduced dielectric constant of the medium (Ajo-Franklin et al. 2006 and references therein).

Resistivity and time domain IP (DCIP) data were measured at a field site in southern Sweden. The site is a former dry cleaning facility situated over a major aquifer, and the ground is heavily contaminated with chlorinated hydrocarbons, namely tetrachloroethylene (PCE) and its degradation products. A wetland is closely situated east of the site. The aim of the measurements was to investigate how well the soil contaminated with free-phase PCE could be delineated with DCIP. Several drillings together with soil and groundwater samplings have been made at the site, providing reference data approximately showing where two main plumes of free-phase PCE in the soil can be expected. Presence of free-phase PCE was expected to give rise to high-resistive anomalies and IP-effects, as previously indicated for instance by Cardarelli and Di Filippo (2009).

The DCIP measurement arrangement on the actual plot consisted of ten roughly parallel 2D profiles and one U-shaped 3D profile enclosing them. The mean length of the profiles was about 80 meters, and spacing between the profiles and between the in-line electrodes were both 2.5 meters. The DCIP measurements were made with the ABEM Terrameter LS instrument using separated cables for transmitting current and receiving potentials. The pole-dipole array was used with the remote electrode located approximately 500 meters away. The DCIP data were inverted in Res3Dinv version 3.08 (Geotomo Software), using robust data and model constrains with incomplete Gauss-Newton optimization methods. Both elevation and coordinates of the electrodes were incorporated in the inversion of the 3D model. The final model RMS error was 3.56 % for resistivity and 4.52 % for chargeability.

Inverted 3D models of resistivity and chargeability are visualised in Fig. 1. According to drillings, the bedrock begins at about -15 mamsl in the western part of the site and at -25 mamsl in the east. The vertical extension of the models reaches down to -12 mamsl, i.e. above the bedrock surface. A layer of heterogeneous fill material with varying resistivities covers the surface throughout the site. The low resistivity values below the fill material in the easternmost part of the resistivity model probably correspond to the thick layers of clay, peat and dy encountered in the drillings towards the wetland. The chargeability model shows that this area also gives rise to IP-effects, which further supports this interpretation.

In the western part of the site, the soil consist of mainly sandy chalk till between roughly -2 to -15 mamsl according on the drillings. The low resistivity section close to the surface could correspond to a documented 1-2 meter thick layer of varved clay situated below the uppermost fill material. The surrounding anomalies with higher resistivity (~100 Ω m) could be interpreted as till. However, they are of limited horizontal extension; the resistivity is much lower in the northern parts of the model (although this is not visible in Fig. 1). Also, the anomalies reach the surface at two locations, even though the drillings suggest a continuous layer of varved clay above the till.

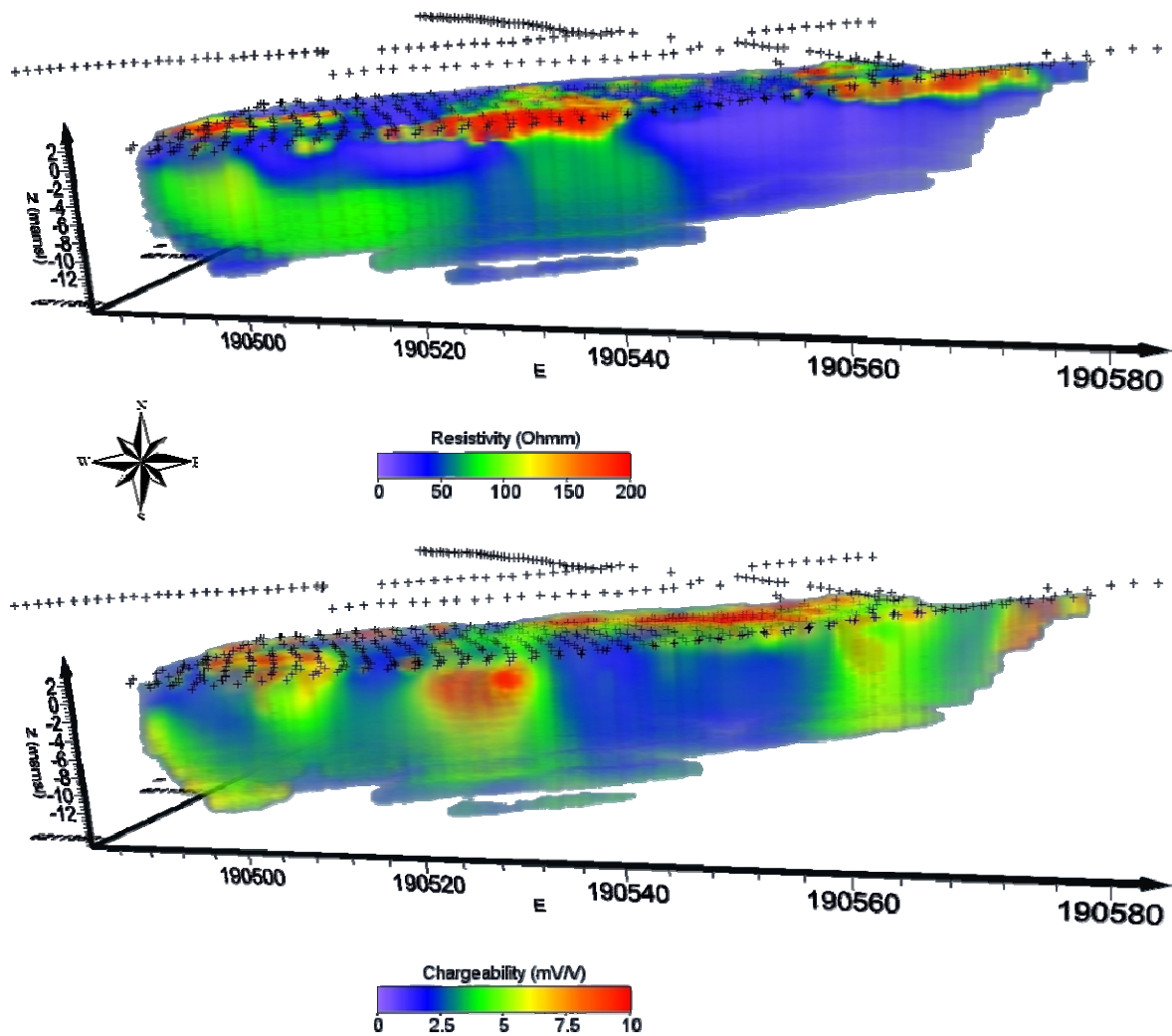


Fig. 1: View over the inverted 3D resistivity model (top) and chargeability model (bottom).

The chargeability model shows two main anomalies with elevated chargeability in the western part of the site. If the resistivity and chargeability models are compared to each other, it can be seen that the IP anomalies coincide with zones of low resistivity. Taken the elevated chargeability in the westernmost edge of the model into account, it seems as if IP-effects occur around the edges of the zones of high resistivity in the western part of the site.

It is probable that the high resistive anomalies in Fig.1 correspond to the sought two plumes of free-phase PCE situated in the sandy chalk till. Their locations correspond approximately to the location expected according to the soil sampling. The shape of the westernmost anomaly suggests that PCE first sank vertically through the till, where after it due to gravitational forces now is migrating eastwards along the tilting surface of the bedrock. The IP-effects encountered in the vicinity of the presumed free-phase PCE-plumes may be caused by the degradation of PCE in interfaces between the contamination and water. This could lead to a gradient of free chloride ions in the pore water surrounding the free-phase PCE. However, the data must be further evaluated against chemical soil and water sampling results in order to establish and understand their origin.

References

- Ajo-Franklin, J.B., Geller, J.T. and Harris, J.M., 2006. A survey of the geophysical properties of chlorinated DNAPLs. *J. Appl. Geophys.*, 59, 177-189.
- Cardarelli, E. and Di Filippo, G., 2009. Electrical resistivity and induced polarization tomography in identifying the plume of chlorinated hydrocarbons in sedimentary formation: a case study in Rho (Milan - Italy). *Waste Management and Research*, 27, 595-602.

Monitoring of a shallow CO₂ injection using time lapse electrical resistivity and induced polarization methods

T. Kremer^{(1),(4)}, V. Allègre⁽¹⁾, M. Schmutz⁽³⁾, E. Williard^{(1),(2)} and A. Maineult^{(1),(4)}

(1) Institut de Physique du Globe de Paris, UMR CNRS 7154, France

(2) Areva Mines, France

(3) ENSEGID, EA4592 G&E, University of Bordeaux, France

(4) Centre de recherches sur le stockage géologique du CO₂ (IPGP / TOTAL / SCHLUMBERGER / ADEME), 1 rue Jussieu, 75238 PARIS cedex

Through a field scale experiment, we investigated the efficiency and the reliability of two electrical methods for the detection and monitoring of a CO₂ leakage. The leak was simulated by injecting gaseous CO₂ at a depth of 6 meters, while electrical resistivity tomography (ERT) and temporal induced polarization (TIP) profiles, centred on the injection well, were acquired at the surface. We monitored the temporal evolution of the electrical resistivity and TIP parameters compared to a reference acquisition performed before the gas injection. The injection lasted for approximately four hours, and the cumulative mass of CO₂ injected approached six kilograms.

Both methods started showing temporal variations thirty minutes after the beginning of the injection. ERT measurements successively showed a decrease in resistivity (Fig. 1) followed by an increase in resistivity that we interpret respectively in terms of gas dissolution and water/gas saturation evolution.

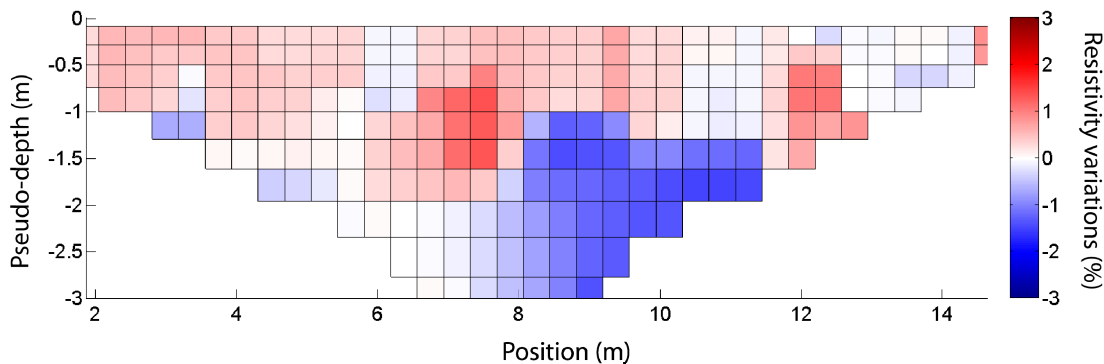


Fig. 1: Resistivity variations with respect to zero-state measurement (i.e. prior to injection), 30 minutes after CO₂ injection started. A decrease of the resistivity values in the lower part of the section can be interpreted as the arrival of a dissolution front induced by the CO₂ injection. The section is centred on the 6-m deep injection well.

Chargeability measurements proved to be much more sensitive to CO₂ injection than resistivity measurements. Measured values showed a continuous increase during the experiment (Fig. 2), suggesting that gas dissolution and saturation evolution alone cannot explain these changes, and that another process is involved.

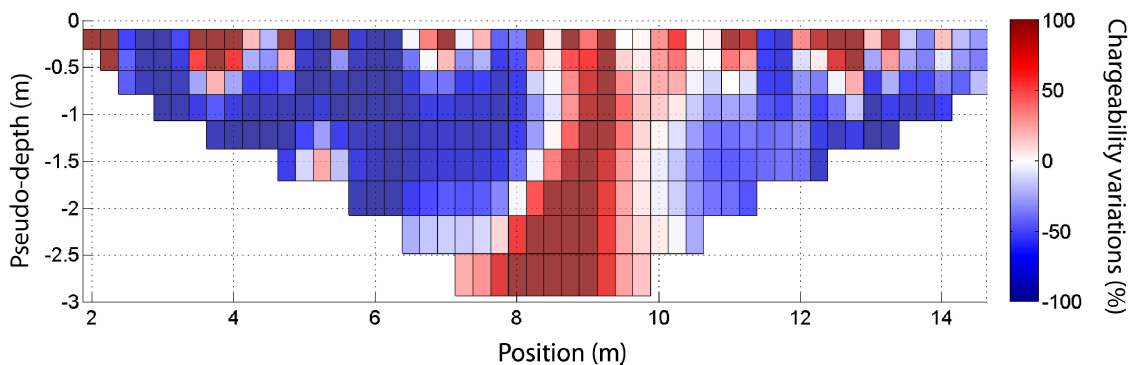


Fig. 2: Chargeability variations after 5 hours of CO₂ injection. Note the strong increase of chargeability values (> 100 %) in the lower central part of the 2D section.

These results are consistent with a previous laboratory study that underlined the larger sensitivity of IP methods to detect CO₂ transfers in the subsurface.

We gratefully acknowledge the support of the ADEME agency, Schlumberger and Total in this project and their permission to present this work. However, the views expressed here are those of the authors who are solely responsible for any errors.

**Frequency-domain induced polarization:
application to a paleovalley, Ugra national park (Russia, Kaluga region)**

V. Kulikov⁽¹⁾ and I. Sterligova⁽¹⁾

(1) *Lomonosov Moscow State University, Faculty of Geology, Russia*

Introduction

Study of ancient paleovalleys is an actual task since they are associated with various placer mineral deposits. One of the largest Miocene paleochannel deposit structures (N1) is located in close vicinity of the geophysical research base (Aleksandrovka village, Ugra national park, Kaluga Region). Based on the parametric borehole data from the research base, it can be assumed that the paleochannel deposits are tens of meters thick. Therefore, this paleovalley is among the deepest and largest ones in the central part of the East European Platform.

The first geophysical survey consisted of magnetometric acquisition at the scale of 1:2,500. Two narrow linear zones of north-western strike appear on the magnetic local component map. It was decided to perform an additional vertical electrical sounding and induced polarization (VES-IP) survey with detail step on several profiles across the strike of the magnetic anomaly to obtain more detailed data about the structure of the identified object in the vertical section.

Data acquisition

Special multichannel stations and multi-electrode arrays are typically used for electrical resistivity tomography surveys. However, there are alternative where measurements are performed with the conventional symmetric four-electrode Schlumberger array and a special linear spacing which allows for 2D data inversion. The VES-IP array used by us was described earlier (Shevnin and Bobachev 2009). The current electrode spacing range ($AB/2$) was measured from 3 to 105 m. Potential electrodes distance 2 and 14 m long were used. The profile step was 10 m in the centre of the anomaly and 20 m on the profile flanks. Four measurement profiles were covered. The distance between the profiles was 60 m. Measurements were performed in the frequency domain at 0.6 and 19 Hz. The apparent polarizability was calculated through the Differential-Phase Parameter (DPP), which can be used for estimating the IP phase, according to the following empirical formula: $\eta_k = -2.5 \times \text{DPP}$ (Kulikov and Shemyakin 1978; Zorin 2013).

Interpretation of the results

The obtained results were interpreted using automatic 2D inversion ZondRes2D software. The interpretation models for electric resistivity tomography profile №2 up to the depth of 20 m are shown in Fig. 1. The vertical scale was doubled for better representation of the near-surface section structure. The resistivity model (Fig. 1b) primarily reflects the lithology. Dry sands have the highest resistivity, while clays are characterized by lower values. The sand lens reaches its maximum thickness of about 8 m at 100-120 m of the profile. A relatively thin horizon with increased polarization values which appear at low frequencies 0.6 Hz was identified at the depth of 4-5 m in the centre of the sand lens (Fig. 1c). Our previous studies in the vicinity of the Alexandrovka based on the IP method showed that this maximum is most likely associated with partial water saturation - capillary fringe zone located above the ground water level in the sands (Kulikov et al. 2013). The rock mass that creates the high-frequency 19 Hz induced polarization anomaly belongs to the conductive horizon located under the western side of the sand lens (Fig. 1d). The position of this anomaly matches well with the maximum of the local magnetic field component (Fig. 1a). This match leads to the assumption that both anomalies have the same nature.

The profile №2 passed in the 60 meters to the wells drilled for confirmation of the magnetic anomaly in the winter of 2013. According to the results of magnetic susceptibility measurements in the wells were found magnetite-containing clays in the interval of 4 to 9.5 m. Deposits with magnetic susceptibility exceeding $200 \cdot 10^{-5}$ SI units were detected in well drilled in the southwestern part of the profile starting from the depth of 23 m. Laboratory measurement results (Kulikov et al. 2013) and our experience of surveys on other sites show that rapid IP field decay is

characteristic of rocks that contain magnetite. This assumption is consistent with the obtained results, since the high-frequency IP anomaly spatially matches the local magnetic field anomaly (Figs 1ad). In our case the magnetite is of alluvial genesis and was deposited along the river-bed.

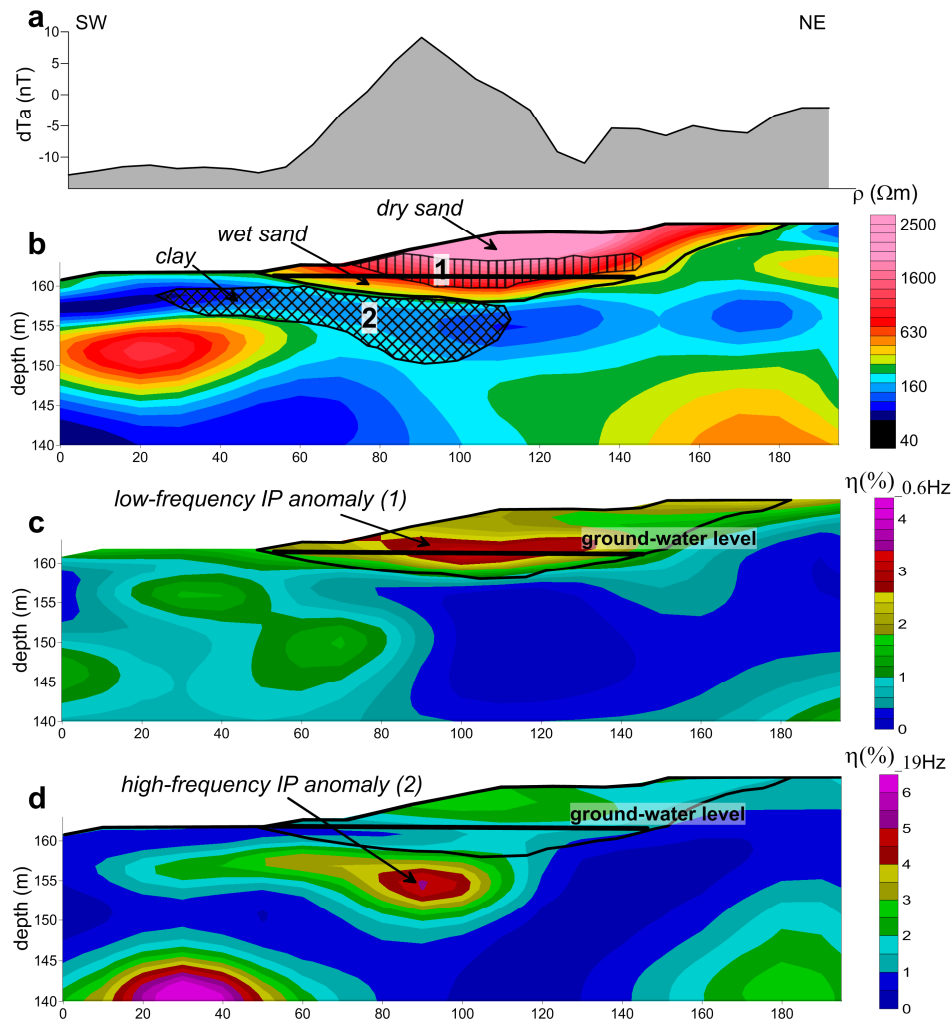


Fig. 1: Magnetic field graph (a), 2D inversion results: (b) resistivity model at frequency 0.6 Hz, (c) polarizability model at 0.6 Hz and (d) 19 Hz.

Conclusions

The geophysical survey carried out using electrical and magnetic exploration methods provided updated data on the structure of a large paleovalley in the National Park Ugra. VES-IP method with detail step and linear spacing were employed to achieve the project objectives. A definite relationship was established between the magnetic field anomalies and high-frequency induced polarization anomalies. Drilling operations carried out based on the magnetic measurement results confirmed that magnetite-containing alluvial deposits were indeed the source of those anomalies. The electrical exploration results can be used as a starting model for interpretation of magnetic survey data, which allows creating a 2D magnetic model of the paleovalley.

References

- Zorin, N. and Yakovlev, A., 2013. Telluric method of natural field induced polarization. 5th Int. Symposium on Three-Dimensional Electromagnetics, 7-9 May 2013, Sapporo, Japan.
- Kulikov, V.A., Gruzdeva, I.D. and Yakovlev, A.G., 2013. A VES-IP survey near the Geophysical Station of Moscow State University, in the Kaluga Region. *Moscow Univ. Geol. Bull.*, 68(3), 191-199.
- Kulikov, A.V. and Shemyakin, E.A., 1978. Geoelectric prospecting using phase method of induced polarization (in Russian). Nedra press, Moscow, 157 p.
- Shevnin, V.A. and Bobachev, A.A., 2009. 2D inversion of data, measured on traditional 1D VES technology (in Russian). *Georazrez*, 3.

Spectral induced polarization in mineral exploration

V. Kulikov⁽¹⁾ and I. Sterligova⁽¹⁾

(1) *Lomonosov Moscow State University, Faculty of Geology, Russia*

Investigation of time (frequency) characteristics of the induced polarization (IP) process is one of the priority areas in today's electrical explorations. The velocity and duration of the IP process are additional independent parameters which can provide further information on the nature of the polarized objects.

Russian company North-West uses a multi-frequency phase measurement technology (INPHASE-IP) developed in the Soviet Union in the 70's of the past century to study the IP characteristics (Kulikov and Shemyakin 1978).

In the INPHASE-IP method, the rock polarizability level is determined based on the differential phase parameter (DPP). Use of DPP was suggested to suppress electromagnetic inductive component which, just like induced polarization, can lead to significant phase shifts in the signal. In the near-field zone approximation, the inductive phase is proportional to the frequency. The differential phase parameter is designed to completely suppress the linear component of the phase without changing the constant component.

$$DPP(\omega_1, \omega_2) = \frac{\phi(\omega_1) \cdot \omega_2 - \phi(\omega_2) \cdot \omega_1}{\omega_2 - \omega_1}$$

where ω_1 and ω_2 are the frequencies, $\phi(\omega_1)$ the full low-frequency phase shift and $\phi(\omega_2)$ the full high-frequency phase shift.

If a square-wave signal (bipolar rectangular pulse) is used in the current line, DPP can be calculated based on phases 1 and 3 of the measured signal harmonics:

$$\Delta\phi(\omega, 3\omega) = \frac{3\phi(\omega) - \phi(3\omega)}{2}.$$

DPP is often converted into apparent polarizability (η_κ^{DPP}) by empirical coefficient $\kappa = -2.5$. This allows converting the resulting data from the negative phase degree dimension to a more conventional unit of measurement used in the IP methods – polarizability percentage.

According to the Cole-Cole formula, the apparent resistivity modulus decreases progressively as the frequency increased, and the phase has one minimum and two symmetrical ascending branches. The phase curve minimum position is determined primarily by time constant τ , the phase amplitude by polarizability value η , and the spectrum width by parameter C . The DPP shape almost exactly follows the shape of the phase curve, but has a more pronounced minimum as well as a minor minimum shift along the x axis (Zorin 2013).

Difference between the DPP values at two frequencies can be used as a simple and reliable method for evaluation of time characteristics of induced polarization. Since the DPP frequency characteristic graphs are virtually symmetrical, the operating frequencies can be selected so that the difference between two DPPs calculated for those frequencies would be negative above one rock and positive above another. This parameter will be proportional to time constant τ (Fig. 1).

The results of INPHASE-IP surveys performed at multiple mining objects showed that DPP can be successfully used in advanced modern applications involving separation of objects with different time characteristics of induced polarization.

Areal electrical surveys based on the electric profiling – induced polarization (EP-IP) method carried out at the Kola Peninsula showed (Fig. 2) that use of multi-frequency DPP measurements enables identification of local intrusive bodies with copper-nickel sulphide mineralization localized in the field of propagation of highly conductive and polarisable carbonaceous shales of the Solenoozerskaya Series (Kulikov 2013).

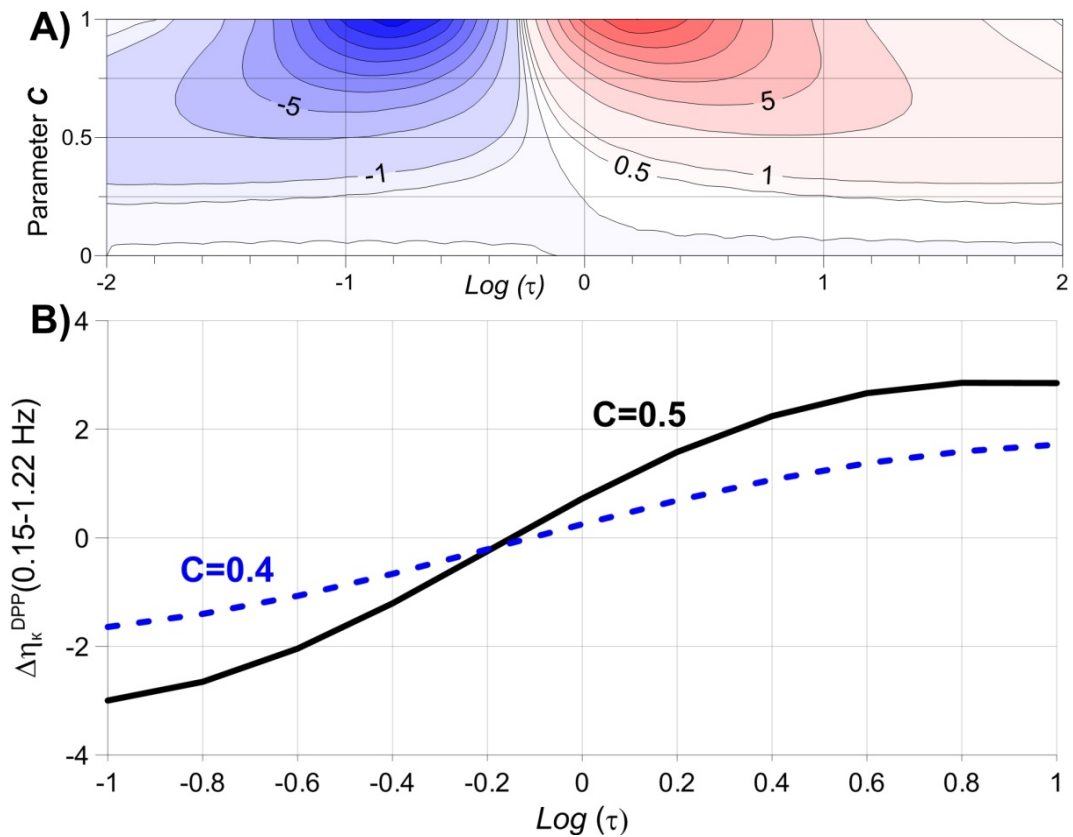


Fig. 1: A) Map of the difference $\Delta\eta_{\kappa}^{DPP}$ at frequencies 0.15 and 1.22 Hz above the homogeneous polarized half-space, depending on the parameters $\log(\tau)$ ($n = 20\%$); B) The diagrams of dependence of $\Delta\eta_{\kappa}^{DPP}$ from $\log(\tau)$ at various parameters C .

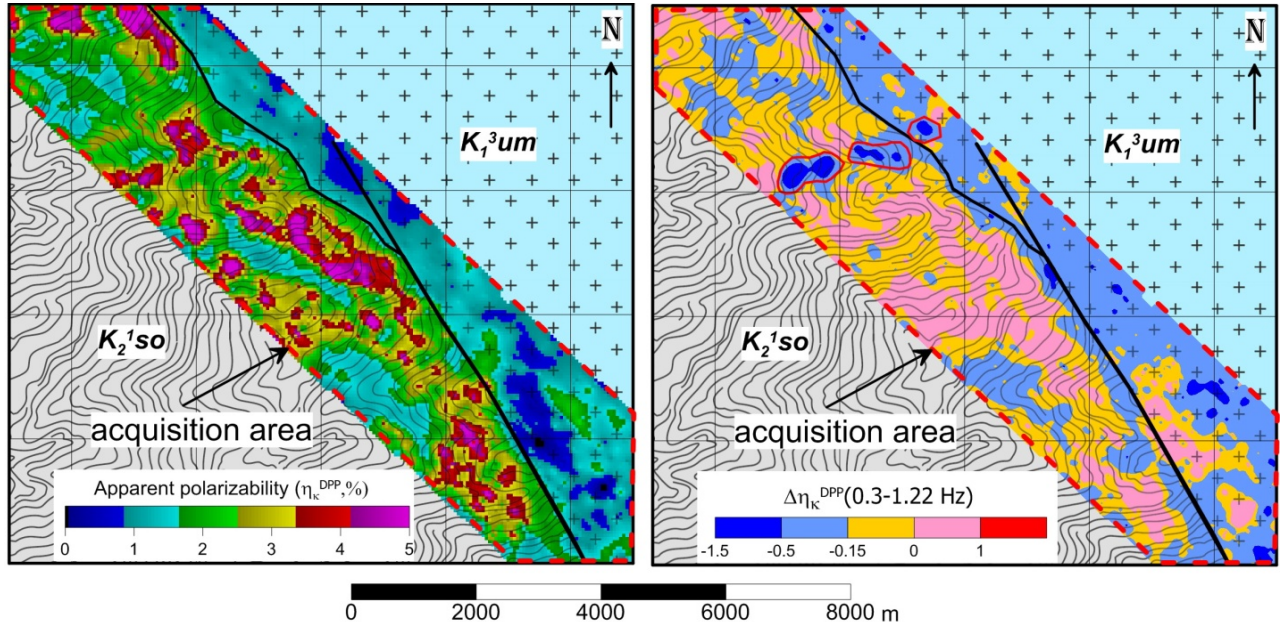


Fig. 2: Map of apparent polarizability η_{κ}^{DPP} (left) and parameter $\Delta\eta_{\kappa}^{DPP}$ (0.3-1.22 Hz) (right).

Explorations carried out at the skarn deposits in Transbaikal using the mean gradient – induced polarization (MG-IP) modification of the method allowed separating silicate and magnetite skarn bodies based on the DPP maps at different frequencies. Skarns with prevailing sulphides (pyrite, chalcopyrite) feature a longer IP field decay time compared to pure magnetite varieties.

Multi-frequency downhole DPP measurements performed within the ore of the Norilsk Intrusion showed that a higher copper-to-nickel ratio in the ore composition causes a shift of the DPP frequency characteristic maximum towards the low-frequency domain, resulting in an increase of induced polarization time parameter τ (Kulikov 2013).

Conclusions

There are many practical methods for evaluation of time (frequency) characteristics of induced polarization in rocks. Information obtained through various measurement methods is essentially equivalent. Here we have an additional parameter of the medium which, together with apparent resistivity and apparent polarizability, can be used in subsequent geological interpretation of geophysical data.

However, in our opinion, the differential phase parameter has a number of technical advantages over other methods.

First of all, phase measurements allow achieving more accurate results. Secondly, DPP substantially suppresses any phase shifts associated with electromagnetic induction shift, which is especially important when working with large spreads.

In addition, as shown by field exploration results, the DPP frequency characteristic maximum for the most common polarisable rocks – carbonaceous shales, sulphide ores etc. is usually located within a limited medium-frequency range, making it convenient for field registration (0.1 – 5 Hz).

The differential phase parameter (DPP) has a simple relation to the Cole-Cole formula parameters. Increase in time constant τ causes a shift of the DPP modulus maximum towards the low-frequency domain, while its width depends on the value of power parameter C .

Having an additional parameter in the form of DPP difference at several frequencies, we can, under certain favourable conditions, separate induced polarization anomalies from carbonaceous and magnetite-containing rocks, various sulphide ore assemblages, and anomalies related to ground water capillary fringes.

References

- Kulikov, A.V. and Shemyakin, E.A., 1978. Geoelectric prospecting using phase method of induced polarization (*in Russian*). Nedra press, Moscow, 157 p.
- Zorin, N. and Yakovlev, A., 2013. Telluric method of natural field induced polarization. 5th Int. *Symposium on Three-Dimensional Electromagnetics*, 7-9 May 2013, Sapporo, Japan.
- Kulikov, V.A., Zorin, N.I., Manzheev, I.T. and Yakovlev, A.G., 2013. Using of differential phase parameter (DPP) for IP anomalies separation (*in Russian*). *Geofizika*, 6, 10-16.

Monitoring sediments pollution of the Garonne River using induced polarization and magnetic susceptibility measurements

M. Llubes⁽¹⁾, M. Macouin⁽¹⁾ and B. Lartiges⁽¹⁾

(1) GET - UMR5563, Observatoire Midi-Pyrénées, France

We characterized the impact of a big city (Toulouse, France) on the pollution of river sediments brought by urban discharges during rainfall. The samples collected at several locations in the river are characterized by IP and magnetic susceptibility measurements. The results show a clear influence of the city on the sediments. However, the curves of magnetic susceptibility and IP data along the river are anti-correlated, contrary to our a priori hypothesis. The nature of anthropogenic particles sluiced by rainfalls could explain this phenomenon. A complementary microscopic and mineralogical analysis of the samples will help us to understand the unexpected result of this study.

Introduction

Cities are the source of many polluting particles, often from human activities: industrial (heavy metals), traffic (hydrocarbons, heavy metals, various oxides), roads and urban construction (cement, paints, tar), and many other. During rain events, these particles are washed into the river, natural topographic receptacle. The spatio-temporal variability, randomness and diversity of origins make it difficult to characterize these emissions and their effect on aquatic environments (Truchot et al. 1994).

The purpose of this study is to characterize the impact of the Toulouse area on the pollution in the sediments of the Garonne. We used two geophysical parameters, chargeability and magnetic susceptibility, to monitor samples along the river.

Sampling and instrumentation

Sediments were sampled at seven sites from Portet-sur-Garonne (Toulouse upstream) to Grenade (downstream of the city) within the riverbed. Each time, we have kept the fraction 50-200 microns for the measures, which allows for more homogeneous samples from one site to another.



Fig. 1: Installation for IP measurements, the sample is in the centre, in the plastic tube.

For this study, we developed a device to measure the induced polarization in the laboratory with very small amounts of soil (about 10 mL). We used non polarisable electrodes (Fig. 1), both for receiving and injection. Measurements are made in temporal IP using a SAS1000 apparatus.

The magnetic susceptibility has been measured in the laboratory on the same samples with a Kappabridge KLY3 AGICO. To complete the interpretation of these data, we separate the heavy particles from some samples, and we observed them by electron microscopy.

Results and discussion

Figure 2 shows the measurement result of chargeability and magnetic susceptibility, ranging from upstream (left side of the figure) to downstream of the city (right side of the figure). Only the first sample (named P2*) is located upstream to Toulouse. Spatial variation is noticed along the

river, with a link to the presence of urbanization very clear effect. The data fluctuate on the stretch that crosses the city, highlighting an inhomogeneous distribution of particulate pollutants.

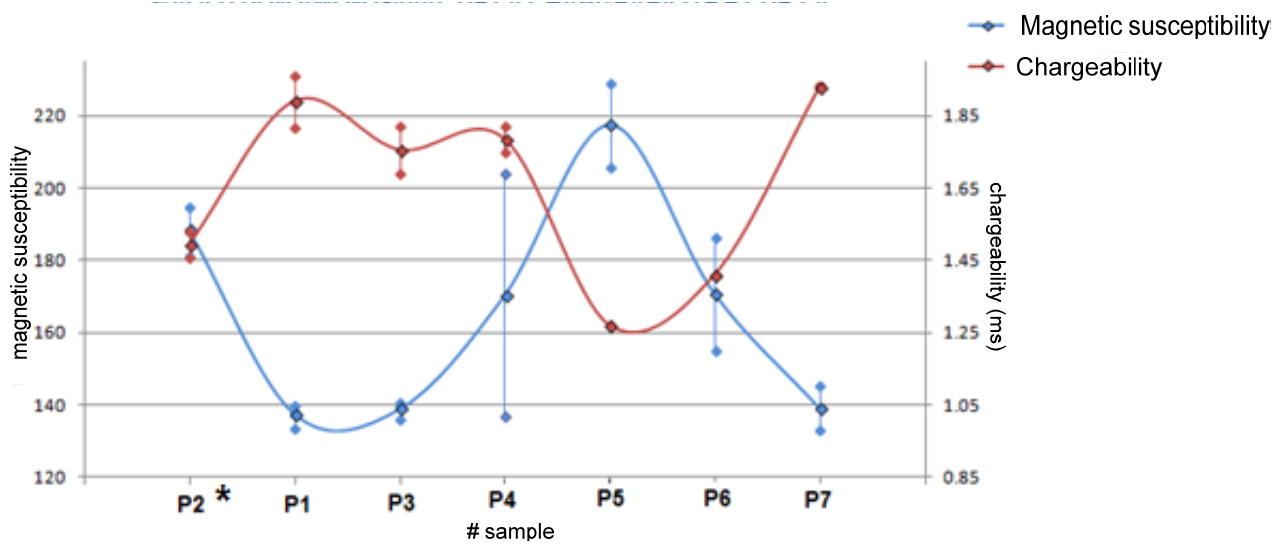


Fig. 2: Measures chargeability and magnetic susceptibility of samples taken along the Garonne (upstream is left downstream right)

Contrary to our expectations, the two geophysical parameters are anti-correlated with an increase in IP in the city, while the susceptibility decreases. The nature of the particles responsible for this phenomenon is certainly the cause of these variations.

Finally, far downstream of Toulouse (last sampling), the influence of urbanization has not decreased, which implies transportation over several km of leached particles.

The electron microscopic analysis was used to validate the presence of numerous anthropogenic particles. However, no precise quantitative estimate could be made, nor on the spatial variations of the quantities of these particles.

Conclusion

This first study validates the use of chargeability and magnetic susceptibility for monitoring pollution in river sediments, even in the case of a weakly polluted river as the Garonne. Characterization and quantification of particles involved remains to be done to identify the sources of the observed phenomenon.

Reference

Truchot, C., Chocat, B., Chatelain, M., Mares, A. and Mouchel, J.M., 1994. La pollution des rejets urbains par temps de pluie: impacts sur les milieux récepteurs. *La houille blanche*, 1-2, 97-105.

Interpretation of a clay rock's desaturation process with IP methods

G. Okay⁽¹⁾, P. Cosenza⁽²⁾, A. Ghorbani⁽³⁾, C. Camerlynck⁽⁴⁾,
J. Cabrera⁽⁵⁾, N. Florsch^{(4),(6)} and A. Revil^{(7),(8)}

(1) *Department of Geomatics, Hacettepe University, Ankara, Turkey*

(2) *CNRS UMR 7285 IC2MP-HydrASA, University de Poitiers-ENSIP, Poitiers, France*

(3) *Department of Mining and Metallurgical Engineering, Yazd University, Yazd, Iran*

(4) *UMR 7619 Metis, Université et Pierre et Marie Curie, Paris, France*

(5) *French Institute of Radioprotection and Nuclear Safety, Fontenay-aux-Roses, France*

(6) *UMI 209 UMMISCO, Institut de Recherche pour le Développement, Paris, France*

(7) *Colorado School of Mines, Department of Geophysics, Golden, USA*

(8) *ISTerre, CNRS, UMR CNRS 5275, Université de Savoie, 73376 cedex, Le Bourget du Lac, France*

This study investigates the desaturation of a clay rock with Electrical Resistivity Tomography (ERT) and Induced Polarization methods used in time (TDIP) and spectral domains (SIP) in the experimental Underground Research Laboratory of Tournemire (Aveyron, France) which belongs to the French Institute of Radioprotection and Nuclear Safety (IRSN). The desaturation process is investigated from the older gallery (East-96), excavated in 1996, in the experimental test site over profiles concerning floors and walls of the gallery. The desaturation has interpreted by two approaches: (1) all electrical parameters and observations gathered for a profile including floor and walls (U profile, see Fig. 1) at a time of acquisition, (2) monitoring the Excavation Damaged Zone's (EDZ) evolution with ERT and TDIP methods during two different periods (June 2008 and February 2009) having different hygrometry values.

The East-96 gallery has no surface-coating (directly clay rock) and the investigated layer is an EDZ including fractures originated from mechanical stress release (new fractures, mm) and hydric modifications due to the ventilation of gallery (hydric fractures, mm) after the excavation. ERT and TDIP measurements were carried out with a Syscal Pro device (IRIS instruments) while SIP measurements were performed (46 mHz – 12 kHz) with the SIP FUCHS-II apparatus (Radic Research). To install electrodes, drillings with holes 12 ± 1 mm in diameter and with a depth of 5.0 ± 0.1 cm are realized. After that, the injection of wet bentonite into these micro-drillings is made. Non-polarizing Cu/CuSO₄ electrodes (6 mm in diameter) were used during injection and potential measurements. Figure 1 shows ERT and TDIP tomograms and the apparent imaginary conductivity spectra obtained from SIP measurements over the U profile. The inversion of the chargeability and the resistivity on U profile has been carried out with the software Res2Dinv from Geotomo (Loke and Barker 1996). We separated the collected data as North wall, South wall and ground into files and then the inversion is applied separately for each section.

Our study over the U profile of East-96 gallery show that hydric fractures on walls cause textural modification on the rock which are interpreted as a continuous layer with high resistivity (100 – 160 Ω m) and low chargeability (≤ 2 mV V⁻¹) values. While at the ground, where we observe new fractures, the EDZ is more important compared to wall's EDZ according to resistivity values. The different state of damage between gallery walls and ground can be related to anisotropy of the rock. Another explication of this difference on the damage can be explained by the work of Ramambasoa (2001). This author indicated that hydric fractures have a hydromechanic behaviour which is a function of ambient hygrometry. In summer (humid period), hydric fractures are closing, while in winter (dry period), hydric fractures are opening. New fractures associated with stress release do not show such kind of hydromechanical behaviour. In consequence, except the mechanical damage, ground seems to be subjected to desaturation process over the all year which amplifies the state of damage at this zone. Thus, new fractures allow desiccation of the clay rock though its cracked-air filled structure penetrating through the depth of the rock (Okay et al. 2013). A

very sensitive parameter to water content (Ghorbani et al. 2009), the apparent imaginary conductivity spectra, obtained for a Wenner array C1P1 = 40 cm, also support this statement. Ground show the lowest polarization amplitude compared to gallery wall. Consequently, the lower amplitude of σ'' support the strongly desaturated state of ground compared to the gallery walls. As an another result, monitoring the EDZ's evolution with TDIP method during two different periods (June 2008 and February 2009) having different hygrometry show the change of resistivity and chargeability confirming Ramambasoa (2001) and the desaturation penetrating in deeper layers of the clay rock.

Finally, SIP tomography obtained from longitudinal profiles at ground show the desaturated state of clay rock with an emphasized visibility with increasing frequency (187, 375 and 750 Hz).

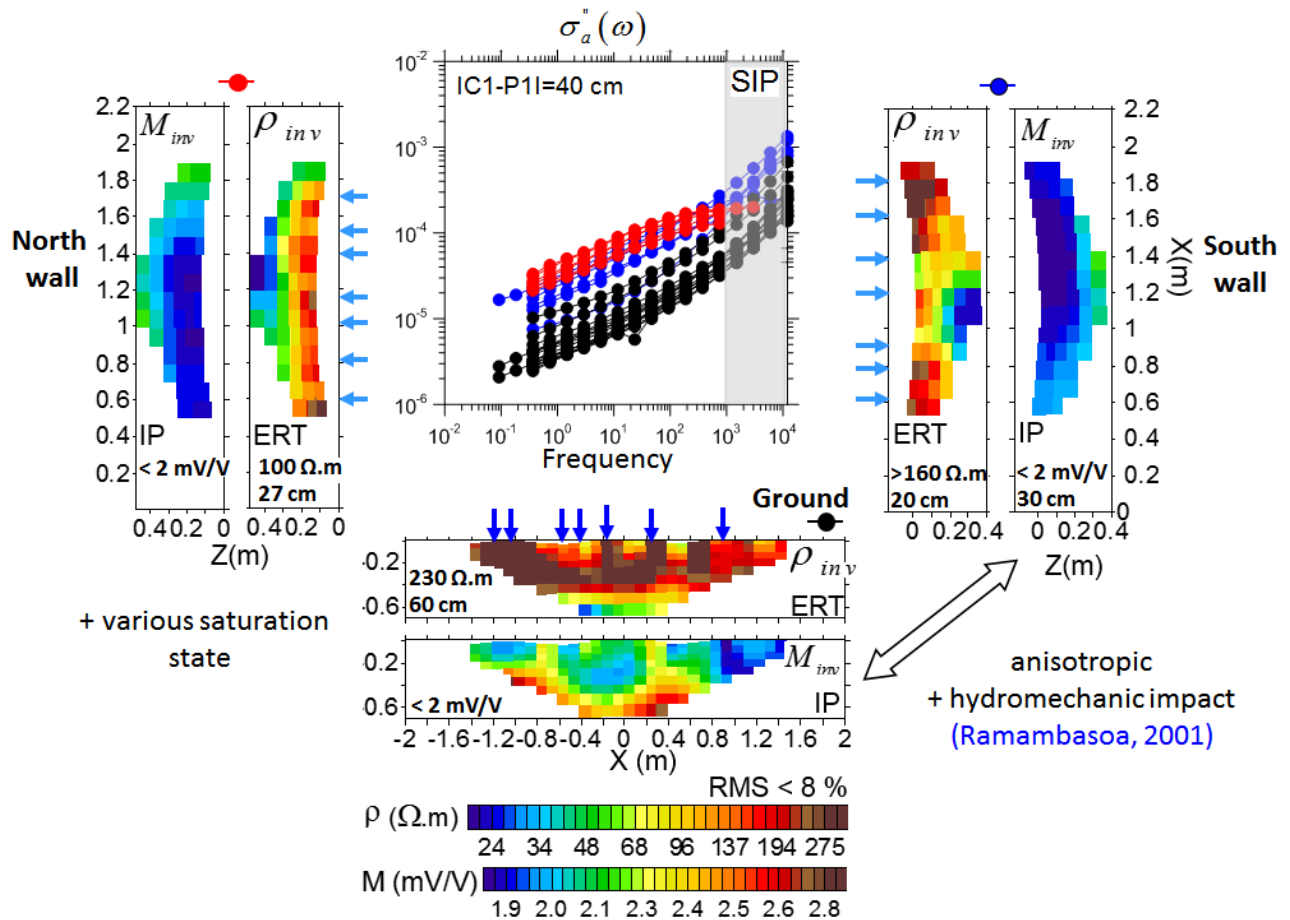


Fig. 1: Electrical resistivity and TDIP tomograms at the East-96 gallery U profile (concerning North wall, South wall and the ground) and the imaginary conductivity spectra. Each curve on the spectra indicates a measurement of a frequency range over a position on the U profile. This means that red curves interpret measurement on the North wall, blue curves interpret measurements on the South wall and black curves indicate measurements on the ground (all with Wenner array).

References

- Ghorbani, A., Cosenza, P., Revil, A., Zamora, M., Schmutz, M. and Florsch, N., 2009. Noninvasive monitoring of water content and textural changes in clay-rocks using spectral induced polarization: a laboratory investigation. *Appl. Clay Sci.*, 43, 493-502.
- Loke, M.H. and Barker, R.D., 1996. Rapid least-squares inversion of apparent resistivity pseudosections by a quasi-Newton method. *Geophys. Prospect.*, 44, 131-152.
- Ramambasoa, N., 2001. Etude du comportement hydromécanique des argilites: application au site de Tournemire. Thèse de Doctorat, Ecole Polytechnique, Palaiseau.
- Okay, G., Cosenza, P., Ghorbani, A., Camerlynck, C., Cabrera, J., Florsch, N. and Revil, A., 2013. Localization and characterization of cracks in clay-rocks using frequency and time-domain induced polarization. *Geophys. Prospect.*, 61, 134-152.

Integrating ERT and IP measurements with traditional environmental sampling – ambiguity reduced or increased? A DNAPL case study from Norway

J. Scheibz⁽¹⁾, S. Bazin⁽¹⁾, A.A. Pfaffhuber⁽¹⁾, G. Fiandaca⁽²⁾,
T. Dahlin⁽³⁾, P. Cappelen⁽¹⁾ and V. Zadorozhnaya⁽⁴⁾

(1) Norwegian Geotechnical Institute, Oslo, Norway

(2) HydroGeophysics, Aarhus Univ., Denmark

(3) Engineering Geology, Lund Univ., Sweden

(4) Council for Geoscience, Pretoria, South Africa

To reduce costs for brownfield investigations while increasing the predictability of contamination plumes, non-invasive and cost efficient investigations methods are needed in addition to classic investigation tools as sampling and drilling. Due to the development of sophisticated equipment and computing tools the combined deployment of Electric Resistivity Tomography (ERT) and Induced Polarization (IP) is a promising tool and of interest for groundwater and contaminated land related issues.

The case study presented here is a small-scale wood preservation plant, located in Central Norway, on which creosote has been applied extensively since 1935. The main sources of the contamination were leaking installations related to a single source that has been stopped. For the environmental risk assessment 56 shallow drillings were conducted on site, soil samples for chemical analyses taken and a drainage installed to stop further spreading. Creosote is a coal-tar distillation product and belongs to the group of dense non-aqueous phase liquids (DNAPL). While being banned in the E.U. it is still widely used for the preservation of wood and abundant as a subsurface contaminant. Due to its density ($1.00 - 1.17 \text{ g cm}^{-3}$ at $25 \text{ }^\circ\text{C}$), it sinks in the groundwater until reaching low permeable barriers and therefore is hard to detect and remediation actions are costly. Furthermore, the low solubility of these fractions makes DNAPL a long time groundwater hazard (Priddle et al. 1994). Being a low conducting and non-polar material makes it a good target for geoelectrical (ERT and IP) mapping.

Our lab test with creosote saturated sandstone showed that even small amounts of creosote lead to a high increase in resistivity and concurrent very low chargeability effects. However defined small scale tests can only be guidelines for field observations Previous ERT/IP measurements (Bazin 2011) were conducted on site using different experimental setups (with different protocols and cable types) and processing software (Res2Dinv, Em1dinv). The latter takes Cole-Cole parameters into account for the inversion process but is currently not available as a commercial tool (Fiandaca et al. 2012). These investigations were a good basis for a first characterization of the site.

Additional ERT/IP measurements were carried out in late 2013 using again the ABEM Terramter LS (12 channels, 81 electrodes) to delineate the plume: four additional high resolution profiles (1 m spacing, 45 to 80 m length) were carried out with the Gradient-Plus protocol. Processing was carried out using Res2Dinv (Loke 2013), limiting the potential of IP-data processing. Data and drilling information were displayed in 3D using RockWorks 16.

According to drilling information, the subsurface can be summarized as followed (Fig. 1):

- Backfill, consisting of peat, woodchips and sawdust: 0.0 – 3.0 m depth (dry: 400 – 1500 Ωm saturated: 20 – 80 Ωm)
- Coarse grained (sand, gravel) sediments: 0.0 – 5.0 m depth (dry: 500 – 2000 Ωm , saturated: 100 – 500 Ωm)
- Fine grained (silty sands and gravels) sediments: 3.0 – 5.0 m depth (saturated: 800 – 300 Ωm)
- Bedrock (Granite and Shale/Limestone): 300 – 2000 Ωm

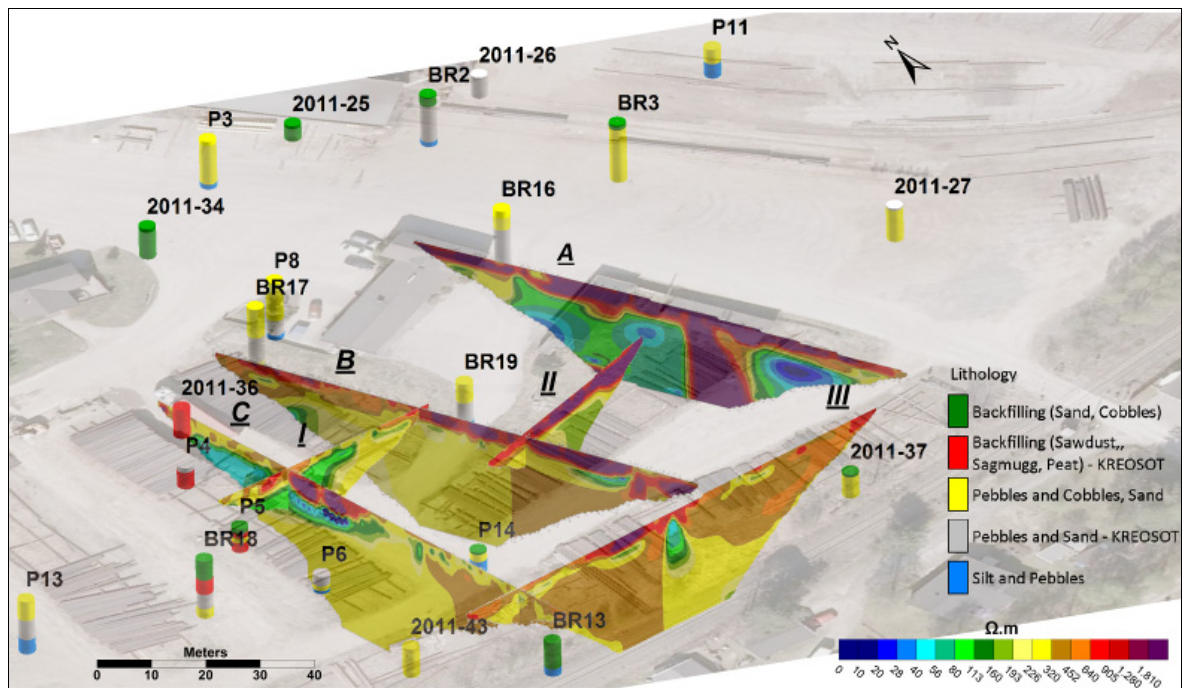


Fig. 1: 3D-visualization of resistivity sections.

Median groundwater levels are between 2.5 – 3.5 m below surface. High concentrations of creosote in the soil (up to 42 gr kg⁻¹) result in up to 1.5 m of free phase on the groundwater table. Bedrock starts at 4 m depth on. Due to glacial processes, the topography of the bedrock is subject of uncertainty and may show large variations. The ERT models reveal high resistivities (> 600 Ωm) along all six profiles limited to the vadose zone which coincide with areas of very low chargeability (5 – 9 mV V⁻¹). Furthermore the extent of these high resistivities decreases away from the contamination source in western direction (Profile A-B-II-C, Fig. 2) and a sharp boundary exists below that depth (2.5 – 3.5 m depth). We therefore suggest that these areas are creosote contaminated backfilling and sediments.

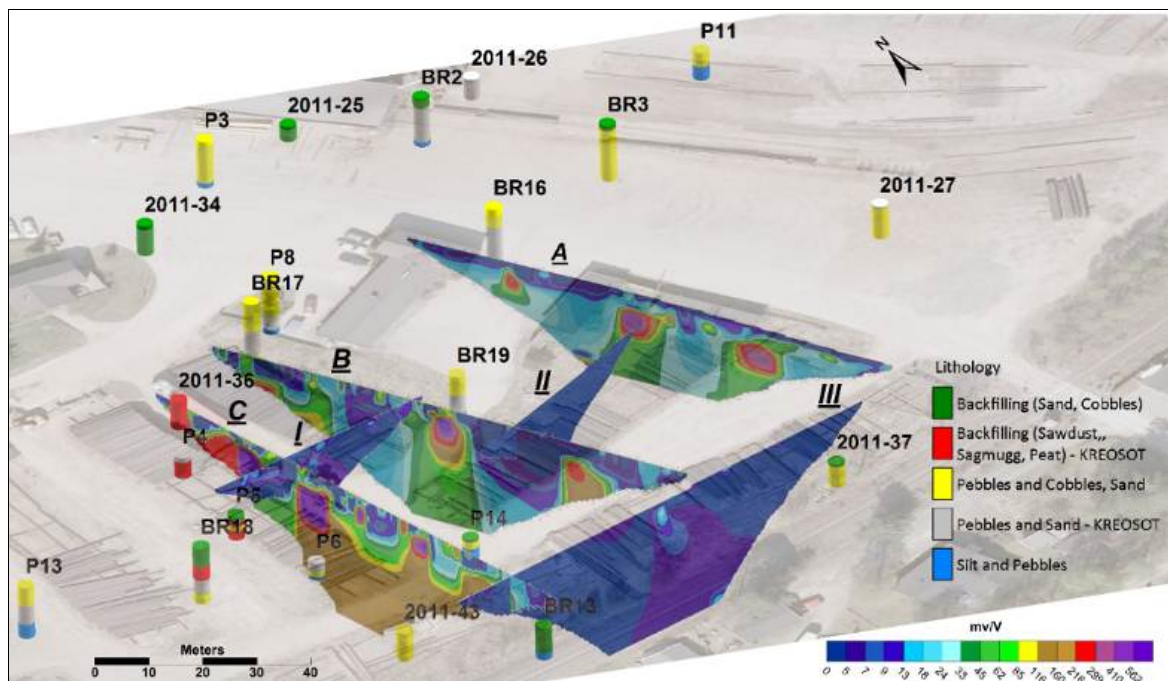


Fig. 2: 3D-visualization of IP sections.

For the groundwater saturated area the ambiguity is manifold. Most resistivity values down to the maximum penetration of about 15 m are homogenous and vary between 200 to 500 Ωm (yellow to brown on Fig. 1) with no visible boundaries that could indicate a potential sediment-bedrock contact. This also applies to the chargeability (profiles A-B and I-II-III: 5 – 50 mV V^{-1}). Additionally some areas show very low resistivity patterns between 10 – 100 Ωm which cannot be related to the known geology or contaminant. Profiles A-B-C (Fig. 1) show furthermore isolated chargeability anomalies ($> 300 \text{ mV V}^{-1}$) of unknown nature. Thanks to the 3D-visualization it was possible to recognize them as linear features which are probably of anthropogenic origin (subsurface installations). At last, Profile C shows from 4 m depth a continuous chargeability anomaly (150 mV V^{-1}) which cannot be interpreted.

We conclude that with our complementary approach it was possible to map the extent of the residual creosote in the vadose zone while the integrated 3D model for the saturated area remains difficult to interpret and subject of further analysis. The 2011 as 2013 surveys showed good matching resistivity distributions which gives confidence in the reliability and repeatability of the acquisition method. Nevertheless further development of our IP-inversion tools is necessary. Full Cole-Cole inversion of profile B data showed the superiority compared to "RES2DINV-style" bulk IP inversion (Bazin et al. 2011). This would improve IP's potential as a commercial tool for environmental site assessment.

References:

- Bazin, S., Pfaffhuber A.A., Fiandaca G., Dahlin T., Cappelen P., French H., and Bloem, E, 2011. Is commercial IP instrumentation ready for operational pollution plume mapping? *Proc. 2nd Int. workshop on Induced Polarization*, 31 October – 2 November 2011, Golden, Colorado
- Fiandaca, G., Auken, E., Gazoty, A. and Christiansen, A.V., 2012. Time-domain induced polarization: Full-decay forward modeling and 1D laterally constrained inversion of Cole-Cole parameters. *Geophysics*, 77, E213-E225.
- Loke, M.H., 2013. Tutorial: 2-D and 3-D electrical imaging surveys (rev. March 2013), <http://www.geotomosoft.com>.
- Priddle, M.W. and MacQuarrie, K.T., 1994. Dissolution of creosote in groundwater: an experimental and modeling investigation, *J. Contam. Hydrol.*, 15, 27-56.

Spectral induced polarization response of soil organic matter

N. Schwartz⁽¹⁾ and A. Furman⁽¹⁾

(1) Technion – Israel Institute of Technology

The spectral induced polarization (SIP) method is increasingly used for the exploration of the subsurface in numerous hydrological and environmental applications. Since the early use of the SIP method a tremendous progress in the understanding of the mechanisms that govern the SIP response of porous media was achieved. Many models that explain the relations between the SIP signature of soil and the soil physical and physicochemical properties were developed (e.g. electrochemical and membrane polarization models). All these models predict that soil polarization is dependent on the surface charge (often measured through the cation exchange capacity, CEC), and that increase of the surface charge will result in an increase of the soil polarization. While these models were calibrate/validate for mineral soil, to the best of our knowledge the effect of soil organic matter (SOM), which although relatively small in volume/weight significantly contribute to the surface charge, on the SIP signature of soil was not directly studied.

Here, we report experimental evidence that demonstrate the impact of SOM on the SIP response of soil. The experiment includes SIP measurements of sandy soil with negligible amount of organic matter, and a mixture of natural organic matter with the same soil. The experiment procedure can be summarized as follow:

- (1) air dry soil were mixed with different amount of air dry organic matter (0 , 0.1 and 1 % w/w);
- (2) water (10 % w/w) was mixed with the dry material using a kitchen mixture for 10 minutes;
- (3) a constant amount of soil was packed in a glass box of known volume (271 cm³), resulting in a consistent water saturation between the samples ($S_w = 43.7$);
- (4) five days after the packing, SIP measurements (10 mHz – 10 kHz) of all the samples (triplicate for each treatment) were taken using four non-polarized electrodes.

In addition to the electrical measurements, the composition of the soil solution, the cation exchange capacity and the exchangeable cation composition were determined.

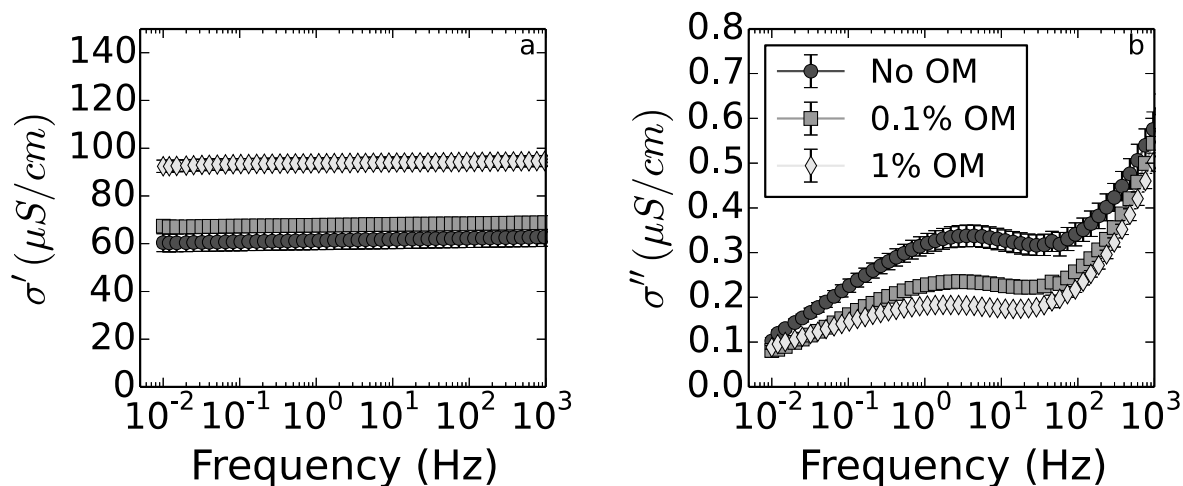


Fig. 1: Mean values and standard deviation (error bar) of the in phase (a) and quadrature (b) conductivity for the three treatments (no organic matter; 0.1 % w/w and 1 % w/w). Note the decrease in relaxation frequency with increasing OM content.

The mean values of the in-phase and quadrature conductivities for the different treatments are shown in Figs 1a and 1b, respectively. The results show that addition of 0.1 % OM to the soil did not significantly change the in-phase conductivity, while addition of 1 % OM resulted in an increase (~60 %) of the in-phase conductivity. The increase of the in-phase conductivity is explained by the presence of soluble salts in the organic matter. Interestingly, addition of organic

matter to the soil resulted in a significant decrease of the soil quadrature conductivity (a measure for the soil polarization) and relaxation frequency (see Fig. 1b). A decrease of ~43 % and ~87 % at 3.5 Hz in the quadrature conductivity for the soil containing 0.1 % and 1 % OM, respectively, was observed. In addition, the relaxation frequency decreases from 1.66 Hz for the 0 % treatment to 1.48 Hz for the 0.1 % treatment and to 0.88 Hz for the 1 % treatment.

The decrease in polarization for soil containing organic matter is not trivial. That is as the CEC of the added OM (103 meq / 100 g) is much higher than the CEC of the soil (2.5 meq / 100 g) and therefore, naively we would expect to see an increase of the soil polarization. To explain the decrease in the soil polarization due to the addition of OM, the interactions between OM and the soil mineral surface is needed to be considered. Interactions between OM and mineral surface can occur, for example through metal bridge, hydrogen bonds, van der Waals interactions and exchange process between natural organic cation and metal cation. These processes are expected to increase the binding energy between the metal cations and the mineral surface, which can explain the observed decrease in polarization and relaxation frequency. Indeed, increase in the binding energy means lower mobility of the metal cation on the soil mineral surface, results in a decrease of polarization and relaxation frequency, as observed in this study.

A comprehensive study of the SIP response of soil contaminated with organic pollutants

N. Schwartz⁽¹⁾, I. Shefer⁽¹⁾ and A. Furman⁽¹⁾

(1) Technion – Israel Institute of Technology

In recent years, there is a growing interest in using geo-electrical methods to detect and monitor organic contaminants, their transport, and their fate within the subsurface. To efficiently relate between the electrical properties measured in a geo-electrical survey and the presence, transport and fate of organic contaminants, an understanding of the influence of organic contaminants on the electrical properties of the porous media is required. Such knowledge is usually empirically based, and is mostly limited to the presence of non-miscible contaminants in the saturated zone. The aim of this work is to determine the effect of organic contaminants on the electrical properties of variably saturated porous media by combining laboratory experiments and theoretical modelling.

The experimental part of this work includes three sessions. In the first we measured the effect of a mixture of organic contaminants, namely motor oil or diesel fuel, on the electrical properties of unsaturated soil. In addition we also measured the effect of the contaminants on the electrical conductivity of the pore water. In the second session we investigated how an exchange process between inorganic and specific organic cations affects the electrical properties of saturated soil (i.e. to eliminate the role of saturation). In this session both the SIP signature of the soil and the chemical properties of the soil solution were monitored during the exchange process. In the third session we investigated the effect of free-phase organic contaminant on the SIP signature of an unsaturated soil. In this experiment we added a single non-polar organic contaminant to an unsaturated soil and measured the SIP signal. In addition we also examined the effect of the added organic contaminant on the chemical composition of the soil solution.

In addition to the experiments, we also modelled the effect of adsorbed organic species on the chemical and electrical properties of porous media. Our model includes a chemical complexation module that was used to determine the surface site density of different chemical species. The results of the model were used as an input to a Stern layer polarization module. The model results were used to construct a mechanistic model for the effect of adsorbed organic contaminant on the SIP signature of porous media.

Our results show that addition of free-phase organic contaminants to unsaturated soil (where water saturation remains constant, i.e. contaminant replace air) does not significantly affect the in-phase electrical conductivity of the soil, but does result in a decrease of the soil polarization and relaxation time. Interestingly, further addition of contaminant did not result in a further change of the soil polarization or the relaxation time. In addition, the chemistry of the soil solution did not change after the addition of the contaminant. We conclude that the effect of free-phase contaminant is through the geometry of the conductive phase (water), and the membrane polarization model can explain the resultant effect on SIP signal.

The results of the first two experiments, that take into account exchange processes between inorganic and ionic organic compounds, show that due to the exchange process the in-phase electrical conductivity increases while the polarization decrease. These results were found to hold for both saturated and unsaturated cases. The exchange process affects the chemistry of both the soil solution and mineral surface, and in turn affects the SIP signal. The chemical and electrical models demonstrate the role of the Stern layer polarization on the SIP signal. The model shows that the lower mobility of the ionic organic compounds at the Stern layer (compared to the inorganic ions) is the main factor affecting the decrease in polarization, and that the increase in the in-phase conductivity resulted from the release of inorganic ions to the soil solution.

Clearly, when a mixture of organic contaminants that contains both polar and non-polar compounds (most real contaminants are essentially a "cocktail") is introduced to the subsurface, the two processes mentioned above (i.e. exchange processes and changes in the conductive phase geometry) are expected to take place simultaneously. Still our results indicate that change in the chemical composition of the mineral-liquid interface is more dominant and is also expected to affect the in-phase electrical conductivity. From application point of view, it is worthwhile to note that in any of the cases considered here and regardless of the governing mechanisms, the polarization of the soil is decreasing in response to the addition of organic contaminant. This is of importance as it can serve as a marker in IP surveys conducted at site suspected to be contaminated with organic pollutants.

To conclude, in this work we show that organic contaminants affect the electrical properties of porous media. We provide new experimental evidence for the effect of free-phase organic contaminant in unsaturated porous media and for the effect of adsorption of ionic organic compounds on the electrical properties of the porous media. A new conceptual model that explain the mechanisms by which organic contaminant affect the SIP response was developed, and for the case of adsorbed organic compounds the conceptual model was tested using an existing model for SIP response of porous media. The results of this work can be used to better interpret electrical data collected at site contaminated with organic pollutants, as well as better design of monitoring systems.

Spectral induced polarization on roll-front type deposits

E. Williard^{(1),(2)}, A. Mainault⁽¹⁾ and M. Béhaegel⁽²⁾

(1) Institut de Physique du Globe de Paris, UMR CNRS 7154, France

(2) Areva Mines, France

Uranium exploration in roll-fronts type deposits is a major issue for mining companies. Indeed, these geological objects are currently exploited at very low production costs.

Roll-front deposits consist of interbedded sequences of permeable and impermeable layers. Uranium mineralization occurs at redox interfaces generated by oxidising groundwater flow in permeable layers. Reduced part is mainly associated with disseminated and low-grade Fe-sulphides (pyrite) while Fe-oxide minerals (hematite, goethite) mark oxidised part. Some high-grade (%) of pyrite can be observed at redox boundaries.

Currently, ore delineation is carried out by successively drilling reduced part (hydrological down-gradient side) then oxidised part (up-gradient side). Aim of this study is to assess the suitability of Spectral Induced Polarization in order to optimize drill hole implementation. Nevertheless, characterization of roll-fronts by geophysical ground survey is challenging due notably to the aquifer high conductivity, clay bed, low-grade mineralization and depth.

Due to the ability of Spectral Induced Polarization (SIP) in providing information about rock mineral composition and notably to detect tenuous signal of metallic particles polarization, SIP was assessed on synthetic samples in laboratory and was implemented on Areva Mongolian permit.

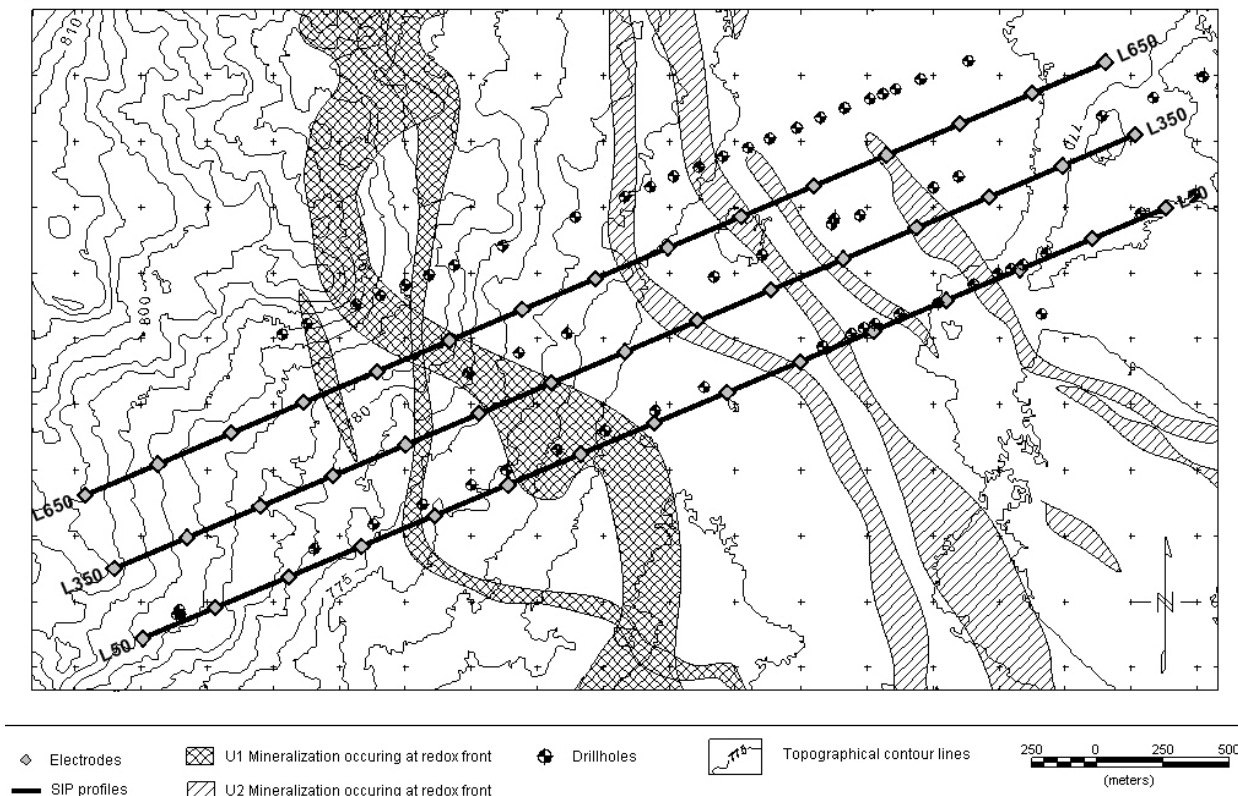


Fig. 1: SIP profiles implementation according roll-front mineralization.

To assess the feasibility of SIP, measurements were carried out on synthetic samples setting up with main characteristics of studied Mongolian roll-front. Indeed, sulphur and hematite dissemination represent only 4.8 % of mineral fraction. Permeable layers are mainly composed by unconsolidated sandstone. This study took also into account the aquifer high conductivity. Samples were saturated with conductive solution of 2.18 mS cm^{-1} composed by main ionic element of Mongolian aquifer. Main results of this laboratory study demonstrated that adding pyrite and

hematite led to a resistivity decrease of amplitude spectra. But only adding pyrite influenced the phase spectra between 5 Hz and 1 kHz. That is to say that, on field involving 4.8 ‰ disseminated minerals, identification of oxidised from reduced area could only be done by pyritic signature. At this stage of this study, we expected a lateral variation of phase shift between reduced and oxidised areas.

SIP method was implemented on a Mongolian roll-front in 2012. Two units are notably investigated and are located between 200 and 350 meters depth. Three parallel profiles of 4.2 km length and separated by 300 m were set up (Fig. 1). The profiles orientation was perpendicular to roll-front deposits. Electrodes spacing was 300 m, with 15 electrodes per line. The equipment used for this acquisition was a GDP 32^{II}, as receiver, and GGT-10, as transmitter, from Zonge International. Spectra were acquired from 0.125 Hz to 72 Hz.

Due to the high conductivity of this environment, large electromagnetic coupling is expected. To interpret the data, three approaches were evaluated to isolate this phenomenon.

First one consists to simply use a 3-point decoupling phase (known also as "Coggon phase", Coggon 1984) based on a power-series representation of the phase spectrum using information at three frequencies. Nevertheless, we demonstrate that the use of this method do not comply with its application limits in our geological context.

Second approach consists in treating SIP method as an EM method by calculating mutual impedance between cables based on a complex resistivity distribution. To achieve this goal, we invert SIP data with Cr1DInv developed by Ghorbani et al. (2009). In our context, results showed that increasing depth of investigation is associated with decrease of problem resolution.

Final approach consists in decomposing ground IP response and EM coupling response in two Cole-Cole dispersion terms. Amplitude spectra at lowest frequency and drill hole logging allowed us to establish a first approximation of ground DC resistivity. To obtain estimates and uncertainty of Cole-Cole parameters, we invert SIP data using Markov-chain Monte Carlo based stochastic algorithm developed by Chen et al. (2008). Results showed that Cole-Cole dispersion terms attributed to EM coupling are well determined but low chargeability of the ground leads to large uncertainty concerning Cole-Cole dispersion terms related to ground IP effects.

In perspective of this study, a sampling survey was undertaken in order to integrate dispersion terms obtained on "real" rock samples. We expect to better constrain initial model and reduce uncertainty related to low chargeability of the ground.

References

- Chen, J., Kemna, A. and Hubbard, S., 2008. A comparison between Gauss-Newton and Markov chain Monte Carlo based methods for inverting spectral induced polarization data for Cole-Cole parameters. *Geophysics*, 73, F247-259.
- Coggon, J.H., 1984. New three-point formulas for inductive coupling removal in induced polarization. *Geophysics*, 49, 307-309.
- Ghorbani, A., Camerlynck, C. and Florsch, N., 2009. CR1Dinv: a Matlab program to invert 1D spectral induced polarization data for the Cole-Cole model including electromagnetic effects. *Comput. Geosci.*, 35, 255-266.

Membrane polarization from molecular to rock scale in dynamic regime

V. Zadorozhnaya⁽¹⁾, N. Abu Zeid⁽²⁾ and G. Santarato⁽²⁾

(1) Council for Geoscience, Pretoria, Republic of South Africa

(2) University of Ferrara, Italy

In recent years V. Zadorozhnaya measured in laboratory a strong non-linear behaviour of electrical resistivity and chargeability in fresh-water saturated samples of several porous rock types. In particular she observed a general increase of resistivity and decrease of chargeability with injected current, together with an increase of both parameters also with time of electric current circulation, (Zadorozhnaya 2008; Zadorozhnaya and Hauger 2009; Zadorozhnaya and Maré 2011).

Based on Fick equation, a model of membrane polarization was developed at pore level, which successfully explained the results (*ibid.*). In particular, the model links the above non-linearity to Pore Size Distribution (PSD) and thus it allows to predict PSD from specifically designed measurements (at least 3 resistivity measurements at 3 different current intensities), in satisfactory agreement with PSD measured using the well-known Hg porosimeter test.

As is known, PSD is linked, although in a heuristic way, to hydraulic conductivity of a porous rock (e.g. Schoen 2004), so that recording a non-linear electrical response should allow predicting hydraulic conductivity through estimation of PSD. Of course, observing the same non linearity in the field by using conventional, or at most specifically adapted, resistivity and induced polarization methods should be of utmost importance for water resources exploration, as an information of strong hydrogeological impact could then be added to the estimation of effective porosity based on the well-known Archie's relationship (Archie 1942).

Electrical non linearity violates the well-established Ohm's law. Such non linearity was never reported in the geophysical literature, at authors knowledge, from usual field measurements. On the other hand, although today the IP response is taken for granted as linear, in the early times of testing the IP method, researchers were aware about possible non linearity associated to circulation of very intense electrical current (Bleil 1953; Iliceto et al. 1982): this non linearity was interpreted as a "saturation" effect, without any further investigation.

Authors also calculated and analysed the shape of induced polarization signals if arbitrary current pulse is to be applied to the sample (dynamic regime of transient IP). The results are very similar to laboratory experiments provided by Swanson et al. (2012).

In fact, laboratory samples are crossed by current densities which are fairly greater than those usually available in the field. As a matter of fact, electric currents of the order of 1 A or less are usually injected into the ground by currently available geo-resistivity-meters both for safety reasons and for portability of equipment. With so small current intensities at injecting electrodes, current density becomes very weak with increasing investigation depth, which is very far from laboratory measuring conditions.

In this work a field test is described, which was carefully planned, selecting a site where a saturated porous aquifer, of the same type as those had shown non linearity in the laboratory was possibly outcropping, to reduce decay of current density with depth of investigation. At the selected site (Northern Apennines, Italy), the porous saturated formation was sandstone, while the aquiclude was clay. Several shallow wells for collecting fresh water for drinking uses are present and were producing water at moment of measurements (May 2013). A commercial geo-resistivity-meter was used, to get measurements in a tomographic way, repeating the acquisition at two fixed and fairly different intensities of injected current, of 50 and 500 mA respectively. The equipment was the model SAS4000 by ABEM Instruments (Sweden), which is built as a current generator, so that injected current is under the control of electronic circuitry embedded in it. A profile of 25 electrodes, spaced 3 m was laid out, allowing for a maximum investigation depth of about 12 m.

The datasets were inverted by using a commercial two-dimensional inversion code and the resistivity models are shown in Fig. 1. The geological interpretation is simple: dark areas indicated by "C" are associated to clay formation, while the grey to dark areas indicated by "A" to saturated

sandstone. A fair increase of resistivity associated to the resistive bodies, i.e. saturated sandstone, is observed, centred at abscissae 31 m and 55 m respectively. Also chargeability models (not shown here) exhibit a behaviour which is quite similar to that observed on lab samples, i.e. a strong decrease with increasing current intensity.

The authors are aware that the field results shown here are so unusual that they need an indispensable validation, both by extending measurement at the test site and by repeating them in other sites, possibly of similar hydrogeological characteristics

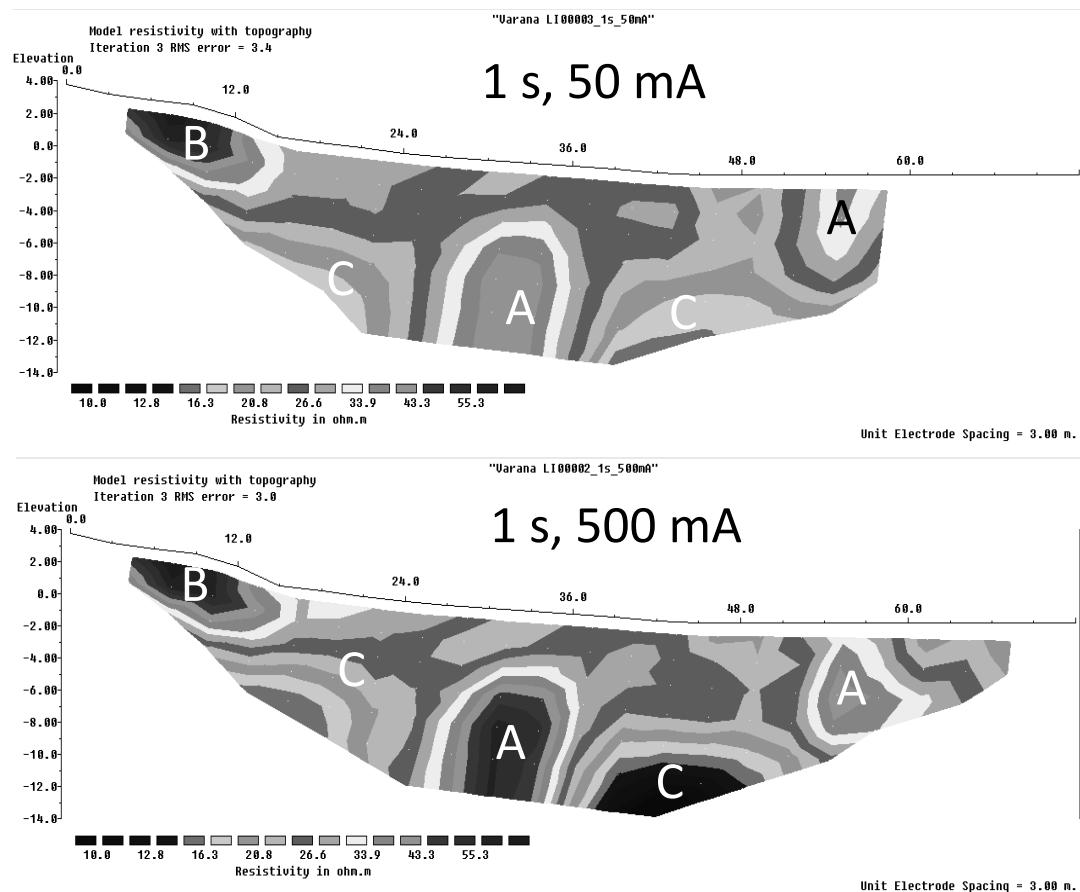


Fig. 1: 2D resistivity model obtained at 50 mA of injected current (above) and at 500 mA respectively (below), 1 s of injection time. A: aquifer bodies; B: drained debris.

References

- Archie, G.E., 1942. The electrical resistivity log as an aid in determining some reservoir characteristics. *Petroleum. Trans. AIME*, 146, 54-62.
- Bleil, D.F., 1953. Induced Polarization: a method of geophysical prospecting. *Geophysics*, 18, 636-661.
- Iliceto, V., Santarato, G. and Veronese, S., 1982. An approach to the identification of fine sediments by Induced Polarization laboratory measurements. *Geophys. Prospect.*, 30, 331-347.
- Schoen, J.H., 2004. Physical properties of rocks: fundamentals and principles of petrophysics. Elsevier, Amsterdam, 583 p.
- Zadorozhnaya, V.Yu. 2008. Resistivity measured by direct and alternating current: why are they different? *Adv. Geophys.*, 19, 45-59.
- Swanson, R.D., Singha, K., Day-Lewis, F.D., Binley, A., Keating, K. and Haggerty, R., 2012. Direct geoelectrical evidence of mass transfer at the laboratory scale. *Water Resources Res.*, 48, W10543.
- Zadorozhnaya, V.Yu. and Hauger, M.H., 2009. Mathematical modeling of membrane polarization occurring in rocks due to applied electrical field. *Izvestiya, Phys. Solid Earth*, 45, 1038-1054.
- Zadorozhnaya, V.Yu. and Maré, L.P., 2011. New model of polarization of rocks: theory and application. *Acta Geophys.*, 59, 262-295.

New shape of TEM: membrane polarization, mechanism and possible interpretation

V. Zadorozhnaya⁽¹⁾, N. Abu Zeid⁽²⁾, G. Santarato⁽²⁾ and S. Bignardi⁽²⁾

(1) Council for Geoscience, Pretoria, Republic of South Africa

(2) University of Ferrara, Italy

It is known that induced polarization (IP) effect affects the polarization process on a TEM sounding. Usually, it is an effect of electroosmosis type. Numerous formulae, which describe the IP-effect of electroosmosis type in geological media, are known. The most widely used IP model is described by the Cole-Cole formula (Cole and Cole 1941; Pelton et al. 1978). In our calculations, we use a simplified Cole-Cole formula, i.e.:

Frequency domain	Time domain
$\sigma(\omega) = \frac{\sigma_z}{1 + \frac{\eta}{i\omega\tau + 1}} \quad (1)$	$\sigma = \frac{\sigma_z}{1 + \eta} \left[1 - \eta \exp\left(-\frac{1 + \eta}{\tau} t\right) \right] \quad (2)$

where ω represents angular frequency, η is the polarizability and τ is the decay constant.

This means that η is the ratio of surplus electrical conductance to the electrical conductance of the pore fluid. The values of polarizability η ranges from 0, for sediments with large pore spaces when the contribution of the electrical double layer (EDL) is negligible, to 1, in sediments such as some types of clay, where the pore spaces are very small.

Many TEM soundings are distorted by the IP effect but not all of the decay curves change in sign. However, equations (1) and (2) show that the amplitude of IP effect does not depend neither on amplitude of electrical current nor on the current pulses duration.

The theory of IP effect caused by constrictivity of pores, developed by Zadorozhnaya (2008), Zadorozhnaya and Hauger (2009) and Zadorozhnaya and Maré (2011), to explain non-linear electrical phenomena measured on saturated samples of porous rocks in laboratory, starts from observing that cations in narrow capillaries are more mobile (transfer more electrical charges) than anions because in narrow capillaries some anions are adsorbed by the EDL and are immobile. This means that the salinity of cations increases. The salinity of anions is increased by the same amount (in case of neutrality of solution). Obviously the excess of salinity at the boundary between pores depends on time of applied current. If pulse length is short, then the excess of the ions becomes small and time of levelling (discharging) is also short. Increasing length of current pulse entails that the membrane effect increases. The direction of ions accumulated at the boundaries is the same as the current flow (Kobranova 1986). On the other hand the direction of discharge is also the same as the direction of transient emf. That is why the resistivity of layers, where membrane IP effect occurs, show considerable decrease.

In 2012, the authors carried out a TEM survey in the Northern Apennines composed of 6 soundings above a subsurface mainly composed by clayey layers. The ZONGE equipment was used. All the 6 TEM soundings were registered using different length of current pulses (frequencies 32, 8 and 4 Hz). Very strange signals were collected. While all decay curves show a typical IP effect, three of them (TEMs 1, 2 and 3, acquired on the northern side of the investigated area) strongly depend on used exciting frequencies, while the remaining three on the south do not. In Fig. 1 TEM 3 and TEM 4 are shown as examples.

For interpretation of TEM soundings, a 1D modelling and inversion code, written in MATLAB by V. Yu. Zadorozhnaya was used. Results of interpretation are given in Table 1. At frequency 32 Hz (right model) the section contains relatively resistive (60 – 90 Ωm) first layer, then resistivity gradually decreases with depth. The resistivity of deep clay layers is about 0.5 Ωm .

This geoelectrical structure shows a good agreement with a 2D, DC resistivity inversion model obtained nearby TEM 3 (not reported here). However, the resistivity of clay considerably decreases when frequencies 8 Hz or 4 Hz have been used (left model). Obviously the resistivity

0.05 Ωm is too small to be a realistic value of any shallow formation, even for a submarine clay deposit. This effect can be explained if we accept that an additional type of IP effect occurs, due to different length of current pulses. We propose that membrane polarization occurring due to constrictivity of pores affects the shape of the TEM signals, which depend on the exciting current time-span.

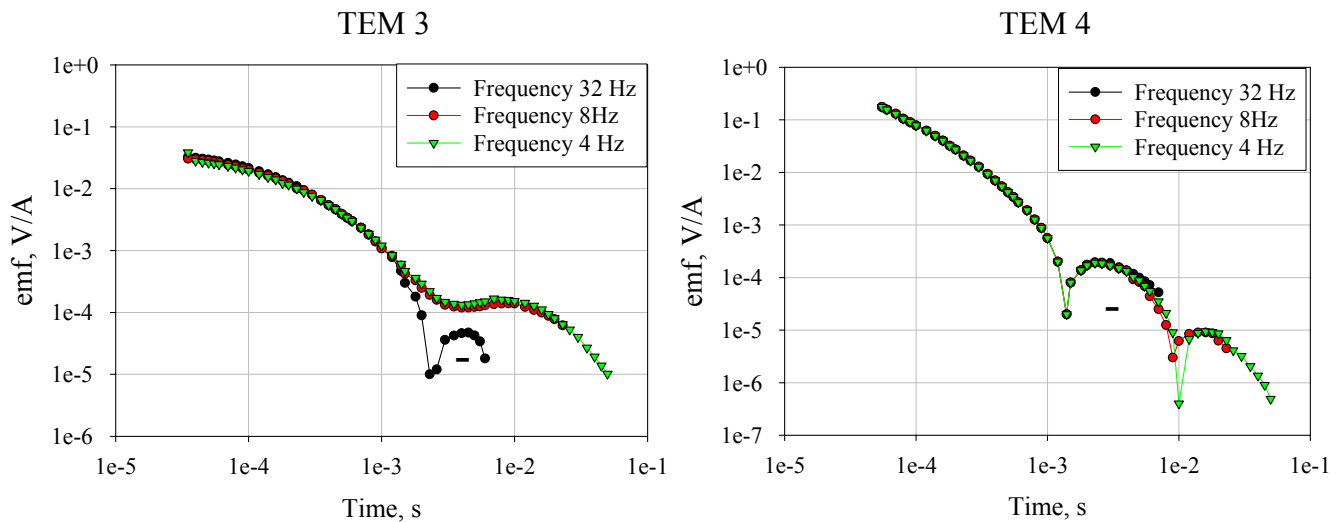


Fig. 1: Decay curves of TEM soundings 3 and 4.

Modelling of TEM 3. Frequency 4-8 Hz					Modelling of TEM 3. Frequency 32 Hz				
# of layer	ρ resistivity ($\Omega\text{ m}$)	h thickness (m)	η chargeability	τ decay constant (s)	# of layer	ρ resistivity ($\Omega\text{ m}$)	h thickness (m)	η chargeability	τ decay constant (s)
1	30	30	-	-	1	90	15	-	-
2	8	45	-	-	2	12	25	-	-
3	0.92	45	0.25	3e-3	3	2.3	19	-	-
4	0.05	45	0.99	3.5e-3	4	0.5	20	0.25	3.5e-3
5	0.05	45	0.99	3e-3	5	0.5	25	0.25	3e-3
6	0.05	45	0.99	3e-3	6	0.6	24	0.25	3e-3

Table 1: 1D models of TEM sounding 3 at 4-8 Hz (left) and at 32 Hz (right).

References

- Cole, K.S. and Cole, R.H., 1941. Dispersion and absorption in dielectrics - I alternating current characteristics. *J. Chem. Phys.*, 9, 341–352.
- Kobranova, V.N., 1986. Petrophysics (*in Russian*). Nedra press, Moscow, 392 p.
- Kulikov, A.V. and Shemyakin, E.A., 1978. Electric survey using phase induced polarization method (*in Russian*). Nedra press, Moscow, 157 p.
- Pelton, W.H., Ward, S.H., Hallof, P.G., Sill, W.R. and Nelson, P.H., 1978. Mineral discrimination and removal of inductive coupling with multi-frequency IP. *Geophysics*, 43, 588-609.
- Zadorozhnaya, V., 2008. Resistivity measured by direct and alternating current: why are they different? *Adv. Geosci.*, 19, 45-59.
- Zadorozhnaya, V.Yu. and Hauger, M.H., 2009. Mathematical modeling of membrane polarization occurring in rocks due to applied electrical field. *Izvestiya, Phys. Solid Earth*, 45, 1038-1054.
- Zadorozhnaya, V.Yu. and Maré, L.P., 2011. New model of polarization of rocks: theory and application. *Acta Geophys.*, 59, 262-295.

SESSION 4
OTHER IP APPLICATIONS

SIP responses of building materials, investigation of correlations with specific surface and dominant pore throat size

S. Kruschwitz⁽¹⁾

(1) Federal Institute for Materials Research and Testing (BAM), Berlin, Germany

Many damage processes in building stones are driven by moisture ingress and subsequent decay due to soling, blistering or different types of corrosion. Hence, measuring moisture and/or any material property that is connected to the absorption/desorption behaviour of a porous medium is helpful for building engineers concerned with conservation or restoration. Since the SIP method is sensitive to both the amount and chemistry of a pore fluid and pore space properties its applicability and practical use as a non-destructive testing tool for moisture damages is studied at BAM.

Scott and Barker (2003) demonstrated for sandstones a good correlation between the frequency of the SIP phase peak and the dominant pore throat size measured in mercury-intrusion experiments. Their observations basically go back to the relaxation model developed by Schwartz (1962) and Schurr (1964) for spherical particles in ion solutions. In their model the particle diameter R of glass beads and the relaxation time τ of the ions in the solution were linked according to:

$$\tau = R^2 / D_s \quad \text{and} \quad D_s = \mu_s kT$$

where D_s is the effective diffusion coefficient, μ_s is the effective ionic mobility, k is the Boltzmann’s constant and T is the absolute temperature and. Scott and Barker argued that in the case of consolidated materials like sandstones the “critical length scale” leading to the relaxation process are not grain sizes, but pore throat sizes.

In order to further explore this relationship for building materials (with a particular focus on sandstones) a new study has been carried out covering with the samples a wide range of textural characteristics. The involved materials comprised sandstones, tuffs, bricks, artificial sand-limestones, asphalt and concrete. The pore-throat size distributions of all samples have been measured in mercury-intrusion experiments and the specific surfaces determined in BET analyses. Most materials had unimodal pore throat size distributions and a dominant pore throat size could be defined. Figure 1 shows the dominant pore throat size versus the position of the phase peak (frequency_peak) and the corresponding peak relaxation time (tau_peak), respectively for the new set of data and literature values.

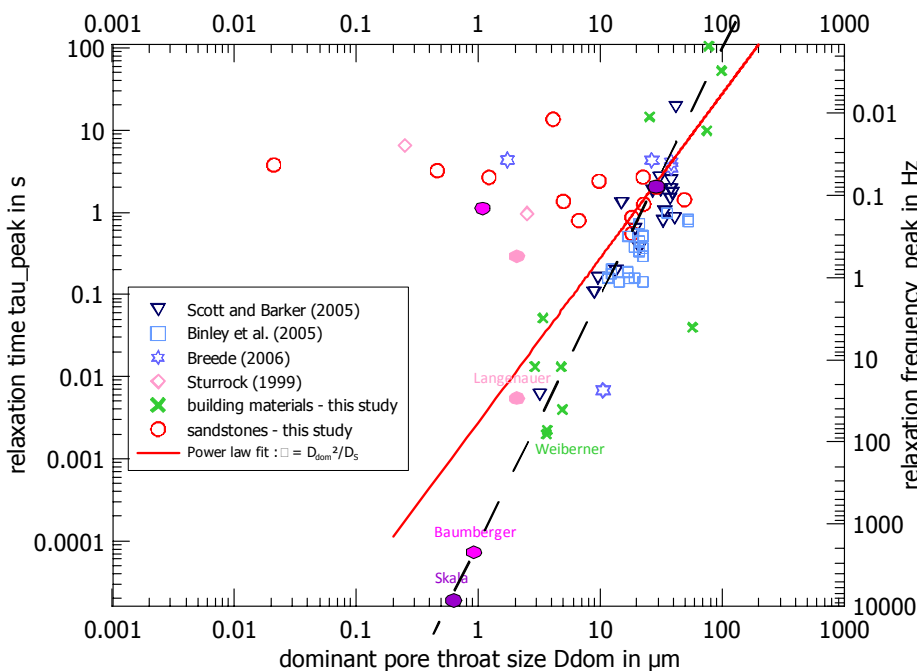


Fig. 1: Dominant pore throat sizes (D_{dom}) versus peak relaxation time (τ_{peak}) for sandstones and building materials saturated with brines of $\approx 0.1 \text{ S m}^{-1}$ fluid conductivity

Interesting are the following observations:

- 1) Some of the samples follow the predicted trend (Scott and Barker 2003) of decreasing relaxation time with decreasing dominant pore throat size. Most all of them are building materials like aerated concretes, bricks and tuffs.
- 2) Almost all sandstones of this study with dominant pore throats below 5-10 μm show relaxation times between 1 and 10 s and do not follow the predicted trend.
- 3) Some of the samples, which had unimodal pore throat size distributions in the mercury-intrusion experiments showed SIP phase curves with two peaks (e.g Baumberger and Langenauer sandstone, displayed in Fig. 2) and were hence marked with two dots in Fig. 1.
- 4) Other samples, which had a bimodal pore-size distribution in the mercury intrusion also shows a bimodal SIP phase curve (like Skala sandstone in Fig. 2), these are also marked with two dots in Fig. 2.
- 5) Between 1-10 μm we observe something like a “transition zone” where it is unclear what exactly controls the relaxation behaviour.

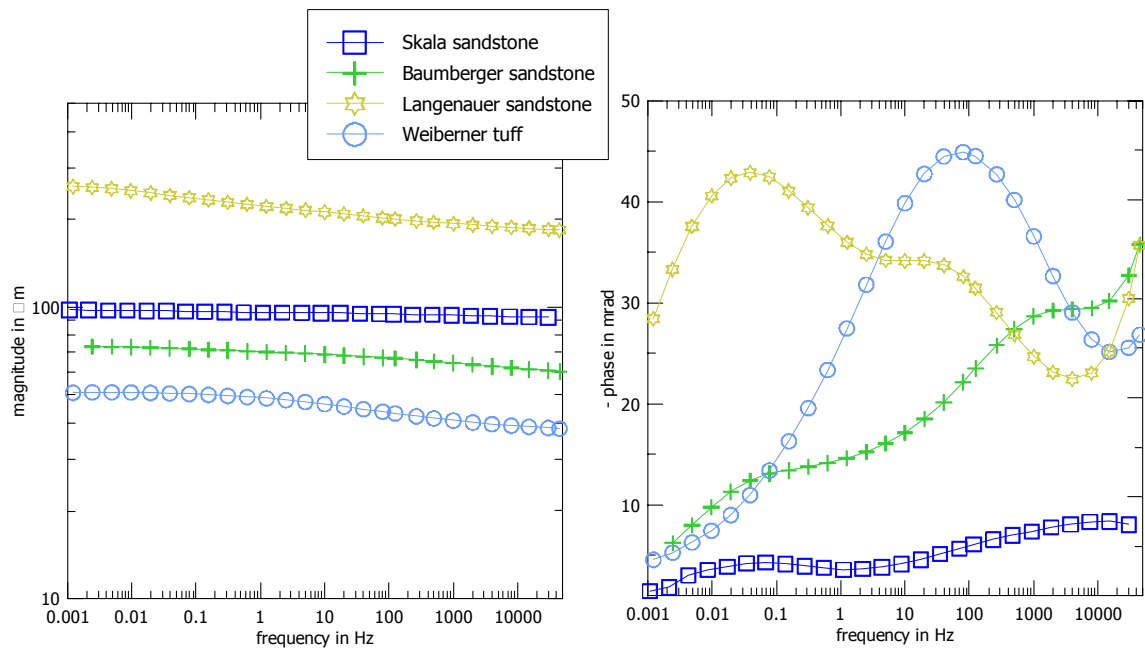


Fig. 2: SIP magnitude (left) and phase (right) spectra of three sandstones and one tuff, all samples are saturated with 0.01 M NaCl ($\sigma_f \approx 0.1 \text{ S m}^{-1}$).

The specific surfaces of the samples not following the predicted trend are usually high and the porosities low (compare with Kruschwitz et al. 2010). Currently the mineral composition and other geometric features of the pore structure are investigated in thin sections and by mineral analysis. A possible explanation for the observed phenomena might be that different relaxation processes are competing. The low-frequency relaxation process might be due to surface roughness or a certain mineral or chemical compound causing slower diffusion.

References

- Kruschwitz, S., Binley, A., Lesmes, D. and Elshenawy, A., 2010. Textural controls on low-frequency electrical spectra of porous media. *Geophysics*, 75, WA113-WA123.
- Schurr, J.M., 1964. On the theory of the dielectric dispersion of spherical colloidal particles in electrolyte solution. *J. Phys. Chem.*, 68, 2407-2413.
- Schwarz, G., 1962. A theory of the low-frequency dielectric dispersion of colloidal particles in electrolyte solution. *J. Phys. Chem.*, 66, 2636-2642.
- Scott, J. and Barker, R., 2003. Determining pore-throat size in Permo-Triassic sandstones from low-frequency electrical spectroscopy. *Geophys. Res. Lett.*, 30(9), 1450.
- Sturrock, J.T., 1999. Predictions of hydraulic conductivity using Spectral Induced Polarizations. MSc Dissertation, Boston College.

Preliminary use of induced polarization measurement to study tree roots growing in earth dikes

B. Mary⁽¹⁾, G. Saracco⁽²⁾, L. Peyras⁽¹⁾, P. Mériaux⁽¹⁾ and M. Vennetier⁽¹⁾

(1) IRSTEA (National Research Institute of Science and Technology for Environment and Agriculture), France

(2) CNRS-CEREGE (European Centre for Research and Education in Environmental Geosciences), UMR 7330, France

Context and motivations

Roots are recognized as an environmental hazard when growing in hydraulic earth structures, especially dikes. Trees' rooting in earth dikes generates two types of risks: internal erosion due to root development in earth embankments or their foundation, and external erosion (slopes and crest) which is often related to trees uprooting by the effects of currents or wind (Fauchard and Mériaux 2004). The aim of this paper is to elaborate non-destructive prospection methods able to detect and evaluate dangerous tree roots growing in earth dike or dam body.

For now, the electrical prospecting method has been used widely especially for the study of root biomass (Amato et al. 2009). Basically the use of a classical electrical resistivity tomography provides an approximation of the distribution and the volume of the root system. Recently Vanderborgh et al. (2013) proposed an overview of the methods used for studying root zone properties. They pointed out many gaps and challenges of the electrical approach. Among the limits underlined, the main is that the classical electrical tomography may be in some cases an indirect determination of the roots system. A promising approach for mapping more accurately the roots system is to consider the complex resistivity. Related to the classical ERT, this method includes a temporal dimension (Kemna et al. 2000). Plant and root materials are expected to polarize much stronger and allows obtaining potentially a specific signature of the roots presence. Some studies (Schleifer et al. 2002; Zanetti et al. 2011; Martin 2012) shown a low-frequency response. Moreover Martin (2012) shown that the bioelectrical properties of a tree stem are affected by seasonal variations. These results are fundamentals and should be consider and improve for the root detection.

Thus, thought both soil and biological material implies polarizations effects, we hope to asses in which type of soil and roots we could discriminate the roots from the soil. This work has been initiated during laboratory experimentations and shown that in most cases, the conductivity of buried root samples increased the whole conductivity of the ground among different type of soil (Zanetti et al. 2011).

This study has two main purposes: first we will try to link the polarizations effects with each parameter such as the properties of the roots (type, diameter, function, decay state...), of the soil (type, water content) and seasonal variations of the tree (sap activity). We will focus here on the determination of the weight of soil water content on the measured signal and thus on the ability to detect of the roots. Then in parallel, we develop different methodologies using temporal and frequency instruments. Following the inversion of the data we hope to compare from Cole-Cole parameters the both approach and to conclude about the ability to upscale it on field.

Results from laboratory experiments

We used for this experiment a representative type of soil of mostly dikes composition. The geoelectrical measurements were performed at the soil surface in plastics tanks containers. The tank number 1 is a control containing only the soil while in the tank number 2 is disposed a root at about 6 cm in depth. First the medium were saturated on water. The measurements were repeated each day to study the evolution of the signal with the decrease of water content of the soil.

It seems that the ability to detect the roots even including polarization effects is highly related to water content of the soil. The resistivity seems not affected by the presence of the roots whatever the water content. We observed a decrease of the chargeability over time with the drying

of medium in both tanks. Nevertheless we noticed that the ratio of the chargeability in the tank with the buried roots on the tank without root tends to be higher as 1 when the medium is drying.

Results from field experiments

We conducted the field experiment with the same parameters used in laboratory. The positions of the roots were determined previously during the tree planting. In Fig. 1 below, the root system is composed of one single primary roots of 22 mm diameter at about 20 cm depth.

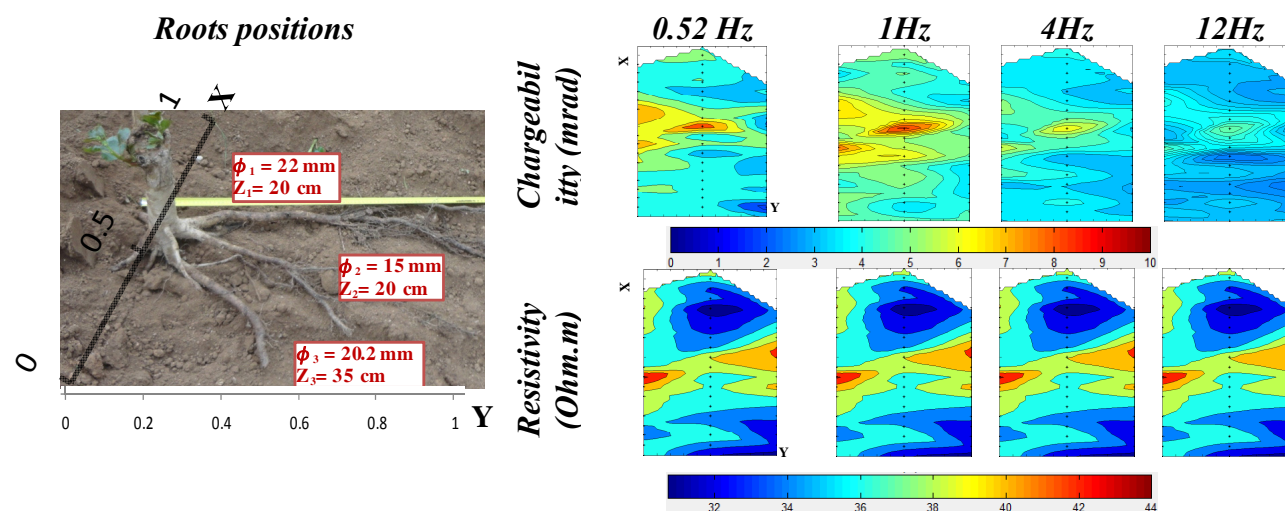


Fig. 1: Mapping of the departure of a poplar primary horizontal root from the trunk; prospect area $x = [0, 1]$ m, $y = [0, 0.2]$ m, "Wenner" configuration with inter-electrode distance $A = 15$ cm.

Here we observed a particular case with a correlation both between electrical resistivity and chargeability and the theoretical positions of the roots. While the roots 2 and 3 seems respectively too small and deep for this inter-electrode distance ($A = 15$ cm), the root 1 may be identified as an anomaly of resistivity and chargeability ($45 \Omega\text{m}$, 10 mrad at 1 Hz) on the surrounding soil ($30 \Omega\text{m}$). Moreover, the roots seems appears much more clearly at low frequency ($< 1 \text{ Hz}$).

At this stage of the study, we shown that the information provides by the polarization physic seems relevant to localize roots in the soil. Unfortunately the signal at very low frequency is very noisy and depends on a lot of external parameters. Therefore efforts should be done for offers a better understanding and conduct prospectation on real conditions.

References

- Fauchard, C. and Mériaux, P., 2004. Méthodes géophysiques et géotechniques pour le diagnostic des digues de protection contre les crues: Guide pour la mise en œuvre et l'interprétation. Editions Quae, France, 124 p.
- Amato, M., Bitella, G., Rossi, R., Gómez, J.A., Lovelli, S. and Ferreira Gomes, J.J., 2009. Multi-electrode 3D resistivity imaging of alfalfa root zone. *Eur. J. Agron.*, 31, 213-222.
- Vanderborght, J., Huisman, J.A., Kruk, J. and Vereecken, H., 2013. Geophysical methods for field-scale imaging of root zone properties and processes. *In: Soil-water-root processes: advances in tomography and imaging* (Eds Anderson, S.H. and Hopmans, J.W.). *Soil Sci. Soc. Am. Special Publication*, 61, 247-282.
- Kemna, A., Binley, A., Ramirez, A. and Daily, W., 2000. Complex resistivity tomography for environmental applications. *Chem. Eng. J.*, 77, 11-18.
- Martin, T., 2012. Complex resistivity measurements on oak. *Eur. J. Wood Prod.*, 70, 45-53.
- Schleifer, N., Weller, A., Schneider, S. and Junge, A., 2002. Investigation of a Bronze Age plankway by spectral induced polarization. *Archaeol. Prospect.*, 9, 243-253.
- Zanetti, C., Weller, A., Vennetier, M. and Mériaux, P., 2011. Detection of buried tree root samples by using geoelectrical measurements: a laboratory experiment. *Plant Soil*, 339, 273-283.

Monitoring of the biodegradation of toluene-contaminated sand in columns by SIP measurements, CO₂ content and its ¹³C/¹²C isotopic signature

C. Noel^{(1),(2)}, J.-C. Gourry⁽¹⁾, I. Ignatiadis⁽¹⁾, F. Battaglia⁽¹⁾ and C. Guimbaud⁽²⁾

(1) BRGM, Orléans, France

(2) LPC2E, CNRS, Orléans, France

Hydrocarbon contaminated soils represent an environmental issue as it impacts on ecosystems and aquifers. Bioremediation uses the ability of bacteria naturally present in the ground to degrade hydrocarbons. It represents an effective solution to fight the pollution but *in situ* monitoring before and during soil treatment is difficult and challenging. Indeed, where significant subsurface heterogeneity exists, conventional intrusive groundwater sampling can be insufficient to obtain a robust monitoring as the information they provide is restricted to vertical profiles at discrete locations, with no information between sampling points.

In order to obtain wider information, complementary methods can be used like geo-electrical techniques. Induced polarization (IP) seems to be the more promising to study the effects of biodegradation processes. Indeed, laboratory and field experiments have shown an enhancement of real and imaginary parts of electrical conductivity while bacterial treatment is progressing (Abdel Aal et al. 2006; Atekwana et Atekwana 2010).

Moreover, microbial activity induced CO₂ production and isotopic deviation of carbon (Aggarwal and Hinchee 1991). The ratio $\delta^{13}\text{C}(\text{CO}_2)$ will come closer to $\delta^{13}\text{C}(\text{hydrocarbon})$.

From these findings, the French project *BIOPHY*, supported by the French National Research Agency (ANR), proposes to use electrical methods and gas analyses to develop a non-destructive method for monitoring *in situ* biodegradation of hydrocarbons in order to optimize soil treatment. Laboratory experiments in columns are carried out to demonstrate its feasibility.

Our objectives were to monitor aerobic microbial activity in toluene-contaminated sand columns using complex electrical resistivity measurements (SIP, Spectral Induced polarization and GEIS, Galvanostatic Electrochemical Impedance Spectroscopy) and measuring concentration and $\delta^{13}\text{C}$ isotopic ratio of produced CO₂.

Materials and methods

Toluene aerobic biodegradation by *Rhodococcus wratislaviensis* (*R. w.*) is studied. Columns (height 50 cm, diameter 15 cm) are constructed in Kynar® and filled with sand from Fontainebleau. They are fed up with a fluid containing toluene (carbon source), bacterial growth medium and H₂O₂ in low concentration to supply O₂ and thus stimulate aerobic metabolic bioprocesses.

Complex electrical conductivity measurements are performed regularly to monitor the bio-activity and progress of toluene degradation. Two methods are used: SIP and GEIS. An electrical current with known amplitude and frequency is applied at two ring electrodes, positioned at both ends of the columns. This induces an electrical current in the porous media and the associated voltage is measured between two Cu/CuSO₄ potential electrodes. The change of amplitude and phase of the received waveform allows measuring complex conductivity σ^* , expressed as a sum of the real (σ') and imaginary (σ'') parts:

$$\sigma^*(\omega) = \sigma'(\omega) + i\sigma''(\omega) \quad \text{with} \quad i = \sqrt{-1} \quad \text{and} \quad \omega = 2\pi f.$$

The CO₂ concentration and $\delta^{13}\text{C}(\text{CO}_2)$ is measured by infrared laser spectroscopy. Chemical composition of fluid is also monitored: toluene quantification, $\delta^{13}\text{C}(\text{toluene})$ and $\delta^{13}\text{C}(\text{DIC})$ (Dissolved Inorganic Carbon) and alkalinity.

Results and discussion

We show the results for two columns in Fig. 1: a biotic and an abiotic control.

For the biotic column, we notice an enhancement of σ'' during decrease of toluene concentration. Moreover, there is an increase of CO₂ concentration in the air just after increase of HCO₃⁻ concentration in the pore fluid; and $\delta^{13}\text{C}(\text{CO}_2)$ approaches $\delta^{13}\text{C}(\text{toluene})$. On the contrary,

for the abiotic column, there is no significant variation of the different parameters. The $\delta^{13}\text{C}(\text{CO}_2)$ was not able to be measured because of the lack of CO_2 in the air of the column.

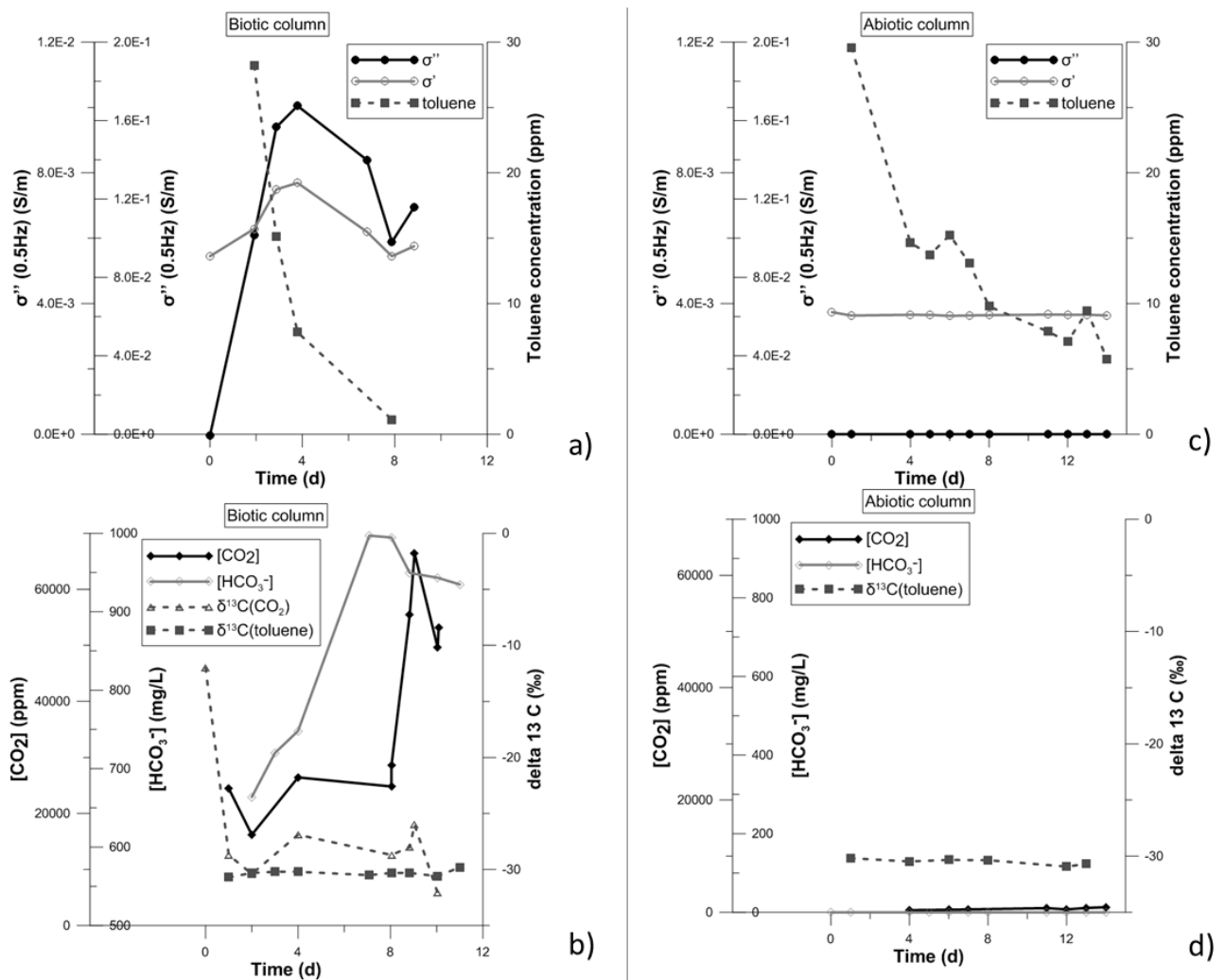


Fig. 1: Results for biotic (left) and abiotic (right) columns. a) and c) Variation over time of real and imaginary parts of complex conductivity at 0.5 Hz and toluene concentration; b) and d) CO_2 and HCO_3^- concentrations; $\delta^{13}\text{C}(\text{CO}_2)$ and $\delta^{13}\text{C}(\text{toluene})$.

Regarding these results, we can say that microbial activity is characterized by CO_2 production and $\delta^{13}\text{C}(\text{CO}_2)$ isotopic deviation, and also by an evolution of complex electrical resistivity in correlation with chemical analyses. Aerobic biodegradation of toluene can be monitored by SIP and gas measurements at laboratory scale and it will be tested soon on the field scale.

References

- Abdel Aal, G.Z., Slater, D.L. and Atekwana, E.A., 2006. Induced-polarization measurements on unconsolidated sediments from a site of active hydrocarbon biodegradation. *Geophysics*, 71, H13-H24.
- Aggarwal, P.K. and Hinchee, R.E., 1991. Monitoring in situ biodegradation of hydrocarbons by using stable carbon isotope. *Env. Sci. Tech.*, 25, 1178-1180.
- Atekwana, E.A. and Atekwana, E.A., 2010. Geophysical signatures of microbial activity at hydrocarbon contaminated sites: a review. *Surv. Geophys.*, 31, 247-283.

**A new model for the spectral induced polarization signature
of bacterial growth in porous media**

A. Revil^{(1),(2)}

(1) *Colorado School of Mines, Golden, CO. USA*

(2) *CNRS, ISTERRE, Grenoble, France*

The complex conductivity of porous materials and colloidal suspensions comprises two components: the in-phase conductivity associated with electromigration of the charge carriers and the quadrature conductivity associated with the reversible storage of the charges at some polarization length scales. We have developed a new quantitative model to investigate frequency-domain induced polarization response of suspensions of bacteria and bacteria growth in porous media. Low-frequency induced polarization of bacteria (alpha-polarization) is related to the properties of the electrical double layer of bacteria. Surface conductivity and alpha-polarization are due to the Stern layer of counterions occurring in a brush of polymers coating the surface of the bacteria and can be related to their cation exchange capacity of the bacteria. This new model can be coupled to reactive transport modelling codes in which the evolution of bacterial populations are usually described by Monod coupled kinetics. We have shown that the growth rate and endogenous decay coefficients of bacteria in a porous sand can be inferred from time lapse frequency-domain induced polarization data.

**Imaging and characterization of crop root systems
using electrical impedance tomography at the rhizotron scale**

M. Weigand⁽¹⁾ and A. Kemna⁽¹⁾

(1) *Department of Geodynamics and Geophysics, University of Bonn, Germany*

A better understanding of root-soil interactions and associated processes is essential to achieve progress in crop breeding and management, prompting the need for high-resolution and non-destructive characterization methods. To date such methods are lacking, in particular for characterizing root growth and function in the field. A promising technique in this respect is electrical impedance tomography (EIT), which utilizes low-frequency electrical conduction and polarization properties of the subsurface in an imaging framework.

Crop roots are of non-woody nature and thus do not give rise to large resistivity contrasts in the subsurface. Therefore a more promising approach is the analysis of polarization signals originating within and in the direct vicinity of the roots. It is well established that cells and cell clusters exhibit polarization signals in alternative current fields due to the electrical double layer which forms at the cell membranes. However, upscaling of these signals to the scale of the whole root system is not trivial due to the complexity of the system and the occurrence of additional large-scale membranes such as the Casparian strip, which could be related to additional polarization responses. Moreover, the strength of the polarization originating at the surface of membranes is influenced by the charge concentrations on both sides of the double layer. This charge concentration is dominated by dissolved nutrients in root systems. Therefore a correlation between nutrient dynamics (uptake, usage, and translocation) and measured low-frequency polarization responses can be expected. In particular, the frequency peak of the low-frequency polarization response provides a link to the length scale at which the dominant polarization processes take place.

We investigated the capability of EIT to image crop root systems in a series of laboratory rhizotron experiments using canola plants grown in hydroponics. Those plants were then placed in a rhizotron container with a width of 30 cm, a height of 78 cm, and a depth of 2 cm, effectively providing a 2D environment for the experiment. The rhizotron was filled with tap water, which served two purposes: first, the root system could be visually mapped, and second, the low nutrient concentration in tap water created a stress situation for the plant system. This stress situation was then monitored using multi-frequency (450 mHz – 45 kHz) EIT measurements with the tomographic acquisition system EIT40 (Zimmermann et al. 2008) over a span of four days with a high temporal resolution (up to seven measurements per day). Corresponding EIT images for all frequencies were computed using the complex resistivity inversion code CRTomo (Kemna 2000). The complex resistivity spectra, as extracted for each of the image pixels, were then analyzed using a Debye decomposition scheme. Hereby the complex resistivity spectra $\rho^*(\omega)$ are described by a superposition of multiple Debye terms:

$$\rho^*(\omega) = \rho_0 \left[1 - \sum_{i=1}^N m_i \left(1 - \frac{1}{1 + j\omega\tau_i} \right) \right]$$

with j the imaginary number, ρ_0 the direct current resistivity, m_i the i -th chargeability value with the corresponding characteristic relaxation time τ_i . A total normalized chargeability:

$$m_{tot}^N = \frac{1}{\rho_0} \sum_{i=1}^N m_i$$

was computed, and the low-frequency peak relaxation time τ_{peak} of the resulting m distribution was used for further analysis.

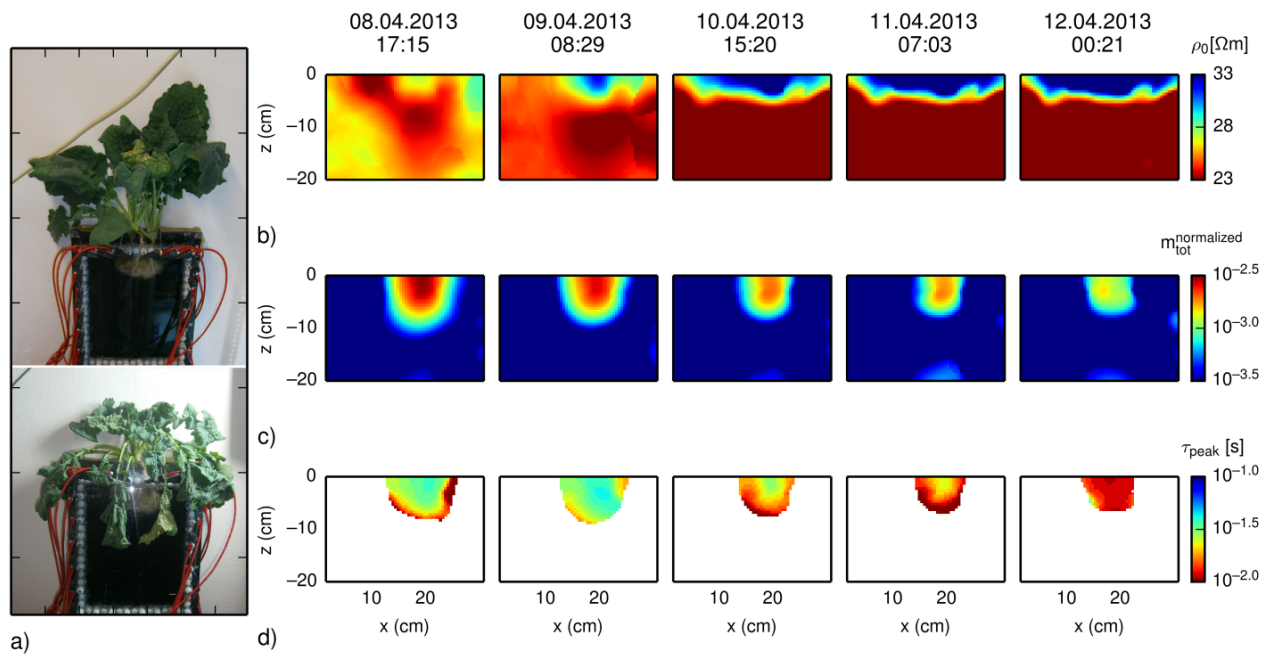


Fig. 1: EIT monitoring of multiple canola plant root systems in a nutrient stress situation over a span of four days. a) Picture of the plant system in the rhizotron at day one (top) and day four (bottom). b - d: Spectral parameters derived from a Debye decomposition of the complex resistivity pixel spectra extracted from imaging results; b) DC resistivity, c) total normalized chargeability, and d) low-frequency peak relaxation time.

As confirmed by visual inspection (Fig. 1a) the plant system reacted to the nutrient stress situation by dying back over the course of four days. Imaging results of the Debye decomposition are shown in Fig. 1b-d for selected time steps. As expected there are only small spatial and temporal changes in the resistivity (Fig. 1b). The emergence of a slightly more resistive zone at the top of the rhizotron does not coincide with the extension of the root system, and a more likely explanation is uptake of ions by the nutrient deprived root system. The total normalized chargeability (Fig. 1c) exhibits a good agreement with the root system's dimensions observed via photographs (Fig. 1a). Also, a steady decline in chargeability can be observed, which we assume corresponds to physiological processes within the root system given the nutrient deficit. The presented τ_{peak} results (Fig. 1d) can be interpreted as indicators of the dominant length scale at which polarization occurs; they show a slight, but steady, decline towards smaller values. This change in turn can either be interpreted as a breakdown of large-scale membranes such as the Casparian strip into smaller chunks, or as a change of the dominant polarization source as the membranes break down due to the nutrient deficit and the dieback of the root system.

The observed changes in relaxation time may serve as a means to characterize physiological processes within root systems, especially to study the response to stress situations. However, the present study only deals with a root system in water. If embedded in a soil matrix, the polarization response of the soil matrix will be superimposed on the root system's response, and further research is needed with regard to the discrimination of the sources of polarization in such an environment.

Nonetheless, our results demonstrate the capability of EIT to non-invasively image and monitor root systems at the rhizotron scale and suggest that EIT can be used as a tool for imaging, characterizing and monitoring crop roots at laboratory and field scales.

References

- Kemna, A., 2000. Tomographic inversion of complex resistivity - theory and application. Ph.D. thesis, Ruhr-Universität Bochum.
- Zimmermann, E., Kemna, A., Berwix, J., Glaas, W., Münch, H.-M. and Huisman, J.A., 2008. A high-accuracy impedance spectrometer for measuring sediments with low polarizability. *Meas. Sci. Technol.*, 19, 094010.

INDEX OF AUTHORS

Abdulsamad F.	48	Giampaolo V.	102	Peyras L.	138
Abu Zeid N.	130, 132	Gourry J.-C.	140	Pfaffhuber A.	120
Agrinier P.	22	Gouws G.	14, 16	Placencia-Gómez E.	30
Akulina K.	78	Guimbaud C.	140	Postic F.	72
Allègre V.	108	Gurin G.	78, 104	Radic T.	74
Auken E.	52, 70, 86 , 94, 96	Haegel F.-H.	8 , 56	Revil A.	20, 24, 32 , 54, 102, 118, 142
Bairlein K.	6	Hördt A.	6, 10 , 28	Roques C.	90
Battaglia F.	140	Huisman J.A.	8, 38, 56 , 58, 80	Rosqvist H.	106
Bazin S.	120	Hupfer S.	12	Santarato G.	130, 132
Béhaegel M.	128	Ignatiadis I.	140	Saracco G.	138
Bignardi S.	132	Ilse K.	14	Scheibz J.	120
Binley A.	38, 52	Ilyin Y.	104	Schmutz M.	22, 48, 76 , 88, 100, 108
Blondel A.	76, 88	Ingham M.	14 , 16	Schwartz N.	36, 124 , 126
Bouzid N.	92	Jakobsen R.	96	Shefer I.	34 , 36 , 126
Bücker M.	6, 10, 40, 98	Joblonowski N.	8	Slater L.	30, 42, 68
Cabrera J.	118	Johansson S.	106	Sparrenbom C.	106
Cahill A.	96	Joseph S.	14, 16	Sterligova I.	110, 112
Camerlynck C.	48, 54, 90 , 100, 118	Keating E.	22	Tarasov A.	78, 104
Capozzoli L.	102	Kelter M.	58	Tichané F.	88
Cappelen P.	120	Kemna A.	18 , 38, 40, 58, 60, 80, 144	Titov K.	78 , 104
Carles M.	88	Kenkel J.	60	Treichel A.	38 , 56, 80
Carlson N.	92	Kessouri P.	20	Undorf S.	40
Christiansen A.V.	52, 86, 96	Kratzer T.	64	van Waasen S.	80
Cosenza P.	24, 118	Kremer T.	22 , 108	Vaudelet P.	76
Curatola F.	68	Kruschwitz S.	136	Vennetier M.	138
Dahlin T.	50 , 70, 94 , 106, 120	Kulikov V.	110 , 112	Vereecken H.	8, 38, 56, 58
Diamantopoulos E.	28	Lartiges B.	116	Votta M.	102
Doetsch J.	52, 96	Leroy P.	24	Weigand M.	18, 144
Doussan C.	72	Llubes M.	116	Weinstein M.	34
Durner W.	28	Longuevergne L.	90	Weller A.	42 , 44
Esser O.	8, 38	Losito G.	26	Williams K.	98
Evdokimov K.	68	Lumetzberger M.	106	Williard E.	108, 128
Fel L.	36	Macnae J.	62 , 64	Wolters B.	80
Fiandaca G.	52 , 70, 86, 96, 120	Macouin M.	116	Woodruff W.	20
Flores Orozco A.	98	Maineult A.	22, 108, 128	Zadorozhnaya V.	120, 130 , 132
Florsch N.	48, 54 , 118	Martin T.	2 , 12	Zhang Z.	44
Franceschi M.	88	Mary B.	138	Zhao Y.	80
Furman A.	34, 36, 124, 126	Masi M.	26	Zimmermann E.	8, 18, 38, 56, 58, 80
Gao Z.	8	Mériaux P.	138	Zorin N.	82
Gazoty A.	86	Noel C.	140		
Ghorbani A.	24, 76, 100 , 118	Noell U.	12		
		Nordsiek S.	6, 28 , 44		
		Ntarlagiannis D.	68		
		Okay G.	24, 118		
		Olsson P.-I.	70 , 106		
		Parisot J.-C.	100		

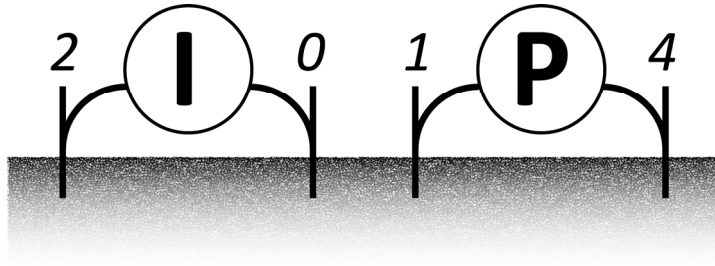
Edited by

Christian Camerlynck (Sorbonne Universités, UPMC - Université Paris 6)
Hervé Chauris (MINES ParisTech)
Alexis Mainault (Centre National de la Recherche Scientifique and UPMC)
Myriam Schmutz (Institut Polytechnique de Bordeaux – ENSEGID)

April 2014

3rd International Workshop on Induced Polarization

6 – 9 April 2014, Ile d'Oléron, France



Following the two previous International Workshops on Induced Polarization organized in Bonn in 2009 and in Golden (Colorado) in 2011, this conference gathers scientists interested in IP to present and discuss the recent developments of the method. This booklet contains the extended abstracts of the oral and poster presentations. Methodological aspects, petrophysical relationships, theoretical and laboratory studies, modelling and inverse problem are addressed, as well as applications to geology, ore prospecting, survey of the environment, hydrology, civil engineering and plant science are presented.

Organizing committee

Christian CAMERLYNCK (UPMC, Paris)
Hervé CHAURIS (MINES ParisTech)
Alexis MAINEULT (CNRS, Paris)
Myriam SCHMUTZ (Institut
Polytechnique de Bordeaux)

Scientific committee

Norman CARLSON (Zonge International, Inc.)
Claude DOUSSAN (INRA, Avignon)
Nicolas FLORSCH (UPMC, Paris)
Andreas KEMNA (Universität Bonn)
James MACNAE (RMIT University, Melbourne)
Tina MARTIN (BGR, Berlin)
Konstantin TITOV (St Petersburg State University)
Andreas WELLER (Technische Universität Clausthal)

Conference organized by



with the support of

